2018

HETEROGENEOUS CATALYTIC DEOXYGENATION OF LIPIDS TO FUEL-LIKE HYDROCARBONS OVER IMPROVED BIMETALLIC NICKEL CATALYSTS

Ryan Andrew Loe
University of Kentucky, ryan.a.loe89@gmail.com
Digital Object Identifier: https://doi.org/10.13023/etd.2018.420

STUDENT AGREEMENT:

I represent that my thesis or dissertation and abstract are my original work. Proper attribution has been given to all outside sources. I understand that I am solely responsible for obtaining any needed copyright permissions. I have obtained needed written permission statement(s) from the owner(s) of each third-party copyrighted matter to be included in my work, allowing electronic distribution (if such use is not permitted by the fair use doctrine) which will be submitted to UKnowledge as Additional File.

I hereby grant to The University of Kentucky and its agents the irrevocable, non-exclusive, and royalty-free license to archive and make accessible my work in whole or in part in all forms of media, now or hereafter known. I agree that the document mentioned above may be made available immediately for worldwide access unless an embargo applies.

I retain all other ownership rights to the copyright of my work. I also retain the right to use in future works (such as articles or books) all or part of my work. I understand that I am free to register the copyright to my work.

REVIEW, APPROVAL AND ACCEPTANCE

The document mentioned above has been reviewed and accepted by the student's advisor, on behalf of the advisory committee, and by the Director of Graduate Studies (DGS), on behalf of the program; we verify that this is the final, approved version of the student's thesis including all changes required by the advisory committee. The undersigned agree to abide by the statements above.

Ryan Andrew Loe, Student

Dr. Mark Crocker, Major Professor

Dr. Mark Lovell, Director of Graduate Studies

HETEROGENEOUS CATALYTIC DEOXYGENATION OF LIPIDS TO FUEL-LIKE HYDROCARBONS OVER IMPROVED BIMETALLIC NICKEL CATALYSTS

DISSERTATION

A dissertation submitted in partial fulfillment of the
requirements for the degree of Doctor of Philosophy in the
College of Arts and Sciences
at the University of Kentucky

By
Ryan Andrew Loe

Lexington, Kentucky

Co-Directors: Dr. Mark Crocker, Professor of Chemistry and
Dr. John Selegue, Professor of Chemistry

Lexington, Kentucky

ABSTRACT OF DISSERTATION

HETEROGENEOUS CATALYTIC DEOXYGENATION OF LIPIDS TO FUEL-LIKE HYDROCARBONS OVER IMPROVED BIMETALLIC NICKEL CATALYSTS

Diminishing petroleum reserves and environmental considerations have strengthened the demand for developing renewable fuel technologies. One alternative is deoxygenating plant oils, animal fats, and waste lipid streams to fuel-like hydrocarbons. These fuels offer a drop-in replacement to petroleum products while potentially becoming carbon neutral, satisfying both fuel and environmental concerns. This fuel is obtained through catalytic deoxygenation via either hydrodeoxygenation (HDO) or decarboxylation/ decarbonylation ($deCO_x$). HDO requires problematic sulfided catalysts and extreme hydrogen pressures to convert lipids to fuel-like hydrocarbons. Therefore, this work focuses on the $deCO_x$ pathway, where hydrogen is not required for deoxygenation to take place. Generally, other authors use Pd or Pt as the active metals for $deCO_x$; however, their cost can be industrially prohibitive. Recently, inexpensive Ni catalysts have shown comparable catalytic $deCO_x$ activity to Pd and Pt, albeit significant catalyst deactivation and catalytic cracking to undesirable products remain problematic. Therefore, this work aims to improve the activity, selectivity, and recyclability of supported Ni catalysts for the $deCO_x$ of lipids. Cu, Sn, and minimal amount of Pt were investigated as secondary promoter metals for Ni catalysts for $deCO_x$. Deoxygenation of waste lipids such as brown grease and yellow grease was also accomplished in an industrially relevant fixed bed reactor.

KEYWORDS: Lipids, Decarbonylation/decarboxylation, Hydrocarbons, Supported Nickel Catalysts.

Ryan Andrew Loe
09/04/18

HETEROGENEOUS CATALYTIC DEOXYGENATION OF LIPIDS TO FUEL-LIKE HYDROCARBONS OVER IMPROVED BIMETALLIC NICKEL CATALYSTS

By

Ryan Andrew Loe

Dr. Mark Crocker
Co-Director of Dissertation

Dr. John Selegue
Co-Director of Dissertation

Dr. Mark Lovell
Director of Graduate Studies

09/04/18

To my wife and family,

for your support, encouragement, and

unconditional love

ACKNOWLEDGMENTS

I would like to thank my advisor, Dr. Mark Crocker, for his guidance, support, and unfaltering patience throughout my time at the University of Kentucky. I am truly grateful for the opportunity to be one of his students. I would also like to thank my doctoral committee members Dr. John Selegue, Dr. Mark Meier and Dr. Stephen Rankin for their ample time spent in committee meetings, oral qualifying exams, and more. Their continued advice and support will forever be appreciated.

I would also like to thank my colleagues and friends at the University of Kentucky Center for Applied Energy Research. Thank you to the undergraduates Lilia Sewell, Makaylah Garrett, Miranda Maier, Morgan Walli, and - now fellow graduate student - Kelsey Huff for your assistance on various projects. Thank you to Tonya Morgan for assistance in analyzing the liquid samples from my hundreds of experiments. Thank you to Leslie Hughes for her help in preparing my publications and assisting in organizing my travel arrangements for a number of conferences. I would like to thank Dr. Eduardo Santillan-Jimenez for getting me to this far. Your advice has always been most helpful whether it is with research or in life.

Thank you to my family for all your love and support along this journey. A special thanks to my wife, Dr. Ashley Loe. You have been my biggest supporter since day one of this adventure and I don't know where I would be without you. There have been many ups and downs along the way, but you have always helped me pull through.

This work was funded by the National Science Foundation under Grants No. 1437604, 1531637, 1305039, and 1355438 and by the U.S. Departments of Energy under award DE-FG36-08GO88043.

TABLE OF CONTENTS

ACKNOWLEDGMENTS iii
LIST OF TABLES vii
LIST OF FIGURES ix
LIST OF SCHEMES xii
Chapter 1: Introduction to upgrading of lipids to fuel-like hydrocarbons and terminal olefins *via* decarbonylation/decarboxylation 1
1.1. Introduction 1
1.2. Lipid Feeds 6
1.3. $DeCO_x$ Catalysts: Active Phases 9
1.4. $DeCO_x$ Catalysts: Support Materials 17
1.5. Reaction Conditions 20
1.6. Reaction Mechanism 24
1.7. Catalyst Deactivation 29
1.8. Conclusions and Outlook 32
Chapter 2. Effect of Cu and Sn promotion on the catalytic deoxygenation of modeland algal lipids to fuel-like hydrocarbons over supported Ni catalysts 41
2.1. Introduction 42
2.2. Experimental 46
2.2.1. Catalyst preparation and characterization 46
2.2.2. Deoxygenation experiments in semi-batch mode 48
2.2.3. Deoxygenation experiments in continuous mode 49
2.2.4. Product analysis 50
2.3. Results and Discussion 51
2.3.1. Catalyst Characterization 51
2.3.2. Blank runs 56
2.3.3. Tristearin deoxygenation in semi-batch mode 57
2.3.4. Stearic acid deoxygenation in semi-batch mode 60
2.3.5. Triolein deoxygenation in continuous mode 62
2.3.6. Algal lipids deoxygenation in continuous mode 63
2.3.7. Spent catalyst characterization 65
2.4. Conclusions 67

Chapter 3. Effect of Cu promotion on cracking and methanation during the Ni-catalyzed deoxygenation of waste lipids and hemp seed oil to fuel-like hydrocarbons 85
3.1. Introduction 86
3.2. Materials and methods 88
3.2.1 Feed lipid analysis 88
3.2.2. Catalyst preparation and characterization 88
3.2.3. Deoxygenation experiments 89
3.2.4. Methanation experiments 90
3.2.5. Analysis of deoxygenation products and spent catalysts 90
3.3. Results and Discussion 92
3.3.1. Catalytic upgrading of 25 wt% yellow grease 92
3.3.2. Catalytic methanation of CO_2 96
3.3.3. Catalytic upgrading of 25 wt% hemp oil 97
3.3.4. Catalytic upgrading of 75 wt% yellow grease 99
3.3.5. Analysis of spent catalysts 101
3.4. Conclusions 102
Chapter 4. Continuous catalytic deoxygenation of waste free fatty acid-based feeds to fuel-like hydrocarbons over a supported Ni-Cu catalyst. 125
4.1. Introduction: 125
4.2. Experimental: 128
4.2.1. Catalyst preparation 128
4.2.2. Catalyst characterization 129
4.2.5. Feed Preparation 130
4.2.4. Continuous fixed-bed deoxygenation experiments 130
4.2.5 Liquid and gaseous product analysis 131
4.3. Results and Discussion 133
4.3.1 Catalytic deoxygenation of fatty acids 133
4.3.2 Catalytic deoxygenation of brown grease at different temperatures 134
4.3.3 Catalytic deoxygenation of brown grease at different H_2 partial pressures 136
4.3.4 Catalyst deactivation and online regeneration 137
4.4. Conclusions 140
Chapter 5. Catalytic deoxygenation of tristearin using Pt as a promoter for supported Ni catalysts. 158

5.1. Introduction 158
5.2. Experimental 161
5.2.1. Catalyst preparation and characterization 161
5.2.2. Deoxygenation experiments 163
5.2.3. Liquid product analysis 164
5.3. Results and Discussion 165
5.3.1. Catalyst Characterization 165
5.3.2 Tristearin deoxygenation in semi-batch mode 168
5.3.4. Spent catalyst characterization 170
5.4. Conclusions 171
Chapter 6. Conclusions and future outlooks 180
6.1. Conclusions 180
6.2 Future Outlooks 183
REFERENCES 186
VITA 202

LIST OF TABLES

Table 1.1. Selected examples of deCOx catalysts and their performance in the deoxygenation of lipid feeds……..34

Table 2.1. Textural properties and metal dispersion of the catalysts studied.……... 69

Table 2.2. Semi-batch mode deoxygenation of tristearin over alumina-supported Ni-based catalysts (580 psi of H_2, 6 h reaction time)……70

Table 2.3. Semi-batch mode deoxygenation of tristearin over 20% Ni/Al_2O_3 catalysts with different metal particle size (260 °C, 580 psi of H_2, 6 h reaction time)…….71

Table 2.4. Semi-batch mode deoxygenation of stearic acid over alumina-supported Ni-based catalysts (300 psi of H_2, 1.5 h reaction time)……72

Table 3.1. GC-MS analysis of the feed and product mixtures in the catalytic upgrading of yellow grease (25 wt% in C12) over 20% Ni/Al_2O_3 at 350 °C and WHSV = 4.7 h^{-1} …….....104

Table 3.2. GC-MS analysis of the feed and product mixtures in the catalytic upgrading of yellow grease (25 wt% in C12) over 20% Ni-5% Cu/Al_2O_3 at 350 °C and WHSV = 4.7 h^{-1} …..……105

Table 3.3. C1-C3 mass balance of the catalytic upgrading of yellow grease (25 wt% in C12) over 20% Ni/Al_2O_3 and 20% Ni-5% Cu/Al_2O_3 at 350 °C and WHSV = 4.7 h^{-1} ……...……...106

Table 3.4. GC-MS analysis of the feed and product mixtures in the catalytic upgrading of hemp oil (25 wt% in C12) over 20% Ni/Al_2O_3 at 350 °C and WHSV = 4.7 h^{-1}……107

Table 3.5. GC-MS analysis of the feed and product mixtures in the catalytic upgrading of hemp oil (25 wt% in C12) over 20% Ni-5% Cu/Al_2O_3 at 350 °C and WHSV = 4.7 h^{-1}…108

Table 3.6. GC-MS analysis of the feed and product mixtures in the catalytic upgrading of yellow grease (75 wt% in C12) over 20% Ni-5% Cu/Al_2O_3 at 375 °C and WHSV = 2.0 h^{-1}……109

Table 3.7. GC-MS analysis of the feed and product mixtures in the catalytic upgrading of yellow grease (75 wt% in C12) over 1 g SiC at 375 °C and WHSV = 2.0 h^{-1} ……..110

Table 4.1. GC-MS analysis of the feed mixtures used in the catalytic upgrading experiments over 20% Ni- 5% Cu/Al_2O_3……142

Table 4.2 GC-MS analysis of the liquid product mixtures in the catalytic upgrading of fatty acid feed (25 wt% in C12) over 20% Ni-5% Cu/Al_2O_3 at 275 °C and WHSV = 1.0 h^{-1}, in 100% H_2……...143

Table 4.3 GC-MS analysis of the liquid product mixtures in the catalytic upgrading of fatty acid feed (25 wt% in C12) over 20% Ni-5% Cu/Al_2O_3 at 325 °C and WHSV = 1.0 h^{-1}, in 100% H_2……...144

Table 4.4 GC-MS analysis of the liquid product mixtures in the catalytic upgrading of fatty acid feed (25 wt% in C12) over 20% Ni-5% Cu/Al_2O_3 at 375 °C and WHSV = 1.0 h^{-1}, in 100% H_2……...145

Table 4.5 GC-MS analysis of the liquid product mixtures in the catalytic upgrading of brown grease lipid feed (50 wt% in C12) over 20% Ni-5% Cu/Al_2O_3 at 325 °C and WHSV = 1.0 h^{-1}, in 100% H_2……..……..146

Table 4.6 GC-MS analysis of the liquid product mixtures in the catalytic upgrading of brown grease lipid feed (50 wt% in C12) over 20% Ni-5% Cu/Al_2O_3 at 325 °C and WHSV = 1.0 h^{-1}, in 100% H_2……...……..147

Table 4.7 GC-MS analysis of the liquid product mixtures in the catalytic upgrading of brown grease lipid feed (50 wt% in C12) over 20% Ni-5% Cu/Al_2O_3 at 375 °C and WHSV = 1.0 h^{-1}, in 20% H_2/Ar……...……..148

Table 4.8 GC-MS analysis of the liquid product mixtures in the catalytic upgrading of brown grease lipid feed (50 wt% in C12) over 20% Ni-5% Cu/Al_2O_3 at 375 °C and WHSV = 0.8 h^{-1}, in 100% H_2 for the first 100 h…….……..149

Table 4.9 GC-MS analysis of the liquid product mixtures in the catalytic upgrading of brown grease lipid feed (50 wt% in C12) over 20% Ni-5% Cu/Al_2O_3 at 375 °C and WHSV = 0.8 h^{-1}, in 100% H_2 for the second 100 h…….…….150

Table 5.1. Textural properties and metal dispersion of the catalysts studied…….173

Table 5.2. Pulsed H_2 chemisorption results of the catalysts screened for the deoxygenation of tristearin……...174

Table 5.3. Semi-batch mode deoxygenation of tristearin over alumina-supported Ni-based catalysts (580 psi of H_2, 260 °C, 3 h reaction time)……...175

LIST OF FIGURES

Figure 2.1. XRD patterns of 20% Ni/Al_2O_3 (a), 20% Ni-1% Cu/Al_2O_3 (b), 20% Ni-2% Cu/Al_2O_3 (c), 20% Ni-5% Cu/Al_2O_3 (d), and 20% Ni-1% Sn/Al_2O_3 (e) calcined under air at 500 °C……73

Figure 2.2. TEM image of 20% Ni/Al_2O_3……...74

Figure 2.3. STEM image of 20% Ni-5% Cu/Al_2O_3 and EDS (inset) of the region highlighted in the image……..…75

Figure 2.4. H_2 TPR profiles of the fresh catalysts……...76

Figure 2.5. High resolution Ni XP spectra of 20% Ni/Al_2O_3 and 20% Ni–5% Cu/Al_2O_3...77

Figure 2.6. DRIFTS spectra of CO adsorbed on 20% Ni/Al_2O_3 and 20% Ni-5% Cu/Al_2O_3 ……78

Figure 2.7. High resolution Ni XP spectra of 20% Ni/Al_2O_3 and 20% Ni-5% Cu/Al_2O_3…79

Figure 2.8. Boiling point distribution plots of the feed and the liquid products obtained from triolein deoxygenation in fixed bed mode at 260 °C and 580 psi over20% Ni/Al_2O_3 (left), and 20% Ni-5% Cu/Al_2O_3 (right)……80

Figure 2.9. Boiling point distribution plots of the feed and the liquid products obtained from algal lipids deoxygenation in fixed bed mode at 260 °C and 580 psi over 20% Ni/Al_2O_3 (left), and 20% Ni-5% Cu/Al_2O_3 (right)……81

Figure 2.10. GC-MS analysis of the algae oil used in this study…….82

Figure 2.11. TGA profiles of catalysts spent upgrading tristearin at 260°C for 6 h in a semibatch reactor (top left), tristearin at 350°C for 6 h in a semibatch reactor (top right), stearic acid at 300 °C for 1.5 h in a semibatch reactor (bottom left), and triolein at 260 °C for 4 h in a fixed bed reactor (bottom right)…….83

Figure 3.1. Lipid profile for the yellow grease and hemp seed oil used.....111

Figure 3.2. BPDPs of 25 wt% yellow grease (feed) and the products collected after 1-8 h of time on stream and GC-MS data showing the evolution of different types of compounds during catalytic upgrading over 20% Ni/Al_2O_3 (a and b) and 20% Ni-5% Cu/Al_2O_3 (c and d) at 350 °C and WHSV = 4.75 h^{-1}…….…….112

Figure 3.3. Amounts of C10, C11, C14, C15 and C16 in the reaction products collected after 1-8 hours of time on stream during the catalytic upgrading of 25wt % yellow grease over 20% Ni/Al_2O_3 (a) and 20% Ni-5% Cu/Al_2O_3 (b) at 350 °C and WHSV = 4.75 h^{-1} ……..…113

Figure 3.4. Composition of incondensable gases collected after 1-8 hours of time on stream during the catalytic upgrading of 25 wt% yellow grease over 20% Ni/Al_2O_3 (a) and 20% Ni-5% Cu/Al_2O_3 (b) at 350 °C and WHSV = 4.75 h^{-1} …….…….114

Figure 3.5. Composition of gases collected after 1-8 hours of time on stream during the catalytic methanation of ~5 vol% CO_2 in H_2 over 20% Ni/Al_2O_3 (a) and 20% Ni-5% Cu/Al_2O_3 (b) at 350 °C …….....115

Figure 3.6. DRIFTS spectra of the spent 20% Ni/Al_2O_3 and 20% Ni-5% Cu/Al_2O_3 catalysts……116

Figure 3.7. BPDPs of 25 wt% hemp oil (feed) and the products collected after 1-8 hours of time on stream and GC-MS data showing the evolution of different types of compounds during catalytic upgrading over 20% Ni/Al_2O_3 (a and b) and 20% Ni-5% Cu/Al_2O_3 (c and d) at 350 °C and WHSV = 4.81 h^{-1}……117

Figure 3.8. Amounts of C10, C11, C14, C15 and C16 in the reaction products collected after 1-8 hours of time on stream during the catalytic upgrading of 25 wt% hemp oil over 20% Ni/Al_2O_3 (a) and 20% Ni-5% Cu/Al_2O_3 (b) at 350 °C and WHSV = 4.81 h^{-1} .....…….118

Figure 3.9. Composition of incondensable gases collected after 1-8 hours of time on stream during the catalytic upgrading of 25 wt% hemp oil over 20% Ni/Al_2O_3 (a) and 20% Ni-5% Cu/Al_2O_3 (b) at 350 °C and WHSV = 4.81 h^{-1}……..……119

Figure 3.10. BPDPs of 75 wt% yellow grease (feed) and the products collected after 1-8 hours of time on stream and GC-MS data showing the evolution of different types of compounds during catalytic upgrading over 20% Ni-5% Cu/Al_2O_3 (a and b) at 375 °C and WHSV = 2.03 h^{-1}……...……...120

Figure 3.11. BPDP of yellow grease (75 wt% in C12) and the products collected after 1-8 hours of time on stream during a blank experiment performed using SiC at 375 °C and WHSV = 2.0 h^{-1}……...…….121

Figure 3.12. Composition of incondensable gases collected after 1-8 hours of time on stream during the catalytic upgrading of 75 wt% yellow grease over 20% Ni/Al_2O_3 (a) and 20% Ni-5% Cu/Al_2O_3 (b) at 350 °C and WHSV = 4.81 h^{-1}…….……122

Figure 3.13. TGA profiles (acquired under air) of catalysts spent in the catalytic upgrading of yellow grease, in the catalytic methanation of CO_2, and in the catalytic upgrading of hemp oil……123

Figure 4.1 GC-MS analysis of the liquid product mixtures in the catalytic upgrading of fatty acid feed (25 wt% in C12) over 20% Ni-5% Cu/Al_2O_3 at a) 275 °C, b) 325 °C, c) 375 °C with a WHSV = 1.0 h^{-1}, in 100% H_2…….……..151

Figure 4.2 GC-MS analysis of the liquid product mixtures in the catalytic upgrading of brown grease lipid feed (25 wt% in C12) over 20% Ni-5% Cu/Al_2O_3 at a) 325 °C and b) 375 °C with a WHSV = 1.0 h^{-1}, in 100% H_2……...152

Figure 4.3. GC-MS of the liquid products (a and c) and refined gas analysis (b and d) of the gaseous products from the deoxygenation of brown grease lipids at different H_2 partial pressures……...153

Figure 4.4. Thermogravimetric analysis of the dried spent catalyst from the deoxygenation of brown grease lipids at 375 °C and 580 psi of 100% H_2 after first 100 h and the second100 h on stream of the regenerated catalyst…….154

Figure 4.5. GC-MS analysis of select liquid samples for the deoxygenation of brown grease lipids after 100 h on stream, *in situ* catalyst regeneration, and a 2nd 100 h on stream at 375 °C and 580 psi of 100% H_2……...155

Figure 4.6. Refined gas analysis on select gas samples from the deoxygenation of brown grease lipids after 100 h on stream, *in situ* catalyst regeneration, and a 2nd 100 h on stream at 375 °C and 580 psi of 100% H_2…….156

Figure 4.7. DRIFTS spectra of the fresh catalyst after reduction, spent catalyst, and the spent catalyst after reduction……....157

Figure 5.1. X-ray diffraction patterns for 20%Ni/Al_2O_3 (a), 20%Ni-0.1%Pt/Al_2O_3 (b), 20%Ni-0.25%Pt/Al_2O_3 (c), and 20%Ni-0.5%Pt/Al_2O_3 (d)……...176

Figure 5.2. Temperature programmed reduction profile of the catalysts screened for the deoxygenation of tristearin……...177

Figure 5.3. Gas chromatograms and BPDPs of the liquid products collected from the deoxygenation of tristearin with 20%Ni/Al_2O_3 (a and b) and 20%Ni-0.5%Pt/Al_2O_3 (c and d) at 260 °C…….....178

Figure 5.4. Thermogravimetric analysis of the spent catalysts from the deoxygenation of tristearin…….....179

LIST OF SCHEMES

Scheme 1.1. Reaction equations for a) Hydrodeoxygenation, b) Decarbonylation, and c) Decarboxylation of stearic acid……..36

Scheme 1.2. a) Water-gas shift, b) Boudouard Reaction, c) Methanation of CO_2, and d) Methanation of CO gas phase reactions during deCO_x……...37

Scheme 1.3. Mechanism for a) hydrolysis b) β-elimination c) γ-hydrognen transfer and d) hydrogenolysis of triglycerides……..38

Scheme 1.4. The proposed reaction mechanism for a) the hydrogenation of palmitic acid to hexadecanal in the presence of H_2 and b) the ketonization of palmitic acid to palmitone in the absence of H_2.……..…..39

Scheme 1.5. Reaction scheme for stearic acid deoxygenation. Adapted from Appl. Catal. B 191 (2016) 147-156……40

Scheme 2.1. Reaction scheme for stearic acid deoxygenation……..….84

Scheme 3.1. Internal cracking of oleic acid and its positional isomers in which the double bond is removed one position in either direction of the C18 chain and where the olefinic cracking products are assumed to undergo hydrogenation……...124

Chapter 1: Introduction to upgrading of lipids to fuel-like hydrocarbons and terminal olefins *via* decarbonylation/decarboxylation

1.1. Introduction

The CO_2 emissions stemming from the use of fossil fuels represent one of the main causes of climate change, which puts social and environmental pressure behind the pursuit of alternative fuels. Furthermore, a number of factors – including the non-renewable nature of fossil fuels, the ever-increasing demand for energy resources, the uneven geographical distribution of oil reserves, as well as geopolitical, technological and economic developments – can result in an uncertain supply and volatile prices of petroleum-derived fuels. Therefore, many countries have come to consider the development of renewable fuels as a means to attain energy independence and national security. Current petroleum consumption surpasses 96 million barrels of crude oil daily worldwide and that demand is expected to increase by 18% by 2040 [1]. Moreover, while hydrocarbon-based fuels such as jet fuel and diesel are widely used in aviation and trucking, viable alternatives to petroleum-derived fuels for these transportation sectors are currently in short supply. The limited availability of alternative fuels is of great concern, particularly since forecasts indicate that fuel consumption for the aviation sector alone will increase 5% annually until 2030 [2] and that the alternative fuel demands by the transportation sector could reach 900 million tons by 2020, which may result in fuel shortages and further environmental disruption [3]. The most advantageous replacement of petroleum-derived fuels – from both an economic and technological standpoint – would be fuel-like hydrocarbons obtained from a renewable source. Indeed, renewable fuels chemically indistinguishable from (and

thus entirely fungible with) petroleum-derived fuels would be fully compatible with the existing engine and fuel distribution infrastructure of nearly every economy around the world [4]. In addition, biofuels have the potential to be carbon neutral, as the amount of CO_2 emitted during biofuel production and use can be equivalent to the amount consumed during the growth of the biomass used as raw material [5]. Additionally, biofuel production could also promote employment and economic activity in rural regions and help countries reduce their dependence on fuels sourced from other nations [6]. Given the aforementioned environmental, economic, energy independence, and national security benefits, the need to develop renewable "drop-in" hydrocarbon biofuels cannot be overstated.

In view of the projected increase in demand, the conversion of plant oils and animal fats into liquid transportation fuels has attracted much attention, the most mature technology developed to date to effect this transformation being the synthesis of biodiesel. This fully commercialized process involves the transesterification of glycerides and/or the esterification of free fatty acids (FFAs) to form the fatty acid methyl esters (FAMEs) that constitute biodiesel. FAMEs offer several advantages over petroleum-derived fuels as they produce lower amounts of sulfur emissions upon combustion [7], offer increased lubricity [7], display high cetane number (a measure of combustion quality under compression ignition), and the mild reaction conditions involved in their synthesis allow for small scale production practically everywhere [8]. However, biodiesel also shows a number of important drawbacks. Indeed, the heat content of FAMEs is 9-13% lower than that of petroleum-derived fuels on a mass basis, the fuel can be contaminated with cations

stemming from the catalysts used during biodiesel synthesis, and the latter affords considerable amounts of glycerol, which effectively constitutes a waste by-product that needs to be disposed of. Biodiesel also displays poor storage stability due to the fact that some of the FAMEs may contain C=C double bonds [9], which can be hydrated to afford hydroxyl groups that induce polymerization [10]. Further, engine compatibility issues can also arise since water – which has a relatively high solubility in FAMEs – can cause corrosion of metal parts [8, 9], while FAMEs also display poor cold flow properties [9]. Finally, biodiesel production *via* transesterification is highly sensitive to the feed employed (the presence of FFAs can deactivate the catalysts employed and contaminate the fuel product with soaps [8]), so FFAs must first be removed from glyceride-based feeds before each stream can be converted to FAMEs separately. Altogether, these disadvantages have limited the ability of biodiesel to displace a significant fraction of petroleum-derived fuels.

Notably, many of the drawbacks associated with biodiesel stem from the high oxygen content of FAMEs, which can be higher than 10 wt% [11, 12]. Therefore, research has aimed to develop processes that convert animal fats and plant oils to fuel-like hydrocarbons by removing the oxygen from these feeds *via* catalytic cracking, hydrodeoxygenation (HDO), or decarbonylation/decarboxylation (deCO_x). Catalytic cracking is a simple process that uses acid catalysts such as zeolites and other alumino-silicates or silicoaluminophosphates to yield fuel-like products. However, the reaction is often unselective and creates naphthalene and other aromatic compounds that can lead to coking and the concomitant deactivation of the catalyst [13]. In contrast, HDO removes

oxygen in the form of water (see Figure 1.1a), and can be a very selective process resulting in high yields of diesel- and jet fuel-like hydrocarbons. HDO products are chemically identical to petroleum-derived fuels and have been reported to offer improved performance and reduced emissions relative to both biodiesel and petrodiesel [11, 14]. The use of HDO to produce fuel-like hydrocarbons (marketed as green or renewable diesel) also represents a mature technology, Neste Oil's NExBTL^{TM} and UOP/Eni's Ecofining^{TM} being noteworthy commercial processes. Although promising, HDO typically involves the use of sulfided catalysts (which may deactivate in the presence of water and contaminate the fuel products with sulfur) and requires high pressures of hydrogen, limiting processing to centralized facilities where this gas can be produced from natural gas deposits [11]. Alternatively, oxygen can be removed from lipids – including glycerides, FFAs, FAMEs and/or mixtures thereof – in the form of CO and CO_2 *via* catalytic decarbonylation and decarboxylation, respectively, generating fuel-like hydrocarbon molecules containing one less carbon atom than the original lipid monomer (see Figures 1b and 1c). Although the carbon loss results in a lower atom efficiency compared to the HDO pathway, the decreased H_2 requirements negate this consequence. Generally, decarbonylation and decarboxylation are considered as deCO_x in the aggregate as opposed to independently, mainly because it is difficult to differentiate the two reaction pathways under most experimental conditions. Indeed, hydrogen is typically present in the reaction atmosphere, resulting in the hydrogenation of any double bonds including the terminal olefins produced *via* decarbonylation, which makes the liquid products resulting from decarbonylation and

decarboxylation indistinguishable. Similarly, the gas products evolved do not constitute a reliable way to differentiate the two reaction pathways, mainly due to the fact that water gas shift, methanation and Boudouard reactions can all take place (see Scheme 1.2b), even if the occurrence of the reverse water gas shift (RWGS) reaction can be ruled out by the low value for the RWGS equilibrium constant at typical $deCO_x$ temperatures [15]. The aforementioned reactions confound CO and CO_2, making it impossible to ascertain the extent to which either decarbonylation or decarboxylation have taken place. Albeit the stoichiometry of the $deCO_x$ reactions shown in Figures 1b and 1c clearly illustrates that external hydrogen is not required for these reactions to proceed, external hydrogen is generally added to the reaction atmosphere in order to improve catalyst performance. Nevertheless, $deCO_x$ processes display considerably lower hydrogen requirements and afford similar yields of fuel-like hydrocarbons than processes based mainly on HDO, which represent some of the main reasons behind the considerable interest that $deCO_x$ processes have received in the last decade [16, 17].

Against this backdrop, this chapter will focus on the most salient work performed to date on the $deCO_x$ of lipids involving heterogeneous catalysts. Given that a considerable amount of raw feedstock will be needed if renewable hydrocarbons are to become a substantial fraction of liquid transportation fuels and help meet projected demands, the most abundant lipid feed sources will be discussed. In regards to the catalysts, there are numerous reports covering many different formulations active in the $deCO_x$ of lipids. While both homogeneous [18, 19] and heterogeneous [20, 21] catalysts have been used to

convert FFAs and esters to hydrocarbons over the last 75 years, interest in this transformation has increased dramatically over the last decade. Moreover, heterogeneous catalysts are more relevant for industrial application due to the ease of catalyst and products separation. Therefore, although several homogenous catalysts have recently been reported [22-26], the more common work involving the heterogeneously catalyzed $deCO_x$ of lipids to hydrocarbons will be the focal point of this discussion. Furthermore, the literature contains reports of many different types of heterogeneous catalysts – including supported transition metals [27-36] and supported carbides [37-41], as well as phosphided [42-47] and sulfided [48-51] formulations – that exhibit $deCO_x$ activity. However, due to the fact that the vast majority of reports deal with supported Group 10 metals, only these catalysts (including bimetallic formulations containing these metals) will be discussed, along with the effect of different supports and reaction conditions. Finally, the most widely accepted reaction mechanisms will be examined.

1.2. Lipid Feeds

In contrast to biodiesel synthesis – which presupposes the separation of feeds into reasonably pure FFA or glyceride streams prior to their transformation into biodiesel *via* acid catalyzed esterification and base catalyzed transesterification, respectively – the deoxygenation of lipids *via* $deCO_x$ has the advantage of being feedstock agnostic, as glycerides, FFAs, FAMEs and/or mixtures thereof can be converted to fuel-like hydrocarbons through a single $deCO_x$ process. As stated previously, the demand for

renewable fuels is immense if a significant fraction of the 80 million barrels of oil consumed daily worldwide is to be displaced. Therefore, raw materials that are both abundant and varied are necessary to render renewable fuels a viable alternative. It has already been demonstrated that a number of oils sourced from agricultural crops – including palm [52, 53], sunflower [54, 55], rapeseed [56], coconut [57] and soybean oil [15, 58] – can be converted to fuel-like hydrocarbons *via* deCO_x. However, the use of edible feedstocks can disrupt the food supply, leading to volatile food prices. Moreover, the clearing of forests and other carbon-rich habitats to create farm land dedicated to these crops can also increase CO_2 emissions and prevent any renewable fuels produced from becoming carbon neutral for decades [59].

Currently, the most widely used renewable fuels are corn ethanol and soybean biodiesel; however, corn and soybeans are both edible feedstocks and the fuels derived from them are net carbon positive, in spite of their lower net greenhouse gas emissions (12% and 41%, respectively) relative to petroleum-derived fuels [60]. Fuels derived from inedible oleaginous plants that can thrive in arid or degraded soils (such as Jatropha curcas) represent a more desirable alternative to avoid disrupting the food supply, realize additional greenhouse gas reductions, and minimize agrichemical pollution [60, 61]. Nevertheless, renewable fuels obtained from these sources alone could only replace a limited amount of petroleum-derived fuels fossil fuels, the demand for renewable diesel alone already exceeding the current production levels of terrestrial oleaginous crops. Fortunately, several potential options to supplement the oil supply exist, including microalgae, the latter having

been extensively reviewed [62-69]. Unfortunately, both the energy consumption and the cost of cultivating and processing algae must be reduced considerably before algae can be deemed a viable feedstock for the production of renewable fuels [67, 70]. Other inedible oleaginous raw materials include waste streams such as tall oil fatty acid (TOFA), yellow grease (waste cooking oil) and brown grease (grease recovered from grease traps). While the low cost of these feeds is certainly advantageous, their use can also prevent them from reaching landfills or water streams. TOFA can be obtained from vacuum distillation of crude tall oil, which is a side stream from the pulp and paper industry with production approaching 845,000 tons in 2004 in the United States alone [71]. TOFA have been successfully deoxygenated by Murzin and co-workers [71, 72]. Yellow grease is another inedible feedstock – produced at a rate of 100 million gallons per day in the United States [73] – for which deoxygenation to hydrocarbons has been demonstrated [74-76]. Brown grease offers similar advantages, although dewatering must precede its conversion to fuel to prevent the hydrothermal deactivation of the catalyst employed unless formulations showing satisfactory stability and performance in the presence of water are used [77]. Although these challenges with brown grease have hindered large scale production, successful deoxygenation to fuel-like hydrocarbons has been demonstrated [77].

It should be noted that in contrast with edible oils and fats, which are mostly triglyceride-based, waste lipid streams are typically rich in FFAs. Admittedly, deCO_x processes can yield fuel-like hydrocarbons from glycerides, FFAs or mixtures containing both; however, other characteristics such as the length and the degree of unsaturation of

the carbon chains must also be taken into account. In addition to the fact that natural fats typically contain hydrocarbon chains of 8-22 carbons – which makes them ideal for the production of fuels – several authors have reported that chain length does not affect the rate of deoxygenation observed over most catalysts [78-81]. However, Lamb *et al*. [82] and Martin *et al*. [83] found that over carbon supports, longer chain fatty acids exhibited an increased initial reaction rate which was attributed to increased tendency for adsorption [82]. Martin found that as the chain length of the FA increased to 18, significant increases in cracking occurred [83]. Chain unsaturation is a more challenging factor due to the fact that the presence of carbon-carbon double bonds favors cracking reactions resulting in catalyst fouling, which in turn leads to catalyst deactivation, and in hydrocarbon products consisting of shorter hydrocarbon chains. Given that the chain length of jet and diesel fuel range between 9 and 20 carbons, excessive cracking can limit the use of the hydrocarbon products. Notably, the difficulties associated with unsaturated feeds can be partially addressed by the type of catalyst and reaction conditions employed, both of which will be addressed in the following sections.

1.3. DeCO$_x$ Catalysts: Active Phases

Over the past 15 years, a number of catalysts have been actively investigated for the deoxygenation of fats and oils. In an initial catalyst screening study performed by Snåre *et al*. [84], several commercially available catalysts comprising different active phases and supports were tested for activity in the deoxygenation of stearic acid, a model fatty acid

compound. Carbon-supported formulations were found to be more active, which was attributed to the amphoteric properties, surface functionalities, and high surface area of the carrier minimizing the effect of coke-induced deactivation. Results obtained over similar supports and, accounting for the metal content, revealed that deoxygenation activity follows the order Pd > Pt > Ni > Rh > Ir > Ru > Os. Therefore, for several years following that report, work on the conversion of lipids to fuel-like hydrocarbons focused on carbon-supported Pd and Pt catalysts. However, Ni-based formulations started garnering attention due to their ability to offer comparable deoxygenation activity to Pd and Pt with certain feeds and reaction conditions [15]. In view of the foregoing, this chapter will focus on supported Pt, Pd and Ni catalysts – along with bimetallic formulations involving these metals – such as those included in Table 1.1. In instances where the deoxygenation ability of different metals is compared, catalysts with the same support and similar metal loadings are used (whenever possible) in an effort to minimize the effect of these variables.

In the initial catalyst screening study performed by Snåre *et al*., which included 5 wt% Pt and 5 wt% Pd on a carbon support, the Pd-based catalyst afforded the best results, including quantitative conversion of stearic acid and a selectivity to C17 hydrocarbons of 99%. In the case of Ni catalysts, higher loadings are typically employed to counter the lower intrinsic activity of this metal relative to Pd and Pt. Interestingly, Wu *et al*. recently reported that 5 wt% Pt/C affords a significantly higher conversion of stearic acid than 20 wt% Ni/C at 330 °C in hydrogen- and solvent-free conditions [85]. However, these results

contrast with data previously reported by Crocker and co-workers [15], which can be attributed to the fact that these authors reduced the catalyst prior to the deoxygenation reaction and performed their experiments using a stirred reactor. Indeed, when Crocker and co-workers tested 1 wt% Pt/C, 5 wt% Pd/C and 20 wt% Ni/C for activity in the deoxygenation of soybean oil (an unsaturated triglyceride feed) at 350 °C under an inert atmosphere, the Ni catalyst displayed a conversion of 92% and a yield of C8-C17 hydrocarbons of 54%. In contrast, the Pd and Pt catalysts displayed significantly lower conversion values (30 and 23%, respectively). Tellingly, the Ni catalyst also afforded a considerably higher yield of light (C_{1-7}) hydrocarbons than the precious metal catalysts, which is indicative of increased cracking. A follow up study by Crocker and co-workers evaluated the effect of the reaction atmosphere on the performance of 20 wt% Ni/C and 5 wt% Pd/C [15]. Results indicate that the conversion of FFA and triglyceride model compounds is increased upon addition of H_2 to the reaction atmosphere. However, the Pd catalyst displays a higher selectivity to C17 hydrocarbons than Ni irrespective of the atmosphere employed, which parallels the previous report and suggests that Ni exhibits increased cracking activity relative to Pd regardless of the hydrogen partial pressure. In short, in spite of the fact that when normalized on the basis of metal loading the reactivity of carbon-supported catalysts follows the order Pd > Pt > Ni, reduced Ni catalysts with high (10-30 wt%) metal loadings can outperform noble metal catalysts, particularly when concentrated feeds are employed. Notably, whereas decarboxylation represents the main

pathway observed over Pd and Ni catalysts, decarbonylation is favored over Pt formulations [84].

In addition to the work summarized above on carbon-supported catalysts, several authors have also tested Pt, Pd, and Ni on Al_2O_3 for activity in the conversion of lipids to hydrocarbons, which has led to additional insights. For instance, Beremblyum *et al*. prepared alumina-supported Pt, Pd, and Ni catalysts with the same 5 wt% metal loading [86], thus enabling the direct comparison of the deoxygenation activity of these metals that is lacking for carbon-supported formulations. When tested for stearic acid deoxygenation at 350 °C in a H_2 atmosphere using a batch reactor, activity followed the order Pd > Pt > Ni, conversion values being 100, 92, and 61%, respectively. Beremblyum *et al*. concluded that decarbonylation constituted the main deoxygenation pathway for all three metals under the conditions employed, the highest olefin yield being observed with Ni. The change in the deoxygenation pathway from decarboxylation to decarbonylation when Ni and Pd are supported on oxidic – as opposed to carbonaceous – supports has also been observed by other authors [82]. Analogous findings vis-à-vis the activity trends discussed above have also been reported for the upgrading of unsaturated lipids [87]. Indeed, albeit at 325 °C in the presence of hydrogen Madsen *et al*. found that 5% Pt/Al_2O_3 and 5% Pd/Al_2O_3 displayed similar activity in the conversion of oleic acid, these authors determined that 5% Pd/Al_2O_3, 5% Pt/Al_2O_3 and 5% Ni/Al_2O_3 afforded tripalmitin conversions of 71, 46 and 10%, respectively. Interestingly, when Srifa *et al*. tested the same three catalysts for activity in the deoxygenation of palm oil using an industrially relevant trickle-bed reactor and reaction

conditions (300 °C, 50 bar of H_2 and LHSV = 1 h^{-1}), each of the catalysts afforded quantitative conversion [53]. Tellingly, these authors also observed that lower quantities of long chain hydrocarbons and propane – as well as higher amounts of methane and ethane – were obtained with the Ni catalyst, which is indicative of the increased cracking activity of Ni resulting in the shortening of both the hydrocarbons chains and of the propane stemming from the triglyceride backbone. In short, the order of activity in the catalytic $deCO_x$ of lipids for Group 10 metals on carbonaceous and oxidic supports is Pd > Pt > Ni, a trend that has also been observed in gas phase reactions [88]. Parenthetically, when these three metals supported on a SAPO-11 zeolite were tested in the isomerization of normal to branched alkanes to obtain fuels with improved cold flow properties, the order of reactivity was found to be Pt > Pd > Ni [89], which suggests that Group 10 precious metals are more intrinsically active than Ni in both isomerization and deoxygenation reactions. Moreover, although higher Ni loadings can be used to match the activity of Pt and Pd, exacerbated cracking and the impact of the latter on both selectivity and deactivation must be considered.

In an effort to more thoroughly understand the $deCO_x$ activity of Group 10 metals, several authors have systematically studied the effect of metal loading and dispersion on catalyst performance. Chen *et al*. tested Pt/SAPO-11 catalysts with loadings ranging from 0.6 to 3% for deoxygenation activity and found that, although metal dispersion decreased with increased metal loading, there was an overall increase in the number of active metal sites, which makes the fact that conversion increased with metal loading unsurprising [90].

Murzin and co-workers studied the effect of metal dispersion on the deoxygenation of palmitic and stearic acid over 1wt% Pd/C and found the optimal Pd dispersion to be 65%. Indeed, while a catalyst with a lower dispersion exhibited lower catalyst activity – which can be explained on the basis that larger particles should result in a reduced number of surface sites – a catalyst with 72% metal dispersion also showed lower activity than the formulation with 65% dispersion in spite of the fact that the average metal particle size of both catalysts was similar. The authors explained this finding invoking a strong metal-support interaction for the 72% dispersion catalyst resulting in changes in the Pd metal structure required for deoxygenation. Murzin and co-workers also found that 5% Pd/C exhibited better conversion and selectivity than 1wt% Pd/C in the deoxygenation of stearic acid; however, increasing the Pd loading further did not result in better conversion or selectivity to fuel-like hydrocarbons [84]. Interestingly, Lamb and co-workers found that Pd dispersion values similar to those used by Murzin led to quick catalyst deactivation during the deoxygenation of octanoic acid over silica-supported catalysts [91]. These authors concluded that when silica is used as the carrier, a much lower dispersion of 16% (corresponding to a metal particle size of 7.5 nm) is preferred, which indicates that the optimal metal dispersion is support-dependent for Pd-based catalysts. Similarly, the optimal metal loading has been reported to be support-dependent for Ni-based catalysts. Indeed, for the supports on which the effect of metal loading has been assessed, the optimal Ni loadings have been found to be 15, 20, 7, 7, and 15 wt% on Al_2O_3 [92], carbon [85], SAPO-11 [93], HSZM-5 [94], and ZrO_2 [95], respectively. For each of these supports, both

lower and higher Ni loadings than the ones listed result in a decrease in the number of active sites. Moreover, increasing the loading to 25 wt% Ni has also been reported to favor the formation of inactive Ni-aluminate on alumina-supported [92]. In short, for a given support, catalyst performance is a function of both metal loading and dispersion.

Bimetallic active phases have attracted a fair amount of interest due to their potential to outperform monometallic formulations in the conversion of lipids to hydrocarbons *via* $deCO_x$. For instance, Savage and co-workers observed some improvements relative to Pt/C when using a bimetallic Pt-Sn/C catalyst in the deoxygenation of stearic acid under hydrothermal conditions [96]. Indeed, the Pt-Sn/C catalyst exhibited higher selectivity to C17 (the main $deCO_x$ product from the stearic acid feed), albeit the addition of Sn also led to a decrease in activity. In contrast, incorporating 5 wt% Re into a Pt-Re bimetallic catalyst doubled the C17 obtained from the deoxygenation of stearic acid yield under hydrothermal conditions compared to a monometallic Pt catalyst [97]. Similarly, Sun *et al*. found Pd/SiO_2 to be selective towards $deCO_x$ products when tested in the in gas phase deoxygenation of octanoic acid, although significant deactivation rates were observed [91]. However, the authors found that deactivation could be curbed through the addition of Au in a 1:1 atomic ratio during catalyst synthesis, which afforded bimetallic particles with Au cores and Pd-rich surfaces. The observed improvement in catalyst stability was attributed to the Au addition resulting in a lower CO adsorption energy on the surface Pd sites. The reduced presence of CO – a known catalyst poison – on the catalyst surface decreases catalyst deactivation, which allowed

the Au-Pd catalyst to display a consistent performance in a fixed-bed reactor for more than 6 h of time on stream. Noticeable improvements in activity, selectivity and stability have also been achieved through the addition of Cu to Ni/Al_2O_3 [74, 75]. Indeed, while 20 wt% Ni/Al_2O_3 displayed a conversion and selectivity to C17 hydrocarbons of 27 and 63% during the deoxygenation of tristearin at 260 °C in a semi-batch reactor, the corresponding values achieved over 20 wt%Ni-5 wt% Cu/Al_2O_3 were 97 and 71%. In view of its promising performance, the 20 wt% Ni-5wt% Cu/Al_2O_3 catalyst was also used to upgrade waste and highly unsaturated feeds such as yellow grease and hemp seed oil using a fixed-bed reactor and industrially-relevant reaction conditions [74]. Saliently, the Ni-Cu catalyst displayed remarkable stability during 8 h of time on stream – yielding >90% diesel-like hydrocarbons at all reaction times sampled – and significantly less cracking relative to the corresponding Ni-only catalyst. The promotional effects observed were determined to be due (at least in part) to the fact that Cu facilitates the reduction of Ni at lower temperatures, which results in the formation of the metallic surface Ni sites believed to constitute the active site for the $deCO_x$ reaction. It should be noted that whereas the bimetallic catalyst afforded excellent yields of diesel-like hydrocarbons, the monometallic formulation displayed quantitative yields of methane. This marked improvement in selectivity observed over alumina-supported Ni-Cu catalysts has also been observed by Yakovlev *et al*. in their work with other supports [98], of which CeO_2 and ZrO_2 were found to be most effective, revealing the presence of the support effects that are discussed below in more detail. Nevertheless, the noteworthy improvements achieved over Ni-Cu catalysts are most encouraging in the

development of inexpensive catalysts for the deoxygenation of lipid feeds, as they illustrate that the promotion of Ni with other earth-abundant metals can result in catalysts rivaling the performance of precious metal-based formulations.

1.4. DeCO$_x$ Catalysts: Support Materials

The 5 wt% Pd/C formulation identified as most promising by Snåre *et al*. in their 2006 contribution [84] remains a benchmark catalyst in the conversion of lipids to hydrocarbons *via* deCO$_x$. In general, the fact that good performance can be achieved through the use of carbonaceous supports can be attributed to the large surface area of these carriers, which remains high (>500 m^2/g) even after loading considerable amounts of metal (e.g., 20 wt%). In addition to the fact that a large surface area can help curb the deactivation stemming from the formation of coke deposits and/or the sintering of supported metals, these carriers display amphoteric properties arising from the presence of various surface functional groups [84]. The latter also impact catalyst performance, as confirmed independently by Gosselink *et al*. and by Chen *et al*., who observed that improvements in catalytic activity could be realized through the addition of polarized functional groups to a carbon nanofiber carrier and a carbon support [99, 100]. However, in the event of coke-induced deactivation carbon-supported catalysts are notoriously difficult to regenerate and recycle, which disfavors their use in industrial settings where coked catalysts are typically regenerated *via* calcination in hot air (a treatment that would destroy a carbon-supported

formulation). In light of this, catalyst development has shifted to more refractory oxidic supports, which can be divided into zeolites and other metal oxides.

Zeolites are acidic and porous aluminosilicate materials with wide applications in catalysis in general and within the petroleum industry in particular. Attempts to use them as deoxygenation catalyst supports have employed various frameworks, including HZSM-5 [92, 94, 101-103], SAPO-11 [89, 90, 104-107], SBA-15 [89, 102, 108], H-Beta [101], HY [93, 101, 109], and 5Å [81, 110]. Typically, deoxygenation occurs through the HDO pathway and increased cracking and isomerization of the hydrocarbon products are observed, which is unsurprising given the characteristic concentration of Brønsted acid sites on the surface of these materials [92, 94, 105]. Modifications to the latter, such as increasing the Si:Al ratio, can lower their acidity and improve the yield of $deCO_x$ products, albeit at the cost of decreased conversion [101]. Indeed, the high conversion values associated with acid catalysts stem from the fact that increased acidity decreases the electronic charge of support oxygen atoms, which in turn leads to a decrease in electron density of the surface metal. As a result, any absorbed hydrogen in the form of a H-metal bond should be more readily activated, increasing the hydrogenation rate of the catalyst along with its selectivity towards the HDO pathway [102]. It is worth noting that while some zeolite-supported catalysts yield near equivalent amounts of HDO and $deCO_x$ products – such as 1 wt% Pt/SAPO-11-Al_2O_3 [58] – others can favor $deCO_x$ over HDO, as is the case for Pd supported on an Al-SBA-15 zeolite with a Si:Al ratio of 22 [102]. Murzin and co-workers also developed a 0.6 wt% Pd/SBA-15 that achieved 96% conversion of

stearic acid with a 98% selectivity to $deCO_x$ products, further confirming that tuning acidity can direct the reaction to proceed *via* the $deCO_x$ pathway [111]. In short, the best performing $deCO_x$ catalysts have low to medium acidity, large pores and high surface area. However, the HDO product yield is significant for the majority of zeolites tested to date, which renders these supports less than ideal for $deCO_x$ catalysts with the possible exception of modified SBA-15.

Other oxidic carriers can be further divided into two categories, namely, reducible (ZrO_2, TiO_2, and CeO_2) and non-reducible (Al_2O_3 and SiO_2) metal oxides. Through their efforts to identify promising supports for $deCO_x$ catalysts comprising 10 wt% Ni as the active phase, Lercher and co-workers found that the use of the reducible supports mentioned above led to complete stearic acid conversion and a C17 selectivity between 87 and 96%, thus outperforming 5 wt% Pd/C [95]. In contrast, the non-reducible supports Al_2O_3 and SiO_2 only achieved conversions of 63 and 45%, respectively. The authors attribute the superior activity attained through the use of the reducible supports to the ability of said carriers to become involved in the deoxygenation reaction, which is further discussed in section 6 below. It should be noted, however, that the Al_2O_3 support employed by Lercher and co-workers had a relatively low surface area (80 m^2/g) compared to Al_2O_3 supports tested by other authors (150-400 m^2/g), the latter leading to better conversions of lipid model compounds to hydrocarbons [92, 112]. Also of note is the fact that although several authors have determined SiO_2 to be a poor support for Ni-based $deCO_x$ catalyst [84, 92, 93, 95], SiO_2 has been proven to be a good support for Pd-based catalysts in gas

phase reactions conditions [21], which indicates that support effects are dependent on the nature of the active phase. These caveats for Al_2O_3 and SiO_2 are noteworthy due to fact that their use as catalyst supports often results in a high selectivity to $deCO_x$ products and decreased cracking, which can be attributed to their moderate acidity. In summary, the best supports for $deCO_x$ catalysts are reducible oxides with moderate acidity and high surface area; thus, efforts to increase the surface area of reducible supports are both clearly indicated and currently underway.

1.5. Reaction Conditions

In addition to the catalyst used, the reaction conditions employed are also a major factor to be considered during the deoxygenation of lipids to hydrocarbons. Therefore, the effect of several variables such as reaction atmosphere, pressure, temperature, and solvents has been studied. In regards to the effect of the reaction atmosphere, it should be noted that H_2 is not stoichiometrically required for the deoxygenation of lipids *via* $deCO_x$, as is clearly shown in Figures 1b and 1c. However, the presence of H_2 in the reaction atmosphere has been found to lead to improvements vis-à-vis both catalyst activity and selectivity to $deCO_x$ products. Hydrogen can be supplied internally from the surface of pre-reduced catalysts [95, 101, 113-115] and/or through the reforming of the solvent [116, 117], or externally by including H_2 in the reaction atmosphere, which provides the most sizeable and durable benefits [9, 56, 118, 119]. Indeed, deoxygenation – particularly that of unsaturated feeds

– occurs more slowly under inert reaction atmospheres [120, 121], and in some cases not at all [56]. However, the main reaction pathway in lipid deoxygenation under inert atmosphere appears to be direct decarboxylation, at least with fatty acid feeds [122]. As hydrogen partial pressure increases, most authors have reported an increase in conversion along with a shift in the deoxygenation pathway towards decarbonylation [71, 108, 117, 120, 122, 123], with further increases in H_2 pressure tending to favor the HDO pathway [101, 124]. Interestingly, Boda *et al*. have shown that above certain H_2 pressures the hydrocarbon yield decreases, which may be due to increased competition between H_2 and the feed for absorption sites on the catalyst surface [125].

Optimizing the hydrogen partial pressure can provide several benefits, such as promoting the hydrogenation of unsaturated feeds. Indeed, a number of authors have shown that hydrogenation of the C=C bonds in the feed takes place prior to its deoxygenation, as saturated species have been found to be the most prominent intermediates even under inert reaction atmospheres [71, 79, 95, 108, 110, 116]. This is of benefit given that the presence of unsaturated species has been shown to form aromatic compounds that risk giving rise to coke (of which they are precursors) and increase the deactivation rate of the catalyst [120, 126, 127]. Given that the CO_x evolved *via* the deCO_x reaction can remain absorbed on the metal active sites and act as a catalyst poison, any hydrogen present can also assist in the removal of CO_x from the catalyst surface. The latter not only prevents catalyst deactivation by keeping the catalyst surface clean and accessible, but it also shifts the reaction equilibrium to the right, particularly when semi-batch and

fixed-bed reactors (in which gaseous products are continuously removed) are employed [116]. In view of the foregoing, the presence of hydrogen can promote the catalytic deoxygenation of lipids *via* $deCO_x$, albeit the extent to which the latter takes place depends on the catalyst [17], reactor [115], and reaction conditions employed [71]. Nevertheless, care must be taken to ensure that hydrogen is not used in the deoxygenation reaction itself (as in HDO) and/or in side reactions (such as methanation) to avoid high H_2 consumption.

Unsurprisingly, the reaction temperature also influences the activity and selectivity values obtained during the catalytic deoxygenation of lipids, especially in situations where both HDO and $deCO_x$ can occur. Although typical deoxygenation reaction temperatures range between 250 and 400 °C, some authors have observed deoxygenation activity at lower temperatures [93, 109, 128] and others have used temperatures in excess of 400 °C [129]. For those reaction conditions in which deoxygenation can take place *via* both HDO and $deCO_x$, lower temperatures favor the former while higher temperatures favor the latter [16, 17, 55, 110, 130]. Elevated reaction temperatures also tend to increase conversion [71, 92, 131, 132], albeit this comes at a cost. Indeed, higher temperatures tend to favor catalytic cracking and dehydration reactions, which are often followed by aromatization or isomerization reactions affording undesirable products [9, 49, 55, 71, 98, 114, 133]. Therefore, the influence of temperature on both conversion and selectivity should not be ignored; however, the catalyst employed as well as other reaction parameters seem to exert more significant effects.

In terms of the reaction solvent, the deoxygenation of lipids has been investigated in both aqueous and organic media and the reaction pathway (HDO or $deCO_x$) appears to be independent of the solvent employed [96, 133-135]. However, there are conflicting reports regarding the effect of H_2O on catalyst activity. Indeed, whereas Chen and co-workers observed a dramatic drop in the conversion of oleic acid over a Pt/C catalyst when H_2O was used as the reaction medium [100], Lu and co-workers observed a 14% increase in the conversion of fatty acid esters when using H_2O compared to dodecane [134]. Naturally, water is particularly beneficial for the conversion of triglycerides since H_2O hydrolyses the C-O bond to afford three fatty acid molecules and glycerol, which reduces H_2 consumption [136] and may even provide the reagents necessary to generate hydrogen *in situ* through the dehydration of FFAs [71] and reforming of glycerol [97]. In fact, the prospect of utilizing H_2O both to generate H_2 *in situ* through the water gas shift reaction and as a solvent during deoxygenation experiments has attracted some interest in recent years [96, 134, 135]. Notably, although it seems that the reaction pathway (HDO or $deCO_x$) is independent of the reaction medium, the relative performance of different catalysts is affected by the solvent employed. For instance, while in aqueous media Pt/C has been reported to be a more active deoxygenation catalyst than Pd/C, the reverse trend has been observed in organic media [79, 133]. Finally, a few studies have shown that among organic solvents, those with lower boiling points tend to lead to better catalytic deoxygenation results [113, 127]. Lamb and co-workers have explained this observation invoking the fact that solvents with high boiling points have lower vapor pressure, which increases the partial

pressure of H_2 to a point that may inhibit the $deCO_x$ reaction as discussed above [116]. In view of the aforementioned effects of reaction atmosphere, pressure, temperature, and reaction medium – as well as on the dependence of these effects on the catalyst employed – the importance of carefully considering the combination of catalyst and reaction conditions in the deoxygenation of lipid to hydrocarbons is clearly indicated.

1.6. Reaction Mechanism

Although the mechanism of lipid deoxygenation to hydrocarbons is dependent on several factors – including the nature of the active phase and the catalyst support as well as the reaction conditions – some general trends have been observed. First, many authors have reported that the saturation of any C=C bonds in the feed occurs prior to deoxygenation, even in the absence of exogenous hydrogen [71, 79, 95, 108, 116, 137]. In fact, Murzin and co-workers have suggested that under inert atmosphere unsaturated lipid chains undergo geometrical and double bond positional isomerizations that, when followed by dehydrogenation reactions, ultimately result in the formation of polyunsaturated and aromatic byproducts *via* intramolecular Diels-Alder reactions [71]. Murzin and co-workers conclude that this reaction chain generates endogenous hydrogen that can saturate the C=C bonds in other unsaturated lipid molecules, which is in overall agreement with reports by other authors [137-140]. Doll and co-workers observed direct decarboxylation of unsaturated feeds leading to olefinic products [28]. Doll *et al*. proposed a tandem isomerization-decarboxylation model in which the C=C bonds undergo positional isomerization. Decarboxylation occurs when the double bonds are in close proximity to the

carbonyl carbon, yielding β-alkenes [28]. The unsaturated products are susceptible to cracking, resulting in chain shortening *via* terminal carbon loss, forming methane. Similar products suggested by Doll's model were observed by Crocker and co-workers with unsaturated feeds [74]. For the resulting saturated lipids, the deoxygenation pathway followed depends on whether the feed is a fatty acid, a triglyceride, or another ester.

During the deoxygenation of saturated triglycerides to hydrocarbons many authors have observed the formation and subsequent disappearance of fatty acids, which suggest that FFAs represent major intermediate molecules [15, 95, 141]. In aqueous media, the fatty acids are expected to be generated through hydrolysis of the C-O ester bonds to afford glycerol and three fatty acid molecules (Scheme 1.3a) [79, 142]. In organic media or solvent-free conditions, a β-elimination mechanism takes place as proposed by Vonghia *et al*. for the cracking of triglycerides over activated alumina [143]. Notably, in their study of the latter reaction, Vonghia *et al*. found two dominate pathways: i) a β-elimination mechanism that produces a carboxylic acid and an unsaturated difatty ester (see Scheme 1.3b); and ii) a γ-hydrogen transfer mechanism resulting in a C-C bond cleavage between the α- and β- carbons producing a terminal olefin with 2 less carbons than the parent fatty acid moiety (Scheme 1.3c). Given that over supported metal catalysts fatty acids have been observed as intermediates during the conversion of triglycerides to hydrocarbons while C_{n-2} hydrocarbons have not, it has been concluded that the β-elimination pathway is more plausible under $deCO_x$ reaction conditions [144]. Naturally, the unsaturated glycerol difatty ester produced through this route can subsequently undergo two sequential

hydrogenation/β-elimination steps to ultimately yield three fatty acid molecules and a propane molecule stemming from the triglyceride backbone. Nevertheless, although the β-elimination mechanism is the most widely reported, the selective hydrogenolysis of the backbone-ester C-O bond – which yields similar products to β-elimination/hydrogenation as illustrated in Scheme 1.3d – has also been suggested [121].

Fatty acid feeds, as well as fatty acids formed as intermediates during triglyceride conversion, are deoxygenated to hydrocarbons through several different pathways, which are also dependent on the active metal, support, and reaction atmosphere employed. Under inert atmospheres, the dominant reaction pathway is the direct decarboxylation of FFAs to form C_{n-1} hydrocarbons and CO_2 [117, 123]. However, as the H_2 partial pressure increases, decarbonylation becomes more prevalent [120, 122], this route affording H_2O, CO, and a C_{n-1} terminal olefin that can be readily hydrogenated to the corresponding alkane in the presence of hydrogen. Notably, two distinct mechanisms have been proposed for this particular pathway. Indeed, Boda *et al*. suggested that under conditions favoring decarbonylation, hydrogenolysis of the C-COOH bond occurs to produce formic acid and a C_{n-1} hydrocarbon [125], which is in line with a report by Berenblyum *et al*. who observed heptadecene and formic acid formation on the surface of Pd clusters in their work on the $deCO_x$ of stearic acid [117]. The formic acid generated is subsequently decarbonylated to CO and H_2O or decarboxylated to CO_2 and H_2, the rate limiting step being the C-C bond cleavage of the fatty acid. The second mechanism was proposed by Lercher and co-workers based on their work on the conversion of lipids to hydrocarbons over a Ni/ZrO_2 catalyst

[95, 121]. In line with the discussion above, Lercher and co-workers proposed that prior to deoxygenation, any C=C double bonds in the feed were hydrogenated, while the selective hydrogenolysis of the backbone-ester C-O bond in triglycerides formed three fatty acids and propane (Scheme 1.3d). The fatty acids formed are then either dissociatively adsorbed on the support at oxygen defect sites to yield a carboxylate species [145-147] or adsorbed on the nickel surface [121]. On the support, abstraction of the α-hydrogen on the carboxylate generates a ketene intermediate, albeit this has only been reported for reducible carriers such as ZrO_2 [95]. The α-hydrogen and the hydrogen stemming from the dissociative adsorption of the fatty acid combine with the oxygen at the defect site, desorption of the water molecule thus formed regenerating the oxygen vacancy. In inert atmospheres, the support-bound ketene intermediate interacts with a neighboring carboxylate species to form an acid anhydride, which decomposes to a symmetrical ketone releasing CO_2 in the process [145]. In H_2 atmospheres, the ketene intermediate migrates from the support to a nickel surface site, where it is hydrogenated to the aldehyde as shown in Scheme 1.4. Miran and co-workers also indicated that a metal oxide support is responsible for the formation of esters from neighboring alcohol products and carboxylic acids. Simultaneously, the fatty acids absorbed on the nickel surface can undergo hydrogenolysis to form the corresponding aldehyde and H_2O. Lercher and co-workers have determined that while the removal of the first oxygen atom can be effected by the support or the nickel surface, the decarbonylation step resulting in the removal of the second oxygen atom can only occur on nickel [95, 121]. Other authors have also observed the

formation of aldehyde intermediates [120, 148] over Pd/Al_2O_3 and Pd/C catalysts, extending the applicability of the pathway proposed by Lercher and co-workers over Ni/ZrO_2 to other metals and supports, albeit (as mentioned above) the direct involvement of the carrier in deoxygenation has only been observed with reducible supports.

Tellingly, other oxygenates such as alcohols and esters have also been observed in the conversion of fatty acids to hydrocarbons [81, 121]. The detection of alcohols is not entirely surprising, since in the presence of hydrogen an alcohol is formed *via* further hydrogenation of an aldehyde and both species exist in equilibrium [121]. Indeed, the hydrogenation process is reversible, meaning that alcohol can be dehydrogenated back to the aldehyde for decarbonylation to ensue. Alternatively, if conditions favoring HDO are employed, the alcohol is hydrogenated/dehydrated to form a hydrocarbon containing the same number of carbon atoms as the fatty acid from which it was derived. However, an alcohol can also undergo esterification with a fatty acid molecule, thus producing the long-chain ester species observed by some authors. In turn, esters can undergo hydrogenolysis to reform the parent alcohol and aldehyde [121], which then undergo the deoxygenation pathway previously described. The multiple reaction pathways involving FFAs discussed above are illustrated in Scheme 1.5.

Lastly, an alternative pathway for the deoxygenation of non-glyceride esters has been proposed by Murzin and co-workers based on their work on the $deCO_x$ of ethyl stearate over Pd/C [127]. Parenthetically, ethyl and methyl esters are important feeds

stemming from lipid extraction methods such as the *in situ* esterification approach employed to recover the oleaginous fraction of algal cells [149]. In the presence of H_2, Murzin and co-workers observed the scission of the bond between the carbonyl carbon and the α-carbon of the alkyl chain, resulting in the generation of n-heptadecane and an ester moiety that subsequently decomposes to yield ethanol and CO. Murzin and co-workers also observed hydrocarbons with less than 17 carbon atoms in the product mixture, which was explained by suggesting that shorter hydrocarbons can be formed from the alkyl chains *via* cracking on acid sites associated with the support or by hydrogenolysis over metallic sites on the surface of palladium particles [121].

1.7. Catalyst Deactivation

Catalyst resistance to deactivation remains one of the main challenges associated with deoxygenation reactions. While a number of deactivation pathways often lead to loss of active metal sites – including leaching, oxidation, sintering, or poisoning – decreases in the surface area and/or the porosity of the support also result in lower catalyst activity. However, neither metal oxidation [150, 151] nor metal leaching [55, 84, 115] appear to be very prevalent under most deoxygenation reaction conditions. Sintering of the active metals not only decreases the metal-specific surface area by increasing the particle size, but this process also lessens the metal-support interaction, which can potentially alter the electronic state of the active metal and affect its activity. Moreover, large metal particles can also block the pores of the support, thus hampering the access of reagent molecules to

catalytically active sites. Notably, although sintering can be significant for carbon-supported Pd and Pt catalysts used under hydrothermal conditions, this does not appear to result in loss of catalytic activity [133]. In contrast, Ni catalysts are readily deactivated under hydrothermal conditions due to oxidation of the metallic Ni active phase [151]. In organic media, sintering seems to be considerable only for catalysts using silicoaluminophosphates as the support [125], which is fortunate since metal dispersion is known to be important for formulations comprising carbonaceous [152] and oxidic supports [125, 153].

In regards to poisoning, impurities in the feeds, including nitrogen-, phosphorus-, and sulfur-containing compounds, can deactivate the catalyst by irreversibly binding to the active metal and to Lewis acid sites on the catalyst support [78, 113, 154]. Similarly, any CO generated during the deoxygenation reaction can also act as a catalyst poison by strongly binding to the surface of the active metal. Indeed, CO is known to dissociatively adsorb on Ni catalyst [155], forming carbonaceous deposits that can act as precursors to coke.

Notably, the most common pathway for catalyst deactivation during the deoxygenation of lipids to hydrocarbons is the accumulation of organic deposits on the catalyst surface. Indeed, carbonaceous deposits reduce the metal-specific surface area by physically covering metal sites or by blocking the pores of the support thus impeding the access of reagents to active sites [156]. Naturally, the reaction atmosphere and the feed employed can exacerbate these processes, as higher deactivation rates have been observed

under inert reaction atmospheres and when unsaturated feeds are used [157]. Remarkably, van Es *et al*. found that under an inert atmosphere, the addition of 0.1 equivalents of mono-unsaturated fatty acids to the reaction medium reduced the deoxygenation activity of Pd catalysts by 60%, irrespective of whether the support was carbonaceous or oxidic [157]. The latter is consistent with the fact that unsaturated compounds can be dehydrogenated to polyunsaturated molecules that may undergo intramolecular Diels-Alder [71, 100, 140] or oligomerization [126] reactions, forming the aromatic or unsaturated aliphatic products observed by many authors. Polymeric and crystalline types of carbonaceous deposits – commonly referred to as coke – are typically more complex [158] and are more strongly adsorbed than smaller and simpler unsaturated species, as evinced by the catalyst deactivation studies performed by Savage and co-workers [159]. Nevertheless, Savage found that for Pt/C catalysts tested under hydrothermal conditions, unsaturated products represent minor contributors to deactivation and coke formation, the collapse of the pores being mainly responsible for deactivation. Interestingly, Li *et al*. found in a recent study that the deactivation of zeolite-supported Ni catalysts is associated with a specific mechanism of coke formation in which carbocations generated on Brønsted acid sites on the catalyst surface stack into disordered and filament-like carbon strands similar to carbon nanotubes that evolve into graphitic coke covering the catalyst surface [158]. Unsurprisingly, which of the multiple pathways for coke-induced deactivation takes precedence seems to depend on the catalyst and reaction conditions employed. However, once deactivation has occurred, catalyst regeneration can be difficult. Fortunately, the

absorption of unsaturated products can be curbed to a large degree by the presence of H_2 in the reaction atmosphere [87, 127, 157, 160]. In fact, for catalysts deactivated due to the surface accumulation of unsaturated products, removal of the adsorbed species from the catalyst surface can be achieved by simply exposing the catalyst to H_2 [161], albeit Ping *et al*. have claimed that a series of solvent washes can also be used to remove most of the organic deposits. Obviously, both unsaturated products and coke can be removed through controlled oxidation [162], which would be the approach favored industrially as it would avoid the use of solvents and excess H_2. As mentioned above, this solution would not be viable for carbon-supported catalysts, which makes the use of metal oxides as carriers more advantageous, at least in terms of catalyst regeneration.

1.8. Conclusions and Outlook

Fuel-like hydrocarbons stemming from the deoxygenation of fats and oils offer several advantages compared to both biodiesel and petroleum-derived fuels [89]. In the deoxygenation of these feeds *via* the $deCO_x$ pathway, various metallic active phases and support materials have been investigated, Pt-, Pd-, and Ni-based catalysts exhibiting the most promising results. More recently, the study of bimetallic active phases has gained traction as these catalysts have shown improved deoxygenation activity and selectivity to $deCO_x$ products compared to their monometallic counterparts [74, 75, 91, 96-98]. The reaction conditions employed also affect the product slate in $deCO_x$ reactions, particularly

when H_2 is used as the reaction atmosphere. However, in order for the $deCO_x$ pathway to be deemed more advantageous than the HDO pathway, it is important to minimize the H_2 consumption. Indeed, although H_2 is not consumed in the removal of oxygen from the lipid feeds, the CO and CO_2 evolved can in some cases be readily converted to methane by the $deCO_x$ catalyst in the presence of H_2. Admittedly, the hydrocarbon products have also been observed to partake in side reactions such as cracking and isomerization; however, these products may not be problematic as lighter and branched hydrocarbons display superior cold flow properties. If H_2 is not used, several unfavorable side reactions can take place – such as oligomerization, ketonization, cyclization, dehydration, aromatization and coking – many of which lead to catalyst deactivation and lower yields of desirable products. These negative side reactions are more prevalent with unsaturated lipids, which are common to most feed sources. Therefore, the consumption of some hydrogen is necessary to saturate these lipids. For this reason, simultaneous deoxygenation and reforming of glycerol [163] or methanol [164] to generate H_2 *in situ* has started to attract interest. The issues of catalyst deactivation and regeneration must also be addressed more broadly and thoroughly in future studies. Nevertheless, although improvements to $deCO_x$ catalyst technology are needed, recent developments in this area are promising.

Table 1.1. Selected examples of deCOx catalysts and their performance in the deoxygenation of lipid feeds

Catalyst	Feed/Catalyst Ratio	Feed/solvent	Reactor type*	Pressure (bar), gas	Temp. (°C)	Time (h)	Conversion (%)	Selectivity	Citation
7% Ni/ HZSM-5	30 g/3 g	Methyl hexadecanoate	BR, stirred	20, H_2	220	1	>90	83% C_5-C_{16}	[94]
10% Ni/HBeta (Si/Al = 75)	1 g/0.2 g	1 g Stearic acid/100 mL C_{12}	BR, stirred	40, H_2	260	8	100	~73% C18 ~15% C17	[101]
7% Ni/SAPO-11	LHSV = 2 h^{-1}	Palm oil	FB	40, H_2	280	6	100	52.8% i-C15-C18 9.6% n-C15-C18	[107]
5% Ni/ZrO_2	1 g/0.5 g	1 g Stearic acid/ 100 mL C_{12}	SBR, stirred	40, H_2	260	8	100	2% C18 90% C17	[95]
10% Ni/ZrO_2	1 g/ 0.5 g	1 g Microalgae oil/ 100 mL C_{12}	SBR, stirred	40, H_2	260	8	100	68% C17	[95]
5% Ni/TiO_2	1 g/0.5 g	1 g Stearic acid/ 100 mL C_{12}	SBR, stirred	40, H_2	260	8	98	5% C18 87% C17	[95]
5% Ni/CeO_2	1 g/0.5 g	1 g Stearic acid/ 100 mL C_{12}	SBR, stirred	40, H_2	260	8	100	0.4% C18 93% C17	[95]
5% Ni/Al_2O_3	1 g/0.5 g	1 g Stearic acid/ 100 mL C_{12}	SBR, stirred	40, H_2	260	8	63	0.7% C18 81% C17	[95]
5% Ni/SiO_2	1 g/0.5 g	1 g Stearic acid/ 100 mL C_{12}	SBR, stirred	40, H_2	260	8	45	1.5% C18 57% C17	[95]
15% Ni/Al_2O_3	~3.1 g/0.5 g	~3.1 g Stearic acid/ 100 mL C_{12}	BR, stirred	8, H_2	290	4	100	80% C17	[92]
20% Ni-5% Cu/Al_2O_3	1.8 g/0.5 g	1.8 g Tristearin/ 22 g C_{12}	SBR, stirred	40, H_2	260	6	97	71% C17	[75]

BR: Batch reactor. SBR: Semi-batch reactor. FB: Fixed-bed reactor.

[a]Actual amounts used not specified, only a ratio was given.

[b]Sn metal loading was 25 mol% of the total metal loading.

Table 1.1 Continued. Selected examples of deCOx catalysts and their performance in the deoxygenation of lipid feeds

Catalyst	Feed/Catalyst Ratio	Feed/solvent	Reactor type*	Pressure (bar), gas	Temp. (°C)	Time (h)	Conversion (%)	Selectivity	Citation
20% Ni/C	20 g/0.22 g	20 g Soybean oil	BR, stirred	6.9, N_2	350	4	92	54% C8-C17	[15]
5% Pd/C	20 g/0.22 g	20 g Soybean oil	BR, stirred	6.9, N_2	350	4	30	17.8% C8-C17	[15]
5% Pd/C	4.5 g/1 g	4.5 g Stearic acid/ 86 g C_{12}	SBR, stirred	6, N_2	300	6	100	95% C17	[84]
5% Pd/Al_2O_3	4 g/1 g	4 g Stearic Acid/ 12 g C_{12}	BR, stirred	14.2, H_2	350	6	100	90.1% C17	[117]
0.6% Pd/SBA-15	1.49 g/0.5 g	1.49 g/ 100 mL C_{12}	SBR, Stirred	17, 5%H_2/Ar	300	5	96	98% C17	[111]
5% Pd-Au/SiO_2	4 µL/min/0.5g	4 µL/min Octanoic acid	FB	1, 10%H_2/Ar	260	5	~45	>97% C_7	[91]
1%Pt/C	20 g/ 0.22 g	20 g Soybean Oil	BR, stirred	6.9, N_2	350	4	42	34.7% C8-C17	[15]
5% Pt/ Al_2O_3	4 g/1 g	4 g Stearic acid/ 12 g C_{12}	BR, stirred	14, H_2	350	6	92.4	45% C17	[86]
5% Pt/SAPO-11	18 g/1 g	Oleic Acid[a]	BR. stirred	20, H_2	325	2	>99	31.8% C17 21% dodecylbenzene	[103]
5% Pt_3-Sn/C[b]	108 µL/5.4 mg	108 µL Oleic acid/1 g of H_2O	BR	[a]	350	2	>95	>90% C17	[96]
5.2% Pt- 4.2% Re/C	20 g/0.5 g	20 g Stearic acid/80 g of H_2O	BR, stirred	34.5, H_2	300	3	92	~80% C17	[97]

BR: Batch reactor. SBR: Semi-batch reactor. FB: Fixed-bed reactor.

[a]Actual amounts used not specified, only a ratio was given.

[b]Sn metal loading was 25 mol% of the total metal loading.

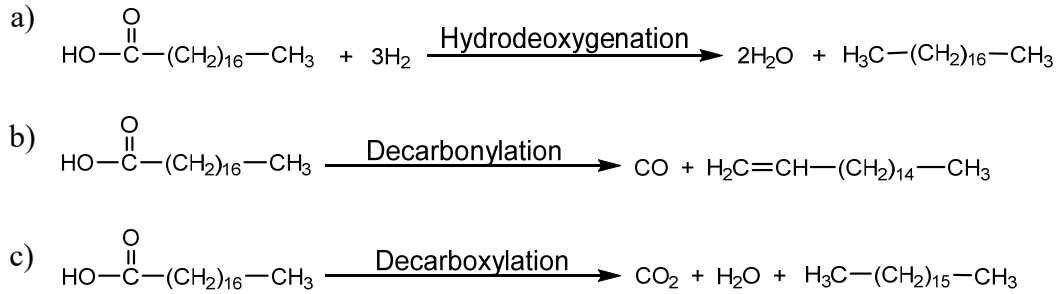

Scheme 1.1. Reaction equations for a) Hydrodeoxygenation, b) Decarbonylation, and c) Decarboxylation of stearic acid.

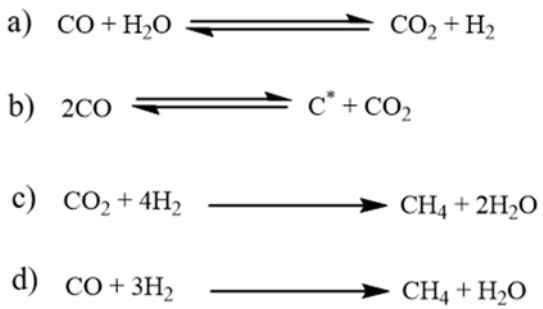

Scheme 1.2. a) Water-gas shift, b) Boudouard Reaction, c) Methanation of CO_2, and d) Methanation of CO gas phase reactions during deCO_x.

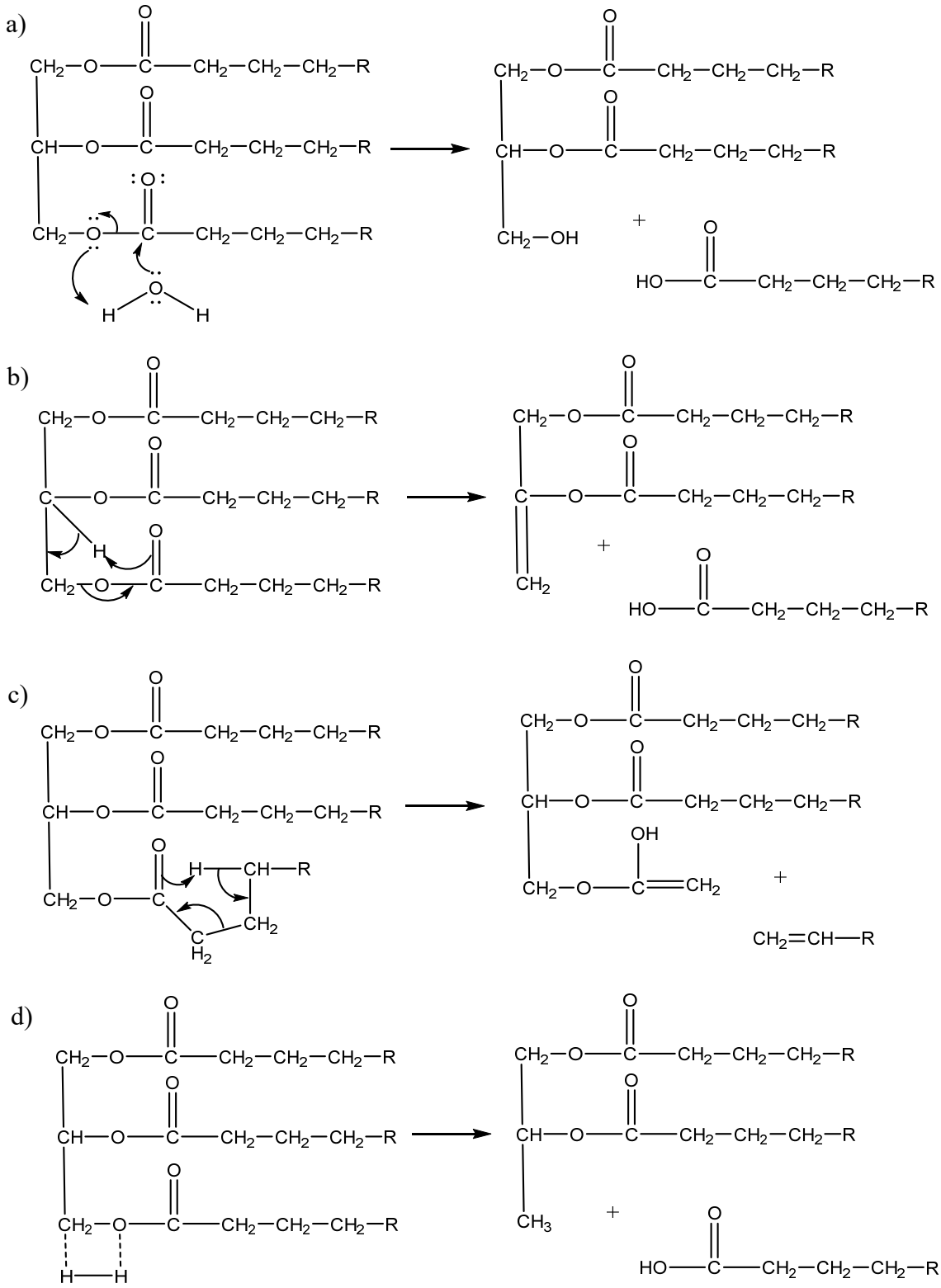

Scheme 1.3. Mechanism for a) hydrolysis b) B-elimination c) g-hydrognen transfer and d) hydrogenolysis of triglycerides.

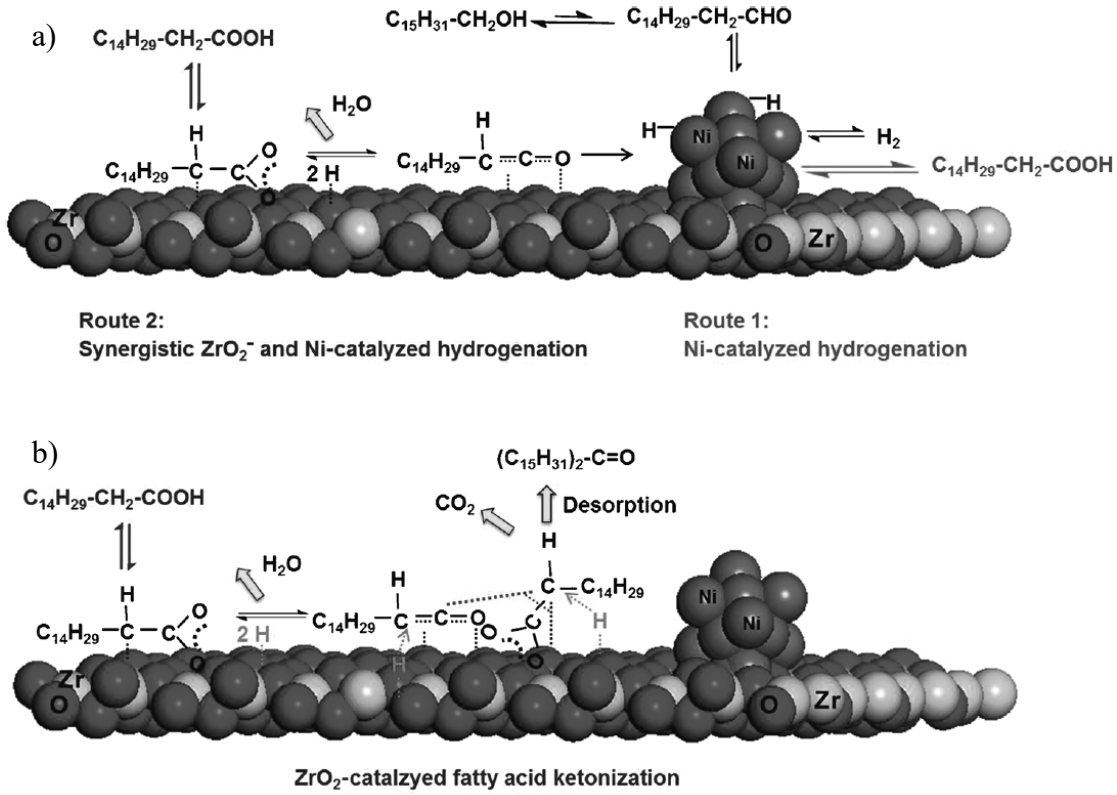

Scheme 1.4. The proposed reaction mechanism for a) the hydrogenation of palmitic acid to hexadecanal in the presence of H_2 and b) the ketonization of palmitic acid to palmitone in the absence of H_2.

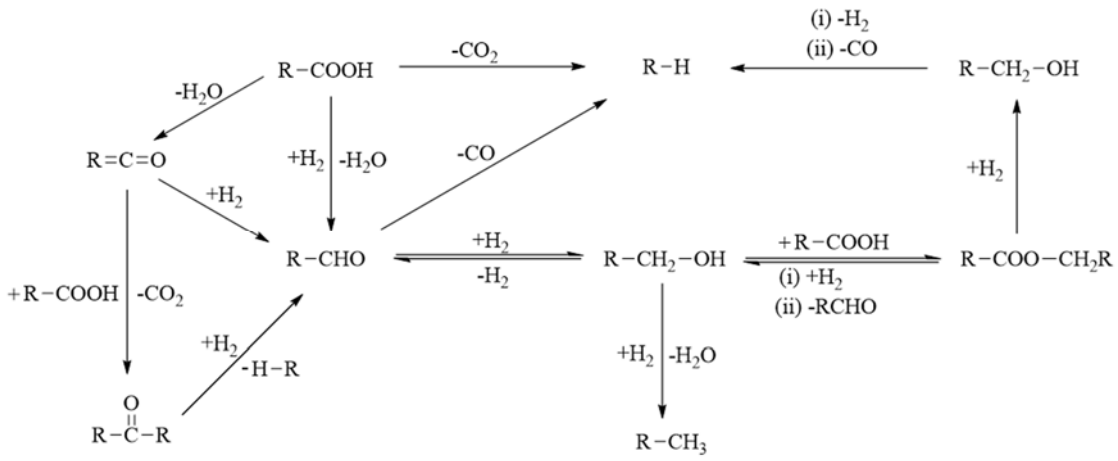

Scheme 1.5. Reaction scheme for stearic acid deoxygenation. Adapted from Appl. Catal. B 191 (2016) 147-156.

Chapter 2. Effect of Cu and Sn promotion on the catalytic deoxygenation of model and algal lipids to fuel-like hydrocarbons over supported Ni catalysts

Disclaimer: The work provided in this chapter is the result of a collaboration with researchers from several institutions. Eduardo Santillan-Jimenez, Samantha Jones, Tonya Morgan, Lilia Sewell, and Yaying Ji contributed from the Center for Applied Energy Research at the University of Kentucky. Mark Issacs and Adam Lee contributed from the European Bioengineering Research Institute at Aston University. Eduardo Santillan-Jimenez was responsible for reactor training, project advising, and assistance in writing and editing. Tonya Morgan performed simulated distillation-gas chromatography analysis of the liquid products obtained from the experiments. Lilia Sewell assisted in repeatability deoxygenation experiments involving tristearin and the catalysts employed in this study. Yaying Ji performed diffuse reflectance infrared Fourier transform spectroscopy on the catalysts employed in this study. Samantha Jones performed the transmission electron microscopy on the 20% Ni/Al_2O_3 and the 20% Ni-5% Cu/Al_2O_3 catalysts. Mark Issacs and Adam Lee performed X-ray photoelectron spectroscopy the 20% Ni/Al_2O_3 and the 20% Ni-5% Cu/Al_2O_3 catalysts.

Note – This chapter was published as an article in the following Journal:

Loe, R., Santillan-Jimenez, E., Morgan, T., Sewell, L., Ji, Y., Jones, S., Isaacs, M.A., Lee, A.F., Crocker, M., (2016). Effect of Cu and Sn promotion on the catalytic deoxygenation of model and algal lipids to fuel-like hydrocarbons over supported Ni catalysts, Appl. Catal. B, 191: 147-156.

2.1. Introduction

The non-renewable nature of fossil fuels and the environmental impacts of the CO_2 emissions resulting from their combustion demand the development of alternative fuels that are both sustainable and carbon neutral. Biofuels fulfill these two conditions, as they derive from a renewable resource – biomass – and they have the potential for closing the carbon cycle without disrupting the food supply when produced from waste and nonedible biomass feedstocks [70, 165, 166]. The production of biodiesel – a biofuel consisting of fatty acid methyl esters (FAMEs) – via the transesterification of vegetable oils or animal fats offers one pathway for the production of renewable liquid fuels. Biodiesel has certain advantages compared to traditional petroleum-derived fuels, such as high cetane number and increased lubricity [167]. However, the high oxygen content of FAMEs gives rise to several drawbacks including poor storage stability and cold flow properties. Therefore, interest has shifted to the development of catalytic methods for the deoxygenation of triglyceride and fatty acid feeds to fuel-like hydrocarbons [167, 168].

Hydrodeoxygenation (HDO) and decarboxylation/decarbonylation ($deCO_x$) represent two processes that have been developed to remove the oxygen from fats and oils in the form of H_2O and CO_2/CO, respectively [9, 169]. Although effective, HDO requires high H_2 pressures and the use of sulfided catalysts, both of which are problematic. Indeed, the H_2 pressures required for HDO limit the process to centralized facilities and the sulfided catalysts risk contaminating the products with sulfur and tend to deactivate in the presence of water, a co-product of the HDO reaction [95, 109]. In contrast, $deCO_x$ proceeds under lower H_2 pressures and does not require the use of sulfided catalysts.

Much of the previous work concerning $deCO_x$ has focused on supported Pd [9, 17, 78, 113, 116, 117, 123, 127, 150, 170] or Pt [126, 141, 171] catalysts, which exhibit high conversion and selectivity to diesel-like hydrocarbons. However, the high cost of these precious metals can forestall their use in large industrial applications. Significantly, inexpensive Ni-based catalysts have exhibited near comparable results to Pd- and Pt-based formulations in converting lipid-based feeds to fuel-like hydrocarbons [15, 119], the Ni-catalyzed transformation of triglycerides and related compounds to green diesel being the subject of a recent review by Kordulis et al. [8]. The fact that good conversions and selectivities have been achieved on Ni catalysts incorporating metal oxide supports – as opposed to high surface area carbon supports – is particularly noteworthy [112]. Indeed, carbon-supported catalysts typically lead to better yields in $deCO_x$ reactions due to the more favorable adsorption of fatty acids on the catalyst [82]; however, $deCO_x$ catalysts are susceptible to deactivation by the accumulation of carbonaceous deposits on their surface [71, 78, 114, 123, 131, 150, 172], which makes metal oxide supports advantageous since they allow for spent catalyst to be easily regenerated by simply combusting these deposits[118].

Although oxide supported Ni catalysts have shown promising activity in $deCO_x$ reactions, they require further improvement if they are to become viable candidates for the production of fuel-like hydrocarbons. Specifically, Ni catalysts have a tendency to produce light hydrocarbons and thus, improving the selectivity towards the longer chain products that constitute diesel fuel (~C10-C20 hydrocarbons [112]) is desirable. As mentioned

above, catalyst deactivation is also an issue for deCO_x catalysts, Ni-based formulations being particularly prone to coking [173]. It can be postulated that these issues are both related to the high activity of Ni for C-C cracking, given that cracking reactions result in the formation of light products and cause the accumulation of organic material on the catalyst, leading to its deactivation. This problem has been addressed in other Ni-catalyzed reactions by the addition of promoters such as Cu and Sn. Compared to monometallic Ni catalysts, supported catalysts containing a Ni-Cu alloy phase have shown superior performance in methane dissociation [174], ethanol reforming [175], acetylene hydrogenation reactions [176] and the hydrodeoxygenation of algae-derived pyrolysis oil [177]. One explanation for this improved performance is that nickel carbide phases can readily form on monometallic Ni catalysts, which leads to the formation of graphitic carbon deposits on the active sites of the catalyst. Since Cu does not form a carbide phase, Ni-Cu catalysts are less prone to coking than their monometallic analogs [175, 178]. Evidence suggests that the formation of carbon deposits on Ni particles occurs at step edges and that these are the sites preferentially occupied by Cu, which explains why Cu-doped Ni catalysts are less prone to deactivation [174]. Also of note in this context is a report by Yakovlev et al. concerning the HDO of anisole and FAMEs, in which Ni-Cu catalysts were found to outperform their monometallic Ni counterparts [98]. The authors of this study attributed the superior performance of the bimetallic catalysts to the ability of copper to simultaneously facilitate nickel oxide reduction and prevent the methanation of oxygen-containing molecules.

Bimetallic catalysts comprising Sn as a Ni promoter have also been shown to outperform Ni-only catalysts in steam reforming [179, 180]. As with Ni-Cu catalysts, the improvement in activity has been attributed to the decrease in coke formation resulting from Sn doping. Indeed, it has been reported that Sn can lower the binding energy of carbon on the Ni surface sites that serve as nucleation centers for the carbon deposits [179], which has the potential to decrease the catalyst deactivation caused by coking. Similar to the case of Ni-Cu catalysts, the promoting effect of Sn can likewise be explained on the basis of metal particle morphology, since Sn atoms can occupy step edge sites which are otherwise the Ni sites most responsible for coking [180].

Based on the foregoing, the effect of promoting Ni with Cu or Sn in the deCO_x of tristearin and stearic acid – used respectively as model triglyceride and fatty acid compounds –was studied in the present work. Initially, reaction temperature and the level of doping were systematically changed in semi-batch experiments to find the optimum set of conditions. The best Ni-promoter combination was then tested in a fixed bed reactor to evaluate the bimetallic catalyst in continuous mode and obtain results more relevant to industrial applications. In fixed bed reactions triolein – a triglyceride with a double bond between the 9^{th} and 10^{th} carbons in each acyl chain – was used as a model unsaturated triglyceride feed. Given that unsaturated feeds are more prone to cracking than saturated feeds [181], thereby exacerbating catalyst deactivation, the use of triolein represents a good test of the ability of promoters to improve both selectivity to long chain hydrocarbons and catalyst resistance to deactivation.

2.2. Experimental

2.2.1. Catalyst preparation and characterization

Catalysts were prepared by excess wetness impregnation using, as appropriate, $Ni(NO_3)_2 \cdot 6H_2O$ (Alfa Aesar), $Cu(NO_3)_2 \cdot 3H_2O$ (Sigma Aldrich), and $SnCl_2 \cdot 2H_2O$ (Gelest, Inc.) as the metal precursors and γ-Al_2O_3 (Sasol; surface area of 216 m^2/g) as the support. Ni loading was kept constant at 20 wt.%, while the Cu or Sn loading was varied. The impregnated materials were dried overnight at 60 °C under vacuum before calcination at 500 °C for 3 h in static air.

The surface area, pore volume and average pore radius of the catalysts were determined by N_2 physisorption using previously described instruments and methods [15]. The average NiO particle size was found by applying the Scherrer equation to the NiO peaks observed in powder X-ray diffractograms, which were acquired using equipment and procedures described previously [112]. Thermogravimetric analysis (TGA) of the spent catalysts was performed under flowing air (50 mL/min) on a TA instruments Discovery Series thermogravimetric analyzer. The temperature was ramped from room temperature to 800 °C at a rate of 10 °C/min. Temperature-programmed reduction (TPR) was used to study the reducibility of the catalysts employing instrumentation and methods described in a previous contribution [112]. For pulsed H_2 chemisorption measurements, the catalyst (250 mg) was first reduced under 10% H_2/Ar flow at 350 °C for 1 h. The U-tube reactor was then purged with Ar at 450 °C for 30 min, and then cooled under flowing Ar to 45 °C. 0.025 mL (STP) 10% H_2/Ar was then pulsed into the Ar carrier gas flowing to the reactor

(at 50 mL/min). Pulsing was continued at 3 min intervals until the area of the H_2 peaks remained constant.

X-ray photoelectron spectroscopy (XPS) was undertaken on a Kratos AXIS HSi spectrometer equipped with a charge neutralizer and monochromated Al K_α excitation source (1486.7 eV), with energies referenced to adventitious carbon at 284.6 eV. High resolution spectra were acquired with a pass energy of 40 eV. Spectral fitting was performed using CasaXPS version 2.3.14, utilizing a common Gaussian-Lorentzian lineshape and FWHM for each element, and the relevant instrumental response factors for quantitification. The minimum number of components required to minimize the residual difference between experiment data and fitting model was employed in all cases.

Diffuse reflectance infrared Fourier transform spectroscopy (DRIFTS) was performed on the 20% Ni/Al_2O_3 and the 20% Ni-5% Cu/Al_2O_3 catalysts during CO adsorption. The catalysts were reduced *in situ* in 10% H_2/N_2 flow (120 mL/min) at 350 °C for 1 h. The reactor was then purged with Ar while the temperature was raised to 450 °C (hold time 30 min) to remove adsorbed hydrogen prior to cooling the catalyst to 50 °C under flowing Ar. Each CO adsorption measurement was performed with 10% CO/He at 50 °C for 30 min, followed by Ar purging to remove gas phase CO and weakly adsorbed CO. Spectra were collected every 30 s during Ar purging until there was no change in IR band intensity.

Materials for electron microscopy were supported on Au grids purchased from Electron Microscopy Sciences. Transmission electron microscopy (TEM) and scanning

transmission electron microscopy (STEM) studies were conducted using a field emission JEOL 2010F with a URP pole piece, GATAN 200 GIF, GATAN DigiScann II, Fischione HAADF STEM detector, Oxford energy-dispersive X-ray detector and EmiSpec EsVision software. STEM measurements were acquired for both samples using a high-resolution probe at 2 Å.

2.2.2. Deoxygenation experiments in semi-batch mode

Tristearin (95%, obtained from City Chemical) and stearic acid (97%, obtained from Acros Organics) were respectively used as model saturated triglyceride and fatty acid compounds. Details on the acid number and the distribution of fatty acids in the tristearin employed are available elsewhere [182]. Experiments were performed in a 100 mL stainless steel, mechanically stirred autoclave. The catalyst (0.5 g) was added in powder form (<150 μm particle size) to the reactor, which was then purged with argon. The catalyst was subsequently reduced at 350 °C under a flow (~60 mL/min) of 10% H_2/N_2 for 3 h prior to cooling to room temperature, purging the reactor with Ar, and adding both solvent and feed (in experiments involving tristearin 22 g of dodecane and 1.8 g of feed was used while in experiments involving stearic acid 28.8 g of solvent and 1.72 g of feed was employed). After the addition of feed and solvent, the autoclave was purged three times with Ar prior to being pressurized with H_2 (to 580 psi and 300 psi for experiments involving tristearin and stearic acid, respectively) and heated to the reaction temperature, which was measured by a K-type thermocouple placed inside a thermowell. A constant flow of 60 mL/min of

H_2 and mechanical stirring of 1,000 rpm was maintained during each experiment. Volatile products were collected from the gas stream exiting the reactor by a condenser kept at room temperature. At the end of these reactions, which lasted 6 and 1.5 h when tristearin and stearic acid were employed, respectively, forced air and an ice bath were used to cool the reactor to room temperature while the system was slowly depressurized. The liquid product mixture and the spent catalyst were removed from the reactor and separated by gravity filtration, the catalyst being washed twice with chloroform to yield additional material. All experiments for which results are shown were performed a minimum of two times.

2.2.3. Deoxygenation experiments in continuous mode

Triolein (glyceryl trioleate, ≥99%) was purchased from Sigma-Aldrich, details on the acid number and the distribution of fatty acids in the triolein being reported elsewhere [183]. Algal lipids were extracted via the Bligh-Dyer method [184] from a sample of dry *Scenedesmus* sp. grown in a photobioreactor fed with the flue gas of a coal-fired power plant [185]. Extracted lipids were then purified using a column containing both activated carbon (DARCO® KB-G purchased from Sigma-Aldrich) and silica gel. Experimental details on algae culturing as well as algal lipids extraction and purification can be found in a recent contribution [185]. Deoxygenation experiments in continuous mode were performed in a fixed bed stainless steel tubular reactor (1/2 in o.d.) equipped with an HPLC pump. The catalyst (0.5 g, particle size 150-300 μm, held in place using a stainless steel frit) was reduced under flowing H_2 at 400 °C for 3 h. Next, the system was taken to the

reaction temperature (260 °C) and pressurized with H_2 to 580 psi. A liquid solution of the feed in dodecane (1.33 wt% triolein) was introduced to the system at a rate of 0.2 mL/min along with a flow of H_2 (50 mL/min). A liquid gas separator (kept at 0 °C) placed downstream from the catalyst bed was used to collect liquid samples.

2.2.4. Product analysis

All feeds and reaction products were analyzed using a GC method specifically devised to identify and quantify the constituents of the feeds used and the products obtained in the upgrading of fats and oils to hydrocarbons, detailed information about the development and application of this method being available elsewhere [186]. Briefly, analyses were performed using an Agilent 7890A GC equipped with an Agilent Multimode inlet, a deactivated open ended helix liner and a flame ionization detector (FID). Helium was used as the carrier gas and a 1 μL injection was employed. The FID was set to 350 °C with the following gas flow rates: H_2=30 mL/min; air=400 mL/min; makeup= 5mL/min. The inlet was ran in split mode (split ratio 25:1; split flow 50 mL/min) using an initial temperature of 100 °C. Inlet temperature was increased immediately upon injection (at a rate of 8 °C/min) to a final temperature of 320 °C, which was maintained for the duration of the analysis. The initial oven temperature of 45 °C was immediately increased upon injection first to 325 °C (at a rate of 4 °C/min) and then to 400 °C (at a rate of 10 °C/min). This temperature was then maintained for 12.5 minutes, making the total run time 90 minutes. An Agilent J&W DB-5HT column (30 m × 250 μm × 0.1 μm) rated to 400 °C

was employed along with a constant He flow of 2 mL/min. Quantification was performed using cyclohexanone as internal standard. Agilent Chemstation and Separation Systems Inc. SimDis Expert 9 software were respectively used to perform chromatographic programming and to process the chromatographic data acquired. Solvents (i.e., chloroform and dodecane) and internal standard (cyclohexanone) were quenched and/or subtracted prior to processing the data, which precluded the acquisition of quantitative data for linear C5-C9 hydrocarbons.

2.3. Results and Discussion

2.3.1. Catalyst Characterization

The X-ray diffractograms in Figure 2.1 show that all catalysts present diffraction peaks – at 37.2°, 43.3°, 62.9°, 75.4° and 79.4° – indicative of NiO [187]. Notably, peaks at 35.5° and 38.7° corresponding to a distinct CuO phase [188] are not observed, which may be the result of the low amount of Cu; indeed, several authors have reported that these peaks are not discernable at low Cu loadings [187, 189]. However, all of the NiO peaks increase in intensity as the Cu metal loading increases. This is consistent with a report by Lee et al., who observed that an increase in the amount of Cu in Ni-Cu/Al_2O_3 catalysts results in an increase in XRD peak intensity and in the formation of Ni-Cu mixed oxides [189].

The textural properties and the average NiO particle size of the catalysts used in this study are collected in Table 2.1. The effect of promoter addition on the average particle size of NiO was studied by applying the Scherrer equation to the X-ray diffractograms of the promoted catalysts. Evidently, at low loadings, the addition of the promoter does not have a direct impact on the NiO particle size, as illustrated by the fact that 20% Ni-2% Cu/Al_2O_3 had the smallest NiO particle size (6.4 nm) of all the catalysts. However, the NiO particle size in the 20% Ni-5% Cu/Al_2O_3 sample (10.7 nm) was the largest among the samples, which points to an increase of particle size at high Cu loadings. TEM and STEM imaging of the 20% Ni/Al_2O_3 and 20% Ni-5% Cu/Al_2O_3 samples was found to be consistent with the average particle sizes reported in Table 2.1, STEM-EDX revealing the presence of Ni-Cu, Ni-only and Cu-only particles in 20% Ni-5% Cu/Al_2O_3 (see Figures 2.2 and 2.3). This agrees with TPR data (vide infra), in which the bimetallic catalysts show separate reduction maxima corresponding to particles of these compositions.

The TPR profiles of the catalysts, which are shown in Figure 2.4, indicate that an increase in Cu loading results in a decrease in the reduction temperature of the catalyst. The 20% Ni/Al_2O_3 catalyst shows a broad reduction peak, which can be attributed to the reduction of NiO to metallic Ni, with a maximum at 507 °C [190]; however, a small shoulder showing a local maximum at 300 °C (assigned to the reduction of large Ni ensembles [190]) can also be seen. The main reduction event also shows an indistinct shoulder above 700 °C that can be assigned to the reduction of a $NiAl_2O_4$ phase, a feature more clearly displayed by the other catalysts examined (vide infra). The TPR profile of

20% Ni-1% Cu/Al_2O_3 shows two similar reduction events, a broad peak with a maximum at 497 °C and a small shoulder with a maximum at 275 °C, these peaks sharing the aforementioned assignments and the shift of their maxima to lower temperature being attributable to the presence of Cu [191]. In addition, the main peak is accompanied by two shoulders, one centered around 385 °C, which can be attributed to the reduction of a NiO-CuO phase [192] and one centered around 710 °C which can be assigned to nickel aluminate ($NiAl_2O_4$) formed from the reaction of NiO with the Al_2O_3 support [193]. Notably, the TPR profile for 20% Ni-2% Cu/Al_2O_3 displays five distinct reduction events: 1) a peak with a maximum at 480 °C attributable to the reduction of NiO to Ni metal; 2) a shoulder of the latter peak, centered around 700 °C, which is assigned to the reduction of $NiAl_2O_4$; 3) a main peak with a maximum at 355 °C attributed to the reduction of a NiO-CuO phase ; 4) a shoulder of this peak centered around 255 °C signaling the reduction of large NiO and/or NiO-CuO ensembles; and 5) a small but well-defined peak with a maximum at 200 °C due to the reduction of copper oxides to Cu metal [187, 191]. This last assignment was confirmed by TPR measurement of a 5% Cu/Al_2O_3 sample (not shown). In line with the aforementioned trends, the TPR profile for 20% Ni-5% Cu/Al_2O_3 also shows several reduction events, including broad peaks centered around 688 °C and 453 °C (due to the reduction of $NiAl_2O_4$ and NiO, respectively), and well-defined peaks with maxima at 355 °C and 180 °C, attributed to the reduction of a NiO-CuO phase and to that of copper oxides, respectively. In short, Cu addition reduces the reduction temperature of NiO in agreement with observations recently reported by Guo et al. [177]. Moreover, the

reduction temperature of both nickel and copper oxides decreases as the Cu loading increases, a phenomenon that has also been observed by other authors [191]. In turn, the decrease in the reduction temperature of Ni resulting from Cu addition leads to the creation of additional Ni^0; XPS of reduced 20%Ni/Al_2O_3 and 20%Ni-5%Cu/Al_2O_3 confirming that the bimetallic catalyst has more than double the concentration of Ni^0 at the catalyst surface (see Figure 2.5). This explains in part the improved performance that certain Ni-Cu catalysts display relative to the Ni-only sample (see sections 3.3-3.6), since Ni^0 is believed to be the catalytically active phase for lipid deoxygenation.

Figure 2.4 also shows the TPR profile for 20% Ni-1% Sn/Al_2O_3, which shows a main peak with a maximum at 500 °C and a shoulder centered around 700 °C, along with a small but well-defined peak with a maximum at 307 °C. The effect of Sn on the TPR profiles seems to be limited to a narrowing of the peaks displayed by the Ni-only catalyst, which is in line with a previous report by Castaño et al., who concluded that metals with a lower surface tension and larger atomic radius than Ni do not form alloys with the latter since they are expelled from the matrix and segregate strongly [194].

H_2 chemisorption was performed on the 20% Ni/Al_2O_3 and the 20% Ni-5% Cu/Al_2O_3 catalysts in order to evaluate the amount of metal active sites present on the catalyst surface after reduction at 350 °C (corresponding to the catalyst reduction temperature applied in the semi-batch experiments). The monometallic and bimetallic catalysts exhibited a H_2 uptake of 0.1569 and 0.4943 mL/g, respectively, corresponding to roughly 8.433×10^{18} and 2.658×10^{19} reduced surface metal sites per gram of catalyst. The larger

volume of H_2 adsorbed at this temperature is consistent with the lower reduction temperature of the metals in the bimetallic catalysts as observed in the TPR measurements and is in good quantitative agreement with the surface Ni^0 content determined directly by XPS.

DRIFTS measurements made on the 20% Ni-5% Cu/Al_2O_3 sample after CO adsorption further confirmed the presence of an electronic interaction between Ni and Cu. As shown in Figure 2.6, when the monometallic Ni catalyst was reduced at 350 °C and CO was subsequently adsorbed at room temperature, band intensity in the CO stretching region was extremely weak. However, when the reduction temperature was increased to 500 °C, two CO adsorption bands were observed. A band at 2036 cm^{-1} can be assigned to CO linearly adsorbed on Ni^0, while a low frequency band at 1960 cm^{-1} can be assigned to CO bridge-bonded to Ni^0 [191]. For the bimetallic Ni-Cu catalyst, significant Ni reduction took place at 350 °C, as evidenced by the presence of strong CO bands. Notably, the CO bands observed at 2036 and 1960 cm^{-1} by 20% Ni/Al_2O_3 after reduction at 500 °C showed a red shift – indicative of an electronic interaction between Ni and Cu – to 2010 and 1890 cm^{-1} in 20% Ni-5% Cu/Al_2O_3 reduced at 350 °C, the first CO band showing a concomitant increase in intensity, implying that the formation of additional Ni^0 sites was facilitated by the presence of Cu [191, 195, 196]. An additional band at 2121 cm^{-1} can be attributed to CO adsorbed on Cu sites [191, 197], which is in agreement with the fact that an intense band was observed in the same position for a 5% Cu/Al_2O_3 reference sample. Other bands (1660, 1435 and 1228 cm^{-1}) can be assigned to bicarbonate formed on the Al_2O_3 support

[198]. XPS further evidences electron transfer between Ni and Cu, with the introduction of copper shifting the Ni $2p_{3/2}$ XP peak to lower binding energy (Figure 2.7), from 854.5 eV in 20% Ni/Al_2O_3 to 853.4 eV in 20% Ni-5% Cu/Al_2O_3, consistent with enhanced nickel reduction.

2.3.2. Blank runs

The results obtained when tristearin and stearic acid are submitted to the reaction conditions described in section 2.2 in the absence of a catalyst have been previously reported and discussed [119]. In short, stearic acid conversion at 300 °C was only 5% and selectivity to C10-C17 and C17 were approximately 85% and 15%, respectively. For blank experiments using tristearin at 360 °C, conversion was around 85% and selectivity to C10-C17 and C17 were ca. 47% and 14%, respectively. These observations are in agreement with thermal (non-catalytic) experiments by other workers [129, 199], the differing reactivity of stearic acid and tristearin being attributed to the more forcing conditions employed with the latter. Notably, an additional blank experiment was performed by subjecting dodecane to tristearin deoxygenation conditions in the presence of a supported Ni catalyst; dodecane proved entirely unreactive and hence, none of the reaction products detected in the experiments described below arose from the reaction solvent.

2.3.3. Tristearin deoxygenation in semi-batch mode

The results of tristearin deoxygenation performed at three different temperatures are summarized in Table 2.2. Conversion increased with increasing temperature, which is unsurprising since triglycerides are reported to thermally decompose to diglycerides, free fatty acids and hydrocarbons at temperatures approaching 360 °C [129]. Moreover, selectivity to both C10-C17 and C17 invariably decreased as the reaction temperature increased for all catalysts showing >99% tristearin conversion, as expected since higher temperatures favor cracking reactions and consequently, lighter hydrocarbons.

Remarkably, whereas the monometallic catalyst afforded only 27% conversion at 260 °C, 20% Ni-5% Cu/Al_2O_3 exhibited 97% conversion. 5% Cu/Al_2O_3 was also tested since Berenblyum et al. found this catalyst to be active in lipid deoxygenation [86, 200]; however, 5% Cu/Al_2O_3 afforded only 11% conversion at 260 °C, which indicates that the superior performance of 20% Ni-5% Cu/Al_2O_3 stems from a synergistic effect between Ni and Cu and not merely from the additive but independent contributions of these two metals. 20% Ni-1% Sn/Al_2O_3 was the worst performing of all formulations included in Table 2.2 at 260 °C, with only 11% conversion. Parenthetically, residual Cl (~2,400 ppm) was detected in this catalyst, which was synthesized using $SnCl_2 \bullet 2H_2O$ as the Sn precursor (see section 2.1). Albeit it is widely known that electronegative elements such as Cl can act as catalyst poisons by reducing electron density at the metal surface, the latter could also result in promotion effects. Indeed, it has been reported that Cl hinders coke deposition on metal nanoparticles, since a decrease in electron density at the metal surface reduces

electron transfer from the metal to the π* orbital of chemisorbed reactant molecules, thereby disfavoring their dissociative adsorption and the concurrent catalyst deactivation [201]. In addition, Cl has also been reported to increase the spillover of hydrogen from the metal to the support, which can eliminate coke precursors via hydrogenation and further reduce coke-induced deactivation [202]. Therefore, Cl may have both poisoning and promotion effects, the investigation of which is outside the scope of the present contribution.

Copper promotion was less apparent at 300 °C, a consequence of the high (98%) conversion exhibited by the monometallic Ni catalyst being similar to that of the Ni-Cu bimetallic catalysts. The Ni-Sn catalyst again exhibited the poorest activity (38% conversion) and selectivity (45% to C10-C17 hydrocarbons), although these values were considerably improved relative to those at 260 °C. Notably, the Cu loading had little impact on the selectivity to C17 or C10-C17 hydrocarbons at 300 °C; however, at 350 °C – a temperature at which conversions invariably exceeded 99% (as expected from the results obtained at 300 °C) – it noticeably influenced selectivity. Indeed, 20% Ni-5% Cu/Al_2O_3 exhibited the highest selectivity to both C10-C17 and C17 hydrocarbons (98% and 49%, respectively), which contrasts with the 88% and 21% selectivity values obtained over the monometallic 20% Ni/Al_2O_3 catalyst. This demonstrates that doping with 5% Cu effectively curbs cracking reactions at 350 °C. Surprisingly, at 350 °C the best catalyst was 20% Ni-1% Sn/Al_2O_3, yielding 99% conversion and C10-C17 and C17 hydrocarbon selectivities of 97% and 56%, respectively. Tin promotion is thus extremely temperature

dependent. It should be noted that further increasing the copper loading to 7.5% did not improve performance relative to the 20% Ni-5% Cu/Al_2O_3 catalyst.

Notably, small amounts of reaction products with a b.p. higher than C17 were also observed. Tellingly, all experiments in Table 2.2 were found to afford product mixtures containing <1% of C18 (C18 results not shown). This suggests that deoxygenation proceeds mainly through $deCO_x$, as also observed in experiments involving stearic acid as the feed (see section 3.4). Interestingly, small amounts of fatty esters such as cetyl stearate and stearyl stearate were also observed in some products mixtures, although this was dependent on both the temperature and the catalysts employed. Indeed, at 260 ° both the Ni-only catalyst and catalysts promoted with 1% of Cu or Sn afforded moderate amounts (~5%) of these esters, which were obtained in lower amounts (~2%) over 20% Ni-2% Cu/Al_2O_3 and not observed over were observed over 20% Ni-5% Cu/Al_2O_3. At 300 °C, only the Sn-promoted catalyst yielded a small amount (~5%) of these esters, whereas at 350 °C the latter were not detected. Thus, it appears that the condensation reactions leading to the formation of cetyl stearate and stearyl stearate are curbed by increasing the reaction temperature and/or the amount of promoters, which is consistent with the fact that these conditions lead to lower concentrations of the intermediates that give rise to ester formation (see section 3.4).

In order to be able to unequivocally attribute improvements in catalytic performance to the presence of promoters, the effect of metal dispersion on catalyst performance must be considered to discount the possibility that the differences in Table

2.2 simply reflect metal particle size effects. To this end, a 20% Ni/Al_2O_3 catalyst with a markedly different average NiO particle size of 16.1 nm was prepared (using butanol in lieu of water in the synthesis described in section 2.1) and its deoxygenation activity at 260 °C was compared to that of the 20% Ni/Al_2O_3 catalyst with an average NiO particle size of 7.4 nm, the results of these experiments being summarized in Table 2.3. While the catalytic properties of these two formulations differed somewhat, it is clear that the effect of copper addition cannot be explained solely in terms of its impact on NiO particle size. Indeed, increasing the particle size of the monometallic catalyst from 7.4 nm to 16.1 nm increased tristearin conversion by 11 % at the expense of a 10% decrease in selectivity to C10-C17 and a 19% decrease in selectivity to C17 (see Table 2.3). This contrasts with the greatly increased conversion and selectivity observed for the 20% Ni-5% Cu/Al_2O_3 at 260 °C (Table 2.2) relative to both 20% Ni/Al_2O_3 catalysts.

2.3.4. Stearic acid deoxygenation in semi-batch mode

Since triglyceride conversion to hydrocarbons via $deCO_x$ has been reported to be intermediated by free fatty acids [15, 112, 119, 203], representative experiments were also performed using stearic acid as the feed in an effort to gain additional insights into the promoting effect of Cu and Sn. The results of these deoxygenation experiments, which were performed at two different temperatures, are shown in Table 2.4. Irrespective of the catalyst or temperature employed, C18 represented at most 1% of the total product yield, indicating that deoxygenation occurred principally via $deCO_x$ (yielding C17) rather than

through HDO (which would afford C18). This is consistent with previous reports indicating that $deCO_x$ is the dominant reaction pathway over Ni-based catalysts [95, 112, 173, 204]. In line with the results obtained using tristearin, 20% Ni-5%Cu/Al_2O_3 and 20% Ni-1% Sn/Al_2O_3 respectively exhibited the highest and lowest stearic acid conversion at both temperatures. Selectivity values were more informative, since selectivities to C10-C17 hydrocarbons at 260 °C were much lower for both the Ni-only and the Ni-Cu catalysts than when tristearin was used as the feed. This is attributed to the intermediates formed during stearic acid deoxygenation. Indeed, the reaction may proceed by routes other than direct decarboxylation – as illustrated in Scheme 2.1 – and consequently, a range of intermediates can form in accordance with previous work by the research groups of Murzin and Lercher [120, 205]. For instance, an ester (in this case stearyl stearate) can form when an alcohol intermediate (stearyl alcohol) undergoes esterification with the stearic acid feed. In turn, the stearyl stearate thus formed requires further hydrogenation of the ester bond to form stearyl alcohol once again before the latter can form the alkane via decarbonylation. Stearyl stearate formation was indeed significant at 260 °C, yields of 13, 16, and 9% being obtained after 1.5 h over 20% Ni/Al_2O_3, 20% Ni-5% Cu/Al_2O_3, and 20% Ni-1% Sn/Al_2O_3, respectively. When the reaction temperature was increased to 300 °C, the yield of C10-C17 hydrocarbons surged while that of stearyl stearate decreased to 0, 4, and 7% over the Ni-only, Ni-Cu and Ni-Sn catalysts, respectively. The significant amounts of stearyl stearate intermediate detected offer a compelling explanation vis-à-vis the lower selectivity to C10-C17 hydrocarbons obtained at lower reaction temperatures. This intermediate is not

observed in experiments involving tristearin as the feed, which can be attributed to the longer reaction times employed for those runs.

2.3.5. Triolein deoxygenation in continuous mode

Continuous processes are favored for industrial applications and hence, the effect of Cu promotion was also assessed by comparing the performance of 20% Ni/Al_2O_3 and 20% Ni-5% Cu/Al_2O_3 in a fixed bed reactor. These experiments were performed using 1.33 wt.% triolein in dodecane as the feed, triolein being chosen not only due to the fact that unsaturated lipids are commonly found in biomass-derived feeds [181], but also because in the $deCO_x$ of lipids to hydrocarbons it has been observed that catalyst deactivation from coking occurs to a greater extent when unsaturated feeds are employed [71]; thus, triolein offers a means to gauge the ability of Cu to improve catalyst resistance to deactivation. Indeed, it has been suggested that unsaturated feeds cause catalyst deactivation due to their stronger adsorption and propensity for cracking, thus leading to coke deposition [181].

Figure 2.8 shows the boiling point distribution plots (BPDP) of both reactants and products from fixed bed experiments sampled at intervals of 1, 2, 3, and 4 h. These BPDPs, which were obtained through a recently published simulated distillation GC protocol [186], show that practically all products formed were hydrocarbons within the boiling range of diesel fuel (~180-350 °C) at all reaction times. Notably, heptadecane (b.p. = 302 °C) represented the major product in all samples, further indicating that $deCO_x$ – as opposed to

HDO – constitutes the main reaction pathway. The superior performance of the Ni-Cu catalyst relative to the Ni-only catalyst is most prominent in the first hour of the reaction, in which long chain (C15-17) hydrocarbons comprised approximately half of the products formed over the monometallic catalyst, whereas C15-C17 constituted about three-quarters of the products afforded by the bimetallic catalyst. It is also noteworthy that while 20% Ni/Al_2O_3 showed evidence of slight deactivation after 4 h, at which time a small amount of the material appeared in the product mixture exhibiting a boiling point characteristic of the feed (600 °C) – this was not the case for 20% Ni-5% Cu/Al_2O_3. Overall, both catalysts achieved close to quantitative conversion in continuous mode at all reaction times sampled, although the bimetallic catalyst displayed higher selectivity to C15-C17 hydrocarbons (which are more desirable than light hydrocarbons since they possess higher cetane numbers) than the monometallic catalyst irrespective of time on stream.

2.3.6. Algal lipids deoxygenation in continuous mode

In view of the promising results obtained in the continuous deoxygenation of triolein, the upgrading of a realistic and topical feed – namely algal lipids [185] – was attempted using identical reaction conditions as those employed with triolein. The BPDP of the algae extract and the reaction products obtained over both 20% Ni/Al_2O_3 and 20% Ni-5% Cu/Al_2O_3 are included in Figure 2.9. As illustrated by the BPDP of the feed, compounds boiling below 320 °C (mostly hydrocarbons) represented ~7% of the algae extract, compounds boiling between 320-500 °C (mostly free fatty acids) comprised ca.

66% of the feed, and compounds boiling >500 °C (mostly triglycerides) constituted ~27% of the extract. In addition to these compounds, GC-MS of the algae extract (shown in Figure 2.10 also revealed the presence of non-negligible amounts of other compounds such as fatty alcohols, phytols and other phytol-like compounds in agreement with a previous report [183]. Catalytic upgrading effectively increased the diesel range hydrocarbon content from ~7% in the feed to 78% and 83% at t = 1 h over 20% Ni/Al_2O_3 and 20% Ni-5% Cu/Al_2O_3, respectively, the corresponding values being 42% and 45% at t = 4 h. In line with a recent report [183], the lower yields of diesel-like hydrocarbons, as well as the higher rate of deactivation observed in these runs relative to experiments involving triolein as the feed, can be attributed to the fact that the algae extract contains highly unsaturated fatty acid chains, as well as compounds such as phytols, which are potentially capable of poisoning catalytically active sites via strong adsorption. Nevertheless, the results presented herein indicate that good diesel yields can be obtained. Notably, just as for the triolein upgrading experiments, the superior performance of the Ni-Cu bimetallic catalyst relative to the Ni-only catalyst is most prominent in the first hour of the reaction, C10-C14 hydrocarbons representing ~23 and 10% of the products obtained over 20% Ni/Al_2O_3 and 20% Ni-5% Cu/Al_2O_3, respectively, once again showing that the Ni-Cu catalyst favors the formation of long chain hydrocarbons.

2.3.7. Spent catalyst characterization

The ability of Ni-Cu catalysts to outperform their Ni-only counterparts has been postulated to arise from decreased coking, which results in reduced catalyst deactivation and enhanced conversion [175, 178]. Representative spent catalysts were therefore subjected to thermogravimetric analysis in air to quantify surface coking, the resulting profiles being collected in Figure 2.11. TGA profiles show a major weight loss event below 400 °C, which could reflect either the desorption and/or combustion of residual reactants, intermediates and/or products or the combustion of poorly structured carbon deposits [182]. Notably, the weight gain centered around 350-400 °C shown by some spent catalysts in Figure 2.11 is due to the oxidation of Ni to NiO [206].

For some catalysts, TGA profiles showed a good correlation between the degree of coking and their conversion. For instance, in experiments performed with tristearin as the feed at 260 °C (Figure 2.11 top left), the spent 20% Ni-5% Cu/Al_2O_3 and 20% Ni-1% Sn/Al_2O_3 exhibited the lowest and highest weight loss, indicating the least and the greatest amount of coke formation, respectively. This is in agreement with the fact that 20% Ni-5% Cu/Al_2O_3 and 20% Ni-1% Sn/Al_2O_3 respectively showed the highest and lowest conversion. Nevertheless, all other catalysts showed almost identical weight losses, which contrasts with the fact that 20% Ni-2% Cu/Al_2O_3 displayed a considerably higher conversion than 20% Ni/Al_2O_3 and 20% Ni-1% Cu/Al_2O_3. For spent catalysts arising from experiments with tristearin as the feed at 350 °C (Figure 2.11 top right), all catalysts

displayed a relatively small – and very similar – weight loss (7.5±1%), which is consistent with the fact that all catalysts afforded quantitative conversions.

The TGA plots of catalysts spent using stearic acid as the feed at a reaction temperature of 300 °C (Figure 2.11 bottom left) also illustrate that albeit in some instances there is a clear correlation between the amount of coke deposited on catalysts and their performance (e.g., 20% Ni-5% Cu/Al_2O_3 showed the least coking and best conversion), in other cases no such correlation exists (albeit 20% Ni-1% Sn/Al_2O showed lower amounts of coke deposits than 20% Ni/Al_2O_3 the monometallic formulation afforded a substantially higher conversion). However, the weight loss difference between the Ni-only and the Ni-Sn catalysts is fairly small (~4%), which suggest that catalyst performance – and specifically the effect of promoters on catalyst performance – can only be explained invoking the amount of carbonaceous deposits on the catalysts surface when the difference in the magnitude of coking is sizable. With this in mind, caution should be taken when interpreting thermogravimetric data such as that in Figure 2.11 bottom right, which shows the TGA plots of catalysts spent in the continuous deoxygenation of triolein. Indeed, while 20% Ni-5% Cu/Al_2O_3 exhibited less coking and better activity than 20% Ni/Al_2O_3, the difference in their associated carbonaceous deposits is too small (<1%) to be significant. The fact that the weight losses of spent catalysts from fixed bed experiments were almost negligible is in itself noteworthy, particularly since an unsaturated feed was employed in an effort to exacerbate catalyst coking and deactivation.

In short, although longer and/or more stringent experiments may be necessary to accentuate coking and thereby uncover the role of promoters in retarding catalyst deactivation arising from accumulated carbonaceous deposits, the present work shows that Ni-Cu deCO_x catalysts have the potential to outperform Ni-only formulations and that in some instances this enhancement can be attributed to the ability of Cu to suppress cracking and coke-induced deactivation, the capacity of Cu addition to curb coking in Ni-based deoxygenation catalysts being consistent with a recent report by Guo et al. [177]. It should be appreciated that these results were acquired using lipid feeds for which the dilution level is far from representative of industrial conditions. Therefore, a future contribution will focus on the use of concentrated waste lipid feeds.

2.4. Conclusions

Semi-batch studies indicate that Cu is a very effective promoter of Ni for the deCO_x of tristearin at 260 °C, tristearin conversion increasing from 27% over 20% Ni/Al_2O_3 to 97% over 20% Ni-5% Cu/Al_2O_3. At 350 °C, Sn is also a promising promoter, increasing selectivity to C17 from 21% over 20% Ni/Al_2O_3 to 56% over 20% Ni-1% Sn/Al_2O_3. Cu also promoted the deoxygenation of stearic acid in semi-batch mode, 20% Ni-5% Cu/Al_2O_3 exhibiting higher stearic acid conversion than 20% Ni/Al_2O_3 at both 260 and 300 °C, as well as considerably higher selectivity to diesel-like hydrocarbons at the higher reaction temperature. The benefit of promoting 20% Ni/Al_2O_3 with 5% Cu was confirmed in fixed bed experiments with a triolein feed, for which the Ni-Cu bimetallic catalyst exhibited

higher selectivity to long chain hydrocarbons than the Ni-only catalyst, particularly at the beginning of the reaction.

Improvements in deCO_x performance arising from Cu or Sn addition to Ni catalysts does not appear related to particle size effects. Copper promotion arises from a combination of factors including the destabilization of NiO and the consequent increase in the proportion of surface Ni^0, which is believed the catalytically active phase for lipid deoxygenation. Thermogravimetric analysis of spent catalysts suggests that Cu promotion may also be ascribed to the suppression of surface coking and hence catalyst deactivation, albeit only when there are significant differences in the amount of carbonaceous deposits between distinct catalysts. This enhanced resistance to coke-induced deactivation may reflect the ability of Cu to curb the cracking activity of Ni-only catalysts and impart superior selectivity to long chain hydrocarbons via both geometric and electronic effects.

Table 2.1. Textural properties and metal dispersion of the catalysts studied.

Catalyst	BET surface area (m^2/g)	Pore volume (cm^3/g)	Avg. pore diameter (nm)	Avg. NiO particle size (nm)*
20% Ni/Al_2O_3	134	0.30	9.0	7.4
20% Ni-1% Cu/Al_2O_3	148	0.32	8.7	7.7
20% Ni-2% Cu/Al_2O_3	137	0.30	8.8	6.4
20% Ni-5% Cu/Al_2O_3	129	0.28	8.8	10.7
20% Ni-1% Sn/Al_2O_3	141	0.46	8.9	6.5

*As measured from the powder X-ray diffractograms of the catalysts calcined under static air for 3 h at 500 °C.

Table 2.2. Semi-batch mode deoxygenation of tristearin over alumina-supported Ni-based catalysts (580 psi of H_2, 6 h reaction time).*

Catalyst	Reaction Temp. (°C)	Conversion (%)[a]	Selectivity to [Yield of] C10-C17 (%)[b, d]	Selectivity to [Yield of] C17 (%)[c, d]
20% Ni/Al_2O_3	260	27	87 [23]	63 [17]
20% Ni-1% Cu/Al_2O_3	260	27	89 [24]	56 [15]
20% Ni-2% Cu/Al_2O_3	260	85	95 [81]	65 [55]
20% Ni-5% Cu/Al_2O_3	260	97	99 [96]	71 [69]
20% Ni-1% Sn/Al_2O_3	260	11	8 [1]	3 [1]
20% Ni/Al_2O_3	300	98	97 [95]	53 [52]
20% Ni-1% Cu/Al_2O_3	300	>99	>99 [98]	54 [53]
20% Ni-2% Cu/Al_2O_3	300	98	98 [96]	55 [54]
20% Ni-5% Cu/Al_2O_3	300	>99	>99 [98]	62 [61]
20% Ni-1% Sn/Al_2O_3	300	38	45 [17]	27 [10]
20% Ni/Al_2O_3	350	>99	88 [87]	21 [21]
20% Ni-1% Cu/Al_2O_3	350	>99	86 [85]	15 [15]
20% Ni-2% Cu/Al_2O_3	350	>99	81 [80]	3 [3]
20% Ni-5% Cu/Al_2O_3	350	>99	98 [97]	49 [49]
20% Ni-1% Sn/Al_2O_3	350	>99	97 [96]	56 [55]

*All experiments for which results are shown were performed a minimum of two times, average standard deviations being 3.1, 3.6, and 9.1% for conversion, selectivity to C10-C17, and selectivity to C17, respectively.

[a] Conversion = wt% of product with b.p. < 375°C.

[b] Selectivity to C10-C17 = 100 × [(wt% of product with b.p. < 314°C – wt% of product with b.p. < 177°C)/(wt% of product with b.p. < 375°C)].

[c] Selectivity to C17 = 100 × [(wt% of product with b.p. < 314°C – wt% of product with b.p. < 295°C)/(wt% of product with b.p. < 375°C)].

[d] The corresponding yield (conversion × selectivity) values are shown between brackets.

Table 2.3. Semi-batch mode deoxygenation of tristearin over 20% Ni/Al_2O_3 catalysts with different metal particle size (260 °C, 580 psi of H_2, 6 h reaction time).

Solvent used in Excess Wetness Impregnation	NiO particle size (nm)*	Conversion (%)[a]	Selectivity to [Yield of] C10-C17 (%)[b, d]	Selectivity to [Yield of] C17 (%)[c, d]
Water	7.4	27	87 [23]	63 [14]
Butanol	16.1	38	77 [29]	44 [17]

*As measured from the powder X-ray diffractograms of the catalysts calcined under static air for 3 h at 500 °C.

[a] Conversion = wt% of product with b.p. < 375°C.

[b] Selectivity to C10-C17 = 100 × [(wt% of product with b.p. < 314°C – wt% of product with b.p. < 177°C)/(wt% of product with b.p. < 375°C)].

[c] Selectivity to C17 = 100 × [(wt% of product with b.p. < 314°C – wt% of product with b.p. < 295°C)/(wt% of product with b.p. < 375°C)].

[d] The corresponding yield (conversion × selectivity) values are shown between brackets.

Table 2.4. Semi-batch mode deoxygenation of stearic acid over alumina-supported Ni-based catalysts (300 psi of H_2, 1.5 h reaction time).*

Catalyst	Reaction Temp. (°C)	Conversion (%)[a]	Selectivity to [Yield of] C10-C17 (%)[b, d]	Selectivity to [Yield of] C17 (%)[c, d]
20% Ni/Al_2O_3	260	39	15 [6]	2 [1]
20% Ni-5% Cu/Al_2O_3	260	54	13 [7]	7 [4]
20% Ni-1% Sn/Al_2O_3	260	30	7 [2]	3 [1]
20% Ni/Al_2O_3	300	92	76 [70]	66 [61]
20% Ni-5% Cu/Al_2O_3	300	98	86 [84]	79 [77]
20% Ni-1% Sn/Al_2O_3	300	39	23 [9]	17 [7]

*All experiments for which results are shown were performed a minimum of two times, average standard deviations being 7.3, 11.9, and 9.1% for conversion, selectivity to C10-C17, and selectivity to C17, respectively.

[a] Conversion = 100 – (wt% of product with b.p. < 375°C – wt% of product with b.p. < 350°C).

[b] Selectivity to C10-C17 = 100 × <(wt% of product with b.p. < 314°C – wt% of product with b.p. < 177°C)/[100 - (wt% of product with b.p. < 375°C – wt% of product with b.p. < 350°C)]>.

[c] Selectivity to C17 = 100 × <[(wt% of product with b.p. < 314°C – wt% of product with b.p. < 295°C)/ [100 - (wt% of product with b.p. < 375°C – wt% of product with b.p. < 350°C)]>.

[d] The corresponding yield (conversion × selectivity) values are shown between brackets.

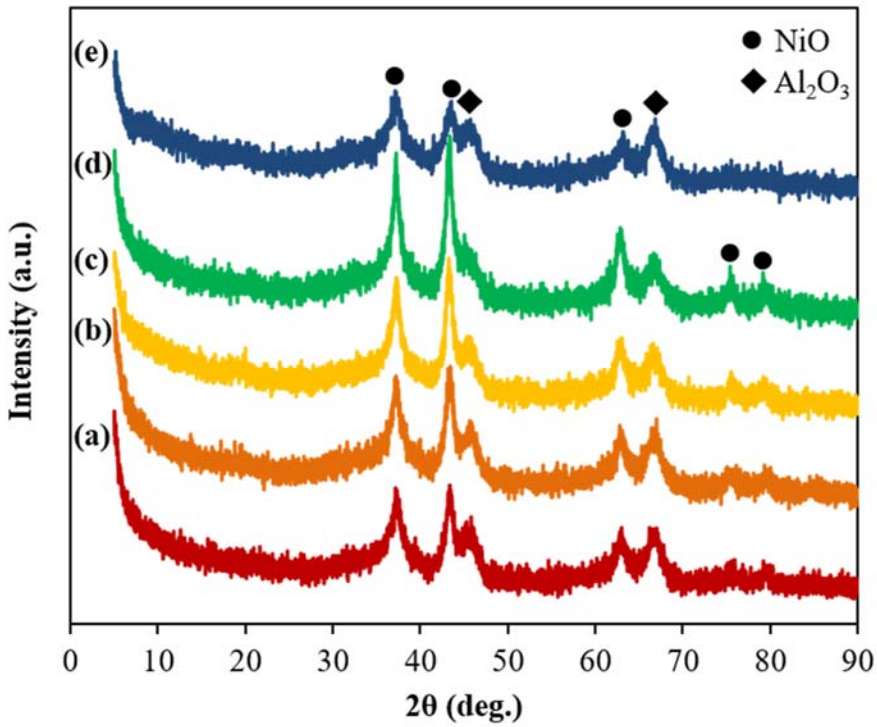

Figure 2.1. XRD patterns of 20% Ni/Al_2O_3 (a), 20% Ni-1% Cu/Al_2O_3 (b), 20% Ni-2% Cu/Al_2O_3 (c), 20% Ni-5% Cu/Al_2O_3 (d), and 20% Ni-1% Sn/Al_2O_3 (e) calcined under air at 500 °C.

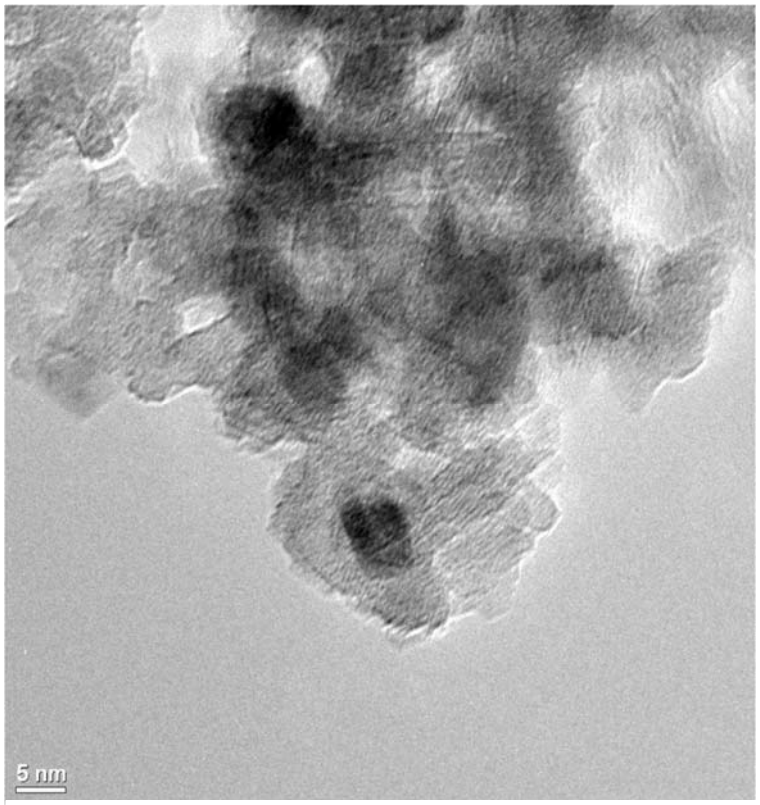

Figure 2.2. TEM image of 20% Ni/Al_2O_3.

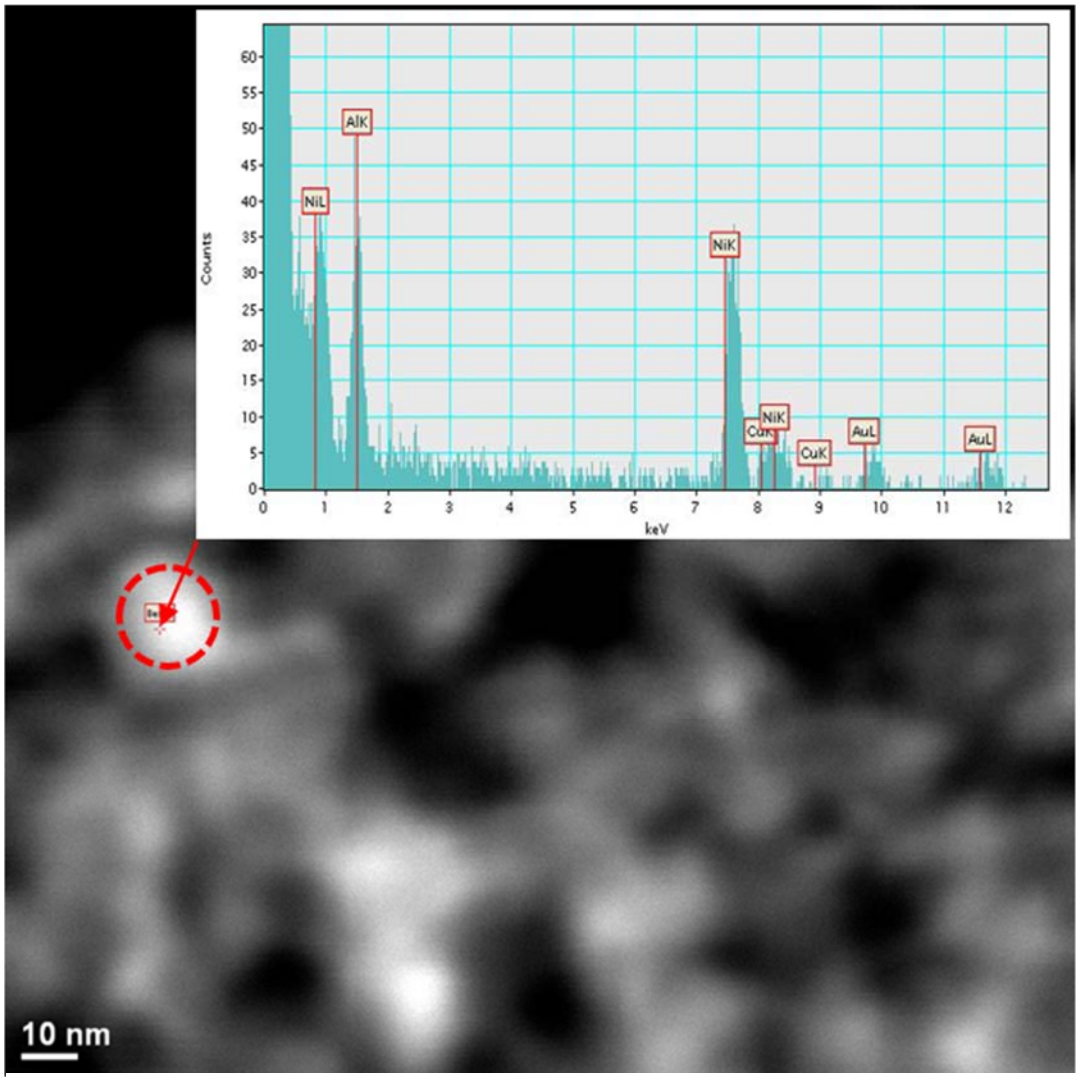

Figure 2.3. STEM image of 20% Ni-5% Cu/Al_2O_3 and EDS (inset) of the region highlighted in the image.

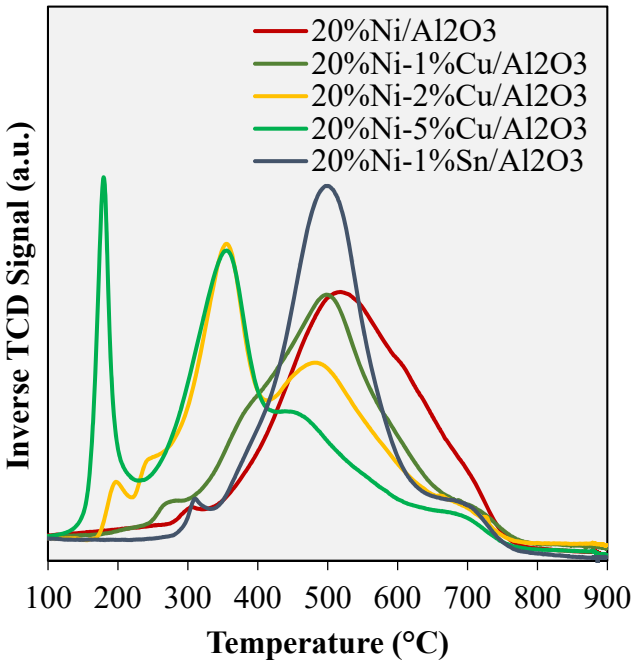

Figure 2.4. H_2 TPR profiles of the fresh catalysts.

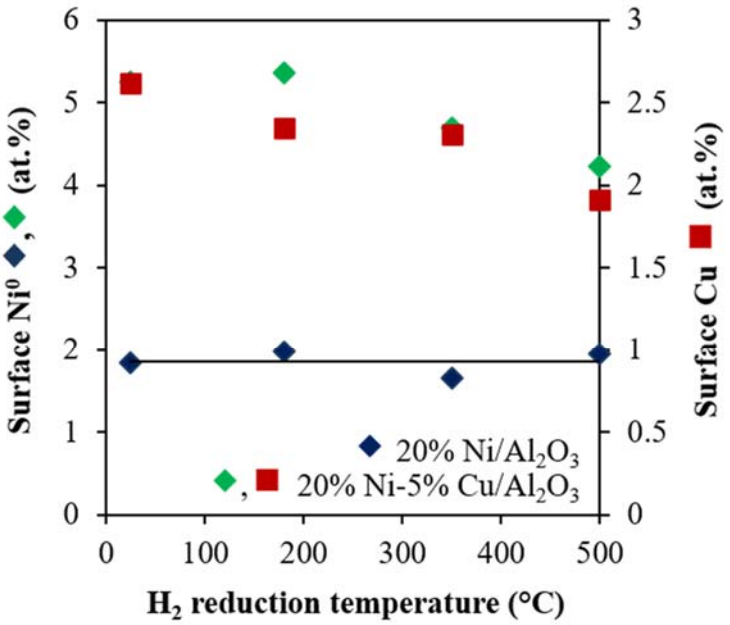

Figure 2.5. Compositional analysis drawn from high resolution Ni XP spectra of 20% Ni/Al_2O_3 and 20% Ni–5% Cu/Al_2O_3

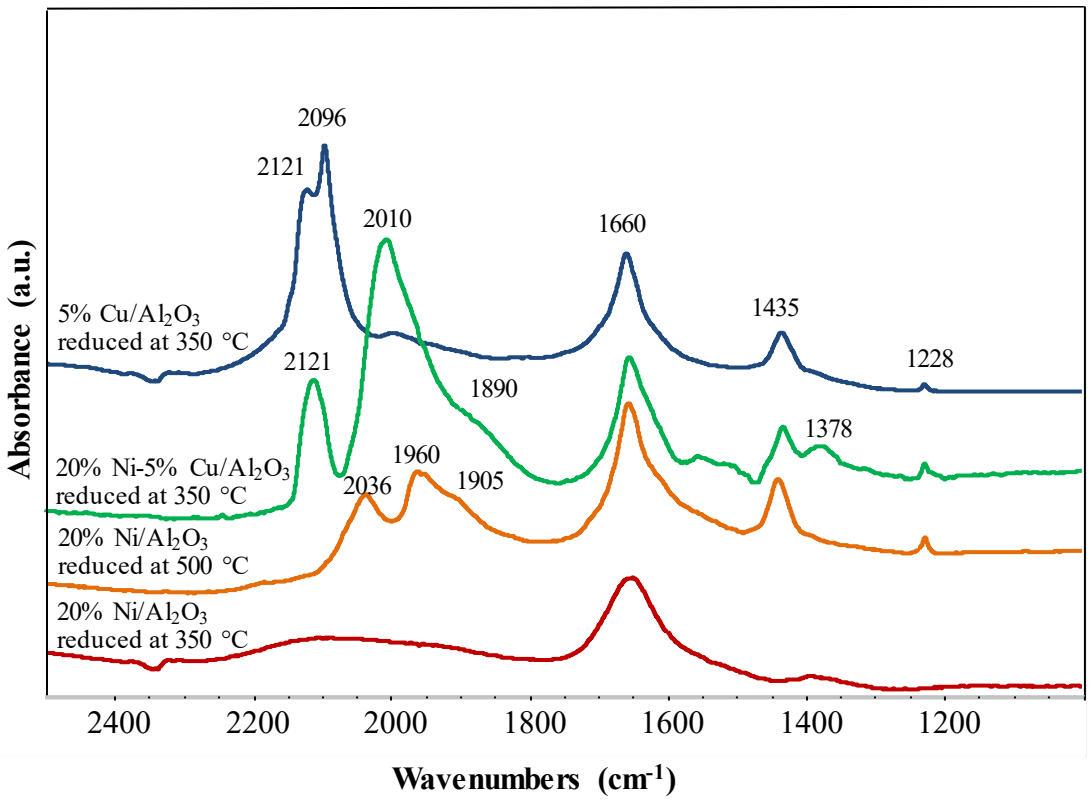

Figure 2.6. DRIFTS spectra of CO adsorbed on 20% Ni/Al_2O_3 and 20% Ni-5% Cu/Al_2O_3.

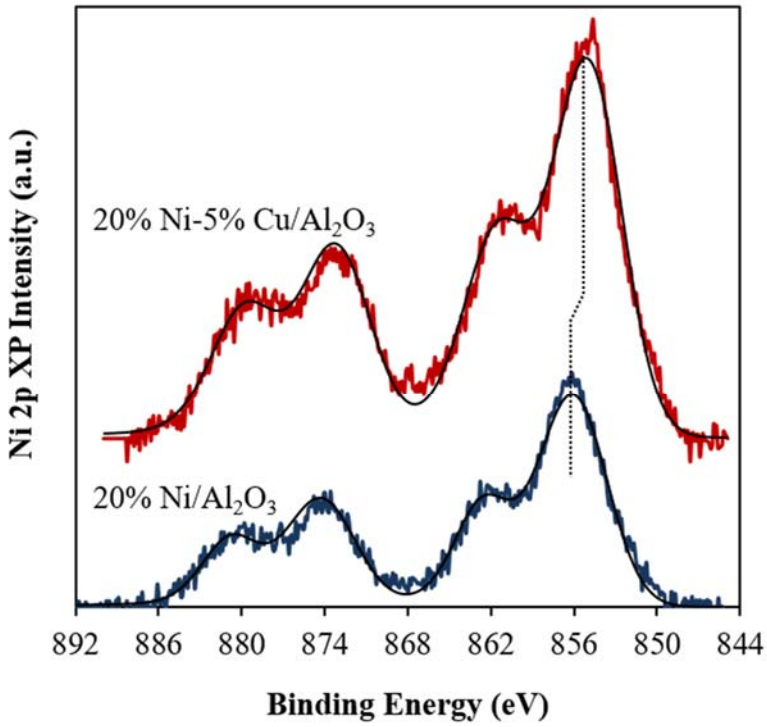

Figure 2.7. High resolution Ni XP spectra of 20% Ni/Al_2O_3 and 20% Ni-5% Cu/Al_2O_3.

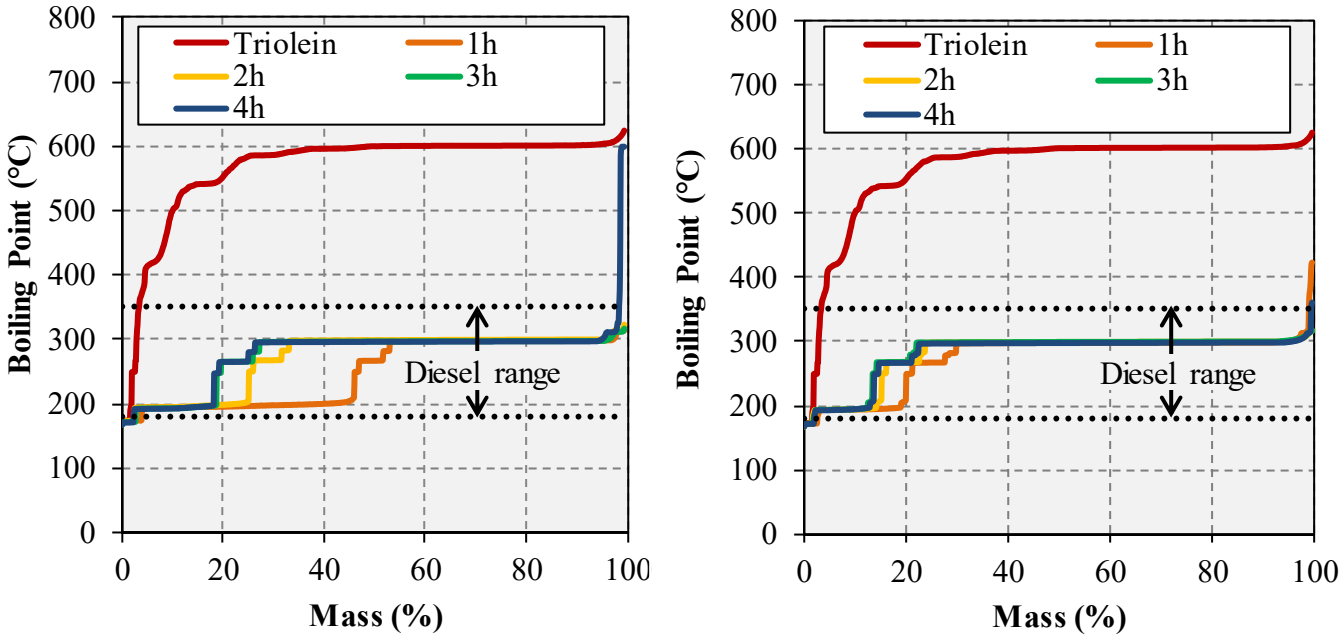

Figure 2.8. Boiling point distribution plots of the feed and the liquid products obtained from triolein deoxygenation in fixed bed mode at 260 °C and 580 psi over20% Ni/Al_2O_3 (left), and 20% Ni-5% Cu/Al_2O_3 (right).

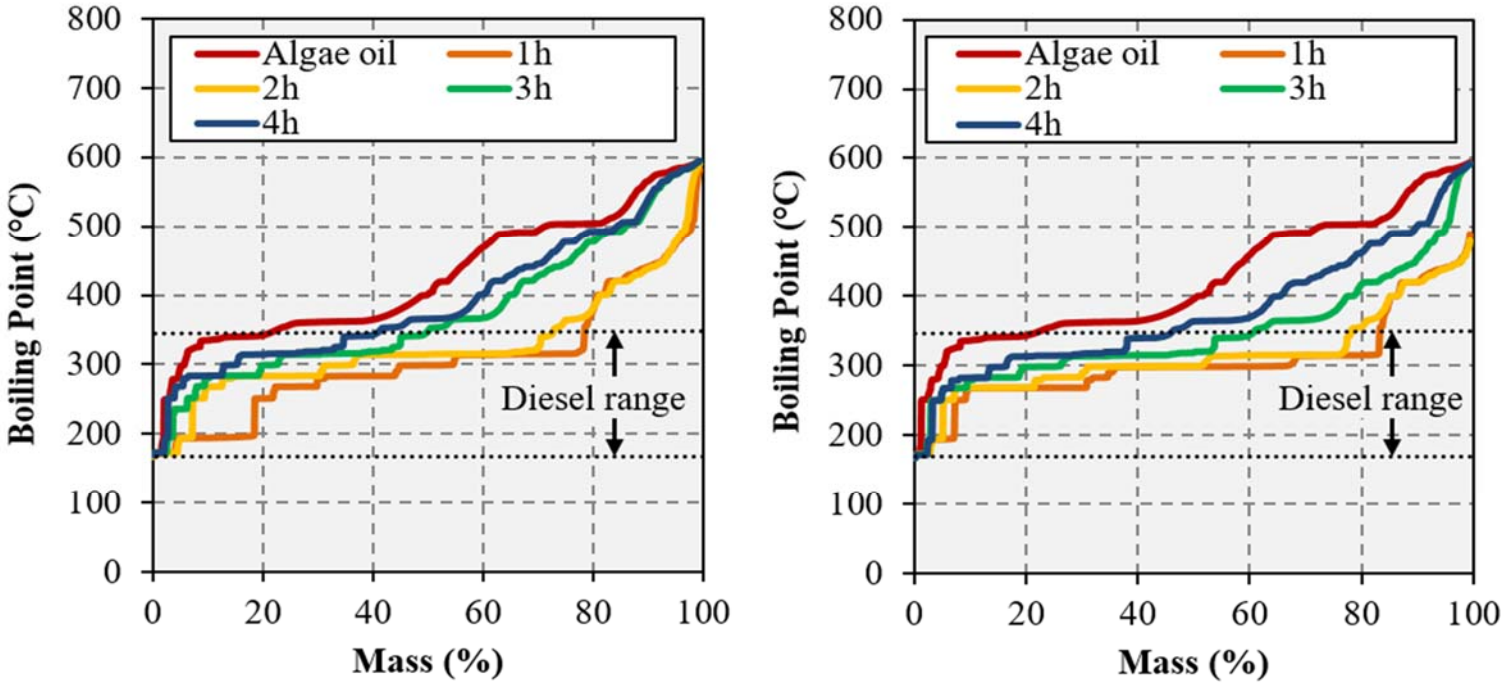

Figure 2.9. Boiling point distribution plots of the feed and the liquid products obtained from algal lipids deoxygenation in fixed bed mode at 260 °C and 580 psi over 20% Ni/Al_2O_3 (left), and 20% Ni-5% Cu/Al_2O_3 (right).

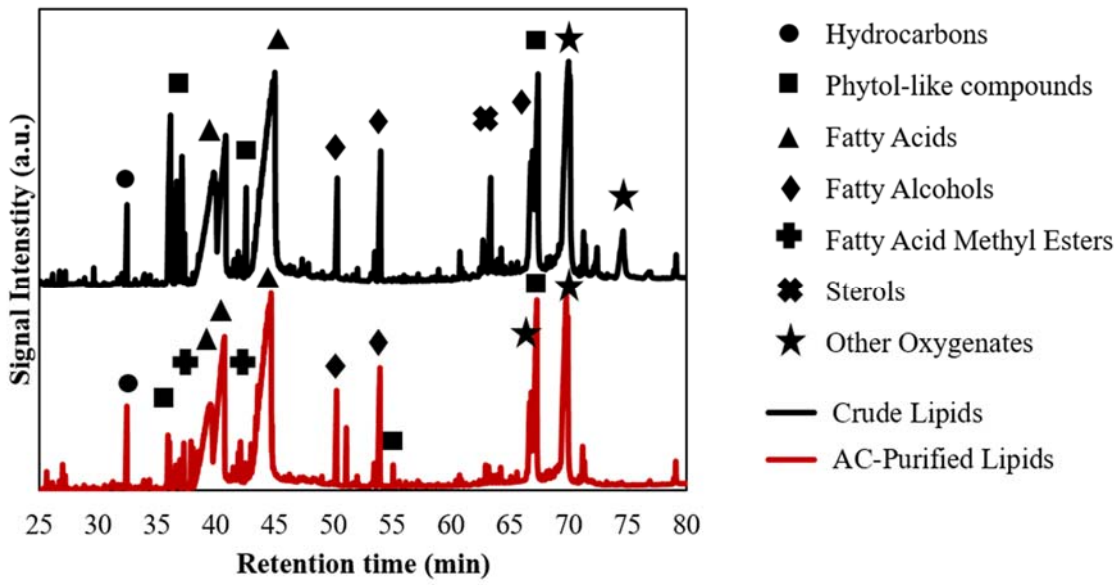

Figure 2.10. GC-MS analysis of the algae oil used in this study.

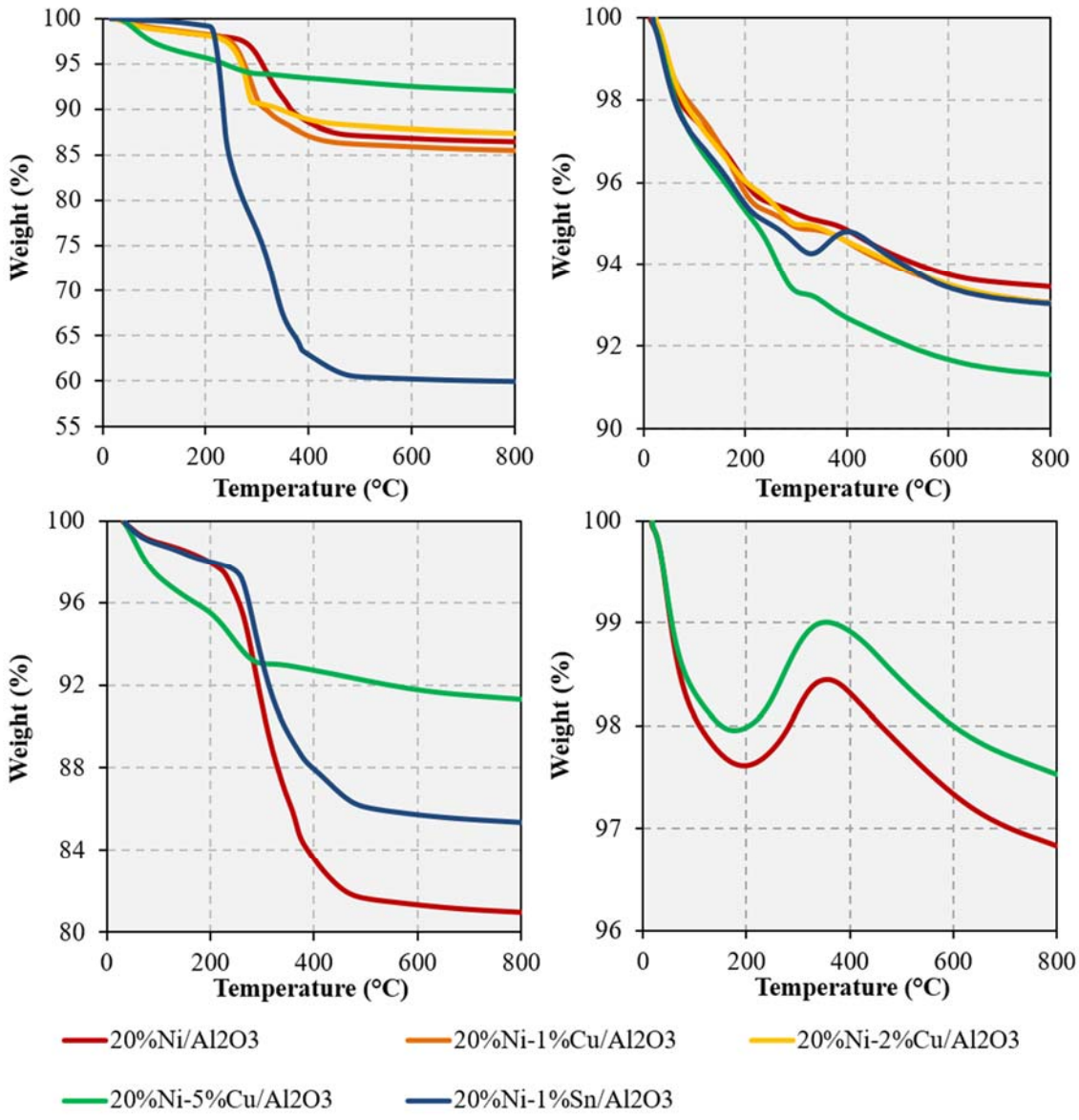

Figure 2.11. TGA profiles of catalysts spent upgrading tristearin at 260°C for 6 h in a semibatch reactor (top left), tristearin at 350°C for 6 h in a semibatch reactor (top right), stearic acid at 300 °C for 1.5 h in a semibatch reactor (bottom left), and triolein at 260 °C for 4 h in a fixed bed reactor (bottom right).

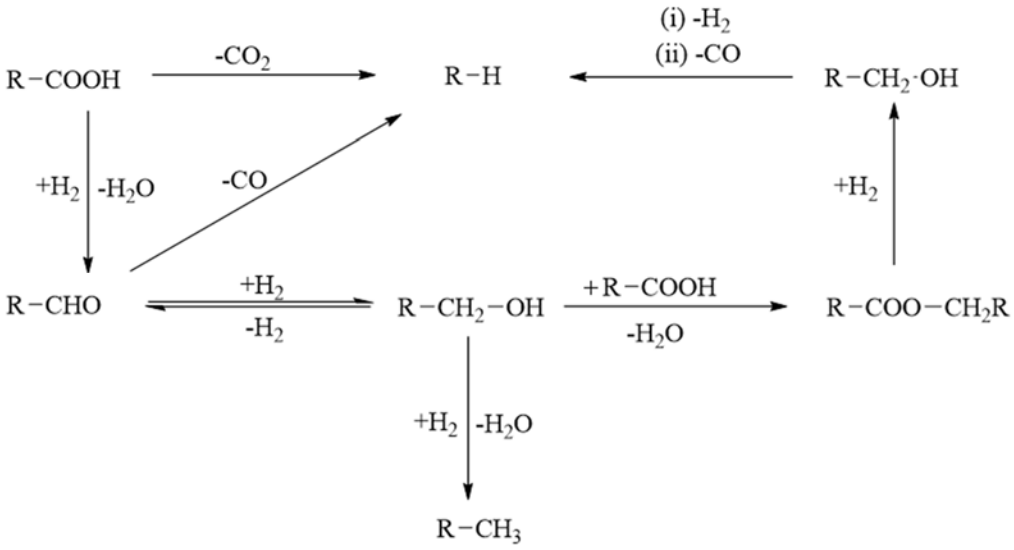

Scheme 2.1. Reaction scheme for stearic acid deoxygenation

Chapter 3. Effect of Cu promotion on cracking and methanation during the Ni-catalyzed deoxygenation of waste lipids and hemp seed oil to fuel-like hydrocarbons

Disclaimer: The work provided in this chapter is the result of a collaboration with Eduardo Santillan-Jimenez and Tonya Morgan from the Center for Applied Energy Research at the University of Kentucky, and Makaylah Garrett from Kentucky State University. Eduardo Santillan-Jimenez was responsible for acquisition of the yellow grease from local middle schools, project advising, and assistance in writing and editing. Makaylah Garrett was responsible for performing reproducibility experiments with 20% Ni/Al_2O_3 and the 20% Ni-5% Cu/Al_2O_3 catalysts, and the deoxygenation of yellow grease and hemp oil. Tonya Morgan performed simulated distillation-gas chromatography and the gas chromatography-mass spectrometry analysis on the liquid products obtained from the experiments.

Note – This chapter was published as an article in the following Journal:

Santillan-Jimenez, E., Loe, R., Garrett, M., Morgan, T., Crocker, M., (2018). Effect of Cu promotion on cracking and methanation during the Ni-catalyzed deoxygenation of waste lipids and hemp seed oil to fuel-like hydrocarbons, Catal. Today, 302: 261-271

3.1. Introduction

A number of sustainability and environmental concerns have spurred interest in biofuels, which are renewable, carbon neutral and do not disrupt the food supply when produced from waste and inedible feedstocks [59, 207]. Waste lipids can be converted via transesterification with methanol to a mixture of fatty acid methyl esters (FAMEs), commonly referred to as biodiesel. While biodiesel offers certain advantages over petroleum-derived fuels [208], the high oxygen content of FAMEs gives rise to several problems – including limited storage stability and engine compatibility issues – that render biodiesel a less than ideal fuel [9]. Thus, attention has shifted to deoxygenation processes capable of converting lipids to fuel-like hydrocarbons, such as hydrodeoxygenation (HDO) and decarboxylation/decarbonylation ($deCO_x$). HDO is a commercial process that is highly selective to diesel-like hydrocarbons, albeit there is a high hydrogen requirement associated with the removal of oxygen as H_2O [109]. Therefore, $deCO_x$ can be viewed as preferable not only because the hydrogen consumption is in principle lower than for HDO, but also because $deCO_x$ is catalyzed by simple supported metal catalysts as opposed to the sulfided metal catalysts used in HDO [109, 209].

Although most $deCO_x$ work has focused on Pd or Pt catalysts, the high cost of these formulations is an impediment to their use in industrial applications. Consequently, inexpensive Ni catalysts have attracted interest for the deoxygenation of lipids to hydrocarbons via $deCO_x$ [8, 15]. Admittedly, Ni catalysts face certain challenges that must be overcome if they are to become an industrially viable alternative for the conversion of

lipids to diesel-like hydrocarbons. Indeed, the high cracking and methanation activity of Ni can favor the formation of short chain liquid hydrocarbons, methane and coke deposits, which reduces the selectivity to diesel, decreases the hydrogen efficiency and results in catalyst deactivation.

Recent results show that the aforementioned issues inherent to supported Ni catalysts can be assuaged to some degree by promoting Ni with Cu. Indeed, we have observed that Ni-Cu bimetallic catalysts afford higher diesel yields as well as reduced coking and deactivation relative to Ni-only formulations in the deCO_x of model lipid feeds such as stearic acid and tristearin [75]. Although the results from our previous study were promising, the study utilized mainly model compounds at low feed concentrations in semi-batch reaction conditions. The current study aimed to further elucidate the effect of Cu promotion under more industrially relevant conditions, namely, the use of a continuous flow fixed bed reactor and realistic, concentrated feedstocks. Previous reports have shown that cracking is more common with increased unsaturation in the feed [210]; therefore, two feedstocks with differing degrees of unsaturation were tested. Yellow grease (used cooking oil) was employed as a waste lipid feedstock composed primarily of triolein, a triglyceride with three 18-carbon acyl chains each containing a double bond between the 9th and 10th carbons. The second feed employed was hemp seed oil, a highly unsaturated feedstock composed mostly of trilinolein, a triglyceride with three 18-carbon acyl chains each containing two double bonds, one between the 9th and 10th carbons and another between

the 12th and 13th carbons. The highly unsaturated nature of hemp seed oil provides a good test of the ability of Cu to mitigate the cracking activity of Ni.

3.2. Materials and methods

3.2.1 Feed lipid analysis

Figure 3.1 shows the lipid profile of both the yellow grease and hemp seed oil used in this study. This was obtained by direct transesterification of the feed with methanol according to the method of Griffiths et al. [211]. The transesterified products were analyzed by an Agilent 6890A gas chromatograph equipped with a HP-88 column (30 m × 0.25 mm × 0.2 μm) and a flame ionization detector. Helium was used as the carrier gas, the flow rate was set to 1 mL/min and a split of 20:1 was employed. The temperatures of the inlet and the detector were 250 and 300 °C, respectively. The temperature program included an initial temperature of 50 °C followed by a ramp of 20 °C/min to 140 °C and a subsequent ramp of 3 °C/min to a final temperature of 240 °C. Calibrations were completed using a Supelco 37 FAME Mixture.

3.2.2. Catalyst preparation and characterization

20% Ni/Al_2O_3 and 20% Ni-5% Cu/Al_2O_3 catalysts were prepared by excess wetness impregnation using $Ni(NO_3)_2 \cdot 6H_2O$ (Alfa Aesar) and $Cu(NO_3)_2 \cdot 3H_2O$ (Sigma-Aldrich) as the metal precursors and γ-Al_2O_3 (Sasol; surface area of 216 m^2/g) as the support. Following impregnation, the materials were dried overnight at 60 °C under vacuum and

then calcined at 500 °C for 3 h in static air. The catalysts and SiC diluent (Kramer Industries, Inc.) were pelletized to the desired particle size (150-300 μm) prior to use. The characterization of these catalysts has been described previously [75].

3.2.3. Deoxygenation experiments

Deoxygenation experiments were performed in a 1/2 in o.d. stainless steel fixed bed reactor equipped with a porous steel frit to support the catalyst bed. Prior to the deoxygenation experiments, the catalyst was reduced *in situ* for 3 h at 400 °C under H_2 (580 psi) with a continuous H_2 flow of 60 mL/min. The system was then taken to the reaction temperature while maintaining the H_2 flow, at which point the feed was introduced using an HPLC pump. Yellow grease (used cooking oil) deoxygenation experiments employed a feed obtained from the cafeteria of a local school and were performed using either 25 wt% yellow grease dissolved in dodecane (99+% Alfa Aesar) or 75 wt% yellow grease in dodecane. The 25 wt% yellow grease experiments were performed at 350 °C, using 0.5 g catalyst and a feed solution flow rate of 12 mL/h, equivalent to a WHSV of 4.75 h^{-1} (note that WHSV refers to only the feed to catalyst ratio, and excludes any amount of dodecane used). The 75 wt% yellow grease experiments were performed at 375 °C with a feed solution flow rate of either 2.76 mL/h or 1.5 mL/h (equivalent to a WHSV of 4.75 h^{-1} and 2.03 h^{-1}, respectively) over a thoroughly mixed catalyst bed containing 0.5 g of catalyst and 0.5 g of SiC as catalyst diluent. Blank experiments were conducted for the 75 wt% yellow grease experiments using 1 g of SiC and a feed flow rate of 1.5 mL/h. Hemp

seed oil (Dr. Adorable Inc.) deoxygenation experiments were performed with 25 wt% hemp seed oil (dissolved in dodecane) at 350 °C, with a feed solution flow rate of 12 mL/h and 0.5 g of catalyst (WHSV of 4.81 h^{-1}). In all experiments, the products were directed into a condenser held at 0°C and liquid products were collected every hour. Incondensable gases were directed to a dry test meter before being collected in Tedlar® gas sample bags that were changed and analyzed hourly. Further details of the equipment and procedures employed have been described elsewhere [6]. Representative experiments were performed in duplicate to ensure reproducibility.

3.2.4. Methanation experiments

Methanation experiments were performed with the equipment and procedures employed for deoxygenation experiments (see section 2.3) using a stream of ~5 vol% CO_2 in H_2 as the feed (63 mL/min).

3.2.5. Analysis of deoxygenation products and spent catalysts

Reaction feeds and product mixtures were analyzed using a combined Simulated Distillation-GC and GC-MS approach. An Agilent 7890B GC System equipped with an Agilent 5977A Extractor MSD and a flame ionization detector (FID) was used for these analyses. A 0.1 μL injection was employed and helium was used as the carrier gas. The Multimode inlet, containing a helix liner, was run in split mode (split ratio 15:1; split flow 48 mL/min) using an initial temperature of 100 °C. Immediately upon injection, the inlet

temperature was increased at a rate of 8°C/min to a final temperature of 380 °C, which was maintained for the duration of the analysis. Similarly, the oven temperature (initially 40 °C) was increased immediately upon injection at a rate of 4 °C/min to 325 °C, followed by a ramp of 10 °C/min to a final temperature of 400 °C held for 12.5 min, the total run time being 91.25 min. An Agilent J&W VF-5ht column (30 m × 250 μm × 0.1 μm; 450 °C max.) was used as the primary column after which the eluents entered a Siltek MXT Connector which split the components into two fractions: one leading to the MSD (J&W Ultimetal Plus Tubing, 11m × 0.25mm ID) and one leading to the FID (J&W Ultimetal Plus Tubing, 5m × 0.25mm ID). MS zone temperatures – including those of the MS source (230 °C) and quadrupole (150 °C) – remained constant for the duration of the analysis. A 1.75 min solvent delay was implemented and the mass spectrometer scanned from 10 to 700 Da. The FID was set to 390 °C with the following flow rates: H_2=40 mL/min; air=400 mL/min; makeup He=25 mL/min. Chromatographic programming was performed using Agilent MassHunter Data Acquisition software. Data acquired using the above GC-FID methods were processed using SimDis Expert 9 software purchased from Separation Systems, Inc. Reaction and GC solvents (i.e., dodecane and either chloroform or carbon disulfide) were subtracted and/or quenched from the chromatogram prior to any calculations. It is important to note that these two GC techniques are complementary: Simulated Distillation-GC was able to analyze the entirety of the samples in spite of lacking the ability to identify individual constituents, whereas GC-MS is a powerful tool for compound identification but is limited in the detection of large molecules such as

triglycerides. Therefore, the data stemming from these two GC techniques were combined in order to obtain a complete picture. Information on the method development for the liquid product analysis is described elsewhere [186]. Incondensable gases and spent catalysts were analyzed using previously described instrumentation and methods [112, 183].

3.3. Results and Discussion

3.3.1. Catalytic upgrading of 25 wt% yellow grease

The results of an experiment in which a solution comprising 25 wt% yellow grease in dodecane was catalytically upgraded over 20% Ni/Al_2O_3 at 350 °C are shown in Figure 3.2a and 3.2b. Notably, the simulated distillation boiling point distribution plot (BPDP) shows that while the entirety of the feed boils in excess of 350 °C (i.e., above the b.p. range of diesel fuel), ca. 95% of the liquid product boiled within the diesel range irrespective of time on stream (see Figure 3.2a), this despite the relatively high WHSV of 4.75 h^{-1} employed (as mentioned in section 2.3, all WHSV values reported correspond to the actual lipid feed rate rather than to the total lipid solution fed). GC-MS analysis of the feed and the reaction products (see Figure 3.2b and Table 3.1) indicated that while the feed consisted of 84.94% triolein, 4.45% oleic acid, 0.69% monoolein, and 9.92% diolein (which is in overall agreement with Figure 3.1), >95% of the liquid product consisted of diesel-like (linear C10-C20) hydrocarbons regardless of time on stream.

The results of an experiment in which the same starting material was upgraded over 20% Ni-5% Cu/Al_2O_3 are included in Figure 3.2c, Figure 3.2d, and Table 3.2 in the

supplementary material. Although the results of this run in terms of the liquid reaction products were similar to those acquired over 20% Ni/Al_2O_3, the Ni-Cu catalyst showed improved selectivity to long chain (C15-C17) hydrocarbons relative to the monometallic formulation, which is consistent with our previous report in which Cu promotion was shown to curb the cracking activity of Ni [75]. Indeed, heptadecane (C17) comprised ~61-70 wt% of the liquid product obtained over the Ni-only catalyst, versus 74-79 wt% of the liquid obtained over the Ni-Cu catalyst according to Simulated Distillation-GC results (see Figures 3.2a and 3.2c). Parenthetically, the small amount (≤2 wt% per Tables 3.1 and 3.2) of C18 in the reaction products indicates that the reaction proceeds via $deCO_x$ as opposed to HDO, which in turn suggests that C16 is formed by cracking and not by HDO of C16 fatty acid chains. A closer look at the less abundant lighter products in the diesel range, namely, C10, C11, C14, C15 and C16 (C12 and C13 could not be determined due to the interference of the reaction solvent), also affords valuable insights vis-à-vis the cracking mechanism (see Scheme 3.1). Indeed, the fact that both catalysts afford larger amounts of long chain (e.g., C16) than short chain (≤C14) hydrocarbons indicates that chain shortening occurs mainly via the removal of terminal carbons as previously suggested by Yakovlev et al. [98]. These results are also consistent with the tandem isomerization-decarboxylation model proposed by Doll and co-workers in which a catalyst dynamically isomerizes a double bond in the aliphatic chain of an unsaturated fatty acid and subsequently decarboxylates isomers with lower activation barriers [28], unsaturated carboxylic acids with a double bond in the α-β or β-γ position relative to the carbonyl carbon being known

to decarboxylate readily to afford olefins [212]. In this manner β-alkenes can form, the cracking of which would result in chain shortening via terminal carbon loss. Nevertheless, a small amount of internal cracking – which can be preceded by the double bond positional isomerization known to occur over Ni catalysts [213] – is also indicated based on the presence of C10 and C11 in the product mixtures and on the fact that small amounts (0.1-0.8 wt%) of C6-C9 are also formed (not shown in Figure 2 for readability). Indeed, using as examples oleic acid and its positional isomers with the double bond removed one position in either direction of the C18 chain, cracking occurs as suggested in the cracking of C34-botryococcenes [10] to afford straight alkanes , in this case a mixture of C6-C11 hydrocarbons as illustrated in Figure 3.3.

Analysis of the incondensable gases formed in these reactions, shown in Figure 3.4, is also informative. The absence of CO and the small amount of CO_2 and propane observed is conspicuous, as these gases would be expected to constitute some of the main deCO_x products [209]. However, CO_x and H_2 can react to form methane, while propane can be cracked to lighter hydrocarbons [8, 214]. The latter is consistent with the fact that while the yield of propane was negligible, ethane was obtained (see Figure 3.4), which suggests that propane is cracked to ethane and methane in agreement with a recent report [214]. Part of the observed methane can also result from shortening of adsorbed fatty acid chains and/or unsaturated hydrocarbon products, which as mentioned above has been reported to occur mainly via terminal methyl group removal [98]. However, another source of methane is likely CO_x hydrogenation, Ni-based catalysts being very active in this reaction [215-

220]. Indeed, this side reaction has been observed to accompany the Ni-catalyzed deoxygenation of lipids to hydrocarbons [53, 98, 204, 214, 221-223]. Additional insights were gained through an effort to close the C1-C3 mass balance (see Table 3.3). For instance, the fact that the theoretical amount of propane resulting from the $deCO_x$ of triglycerides in the feed (entry 7 in Table 3.3) is practically identical to the sum of propane and ethane produced (entries 8+10 in Table 3.3) suggests that ethane results exclusively from propane cracking rather than from the shortening of alkyl chains via terminal C2 loss. In total, the methanation of the CO_x resulting from the $deCO_x$ of lipids in the feed, the cracking of propane and the shortening of alkyl chains to form C16 and C14 via terminal C1 loss account for ~50% of the methane produced, the remainder likely resulting from the shortening of alkyl chains to form lighter (≤C13) alkanes.

The results shown in Figure 3.4 are also of interest due to the fact that the Ni-Cu catalyst was observed to afford consistently lower amounts of methane at all reaction times sampled, this effect being more prominent at the beginning of the reaction. Indeed, Yakovlev et al. observed Ni-Cu catalysts to yield less methane than Ni-only catalysts while investigating the deoxygenation of FAMEs to hydrocarbons [98], although Harnos et al. did not observe copper addition to result in reduced methanation in their study of the deoxygenation of sunflower oil to hydrocarbons [204]. Our results indicate that Ni-Cu catalysts do afford reduced methane formation, which in principle may be attributed to a) reduced cracking of the fatty acid chains; b) the inactivity of unalloyed Cu in methanation [224] – this inactivity being confirmed by Berenblyum et al. during the deoxygenation of

stearic acid to hydrocarbons over Cu/Al_2O_3 [200] – and/or c) the fact that Cu in Ni-Cu alloys has been found to curb the methanation activity of Ni [224]. The latter has been explained by Saw et al. by invoking the ability of the Ni-Cu alloy to prevent CO dissociation, thus avoiding the formation of the carbon (e.g., formate) species that are known to intermediate the formation of methane via CO_2 hydrogenation [225]. Against this backdrop, the methanation of CO_2 was investigated over both the Ni-only and the Ni-Cu catalysts in an effort to elucidate which mechanism(s) could explain the ability of the Ni-Cu catalyst to reduce methane formation.

3.3.2. Catalytic methanation of CO_2

The results of CO_2 methanation experiments – which were performed as described in section 2.4 using a stream of ~5 vol% CO_2 in H_2 as the sole feed – are included in Figure 3.5. Both catalysts afforded very similar results, the small differences observed being attributed to a small variance in the CO_2 content of the feed, which was 5.0 and 5.5 vol% for the run involving the Ni-Cu and the Ni-only catalyst, respectively. Interestingly, an induction period in which the effluent gas composition shifts from almost pure H_2 (t = 1 h) to mixtures of H_2 and methane displaying increasingly high methane content (t = 2 to 8 h) is observed in Figure 3.5, this induction period being also observed in deCO_x experiments (see Figure 3.4). In order to explain this induction period, spent catalysts were analyzed via diffuse reflectance infrared Fourier transform spectroscopy (DRIFTS), the resulting spectra (see Figure 3.6) exhibiting bands at 991, 1370 and 1489 cm^{-1} that can be

assigned to alumina-bound carbonates [226]. This indicates that the induction period is associated with the accumulation of CO_2 on the catalyst surface, which results in CO_2 first being absent in the gas phase at the beginning of the reaction due to its complete adsorption on the surface, after which its concentration increases as the surface becomes saturated.

Thus, the ability of 20% Ni-5% Cu/Al_2O_3 to mitigate methane formation relative to 20% Ni/Al_2O_3 can be assigned to reduced cracking, which is consistent with the fact that chain shortening was found to occur mostly via terminal carbon loss (vide supra) and that lower amounts of C14 and C16 were obtained over the Ni-Cu catalyst (see Figure 2). In fact, methane stemming from the terminal carbon loss associated with C14 and C16 formation accounts for >40% of the excess methane produced by the monometallic relative to the bimetallic catalyst (as calculated from entries 4, 14 and 17 in Table 3.3), the remainder of this excess likely resulting from the formation of lighter alkanes, including the C12 and C13 that could not be detected due to the interference of the reaction solvent (vide supra).

3.3.3. Catalytic upgrading of 25 wt% hemp oil

Previous reports have shown that higher degrees of unsaturation in lipid feeds result in increased cracking during deoxygenation [210]. In order to assess the effect of unsaturation under the experimental conditions employed, 25 wt% hemp seed oil was upgraded over both the 20% Ni/Al_2O_3 and the 20% Ni-5% Cu/Al_2O_3 catalysts, the results of these runs being summarized in Figure 3.7 and Table 3.4. As shown in Table 3.4, the

GC-MS data showed the feed was composed of >99% trilinolein. According to the BPDP in Figure 3.7a, the 20% Ni/Al_2O_3 catalyst afforded ca. 90% C10-C17 hydrocarbons regardless of the hour sampled, which represents only a slightly lower yield than that obtained with yellow grease as the feed (see section 3.1). However, C17 comprised 49-62 wt% of the liquid products, which is significantly lower than the amount of C17 obtained when yellow grease was employed, indicating that the higher degree of unsaturation in the feed does indeed lead to increased cracking.

The BPDP of the liquid products resulting from the deoxygenation of 25 wt% hemp seed oil over 20% Ni-5% Cu/Al_2O_3 are shown in Figure 3.7c. The BPDP indicates that C17 represents ~80% of the liquid products, which is a significant increase relative to the C17 concentration in the products obtained using the monometallic Ni catalyst. The MS data presented in Table 3.5 show that there is only a minor amount of unsaturated products (<1%) indicating that hydrogenation of the double bonds occurs rapidly under these conditions, producing linear chain alkanes. Notably, the selectivity to C16, shown in Figure 3.8, averages ~8.2% and ~3.7% for the Ni and Ni-Cu catalyst, respectively, indicating there is a significant decrease in the end chain cracking over the Ni-Cu catalyst. Tellingly, the selectivity to C10 and C11 is also considerably lower over the Ni-Cu catalyst, indicating a decrease in internal chain cracking near the double bond originally spanning the 9th and 10th in the feed chains, which once again illustrates the ability of Cu to curb cracking even when highly unsaturated feeds are employed. The analysis of the incondensable products stemming from deoxygenation of hemp seed oil over both catalysts

is shown in Figure 8. The amount of methane increases with time on stream – as was also the case in the yellow grease and CO_2 methanation experiments (vide supra) – for both the Ni and Ni-Cu catalyst. However, at any given time, the amount of methane produced by the Ni-Cu catalyst was slightly less than half that of the Ni catalyst.

3.3.4. Catalytic upgrading of 75 wt% yellow grease

Given that the use of concentrated feedstocks is favored in industrial settings, experiments were performed under more industrially-relevant reaction conditions. In an initial experiment performed at 375 °C in which 75 wt% yellow grease in dodecane (WHSV = 4.75 h^{-1}) was used as the feed and a 1:1 mixture of 20% Ni-5% Cu/Al_2O_3 and SiC was employed as the catalyst bed, promising results were obtained in the form of diesel yields as high as 70% at t = 3 h (no liquid products were obtained in the initial hours of this and subsequent experiments due to the reduced flow rate of the feed and the increased volume of the catalyst bed), this value dropping to 60% after 8 h on stream. In an effort to improve diesel yield and catalyst stability, the WHSV was reduced to 2.03 h^{-1}, the results of this experiment being summarized in Figure 3.10 and Table 3.6. According to the MS analysis in Table 3.6, hydrocarbons constitute 100% of the reaction products irrespective of time on stream, which indicates the complete deoxygenation of the feed. Notably, a diesel yield of 92% was obtained at t = 3h, this value reaching 94% at t = 8 h; equally noteworthy is the fact that selectivity to long chain hydrocarbons also increased with time on stream, C17 selectivity increasing from 34% at t = 3 h to 74% at t = 8 h (see Figure

3.10a). These results suggest that while the catalyst retains its deoxygenation activity at all reaction times sampled, cracking reactions become disfavored with time on stream (see Figure 3.10a).

Given the different set of conditions (higher feed concentration, lower WHSV, use of SiC diluent and higher temperature) employed in this experiment, a blank run was performed using an identical set of conditions and 1 g of SiC as the catalyst bed in order to assess the extent to which the aforementioned results could be attributed to thermal – as opposed to catalytic – phenomena. The simulated distillation analysis of the liquid products obtained in this blank run (see Figure 3.11) indicated that only ~3% boil in the diesel range; however, a significant portion boiled at lower temperatures than the feed. GC-MS analysis of the product mixtures (see Table 3.7), revealed the vast majority of products showing a lower boiling point than the feed to be oleic, stearic, palmitic and lauric acids, consistent with the thermal conversion of the glycerides to fatty acids. According to the GC-MS data, glycerides and fatty acids comprise >93.8% of the product mixtures regardless of time on stream; thus, it can be concluded that under these experimental conditions the thermal contributions to the conversion of yellow grease to fuel-like hydrocarbons are minor.

Surprisingly, when the same experiment was repeated using a 1:1 mixture of 20% Ni/Al_2O_3 and SiC as the catalyst bed, no liquid products were recovered at any of the reaction times sampled (t = 1-8 h), the only condensable material obtained being a mixture of unconverted feed and solvent recovered from the condenser at the end of the experiment.

These results were consistent with the analysis of the gaseous products, which showed methane concentrations up to an order of magnitude higher than those observed when 20% Ni-5% Cu/Al_2O_3 was employed (see Figure 3.12). These results make clear that under these reaction conditions, the use of 20% Ni/Al_2O_3 is not conducive to the formation of fuel-like hydrocarbons, as the feed remains either unconverted or undergoes excessive cracking to form considerable amounts of methane. Comparison of the results obtained with 20% Ni/Al_2O_3 and 20% Ni-5% Cu/Al_2O_3 catalysts under industrially-relevant reaction conditions therefore provides a clear illustration of the advantages offered by the bimetallic catalyst: whereas under these conditions 20% Ni/Al_2O_3 failed to yield any liquid products regardless of time of stream, 20% Ni-5% Cu/Al_2O_3 afforded diesel yields of ≥92% at all reaction times sampled.

3.3.5. Analysis of spent catalysts

Ni-based formulations are known to be particularly susceptible to coking during the deoxygenation of lipids to fuel-like hydrocarbons [173, 182] due to a number of reactions – including olefin oligomerization [200] and CO disproportionation [227] – that afford carbonaceous deposits. Spent catalysts were therefore subjected to TGA in air in an effort to quantify the amount of organic material on the catalyst surface (see Figure 3.13). The resulting traces show three types of events, namely, (i) weight loss below 400 °C attributable to the desorption and/or combustion of residual reactants and/or products including poorly structured carbon deposits (water being ruled out since catalysts were dried at 80 °C in a vacuum oven prior to TGA), (ii) weight gain events between 150 and

360 °C due to the oxidation of the supported metal(s), and (iii) a final weight loss event above 400 °C attributable to the combustion of polyaromatic coke deposits [75, 182]. The extent of coking was found to be commensurate with that observed in previous experiments performed using a dilute model lipid feed [75], which is in itself noteworthy since the combination of using a waste lipid feed, a 40-fold increase in WHSV and a doubling of time on stream failed to increase coke formation. Moreover, the spent Ni-Cu catalyst displayed lower amounts of coke deposits relative to the monometallic Ni catalyst, which is consistent with the fact that Cu addition helps to suppress cracking given that coking is an inherent byproduct of high temperature heterogeneous catalytic cracking reactions [228]. These results are also in line with previous reports in which copper hydrides formed at high hydrogen pressures were found to curb olefin oligomerization [200] – in addition to the fact that both Ni and Cu are known to catalyze the hydrogenation of olefins to alkanes during the deCO_x of lipids to hydrocarbons [183, 200] – and with reports claiming that CO disproportionation on Ni catalysts may also be mitigated via Cu addition [224]. In fact, a number of authors have observed Ni-Cu catalysts to accumulate less carbonaceous deposits than their Ni-only counterparts in reactions as varied as water-gas shift (WGS) [224], the HDO of algae-derived bio-oils [177], and the conversion of lipids to fuel-like hydrocarbons via deCO_x [75].

3.4. Conclusions

Ni/Al_2O_3 and $Ni\text{-}Cu/Al_2O_3$ were found to be effective catalysts for the conversion

of yellow grease (25 wt% in dodecane) to linear alkanes at 350 °C. For both catalysts, ca. 95% of the liquid product boiled within the diesel fuel range, the Ni-Cu catalyst showing improved selectivity to long chain (C15-C17) hydrocarbons relative to the monometallic formulation. Chain shortening was found to occur mainly via the removal of terminal carbons, although a small amount of internal cracking, which can be preceded by double bond positional isomerization, also occurs based on the presence of C6-C11 in the product mixtures. Control experiments showed no difference in the methanation activity of Ni/Al_2O_3 and $Ni\text{-}Cu/Al_2O_3$. Hence, the reduced methane formation observed for the Ni-Cu catalyst is consistent with its lower cracking activity. The Ni-Cu catalyst was also effective in curbing cracking of a more unsaturated feed, hemp seed oil, converting it to diesel-like hydrocarbons without excessive cracking. Cu promotion was most pronounced in the upgrading of 75 wt% yellow grease, the Ni-Cu catalyst yielding ≥92% diesel-like hydrocarbons (regardless of the time on stream) whereas no liquid products were obtained over Ni/Al_2O_3.

Table 3.1. GC-MS analysis of the feed and product mixtures in the catalytic upgrading of yellow grease (25 wt% in C12) over 20% Ni/Al_2O_3 at 350 °C and WHSV = 4.7 h^{-1}.

Compound	Feed	1 h	2 h	3 h	4 h	5 h	6 h	7 h	8 h
Total Hydrocarbons	**-**	**100.0**	**100.0**	**100.0**	**100.0**	**100.0**	**100.0**	**100.0**	**100.0**
Normal Alkanes	-	*99.11*	*98.84*	*99.27*	*99.01*	*98.87*	*98.76*	*98.42*	*99.04*
Decane (C10)	-	1.89	1.32	1.17	1.02	0.95	0.91	0.88	0.84
Undecane (C11)	-	5.68	4.50	3.96	3.56	3.24	3.03	2.83	2.48
Tetradecane (C14)	-	0.89	0.68	0.58	0.55	0.47	0.44	0.44	0.38
Pentadecane (C15)	-	10.49	10.10	10.14	10.56	9.90	9.94	10.59	10.29
Hexadecane (C16)	-	4.62	4.00	3.72	3.67	3.25	3.03	2.87	2.66
Heptadecane (C17)	-	70.49	73.14	74.90	74.39	75.70	76.11	75.67	77.47
Octadecane (C18)	-	1.63	1.71	1.69	1.83	1.94	1.95	1.90	1.97
Nonadecane (C19)	-	2.14	2.05	1.91	2.14	2.15	2.08	1.91	1.79
Icosane (C20)	-	0.70	0.72	0.64	0.71	0.68	0.67	0.69	0.59
Heneicosane (C21)	-	0.58	0.63	0.56	0.58	0.59	0.60	0.64	0.57
Branched Alkanes	-	*0.16*	*0.64*	*0.19*	*0.47*	*0.50*	*0.69*	*0.82*	*0.57*
Cholestane	-	0.16	0.37	0.19	0.33	0.34	0.35	0.39	0.37
Stigmastane	-	-	0.27	0.00	0.14	0.16	0.34	0.43	0.20
Olefins	-	*0.37*	*0.23*	*0.22*	*0.23*	*0.30*	*0.20*	*0.31*	-
Heptadecene (C17:1)	-	0.37	0.23	0.22	0.23	0.30	0.20	0.31	-
Unidentified	-	*0.36*	*0.29*	*0.32*	*0.29*	*0.33*	*0.35*	*0.45*	*0.39*
Total Oxygenates	**100.0**	**-**	**-**	**-**	**-**	**-**	**-**	**-**	**-**
Fatty Acids	*4.45*	-	-	-	-	-	-	-	-
Oleic Acid (C18:1)	4.45	**-**	**-**	**-**	**-**	**-**	**-**	**-**	**-**
Monoolein	*0.69*	-	-	-	-	-	-	-	-
Diolein	*9.92*	**-**	**-**	**-**	**-**	**-**	**-**	**-**	**-**
Triolein	*84.94*	-	-	-	-	-	-	-	-

Table 3.2. GC-MS analysis of the feed and product mixtures in the catalytic upgrading of yellow grease (25 wt% in C12) over 20% Ni-5% Cu/Al_2O_3 at 350 °C and WHSV = 4.7 h^{-1}.

Compound	Feed	1 h	2 h	3 h	4 h	5 h	6 h	7 h	8 h
Total Hydrocarbons	-	**100.0**	**100.0**	**100.0**	**100.0**	**100.0**	**100.0**	**100.0**	**100.0**
Normal Alkanes	-	*99.74*	*99.78*	*100.0*	*100.0*	*99.61*	*100.0*	*99.30*	*100.0*
Undecane (C11)	-	5.76	4.54	4.05	3.63	3.26	3.08	2.83	2.49
Tetradecane (C14)	-	0.96	0.69	0.59	0.57	0.47	0.45	0.45	0.40
Pentadecane (C15)	-	10.77	10.32	10.35	10.76	10.08	10.16	10.78	10.49
Hexadecane (C16)	-	4.75	4.09	3.80	3.74	3.32	3.10	2.92	2.71
Heptadecane (C17)	-	72.33	74.92	76.32	75.92	77.03	77.77	77.09	78.90
Octadecane (C18)	-	1.66	1.74	1.72	1.87	1.97	2.01	1.93	2.01
Nonadecane (C19)	-	2.20	2.09	1.95	2.19	2.19	2.13	1.94	1.82
Heneicosane (C21)	-	0.72	0.74	0.65	0.73	0.69	0.68	0.71	0.60
Tricosane (C23)	-	0.58	0.64	0.57	0.59	0.60	0.62	0.65	0.58
Branched Alkanes	-	-	*0.22*	-	-	-	-	*0.23*	-
Cholestane	-	-	0.22	-	-	-	-	0.23	-
Olefins	-	*0.26*	-	-	-	-	-	-	-
Heptadecene (C17:1)	-	0.26	-	-	-	-	-	-	-
Unidentified	-	-	-	-	-	*0.39*	-	*0.47*	-
Total Oxygenates	**100.0**	**-**	**-**	**-**	**-**	**-**	**-**	**-**	**-**
Fatty Acids	*4.45*	-	-	-	-	-	-	-	-
Oleic Acid (C18:1)	4.45	-	-	-	-	-	-	-	-
Monoolein	*0.69*	-	-	-	-	-	-	-	-
Diolein	*9.92*	-	-	-	-	-	-	-	-
Triolein	*84.94*	-	-	-	-	-	-	-	-

Table 3.3. C1-C3 mass balance of the catalytic upgrading of yellow grease (25 wt% in C12) over 20% Ni/Al_2O_3 and 20% Ni-5% Cu/Al_2O_3 at 350 °C and WHSV = 4.7 h^{-1}.

Entry	Description	20% Ni/Al_2O_3	20% Ni-5% Cu/Al_2O_3
1	Max. amount of CO_x via deCO_x of lipid feed	8.00 mmol	8.00 mmol
2	Amount of CO_x in the gaseous products	0.03 mmol	0.03 mmol
3	Amount of CO_x to account for (1-2)	7.97 mmol	7.97 mmol
4	Amount of CH_4 in the gaseous products	36.93 mmol	27.47 mmol
5	Amount of CH_4 stemming from CO_x (3)	7.97 mmol	7.97 mmol
6	Amount of CH_4 to account for (4-5)	28.96 mmol	19.50 mmol
7	Max. amount of C_3H_8 via deCO_x of TAGs[a]	2.70 mmol	2.70 mmol
8	Amount of C_3H_8 in reaction products	0.32 mmol	0.30 mmol
9	Amount of C_3H_8 to account for (7-8)	2.38 mmol	2.40 mmol
10	Amount of C_2H_6 in the gaseous products	1.90 mmol	2.19 mmol
11	Amount of C_3H_8 cracked to C2 and C1 (10)	1.90 mmol	2.19 mmol
12	Amount of C_3H_8 still to account for (9-11)	0.48 mmol	0.21 mmol
13	Amount of CH_4 still to account for (6-11)	27.06mmol	17.31 mmol
14	Amount of C16 in the liquid products	4.80 mmol	1.77 mmol
15	Amount of CH_4 still to account for (13-14)[b]	22.26 mmol	15.39 mmol
16	Amount of C15 in the liquid products[c]	5.52 mmol	5.63 mmol
17	Amount of C14 in the liquid products	1.20 mmol	0.31 mmol
18	Amount of CH_4 unaccounted for (15-17×3)[b]	18.66 mmol	14.46 mmol

[a] Triacylglycerides (triglycerides).

[b] Assuming the entirety of these products stems from the cracking of C17 via the sequential loss of terminal carbons.

[c] No C15 is assumed to stem from the cracking of C17 via sequential loss of terminal carbons since the amount of C15 in the liquid products is practically identical to the theoretical amount (5.68 mmol) of C15 that would be produced from the deCO_x of the C16 fatty acid chains present in the feed (see Figure 3.1).

Table 3.4. GC-MS analysis of the feed and product mixtures in the catalytic upgrading of hemp oil (25 wt% in C12) over 20% Ni/Al_2O_3 at 350 °C and WHSV = 4.7 h^{-1}.

Compound	Feed	1 h	2 h	3 h	4 h	5 h	6 h	7 h	8 h
Total Hydrocarbons	**-**	**100.0**	**100.0**	**100.0**	**100.0**	**100.0**	**100.0**	**100.0**	**100.0**
Normal Alkanes	-	*99.02*	*98.79*	*98.32*	*98.96*	*98.76*	*98.69*	*98.13*	*98.76*
Decane (C10)	-	4.70	3.34	3.52	2.25	2.45	2.22	1.04	1.23
Undecane (C11)	-	9.81	6.83	6.77	5.11	5.02	5.51	4.23	3.09
Tetradecane (C14)	-	4.40	3.55	3.32	2.99	2.98	2.83	3.59	3.92
Pentadecane (C15)	-	11.90	11.54	11.34	11.37	11.20	10.92	12.02	11.77
Hexadecane (C16)	-	10.32	9.54	9.29	9.10	8.91	9.09	8.80	8.77
Heptadecane (C17)	-	53.45	58.84	58.54	61.46	61.21	60.37	61.32	62.16
Octadecane (C18)	-	2.31	2.53	2.63	2.73	2.97	2.85	3.04	2.95
Nonadecane (C19)	-	0.77	0.90	0.74	0.80	0.86	0.85	0.85	0.84
Icosane (C20)	-	0.22	0.20	0.19	0.33	0.22	0.35	0.22	0.24
Henicosane (C21)	-	0.52	0.42	0.48	0.52	0.51	0.60	0.56	0.59
Docosane (C22)	-	0.17	0.13	0.15	0.16	0.16	0.22	0.20	0.17
Tricosane (C23)	-	0.21	0.34	0.42	0.57	0.64	0.79	0.62	0.82
Tetracosane (C24)	-	0.07	0.10	0.15	0.20	0.21	0.28	0.23	0.24
Pentacosane (C25)	-	0.10	0.16	0.27	0.43	0.51	0.64	0.49	0.67
Hexacosane (C26)	-	0.07	0.13	0.23	0.45	0.53	0.62	0.46	0.67
Heptacosane (C27)	-	-	0.07	0.03	0.08	0.06	0.10	0.05	0.11
Octacosane (C28)	-	-	0.05	0.10	0.11	0.13	0.24	0.16	0.26
Nonacosane (C29)	-	-	0.04	0.05	0.15	0.08	0.09	0.08	0.10
Triacontane (C30)	-	-	0.08	0.08	0.14	0.10	0.10	0.16	0.15
Olefins	-	*0.98*	*1.21*	*1.68*	*1.04*	*1.24*	*1.31*	*1.87*	*1.24*
Heptadecene (C17:1)	-	0.98	1.21	1.68	1.04	1.24	1.31	1.87	1.24
Total Oxygenates	**100.0**	**-**	**-**	**-**	**-**	**-**	**-**	**-**	**-**
Triglycerides	*100.0*	-	-	-	-	-	-	-	-
Trilinolein	100.0	-	-	-	-	-	-	-	-

Table 3.5. GC-MS analysis of the feed and product mixtures in the catalytic upgrading of hemp oil (25 wt% in C12) over 20% Ni-5% Cu/Al_2O_3 at 350 °C and WHSV = 4.7 h^{-1}.

Compound	Feed	1 h	2 h	3 h	4 h	5 h	6 h	7 h	8 h
Total Hydrocarbons	**-**	**99.83**	**100.0**	**100.0**	**100.0**	**100.0**	**100.0**	**100.0**	**100.0**
Normal Alkanes	-	*99.17*	*99.37*	*99.33*	*99.41*	*99.45*	*99.36*	*99.31*	*99.35*
Decane (C10)	-	0.43	0.24	0.30	0.31	0.14	0.16	0.18	0.40
Undecane (C11)	-	1.85	2.64	2.10	2.03	2.41	1.29	2.42	1.93
Tetradecane (C14)	-	0.67	1.25	0.71	0.66	0.77	0.60	0.58	0.79
Pentadecane (C15)	-	8.40	11.40	10.87	11.22	11.03	11.48	11.18	10.99
Hexadecane (C16)	-	5.64	4.93	4.46	4.24	3.83	4.04	3.79	3.43
Heptadecane (C17)	-	78.56	75.48	77.47	77.55	77.99	78.63	77.86	78.49
Octadecane (C18)	-	1.84	1.73	1.67	1.64	1.73	1.64	1.69	1.81
Nonadecane (C19)	-	0.80	0.90	0.81	0.82	0.77	0.75	0.77	0.77
Icosane (C20)	-	0.06	0.09	0.08	0.11	0.06	0.05	0.08	0.08
Henicosane (C21)	-	0.49	0.46	0.53	0.47	0.45	0.45	0.46	0.44
Docosane (C22)	-	0.10	0.06	0.10	0.06	0.06	0.04	0.06	0.03
Tricosane (C23)	-	0.16	0.14	0.19	0.14	0.15	0.13	0.14	0.11
Tetracosane (C24)	-	0.03	0.01	0.00	0.08	0.02	0.02	0.02	0.03
Pentacosane (C25)	-	0.07	0.01	0.01	0.03	0.01	0.02	0.04	0.02
Hexacosane (C26)	-	0.05	0.02	0.02	0.03	0.01	0.04	0.02	0.02
Olefins	-	*0.66*	*0.63*	*0.67*	*0.59*	*0.55*	*0.64*	*0.69*	*0.65*
Heptadecene (C17:1)	-	0.66	0.63	0.67	0.59	0.55	0.64	0.69	0.65
Total Oxygenates	**100.0**	**0.17**	**-**	**-**	**-**	**-**	**-**	**-**	**-**
Triglycerides	*100.0*	*0.17*	-	-	-	-	-	-	-
Trilinolein	100.0	-	-	-	-	-	-	-	-
Tristearin	-	0.17	-	-	-	-	-	-	-

Table 3.6. GC-MS analysis of the feed and product mixtures in the catalytic upgrading of yellow grease (75 wt% in C12) over 20% Ni-5% Cu/Al_2O_3 at 375 °C and WHSV = 2.0 h^{-1}.

Compound	Feed	1 h	2 h	3 h	4 h	5 h	6 h	7 h	8 h
Total Hydrocarbons	-	**-**	**-**	**100.00**	**100.00**	**100.00**	**100.00**	**100.00**	**100.00**
Normal Alkanes	-	-	-	*91.95*	*93.38*	*95.10*	*95.29*	*95.68*	*96.46*
Decane (C10)	-	-	-	8.91	4.64	2.94	1.30	1.53	0.90
Undecane (C11)	-	-	-	13.84	8.04	5.23	3.29	2.96	1.91
Tetradecane (C14)	-	-	-	6.92	4.75	3.11	2.26	1.79	1.24
Pentadecane (C15)	-	-	-	12.11	11.46	10.41	10.01	9.23	9.10
Hexadecane (C16)	-	-	-	16.28	16.84	14.31	12.17	10.33	8.98
Heptadecane (C17)	-	-	-	32.04	43.73	53.10	58.62	60.74	64.56
Octadecane (C18)	-	-	-	1.08	2.02	2.70	3.44	3.92	4.00
Nonadecane (C19)	-	-	-	0.55	1.17	1.75	2.11	2.37	2.48
Icosane (C20)	-	-	-	0.09	0.24	0.35	0.37	0.44	0.36
Henicosane (C21)	-	-	-	0.10	0.26	0.48	0.60	0.72	0.78
Docosane (C22)	-	-	-	0.01	0.11	0.24	0.27	0.33	0.28
Tricosane (C23)	-	-	-	0.02	0.08	0.26	0.38	0.56	0.68
Tetracosane (C24)	-	-	-	-	0.02	0.11	0.20	0.27	0.33
Pentacosane (C25)	-	-	-	-	0.01	0.08	0.19	0.33	0.54
Hexacosane (C26)	-	-	-	-	-	0.02	0.08	0.16	0.32
Branched Alkanes	-	-	-	*8.05*	*6.62*	*4.90*	*4.71*	*4.32*	*3.54*
Total Oxygenates	**100.0**	**-**	**-**	**-**	**-**	**-**	**-**	**-**	**-**
Fatty Acids	*4.45*	-	-	-	-	-	-	-	-
Palmitic Acid	-	-	-	-	-	-	-	-	-
Stearic Acid	-	-	-	-	-	-	-	-	-
Oleic Acid (C18:1)	4.45	-	-	-	-	-	-	-	-
Monoolein	*0.69*	-	-	-	-	-	-	-	-
Diolein	*9.92*	-	-	-	-	-	-	-	-
Triolein	*84.94*	-	-	-	-	-	-	-	-

Table 3.7. GC-MS analysis of the feed and product mixtures in the catalytic upgrading of yellow grease (75 wt% in C12) over 1 g SiC at 375 °C and WHSV = 2.0 h^{-1}.

Compound	Feed	1 h	2 h	3 h	4 h	5 h	6 h	7 h	8 h
Total Hydrocarbons	**-**	**-**	**3.77**	**4.78**	**5.80**	**6.18**	**5.60**	**6.14**	**4.73**
Normal Alkanes	-	-	*0.64*	*0.45*	*0.27*	*0.23*	*0.14*	*0.16*	*0.18*
Pentadecane (C15)	-	-	0.08	0.08	0.07	0.06	0.05	0.06	0.05
Heptadecane (C17)	-	-	0.56	0.37	0.20	0.17	0.09	0.10	0.13
Olefins	-	-	*3.13*	*4.33*	*5.53*	*5.95*	*5.46*	*5.98*	*4.55*
8-heptadecene	-	-	0.49	0.25	0.50	0.50	0.36	0.45	0.34
Hexacosynes	-	-	2.18	3.59	4.41	4.83	4.41	5.01	3.68
Stigmasta-3,5-diene	-	-	0.46	0.49	0.62	0.62	0.69	0.52	0.53
Total Oxygenates	**100.0**	**-**	**96.23**	**95.22**	**94.20**	**93.82**	**94.40**	**93.86**	**95.27**
Fatty Acids	*4.45*	-	*42.11*	*45.57*	*42.97*	*43.99*	*40.49*	*45.18*	*36.21*
Lauric Acid	-	-	0.33	0.54	0.56	0.63	0.61	0.70	0.55
Palmitic Acid	-	-	2.95	3.56	3.84	3.61	3.67	3.94	3.39
Oleic Acid (C18:1)	4.45	-	33.38	36.22	34.04	35.65	32.79	36.52	29.21
Stearic Acid	-	-	5.45	5.25	4.53	4.10	3.42	4.02	3.06
Monoolein	*0.69*	-	1.14	1.25	1.30	0.85	1.45	1.62	1.84
Diolein	*9.92*	-	1.16	2.73	3.49	2.81	2.99	2.25	1.16
Triolein	*84.94*	-	51.82	45.67	46.44	46.18	49.47	44.80	56.06

:

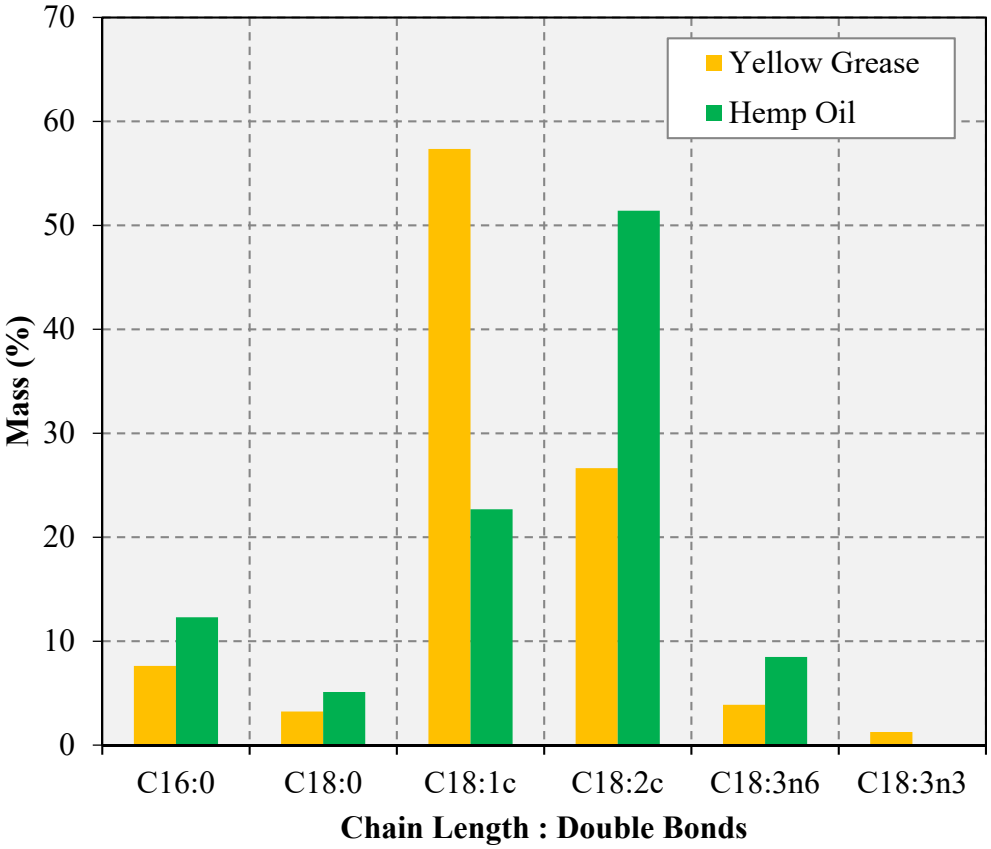

Figure 3.1. Lipid profile for the yellow grease and hemp seed oil used.

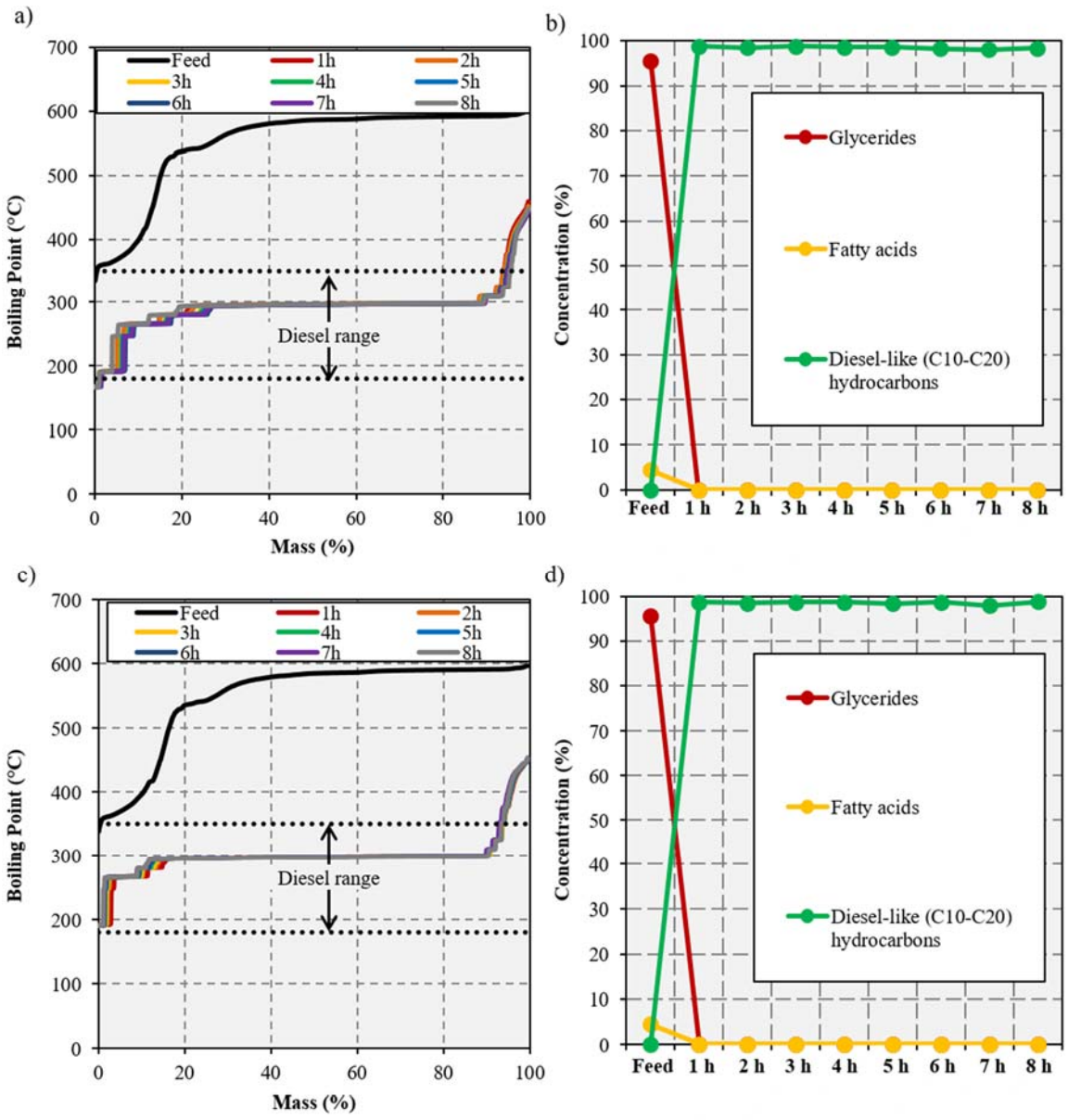

Figure 3.2. BPDPs of 25 wt% yellow grease (feed) and the products collected after 1-8 h of time on stream and GC-MS data showing the evolution of different types of compounds during catalytic upgrading over 20% Ni/Al_2O_3 (a and b) and 20% Ni-5% Cu/Al_2O_3 (c and d) at 350 °C and WHSV=4.75 h^{-1}.

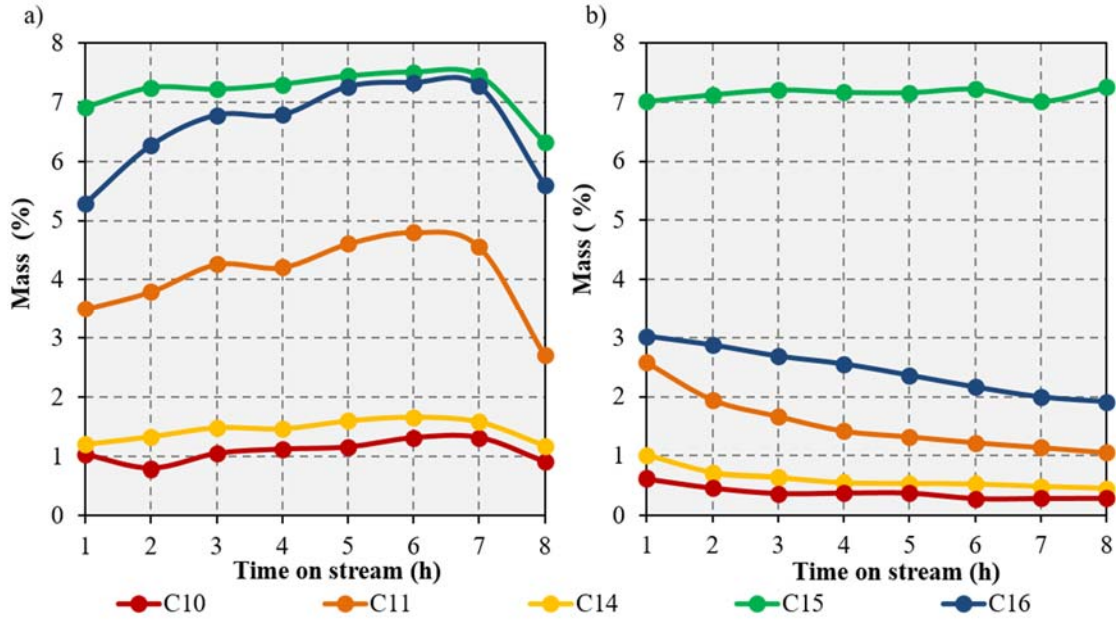

Figure 3.3. Amounts of C10, C11, C14, C15 and C16 in the reaction products collected after 1-8 hours of time on stream during the catalytic upgrading of 25wt % yellow grease over 20% Ni/Al_2O_3 (a) and 20% Ni-5% Cu/Al_2O_3 (b) at 350 °C and WHSV=4.75 h^{-1}.

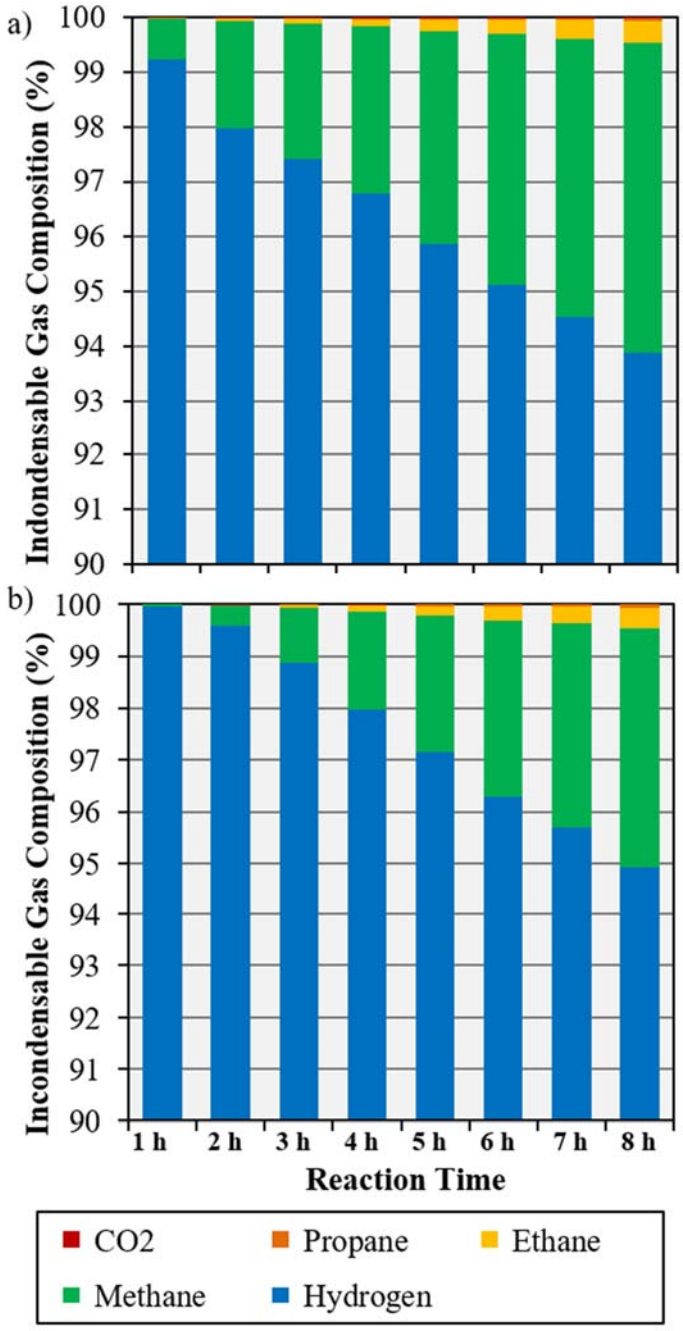

Figure 3.4. Composition of incondensable gases collected after 1-8 hours of time on stream during the catalytic upgrading of 25 wt% yellow grease over 20% Ni/Al_2O_3 (a) and 20% Ni-5% Cu/Al_2O_3 (b) at 350 °C and WHSV=4.75 h^{-1}.

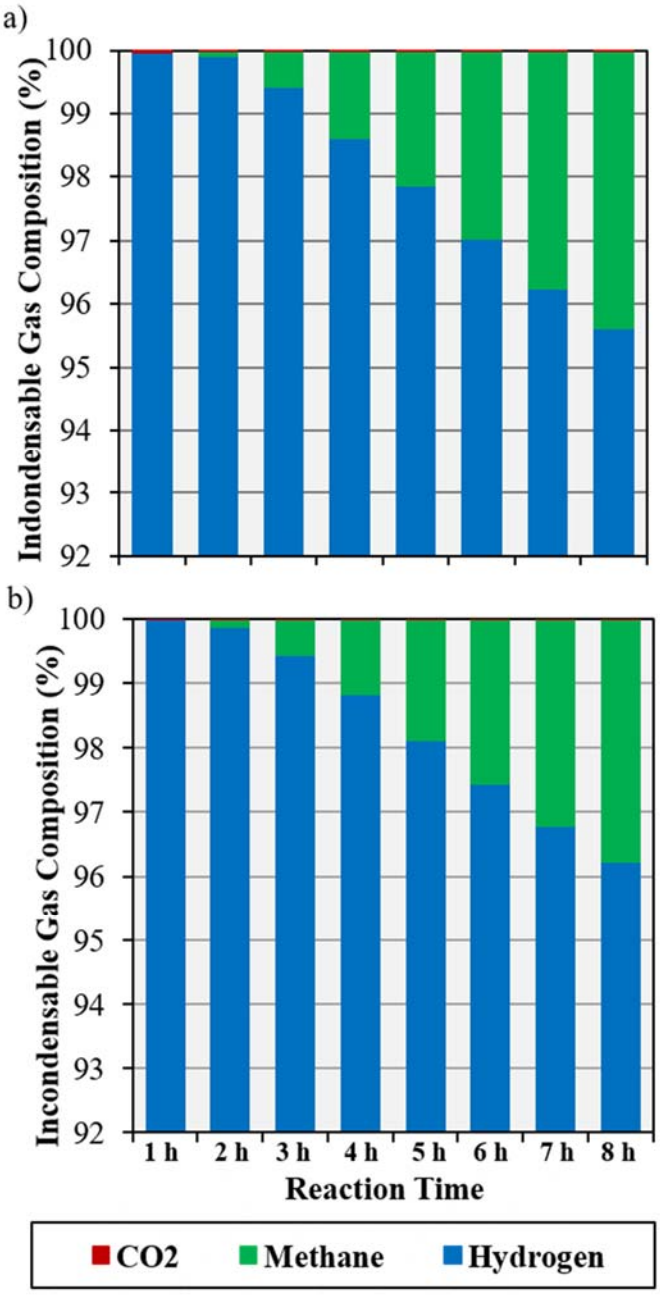

Figure 3.5. Composition of gases collected after 1-8 hours of time on stream during the catalytic methanation of ~5 vol% CO_2 in H_2 over 20% Ni/Al_2O_3 (a) and 20% Ni-5% Cu/Al_2O_3 (b) at 350 °C.

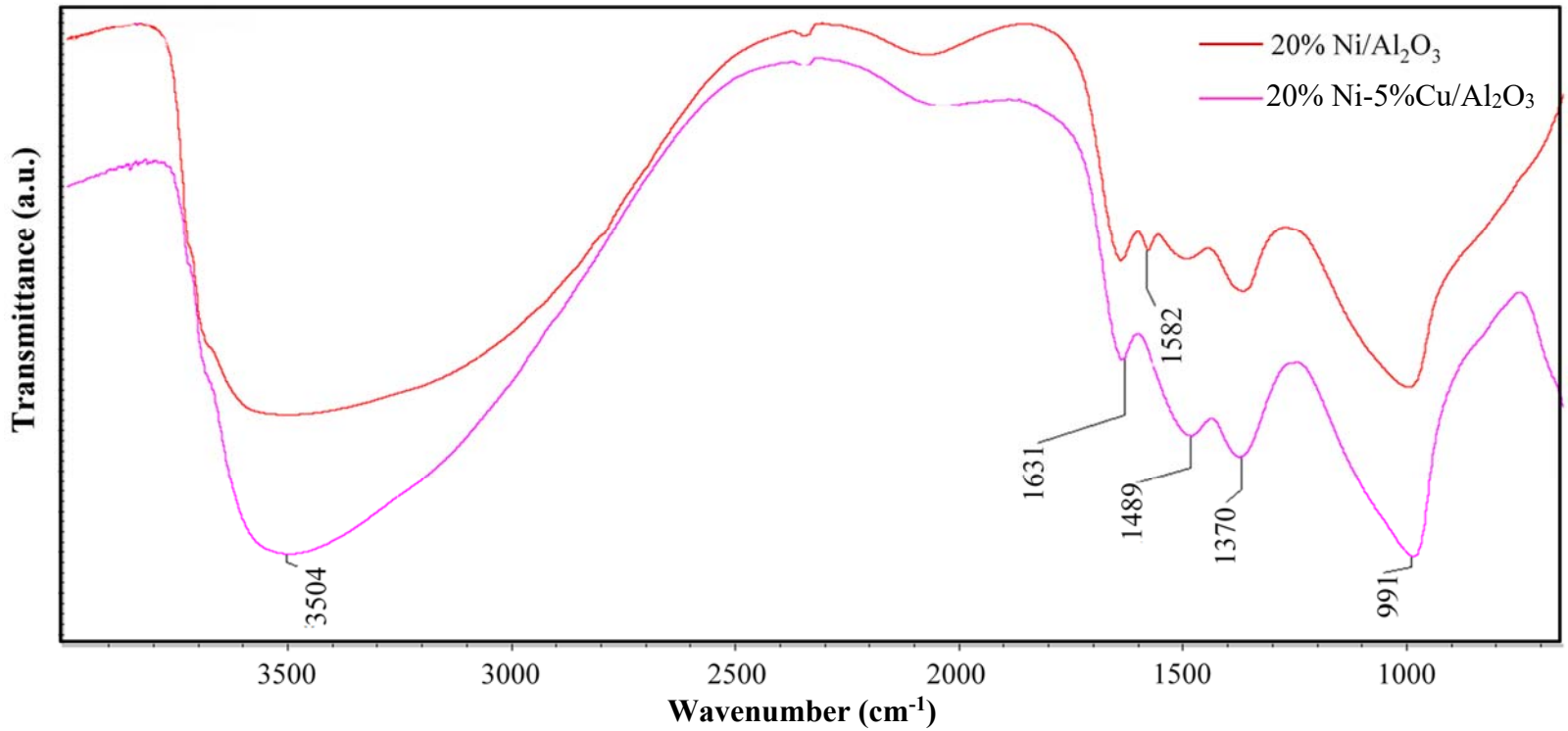

Figure 3.6. DRIFTS spectra of the spent 20% Ni/Al_2O_3 and 20% Ni-5% Cu/Al_2O_3 catalysts.

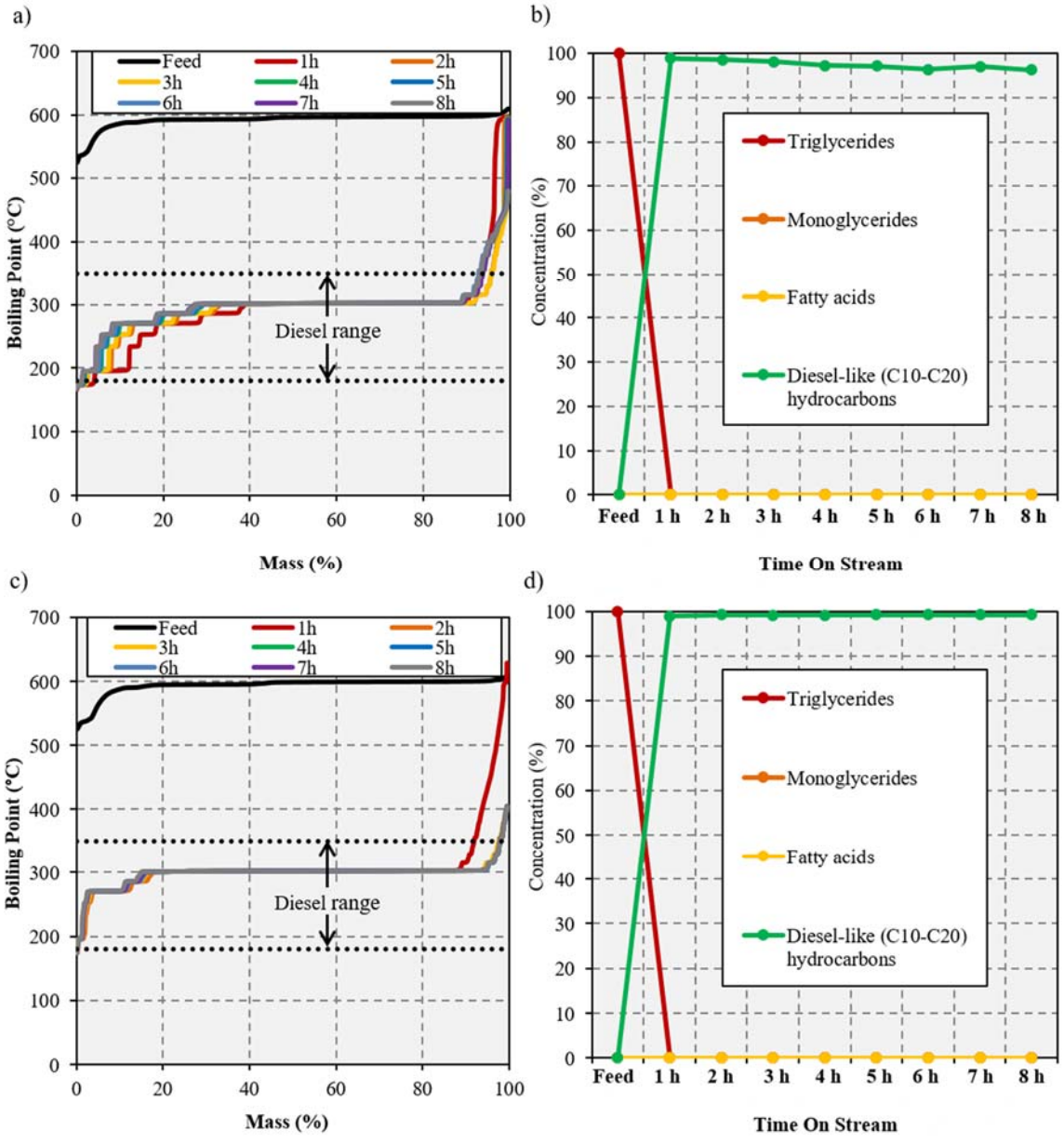

Figure 3.7. BPDPs of 25 wt% hemp oil (feed) and the products collected after 1-8 hours of time on stream and GC-MS data showing the evolution of different types of compounds during catalytic upgrading over 20% Ni/Al_2O_3 (a and b) and 20% Ni-5% Cu/Al_2O_3 (c and d) at 350 °C and WHSV=4.81 h^{-1}.

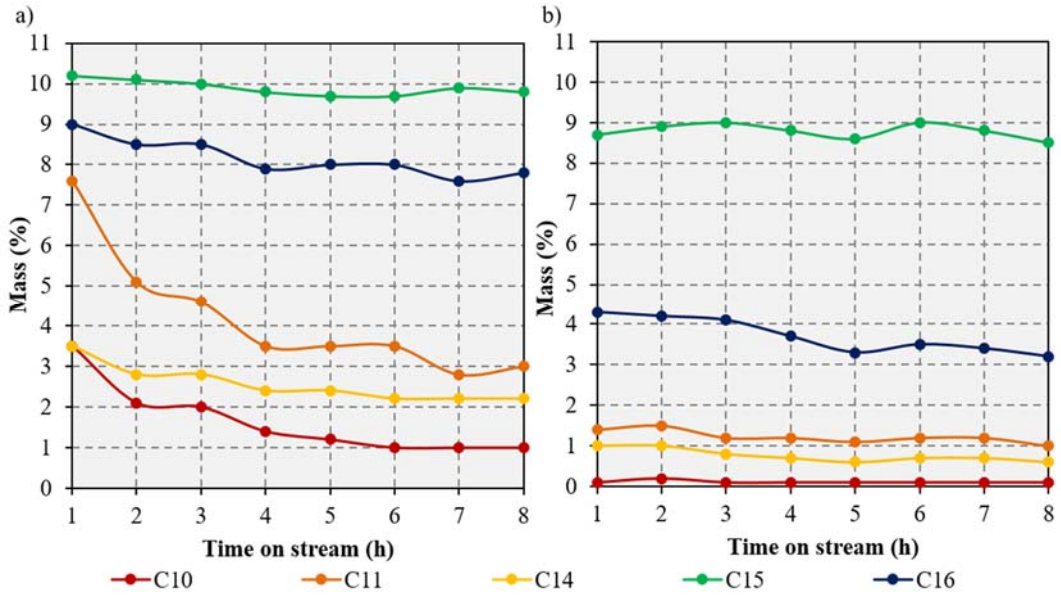

Figure 3.8. Amounts of C10, C11, C14, C15 and C16 in the reaction products collected after 1-8 hours of time on stream during the catalytic upgrading of 25 wt% hemp oil over 20% Ni/Al_2O_3 (a) and 20% Ni-5% Cu/Al_2O_3 (b) at 350 °C and WHSV=4.81 h^{-1}.

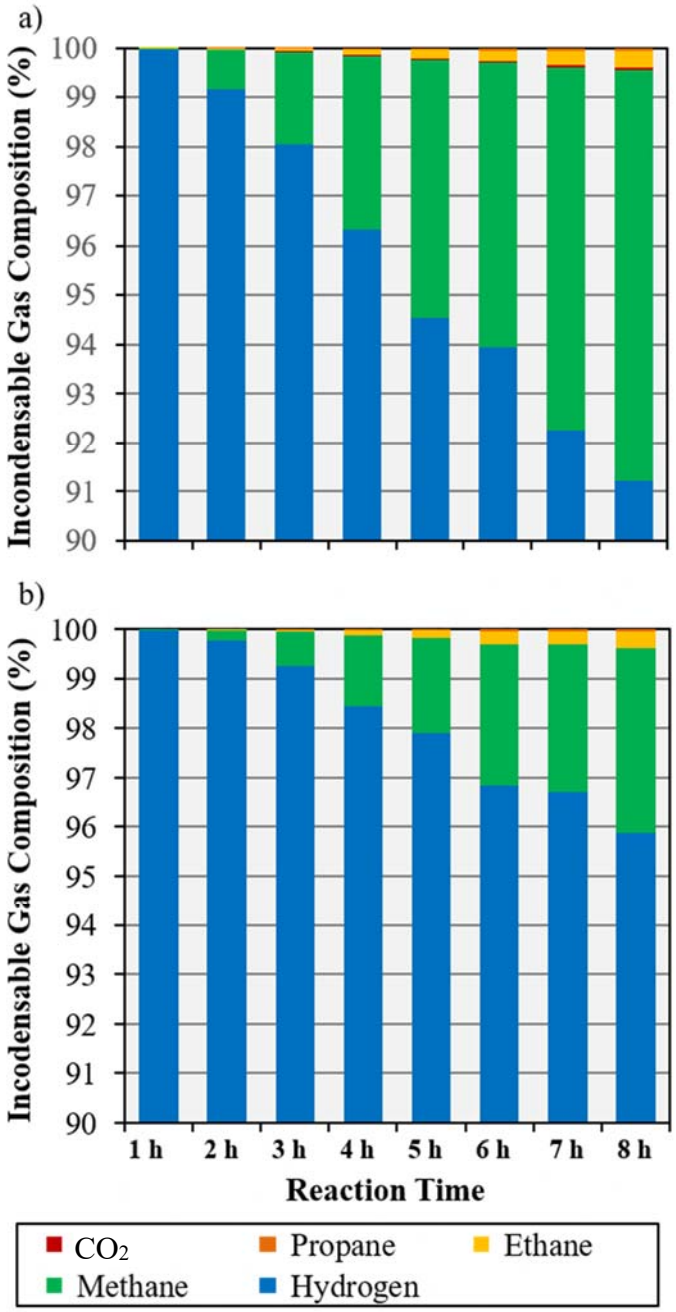

Figure 3.9. Composition of incondensable gases collected after 1-8 hours of time on stream during the catalytic upgrading of 25 wt% hemp oil over 20% Ni/Al_2O_3 (a) and 20% Ni-5% Cu/Al_2O_3 (b) at 350 °C and WHSV=4.81 h^{-1}.

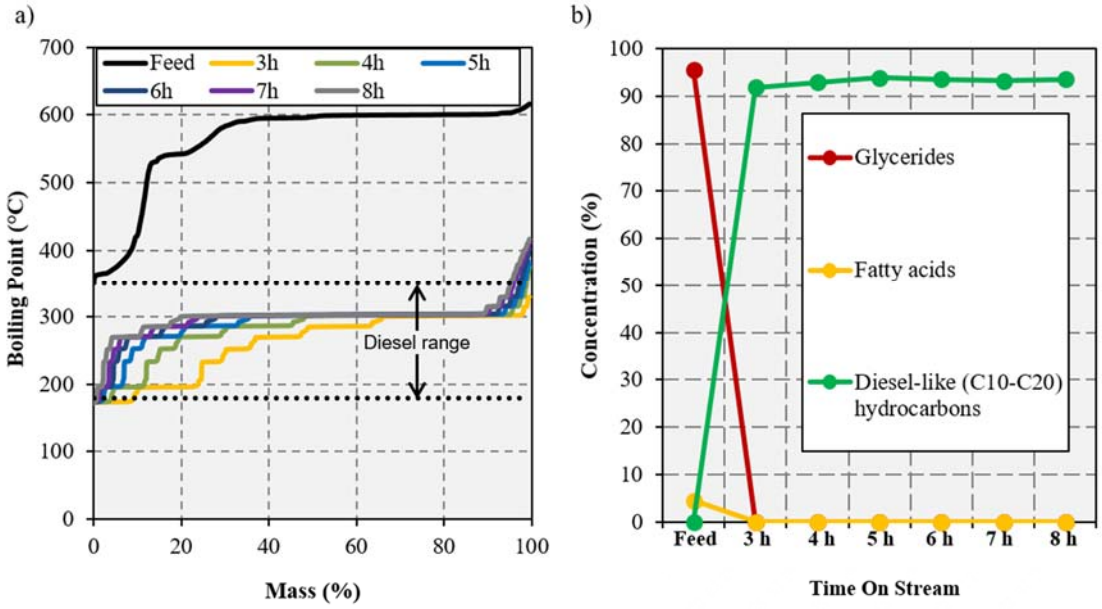

Figure 3.10. BPDPs of 75 wt% yellow grease (feed) and the products collected after 1-8 hours of time on stream and GC-MS data showing the evolution of different types of compounds during catalytic upgrading over 20% Ni-5% Cu/Al_2O_3 (a and b) at 375 °C and WHSV=2.03 h^{-1}.

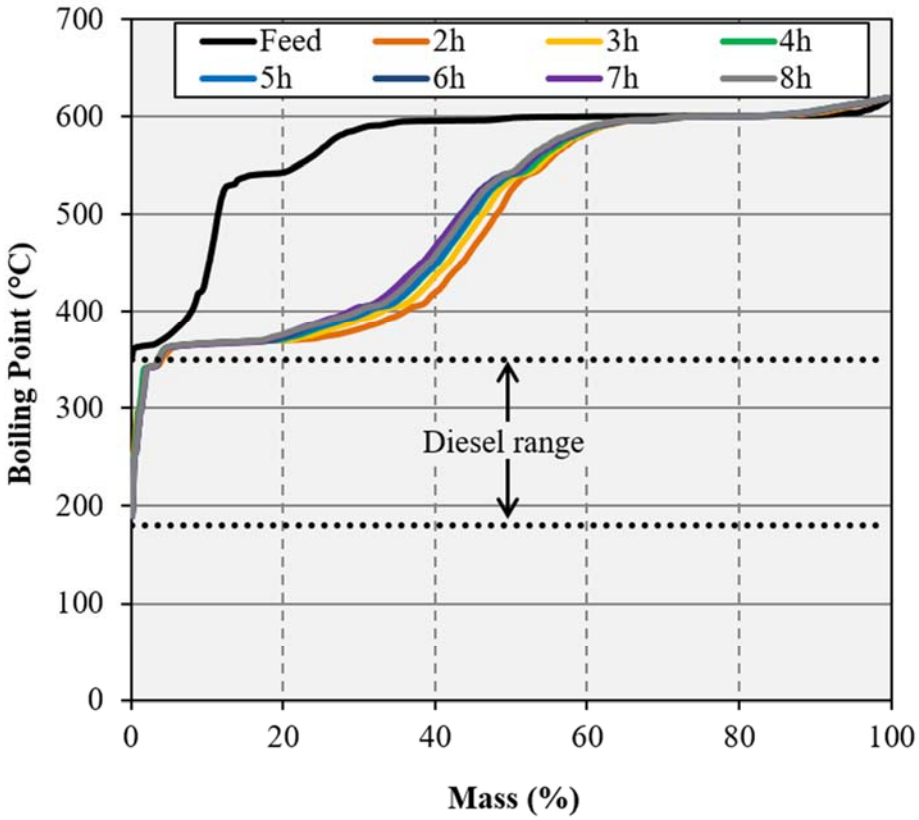

Figure 3.11. BPDP of yellow grease (75 wt% in C12) and the products collected after 1-8 hours of time on stream during a blank experiment performed using SiC at 375 °C and WHSV=2.0 h^{-1}.

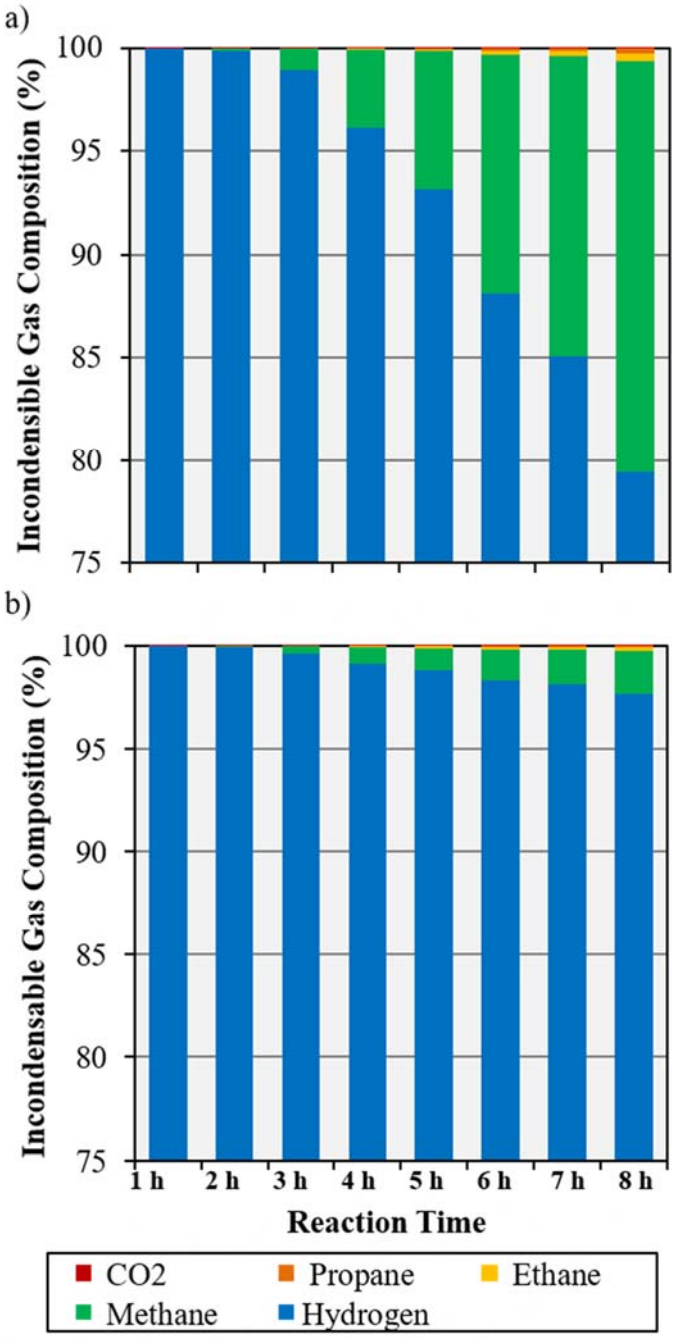

Figure 3.12. Composition of incondensable gases collected after 1-8 hours of time on stream during the catalytic upgrading of 75 wt% yellow grease over 20% Ni/Al_2O_3 (a) and 20% Ni-5% Cu/Al_2O_3 (b) at 350 °C and WHSV=4.81 h^{-1}

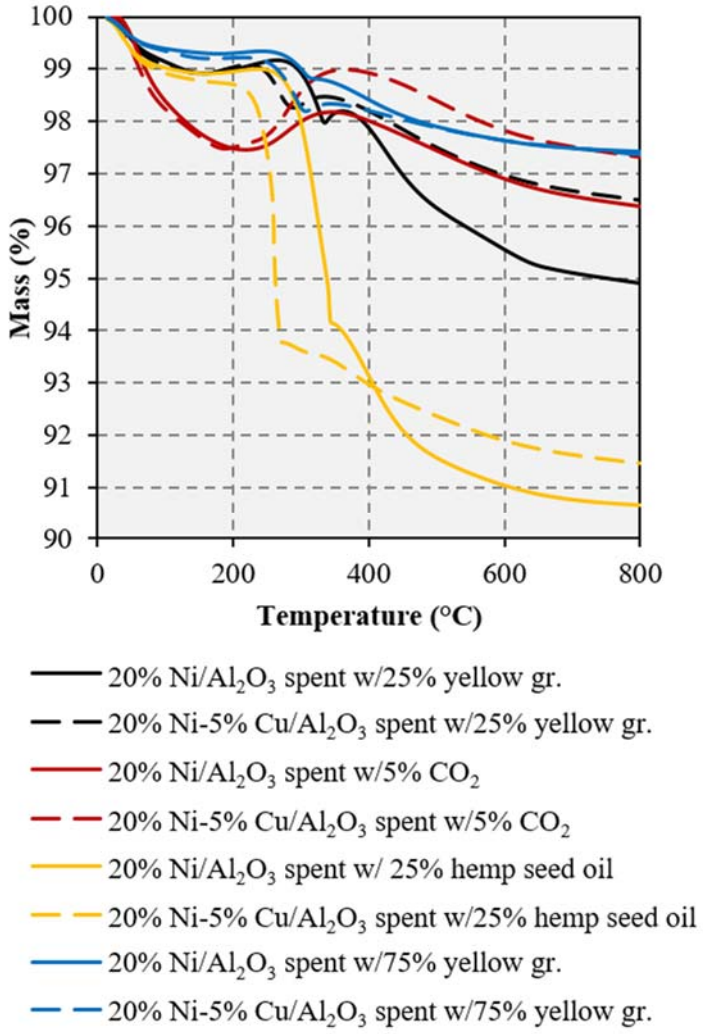

Figure 3.13. TGA profiles (acquired under air) of catalysts spent in the catalytic upgrading of yellow grease, in the catalytic methanation of CO_2, and in the catalytic upgrading of hemp oil.

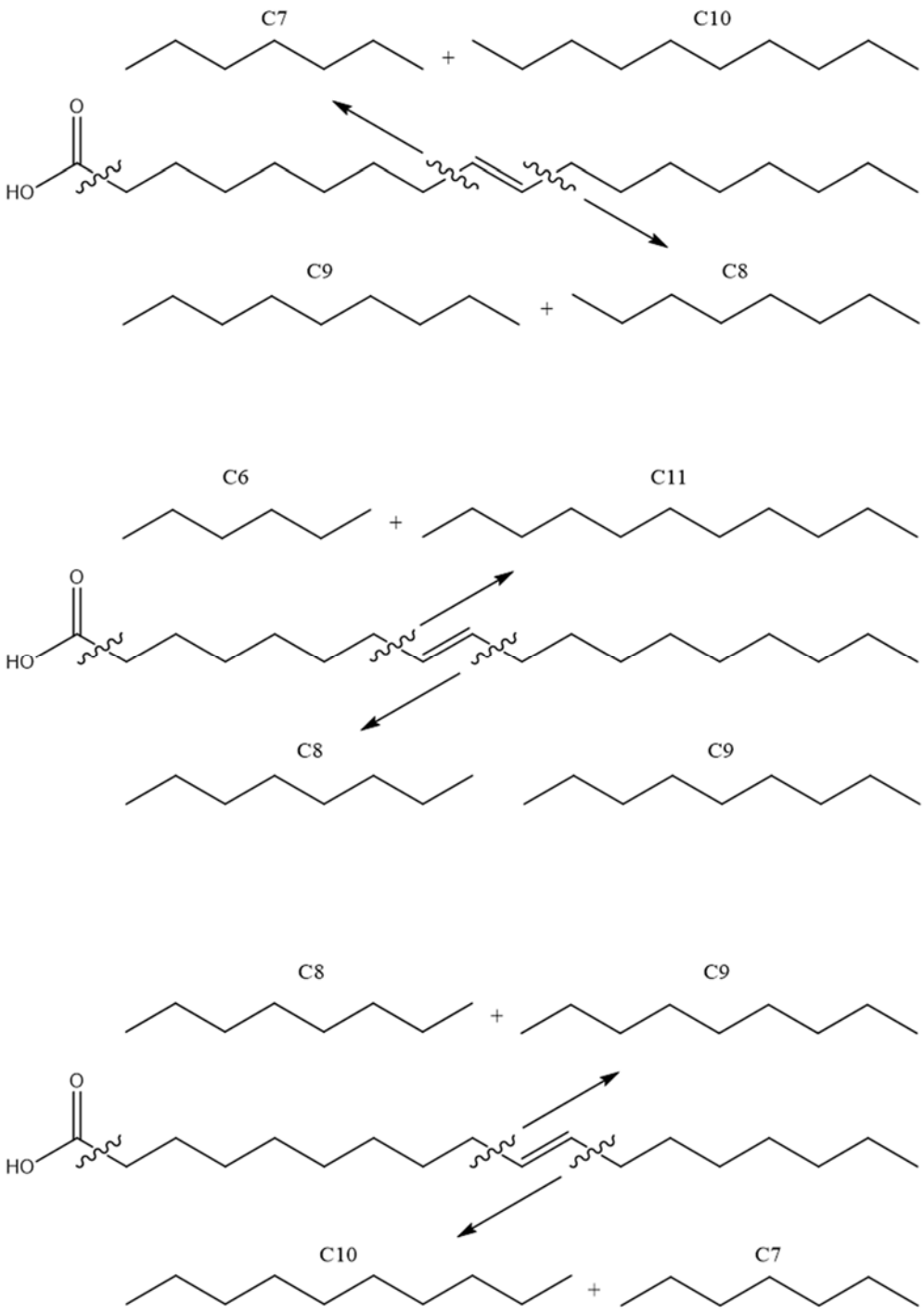

Scheme 3.1. Internal cracking of oleic acid and its positional isomers in which the double bond is removed one position in either direction of the C18 chain and where the olefinic cracking products are assumed to undergo hydrogenation.

Chapter 4. Continuous catalytic deoxygenation of waste free fatty acid-based feeds to fuel-like hydrocarbons over a supported Ni-Cu catalyst.

4.1. Introduction

Due to the high fuel demand in the transportation sector, renewable fuels will require multiple feed sources. Currently, two main feeds – namely, corn and soybean oil – are used in considerable amounts in an attempt to move our energy consumption closer to carbon neutrality [59, 60]. Indeed, the use of biofuels derived from corn and soybean oil results in a decrease in greenhouse gas emissions (compared to petroleum-derived liquid fuels) of 12 and 41%, respectively [60]. However, an ever growing population presents critical challenges, including the need for these crops to meet an increased food demand and the moral conflicts tied to the rise in food prices observed when edible crops are used for fuel production [229]. Alternatives such as the use of inedible oleaginous plants that thrive in arid or degraded soil – such as Jatropha curcas – prevents disruption of the food supply and minimizes agrichemical pollution [60, 61]. Unfortunately, the current scale of cultivation of these crops is insufficient to meet fuel demand. Recently, microalgae have been shown to produce oil in greater quantities than terrestrial crops but the energy consumption and cost associated with both cultivation and processing are issues that still need to be addressed [67, 69]. In short, additional oleaginous feed sources are still required to meet the fuel demand. Therefore, fats, oils and grease (FOG) waste streams have garnered considerable interest as feedstock for the production of renewable fuels due to their low cost and widespread availability.

Promising oleaginous waste streams for renewable fuel production include yellow grease (waste cooking oil) and brown grease. While yellow grease has already been discussed in a previous chapter, brown grease consists of FOG collected from grease traps,

i.e., devices engineered to separate insoluble oils and other material from commercial kitchen wastewater streams [230]. Many studies have struggled to identify a precise amount of usable brown grease in part due to its current method of collection and disposal. Indeed, only some municipalities require brown grease to be delivered directly to wastewater treatment plants, where volumes can be closely monitored [230]. Nevertheless, the United States Department of Energy has recently estimated that the annual production of brown grease in the United States alone ranges from 1.5 to 1.7 million tons [230], nearly all of which is either incinerated or transported to landfills. Therefore, the valorization of this stream is of significant interest. However, brown grease remains a problematic feed because of its high water content and contamination with waste food and other insoluble materials. Moreover, albeit biodiesel represents the primary renewable fuel to which oleaginous feeds are currently converted, this transformation takes place industrially via transesterification of esters. Notably, the high free fatty acid (FFA) content of brown grease is problematic in this process, as it results in catalyst deactivation and contamination of the fuel with soap products [7]. Admittedly, the fatty acids can be separated from triglyceride-based streams (typically via steam stripping) and converted to fuels via acid-catalyzed esterification but the process is not widely utilized. Therefore, the valorization of brown grease and other fatty acid-based feeds – including the waste FFAs stemming from the purification of triglyceride feeds via steam distillation in the biodiesel industry – through another process is desirable.

The catalytic deoxygenation of FOG to fuel-like hydrocarbons has been discussed as an alternative approach to transesterification and/or esterification for the production of renewable fuels. Moreover, the advantages of performing the deoxygenation via

decarboxylation/decarbonylation ($deCO_x$) as opposed to via hydrodeoxygenation (HDO) have been discussed in previous chapters. Unfortunately, the majority of $deCO_x$ investigations to date employ model lipid compounds in lieu of realistic feedstocks and even fewer studies incorporate oleaginous waste streams as opposed to oils derived from terrestrial plants. Nevertheless, the catalytic deoxygenation of some FOG waste streams to fuel-like hydrocarbons has been reported [71, 72, 74, 77], albeit most work has focused on the use of costly noble metal catalyst which can be industrially prohibitive. Notably, the use of an inexpensive 20% Ni-5% Cu/Al_2O_3 catalyst to deoxygenate yellow grease has been demonstrated with near quantitative yields of fuel-like hydrocarbons [74], although it should be noted that the feed used was >85% triglycerides. Indeed, the majority of realistic feedstocks employed in deoxygenation studies – such as soybean oil [58] – are mostly composed of triglycerides, which is of significance since carboxylic acids have been shown to be less active towards deoxygenation than esters [231]. This is concerning due to the fact that the majority of waste streams in general, and brown grease in particular, predominately consist of fatty acids. Therefore, catalysts considered for this process must possess the ability to convert concentrated fatty acid feeds if they are to avoid the feed-related limitations found in biodiesel production. Another potential complication of waste streams is a high degree of unsaturation. Relative to saturated feeds, unsaturated feeds typically yield more undesirable cracking products [87] and cause decreased catalyst activity, stemming from competitive adsorption and reaction of the carbon-carbon double bonds [77]. Therefore, catalyst development must take into account these considerations.

There have been few attempts to use brown grease as a feed for renewable fuel production reported in the literature. Indeed, some authors have investigated the use of

brown grease as a feed for biodiesel synthesis using homogenous catalysts [232]. However, the oxygen content in the resulting fuel limits its ability to function as a drop-in replacement for fossil fuels. Alternatively, Sari *et al*. were able to deoxygenate brown grease to fuel-like hydrocarbons, albeit these authors employed a Pd/C catalyst comprising an expensive active metal and a support that precludes the catalyst from being easily regenerated upon deactivation [77]. Moreover, experiments were performed in batch and semi-batch reactors, the use of which would be prohibitive in industrial settings due to the labor and downtime required to remove products and add new feed. Therefore, for the purposes of this study, realistic fatty acid feeds as well as an industrially relevant set of reactor and reaction conditions were employed. To the best of the author's knowledge, non-sulfided Ni catalysts have not been tested to date in a continuous fixed bed reactor with a realistic feed and allowed to reach steady state, which implies that catalysts stability and the prospect of online catalyst regeneration have not been studied either. Therefore, investigating the ability of the inexpensive Ni-Cu catalyst described in previous chapters to convert realistic FFA feeds under industrially relevant conditions is necessary if the technology is to become a commercially viable option for fuel production.

4.2. Experimental

4.2.1. Catalyst preparation

Catalysts were prepared by excess wetness impregnation using $Ni(NO_3)_2 \bullet 6H_2O$ (Alfa Aesar) and $Cu(NO_3)_2 \bullet 3H_2O$ (Sigma Aldrich) as the metal precursors. Beads of γ-Al_2O_3 (Sasol; surface area of 216 m^2/g) were used as the support and were crushed to a particle size of <150 μm before the impregnation. The target metal loadings for the catalyst

were 20 wt% Ni and 5 wt% Cu. The impregnated catalyst was dried overnight at 60 °C under vacuum prior to calcination for 3 h at 500 °C in static air. The catalyst and SiC catalyst diluent (Kramer Industries) were sieved separately to a particle size between 150-300 μm and stored in a vacuum oven at 60 °C until used.

4.2.2. Catalyst characterization

The surface area, pore volume and average pore radius of the fresh and spent catalyst were determined by N_2 physisorption using previously described instruments and methods [15]. A small sample of the catalyst after the first 100 h on stream (in an experiment involving two 100 hour cycles and an intermediate catalyst regeneration step) was subjected to thermogravimetric analysis (TGA) under flowing air (50 mL/min) on a TA instruments Discovery Series thermogravimetric analyzer. The temperature was ramped from room temperature to 800 °C at a rate of 10 °C/min. The same TGA procedure was used on the spent catalyst after the second 100 h cycle. Diffuse reflectance infrared Fourier transform spectroscopy (DRIFTS) was performed on the fresh and the spent catalyst after CO adsorption. The catalysts were dried under flowing Ar (50 mL/min) at 200 °C for 2 h and allowed to cool to 25 °C. The catalyst was then subjected to flowing 1% CO/Ar (50 mL/min) at 25 °C for 1 h, followed by Ar purging to remove gas phase CO and weakly absorbed CO before the spectrum was collected. The catalyst sample was then heated to 200 °C under flowing Ar (50 mL/min) and complete CO desorption was monitored by a return of the DRIFTS signal to a previously established baseline. The gas flow was then switched to 10% H_2/N_2 (50 mL/min) as the temperature was increased to 400 °C and held for 1 h. The catalyst was then cooled to 25 °C under flowing Ar (50

mL/min) to remove excess H_2. The catalyst was again subjected to flowing 1% CO/Ar (50 mL/min) at 25 °C for 1 h, followed by Ar purging to remove gas phase CO and weakly absorbed CO before spectra were collected.

4.2.5. Feed Preparation

A waste FFA feedstock was obtained from the steam stripping of triglyceride-based feeds used for biodiesel synthesis. Brown grease from waste water grease traps was supplied by Pincelli and Associates. The brown grease was mixed vigorously with 25 wt% chloroform (HPLC grade, supplied by J.T. Baker) for 2 h at 30 °C. The resulting solution was filtered with occasional heating to counter the solidification of fats. The water layer from the resulting filtrate was then decanted and the remaining organic mixture was dried using Na_2SO_4. The chloroform was removed by rotatory evaporation and the remaining lipids were diluted to the desired concentration with n-dodecane (99+%, Alfa Aesar).

4.2.4. Continuous fixed-bed deoxygenation experiments

Experiments were operated in continuous mode using a fixed bed stainless steel tubular reactor (1/2 in o.d.) with a stainless steel porous frit to hold the catalyst bed in place. A mixture of equal parts catalyst and SiC diluent (by weight, 1 g total) was used for all experiments, except the blank (sans catalyst) run in which 1 g of the diluent was employed. The catalyst was reduced *in situ* at 400 °C for 3 h under flowing H_2 (60 mL/min). Temperature was monitored using two K-type thermocouples, one introduced from above and made to contact the catalyst bed and one introduced from below and made to contact the aforementioned porous frit under the catalysts bed. For experiments in which the

reaction atmosphere was not pure H_2, the reactor was purged after the reduction with Ar and pressurized with the reaction gas to 580 psi. The pressure was monitored both upstream and downstream of the catalyst bed by Omega digital pressure gauges. After the system was pressurized, the catalyst bed was heated to the desired reaction temperature (275-375 °C). The liquid feed solution was introduced to the reactor using a Harvard Apparatus syringe pump equipped with an 8 mL syringe, either at 0.043 mL/min for the FFA feed (25 wt% in C12) or at 0.021 mL/min for brown grease (50 wt% in C12) to achieve a weight hour space velocity (WHSV) of 1 h^{-1}. The flow of the reaction gas was held at 60 mL/min for the duration of the experiment. Liquid products were sampled from a liquid-gas separator (kept at 0 °C) placed downstream from the catalyst bed. Incondensable gases were directed to a dry test meter before being collected in Tedlar® gas sample bags. Gas sample bags were changed every time a liquid sample was taken to ensure that the gas samples analyzed and the liquid samples collected could be correlated.

4.2.5 Liquid and gaseous product analysis

The liquid products were analyzed using a combined simulated-distillation-GC and GC-MS method specifically devised to identify and quantify the products obtained in the upgrading of fats and oils to hydrocarbons. Detailed information about the development and application of this method is available elsewhere [233]. Briefly, the analyses were performed using an Agilent 7890B GC system equipped with an Agilent 5977A extractor MSD and flame ionization detector (FID). The multimode inlet, which contained a helix liner, was run in a split mode (15:1; split flow, 48 mL/min) with an initial temperature of 100 °C. Helium was used as the carrier gas and a 1 μL injection was employed. Upon

injection, the inlet temperature was immediately increased to 380 °C at a rate of 8 °C/min, and the temperature was maintained for the course of the analysis. The oven temperature was increased upon injection from 40 °C to 325 °C at a rate of 4 °C/min, followed by a ramp of 10 °C/min to 400 °C, which was maintained for 12.5 min. The total analysis run time was 91.25 min. An Agilent J&W VF-5ht column (30 m × 250 μm × 0.1 μm) rated to 450 °C was used. Column eluents were directed to a Siltek MXT connector that split the flow into two streams, one leading to the MSD (J&W Ultimetal Plus Tubing, 11 m X 0.25 mm i.d.) and one leading to the FID (J&W Ultimetal Plus Tubing, 5 m X 0.25 mm i.d.). The MS zone temperatures (MS source at 230 °C and quadrupole at 150 °C) were held constant for the duration of the analysis. A 1.75 min solvent delay was implemented and the MSD scanned from 10 to 700 Da. The FID was set to 390 °C with the following gas flow rates: H_2 at 40 mL/min; air at 400 mL/min; He makeup at 25 mL/min. Quantification was performed using cyclohexanone as an internal standard. Agilent MassHunter Acquisition and SimDis Expert 9 (purchased from Separation Systems Inc.) software were respectively used to perform chromatographic programming and to process the GC-FID data acquired. Solvents (i.e., chloroform and dodecane) were quenched and/or subtracted prior to processing the data.

Gaseous samples were analyzed using an Agilent 3000 Micro-GC equipped with 5 Å molecular sieve, PoraPLOT U, alumina and OV-1 columns. The GC was calibrated for all of the gaseous products obtained, including CO_x as well as straight chain C1-C6 alkanes and alkenes.

4.3. Results and Discussion

4.3.1. Catalytic deoxygenation of fatty acids

Detailed characterization of the 20% Ni-5% Cu/Al_2O_3 catalyst employed in this study has been presented in a previous chapter. The composition of the FFA feed obtained by steam stripping a biodiesel feedstock – as determined by simulated distillation GC-MS – is shown in Table 4.1. The feed is mainly composed of 96.2% fatty acids, 2.3% fatty acid esters and 0.6% olefins. The most abundant fatty acids are oleic acid, palmitic acid, and stearic acid (corresponding to ca. 63.5, 21.2 and 9.0 % of the fatty acids, respectively), indicating that the feed is primarily *unsaturated* fatty acids. This feed was upgraded over a 20% Ni-5% Cu/Al_2O_3 catalyst in a fixed bed reactor using a WHSV of 1 h^{-1} and reaction temperatures ranging from 275 to 375 °C. The results of simulated distillation GC-MS analysis of the liquid products from each hour of time on stream are shown in Figure 4.1 and Tables 4.2-4.4. At 275 °C the diesel-like hydrocarbons (C10-C20) yield decreased from 87.5% at 1 h to 69.1% at 8 h on stream, while the selectivity to heavier products (C21-C35) progressively increased over the same time period. The heavy products, listed in Table 4.2, are mainly long chain esters that are formed when alcohol intermediates undergo esterification with fatty acids on the catalyst surface [121]. These side reaction products are less prominent at high reaction temperatures, as evinced by the lack of any oxygenates (heavy or otherwise) observed at 375 °C, albeit the small amount of heavier (C21-C35) hydrocarbons formed at this temperature likely stems from the direct decarboxylation of long chain ester intermediates [121]. Alternatively, these esters can undergo hydrogenolysis to form alcohols and aldehydes, while the former can also be dehydrogenated to the latter as these two products have been show to exist in equilibrium

under hydrogen-rich conditions [121]. In turn, aldehydes can undergo decarbonylation to form diesel-like hydrocarbons. At 325 °C the diesel-like hydrocarbons yield is ≥88% irrespective of time on stream. Notably, near complete deoxygenation occurs at this temperature, with the highest amount of oxygenates accumulating during the last hour of the experiment, totaling only 0.2% of the liquid products. Heavy hydrocarbon products are still formed, but in significantly less quantities than those obtained at 275 °C. Complete deoxygenation occurs at all reaction times sampled when the reaction temperature is increased to 375 °C, the selectivity to diesel-like hydrocarbons being ≥98% irrespective of time on stream. The increase in selectivity to diesel-like hydrocarbons as the reaction temperature increases is most likely due to: 1) the cracking of the long chain hydrocarbons (≥C20) that are observed at lower reaction temperatures; and 2) direct deoxygenation of the fatty acids without formation of the long chain ester intermediate.

4.3.2. Catalytic deoxygenation of brown grease at different temperatures

The GC-MS analysis of the lipids extracted from the brown grease feed is displayed in Table 4.1. The composition is similar to the fatty acid feed with the most abundant FFAs being oleic acid, palmitic acid, and stearic acid. In addition, the brown grease contains 2.66% glycerides (mostly diolein), signifying that the feed contains predominately unsaturated lipids. Notably, this composition is comparable to other brown grease samples described in the literature [77, 234, 235], which confirms that the simple extraction method employed was acceptable in obtaining lipids representative of those contained in brown grease. The lipid concentration for these experiments was increased (from that used in the FFA upgrading runs discussed in Section 4.3.1 above) to 50 wt% lipids in dodecane, while

the WHSV was kept at 1 h^{-1}. The most promising reaction temperatures identified through the FFA upgrading runs – namely, 325 and 375 °C – were investigated to assess the effect of the feed concentration on the deoxygenation of brown grease lipids. The simulated distillation GC-MS results of the liquid products obtained during each hour are shown in Figure 4.2 and Tables 4.5 and 4.6. Quantitative conversion of the brown grease lipids was achieved with the 20% Ni-5% Cu/Al_2O_3 catalyst regardless of the reaction temperature employed. However, the deoxygenation of the brown grease lipids at 325 °C yields more than double the amount of heavy products that was obtained in the free fatty acid experiments under the same temperature, reaching 11% of the total liquid products at 8 h on stream. Other authors have seen an increase in heavy products as the feed concentration increases and suggested that this stems from an increase in the amount of fatty acids present on the catalyst surface [77]. The rise in fatty acid concentration increases the possibility of esterification reactions with the alcohol intermediates, forming long chain esters that can undergo direct decarboxylation to yield heavy hydrocarbons as discussed previously. However, the esters observed in the FFA upgrading experiments were not detected in the brown grease upgrading reaction products, suggesting that rapid decarboxylation occurs upon the formation of the ester intermediates. Remarkably, >94% of the liquid products obtained at each hour from the deoxygenation of the brown grease lipids at 375 °C are diesel-like hydrocarbons. At 375 °C there were a number of liquid products deemed to be hydrocarbons by the GC-MS, although their specific identity could not be determined. Nevertheless, according to the simulated distillation GC of these unidentifiable products, they all boil within the diesel range (180-350 °C). The heavy product formation also

decreased at the higher reaction temperature, the total amount obtained being <6% of the liquid products irrespective of time on stream.

4.3.3. Catalytic deoxygenation of brown grease at different H_2 partial pressures

The presence of H_2 in the reaction atmosphere has been shown to be beneficial for catalyst performance during the deCO_x of lipids even if H_2 is not directly involved in the deoxygenation reaction [9, 56, 182]. Interestingly, some authors have also shown that supported Pd catalysts perform better under lower H_2 partial pressure conditions than under pure H_2 atmospheres [119], and the same effect has been reported for some Ni catalysts [118]. Therefore, it is instructive to investigate the effect of H_2 partial pressure on the deoxygenation of the waste oleaginous feeds used in this study. To this end, the deoxygenation of brown grease was conducted under a reaction atmosphere of 20% H_2/Ar at 375 °C, the GC-MS analysis of the liquid products being shown in Figure 4.3 and Table 4.7, while the incondensable gaseous products are also shown in Figure 4.3 as well. Under 20% H_2, the 20% Ni-5% Cu/Al_2O_3 catalyst quantitatively converts the brown grease feed, leaving no trace of the starting material at any reaction time sampled (see Figure 4.3c). However, the amount of diesel-like hydrocarbons in the reaction products decreases to 86-89% of the total liquid products relative to the 94-98% values observed when the reaction is performed under pure H_2 (see Figure 4.3a). Additionally, the amount of heavy products increases when the reaction is performed under reduced H_2 partial pressure, albeit it is worth noting that only a relatively a small amount (an average of 14.8%) of the total heavy products collected are long chain esters. The increase in the amount of long chain hydrocarbons suggests that after the formation of the ester, the lower H_2 partial pressure

favors direct decarboxylation of ester, as opposed to their hydrogenolysis to afford alcohols and aldehydes [121]. Interestingly, while there is only a small decrease in the yield of diesel-like products, the gaseous products show a noticeable decrease in methane formation when the reaction is performed under reduced H_2 partial pressure (see Figures 4.4b and 4.4d). Indeed, while the amount of CO or CO_2 present in the gaseous products obtained using pure H_2 conditions is negligible and methane represents the vast majority of the gaseous products, when 20% H_2 is employed the gas products contain considerably more CO_2 and less methane than the gas products formed under pure H_2. Therefore, under reduced H_2 partial pressures, methanation of CO_x is disfavored and does not proceed to completion. Instead, the methane formed at lower H_2 partial pressures is likely formed from the fatty acids alkyl chains via the end-chain cracking mechanism discussed in the previous chapter.

4.3.4. Catalyst deactivation and online regeneration

As suggested by the fact that the composition of the gas products is still changing at the end of the reactions discussed up to this point – including the upgrading of the waste FFA feed and the brown grease lipids (but also that of the yellow grease and hemp seed oil feed previously reported [151]) – it can be argued that enough time has not been allowed to elapse for steady state conditions to be attained. Obviously, the latter also hinders an assessment of whether significant catalyst deactivation occurs when a 20% Ni-5% Cu/Al_2O_3 formulations is used to upgrade a realistic feed using industrially relevant reaction conditions. Therefore, the most promising conditions in this study, i.e., 375 °C and a pure H_2 atmosphere – were employed in a run in which the deoxygenation reaction time

was extended to 100 h on stream. After this (first) 100 h cycle, the catalyst was regenerated *in situ* by washing, drying, calcining (in air), and re-reducing the catalyst (under flowing H_2). Parenthetically, the catalyst was calcined for 5 h at 450 °C, which is both the top temperature rating of the furnace employed and a temperature at which the majority of the carbonaceous deposits can be eliminated according to the results of TGA (Figure 4.4). Results from the analysis of representative liquid samples (recovered at 24 h intervals) are shown in Figure 4.5 and Table 4.8, the analysis of the gaseous products from the hours in which a gas sample was taken being shown in Figure 4.6. It should be noted that the results shown correspond to products recovered in a single hour and not to products accumulated over a 24 h period, such that the catalyst performance can be assessed at the specified time intervals with a "time resolution" equal to one hour.

During the first 100 h on stream, quantitative conversion of the brown grease lipids is achieved during the initial 48 h. After that, the amount of fatty acids in the products begins to increase, reaching a total of 8.1% of the total liquid products collected at the end of the first 100 h cycle. The yield of diesel-like hydrocarbon is >92% of the liquid products for the first 48 h on stream, this value decreasing to 82.8% after 96 h on stream. Notably, the amount of methane produced also decreases with time on stream, while the amount of CO_x increases (left of Figure 6). This suggests that sites responsible for methanation and/or end chain cracking are being selectively poisoned as the reaction progresses, which represents a noteworthy result since hydrogen consumption should correspondingly decrease with time on stream without sacrificing significant deoxygenation activity. Equally encouraging is the fact that catalyst performance improves after the catalyst is regenerated *in situ*. Indeed, not only is the yield of diesel-like hydrocarbons ~90% or

greater for 72 h on stream, but methane formation is negligible during the second 100 h cycle (right of Figure 6). Interestingly, improvements in performance following catalyst regeneration have been reported for other Ni-based formulations, which was attributed to an increase in the number of strong basic sites during the treatment of the spent catalyst in hot air [118]. Albeit the basicity of the catalyst employed was not assessed in this study, room temperature CO adsorption of the fresh and spent catalyst was investigated via DRIFTS and the resulting spectra are shown in Figure 4.7.

The adsorption of CO on the fresh catalysts produced a strong absorbance peak at 2100 cm^{-1}. Since adsorption of CO on the spent catalyst did not afford this peak, the catalyst was reduced *in situ* to ensure oxidation did not occur when the catalyst was exposed to air. The reduced spent catalyst also lacked a CO adsorption peak, which indicates that the surface active sites that readily adsorb CO are irreversibly poisoned under the reaction conditions employed. This could explain the reduced methane formation observed, as less CO_x adsorb on the catalyst surface. Moreover, the C1 gaseous products observed are almost entirely CO and CO_2, which is consistent with decreased methanation. However, another possibility is that the poisoning of the catalyst may have an electronic effect on surface Ni sites. Indeed, other authors have observed improved catalytic performance when the CO binding energy to the Ni sites is lowered, which frees up the active sites more readily upon deCO_x thereby resulting in enhanced activity [236]. The CO produced *via* decarbonylation is also a known catalyst poison and thus, a lower amount and/or a reduced residency time of CO on the catalyst surface should also benefit catalytic activity [155].

The TGA results in Figure 4.4 show that the total mass loss display by the spent catalyst is 9.5 and 5.1% after the first and second 100 h cycle, respectively. This suggests

that less coke formation occurs after the catalyst regeneration step between these cycles. Catalytic cracking of the feed is known to exacerbate catalyst deactivation and to be particularly problematic for Ni catalysts [8]. Tellingly, light hydrocarbons such as ethane and propane are observed in greater abundance in the gaseous products evolved during the first 100 h cycle relative to the amount observed during the second 100 h cycle. This is consistent with the notion that the increased coking observed during the first 100 h stems from a higher cracking activity. Sites responsible for cracking reactions appear to have been be irreversibly poisoned during the first 100 h cycle. Additionally, adsorbed CO contributes to coking through the Boudouard reaction (Scheme 1.2b) leaving carbon deposits on the surface. Therefore, the lower CO adsorption discussed previously could and reduced cracking observed explain the decrease in carbonaceous deposits formed on the catalyst surface during the second 100 h cycle.

4.4. Conclusions

The 20% Ni-5% Cu/Al_2O_3 catalyst was found to be effective in the catalytic deoxygenation of fatty acid waste streams. Near quantitative conversion of a free fatty acid feed obtained by steam stripping a biodiesel feedstock (25 wt% in dodecane) was achieved at all the reaction temperatures employed, i.e., 275, 325 and 275 °C. Notably, an increase in lipid concentration – from the 25 wt% used in experiments involving the feed obtained by steam stripping a biodiesel feedstock to the 50 wt% used in experiments involving the lipids extracted from brown grease – does not prevent the catalyst from achieving quantitative conversion, as brown grease lipids were completely deoxygenated to hydrocarbons in experiments performed at 325 and 375 °C. While the 20% Ni-5%

Cu/Al_2O_3 catalyst yielded a larger amount of heavy chain hydrocarbons during the upgrading of brown grease under reduced H_2 partial pressure; however, the methanation of CO_x (and the associated H_2 consumption) was significantly reduced. Remarkably, the 20% Ni-5% Cu/Al_2O_3 catalyst was able to afford yields of diesel-like hydrocarbons in excess of 80% at all reaction times during a brown grease upgrading experiment lasting 100 h. Moreover, the catalyst was successfully regenerated *in situ* and displayed improved deoxygenation and decreased methanation activity during a second 100 h cycle, which has been ascribed to the irreversible poisoning of CO adsorption sites and/or to the decrease in the CO binding energy to Ni sites. Indeed, the lower concentration of CO on the catalyst surface decreases catalyst poisoning from CO – resulting in the superior activity and stability observed by the regenerated catalyst – as well as the likelihood of methane formation. In short, when tested under industrially relevant reaction conditions 20% Ni-5% Cu/Al_2O_3 has proven capable of i) quantitatively converting realistic triglyceride [74] and waste free fatty acid-based feeds to fuel-like hydrocarbons; ii) affording very good yields (>80%) of diesel-like hydrocarbons for up to 100 h of time on stream; and iii) being regenerated *in situ* to afford improved deoxygenation activity, superior stability and reduced methanation activity (along with the associated hydrogen savings).

Table 4.1. GC-MS analysis of the feed mixtures used in the catalytic upgrading experiments over 20% Ni- 5% Cu/Al_2O_3.

Compound	Fatty Acid Feed	Brown Grease
Alkenes	**0.63**	**-**
Neophytadiene	0.30	-
squalene	0.33	-
Fatty Acids	**96.21**	**97.33**
Decanoic Acid (C10:0)	-	0.07
Lauric acid (C12:0)	-	0.13
Myristic Acid (C14:0)	0.88	1.55
Pentadecanoic acid (C15:0)	-	0.10
Palmitoleic acid (C16:1)	1.64	0.72
Palmitic acid (C16:0)	21.21	20.42
Heptadecanoic acid (C17:0)	-	0.33
oleic acid (C18:1)	63.52	64.52
stearic acid (C18:0)	8.96	8.73
cis-13-eicosenoic acid (C20:1)	-	0.53
eicosanoic acid (C20:0)	-	0.23
Esters	**2.28**	**-**
Methyl Palmitate	0.26	-
methyl linoleate	0.65	-
methyl oleate	0.76	-
stearyl oleate	0.61	-
Alcohols	**0.39**	**-**
Phytol	0.39	-
Glycerides	**-**	**2.66**
dipalmitin	-	0.34
diolein	-	1.91
Tripalmitin	-	0.05
Tristearin	-	0.22
Triglyceride mixed chain	-	0.14
Unidentified	**0.49**	**-**

Table 4.2 GC-MS analysis of the liquid product mixtures in the catalytic upgrading of fatty acid feed (25 wt% in C12) over 20% Ni-5% Cu/Al_2O_3 at 275 °C and WHSV = 1.0 h^{-1}, in 100% H_2.

Compound	1 h	2 h	3 h	4 h	5 h	6 h	7 h	8 h
Normal Alkanes	**84.84**	**80.26**	**78.38**	**77.46**	**74.75**	**72.93**	**69.85**	**66.36**
Decane (C10)	0.21	0.13	0.13	0.14	0.12	0.17	0.12	0.17
Undecane (C11)	1.10	0.51	0.59	0.39	0.50	0.44	0.50	0.31
Tridecane (C13)	1.44	1.70	1.69	1.37	1.25	1.37	1.52	1.28
Tetradecane (C14)	0.19	0.31	0.33	0.31	0.25	0.28	0.24	0.14
Pentadecane (C15)	21.57	20.29	20.68	20.81	18.92	18.63	18.90	17.90
Hexadecane (C16)	1.01	0.98	1.02	0.70	1.00	0.71	0.77	0.71
Heptadecane (C17)	55.99	53.18	50.41	50.69	49.55	47.73	44.01	41.51
Octadecane (C18)	1.11	1.04	1.00	0.85	0.84	0.99	0.83	0.71
Nonadecane (C19)	0.95	0.72	0.82	0.66	0.77	0.71	0.90	0.89
Heneicosane (C21)	0.60	0.69	0.83	0.44	0.79	0.74	0.82	1.26
Tricosane (C23)	0.37	0.43	0.59	0.73	0.55	0.85	0.89	1.11
Hexacosane (C26)	0.30	0.28	0.29	0.37	0.21	0.31	0.35	0.37
Olefins	**0.61**	**0.53**	**0.83**	**0.88**	**0.83**	**0.69**	**0.82**	**0.73**
Heptadecene (C17:1)	0.48	0.34	0.50	0.66	0.48	0.33	0.46	0.36
Octadecene (C18:1)	0.13	0.19	0.33	0.22	0.35	0.36	0.36	0.37
Branded Alkanes	**5.97**	**6.86**	**6.83**	**7.83**	**8.67**	**9.02**	**9.70**	**10.52**
phytane	2.70	2.74	2.90	2.97	3.02	3.25	3.58	3.52
Squalane	0.51	0.52	0.55	0.58	0.51	0.56	0.55	0.67
Coprostane	0.56	0.83	0.62	0.70	0.79	0.86	0.86	0.98
Cholestane	0.77	1.05	0.97	1.37	1.66	1.70	1.67	1.99
stigmastane	0.47	0.54	0.56	0.62	0.75	0.66	0.65	0.73
stigmastane	0.96	1.18	1.23	1.59	1.94	1.99	2.39	2.63
Total Oxygenates	**8.60**	**12.37**	**13.94**	**13.84**	**15.76**	**17.36**	**19.62**	**22.38**
Methyl Stearate	0.50	1.30	1.77	2.12	3.42	4.25	4.78	6.47
Lauryl Stearate	1.09	1.27	1.94	2.18	2.36	2.67	3.24	3.38
cetyl palmitate	2.61	3.52	3.84	3.76	3.95	4.25	4.59	4.78
Cetyl Stearate	3.00	4.03	4.31	3.72	3.65	3.75	4.20	3.98
Stearyl Stearate	1.40	2.25	2.08	2.06	2.38	2.44	2.81	3.77

Table 4.3 GC-MS analysis of the liquid product mixtures in the catalytic upgrading of fatty acid feed (25 wt% in C12) over 20% Ni-5% Cu/Al_2O_3 at 325 °C and WHSV = 1.0 h^{-1}, in 100% H_2.

Compound	1 h	2 h	3 h	4 h	5 h	6 h	7 h	8 h
Normal Alkanes	**97.84**	**91.08**	**95.69**	**96.33**	**95.43**	**95.90**	**96.07**	**95.23**
Decane (C10)	1.54	2.83	1.51	1.55	1.45	1.43	1.50	1.43
Undecane (C11)	2.13	2.48	1.50	1.44	1.59	1.60	2.10	1.25
Tridecane (C13)	1.74	3.13	1.66	1.68	1.65	1.64	1.40	1.66
Tetradecane (C14)	0.90	2.32	0.89	0.75	0.76	0.82	0.80	0.90
Pentadecane (C15)	25.48	16.89	25.69	25.45	24.37	24.22	23.36	23.24
Hexadecane (C16)	3.16	7.98	3.53	3.47	3.73	3.79	3.83	4.10
Heptadecane (C17)	51.99	37.30	52.00	52.31	51.50	51.90	52.12	51.58
Octadecane (C18)	5.77	10.83	4.32	4.83	5.74	5.55	5.76	6.10
Nonadecane (C19)	1.19	1.43	0.82	0.81	0.83	1.07	0.86	1.01
Icosane (C20)	0.26	0.88	0.23	0.32	0.25	0.21	0.34	0.26
Heneicosane (C21)	0.55	0.66	0.35	0.45	0.43	0.36	0.50	0.26
Docosane (C22)	0.35	0.75	0.21	0.29	0.20	0.20	0.29	0.20
Tricosane (C23)	0.39	0.78	0.46	0.31	0.35	0.42	0.38	0.34
Tetracosane (C24)	0.33	0.48	0.37	0.36	0.28	0.39	0.41	0.32
Pentacosane (C25)	0.33	0.42	0.34	0.42	0.32	0.33	0.41	0.37
Hexacosane (C26)	0.42	0.35	0.53	0.42	0.51	0.50	0.60	0.47
Heptacosane (C27)	0.26	0.29	0.27	0.33	0.31	0.17	0.22	0.32
Octacosane (C28)	0.14	0.21	0.11	0.11	0.16	0.11	0.13	0.12
Nonacosane (C29)	0.16	0.35	0.17	0.17	0.15	0.22	0.22	0.22
Triacontane (C30)	0.14	0.12	0.09	0.18	0.05	0.09	0.07	0.09
Hentriacontane (C31)	0.28	0.22	0.23	0.26	0.28	0.32	0.28	0.33
Tritriacontane (C33)	0.26	0.20	0.30	0.31	0.38	0.39	0.37	0.48
Pentatriacontane (C35)	0.07	0.18	0.11	0.11	0.14	0.17	0.12	0.18
Olefins	**1.96**	**6.41**	**1.71**	**1.28**	**1.81**	**1.60**	**1.36**	**1.60**
Heptadecene (C17:1)	1.96	3.90	1.59	1.06	1.64	1.39	1.10	1.19
Octadecene (18:1)	-	2.51	0.12	0.22	0.17	0.21	0.26	0.41
Branched Alkanes	**-**	**2.48**	**2.62**	**2.39**	**2.76**	**2.51**	**2.57**	**2.98**
Phytane	-	2.48	2.62	2.39	2.76	2.51	2.57	2.98
Total Oxygenates	**0.19**	**-**	**-**	**-**	**-**	**-**	**-**	**0.20**
Cetyl Stearate	0.13	-	-	-	-	-	-	0.14
Stearyl Stearate	0.06	-	-	-	-	-	-	0.06

Table 4.4 GC-MS analysis of the liquid product mixtures in the catalytic upgrading of fatty acid feed (25 wt% in C12) over 20% Ni-5% Cu/Al_2O_3 at 375 °C and WHSV = 1.0 h^{-1}, in 100% H_2.

Compound	1 h	2 h	3 h	4 h	5 h	6 h	7 h	8 h
Normal Alkanes	**100.00**	**100.00**	**100.00**	**100.00**	**100.00**	**100.00**	**100.00**	**100.00**
Octane (C8)	1.74	1.21	1.03	0.98	0.95	0.84	0.75	0.68
Decane (C10)	1.38	0.75	0.62	0.60	0.47	0.53	0.52	0.52
Tridecane (C13)	0.99	0.87	0.77	0.75	0.71	0.78	0.74	0.75
Tetradecane (C14)	1.30	1.27	1.24	1.26	0.83	1.27	1.22	1.27
Pentadecane (C15)	14.05	12.46	11.85	11.89	11.93	11.86	11.52	11.77
Hexadecane (C16)	14.79	14.98	14.81	14.84	14.71	14.78	14.63	14.67
Heptadecane (C17)	35.04	33.41	32.46	31.88	31.42	31.04	31.45	31.69
Octadecane (C18)	28.95	32.69	34.53	35.12	36.49	36.15	36.20	36.09
Nonadecane (C19)	0.50	0.63	0.65	0.67	0.60	0.71	0.87	0.74
Icosane (C20)	0.29	0.38	0.41	0.44	0.44	0.45	0.51	0.37
Heneicosane (C21)	0.16	0.23	0.25	0.26	0.22	0.30	0.29	0.27
Docosane (C22)	0.06	0.22	0.20	0.17	0.19	0.22	0.25	0.19
Tricosane (C23)	0.12	0.19	0.25	0.30	0.27	0.29	0.31	0.30
Hentriacontane (C31)	0.11	0.15	0.19	0.26	0.24	0.29	0.28	0.27
Dotriacontane (C32)	0.27	0.31	0.36	0.36	0.33	0.32	0.29	0.28
Tritriacontane (C33)	0.25	0.25	0.39	0.22	0.20	0.16	0.16	0.14

Table 4.5 GC-MS analysis of the liquid product mixtures in the catalytic upgrading of brown grease lipid feed (50 wt% in C12) over 20% Ni-5% Cu/Al_2O_3 at 325 °C and WHSV = 1.0 h^{-1}, in 100% H_2.

Compound	1 h	2 h	3 h	4 h	5 h	6 h	7 h	8 h
Normal Alkanes	**92.05**	**90.64**	**90.53**	**93.00**	**92.64**	**92.97**	**94.06**	**97.08**
Decane (C10)	1.79	1.50	1.64	1.67	1.67	1.25	1.22	1.32
Undecane (C11)	1.45	1.32	1.39	1.43	1.31	1.24	1.25	1.72
Tridecane (C13)	2.21	2.24	2.27	2.30	1.81	2.18	2.06	2.70
Tetradecane (C14)	1.99	1.78	1.69	1.61	1.46	1.40	1.45	1.65
Pentadecane (C15)	13.62	14.32	15.03	16.14	16.30	15.38	13.40	15.72
Hexadecane (C16)	10.24	8.82	8.12	7.32	7.88	4.92	7.29	8.34
Heptadecane (C17)	33.72	35.68	36.67	37.31	37.14	41.23	45.05	37.78
Octadecane (C18)	18.56	15.71	14.03	13.77	13.60	12.73	11.73	14.89
Nonadecane (C19)	1.14	1.24	1.27	1.26	1.21	1.30	1.08	0.96
Icosane (C20)	0.70	0.70	0.68	0.79	0.81	0.70	0.70	0.97
Heneicosane (C21)	0.61	0.78	0.65	0.57	0.50	1.11	1.91	3.70
Docosane (C22)	0.51	0.46	0.48	0.46	0.52	1.12	0.59	0.67
Tricosane (C23)	0.64	0.61	0.62	0.83	0.69	1.00	0.77	0.62
Tetracosane (C24)	0.59	0.57	0.52	0.82	0.53	0.70	0.52	0.56
Pentacosane (C25)	0.55	0.54	0.56	0.60	0.56	0.93	0.59	0.67
Hexacosane (C26)	0.55	0.58	0.59	0.75	0.68	0.97	0.51	0.60
Heptacosane (C27)	0.43	0.51	0.48	0.54	0.54	0.64	0.54	0.76
Octacosane (C28)	0.32	0.36	0.35	0.41	0.39	0.61	0.38	0.62
Nonacosane (C29)	0.35	0.37	0.40	0.51	0.49	0.66	0.59	0.46
Triacontane (C30)	0.17	0.21	0.23	0.31	0.40	0.30	0.23	0.24
Hentriacontane (C31)	0.58	0.67	0.78	0.92	0.97	0.90	0.50	0.54
Tritriacontane (C33)	0.86	1.02	1.27	1.59	1.84	1.11	0.92	0.75
Pentatriacontane (C35)	0.47	0.65	0.81	1.09	1.34	0.59	0.78	0.84
Branched Alkanes	**4.13**	**4.17**	**3.89**	**3.57**	**3.12**	**2.00**	**1.20**	**1.02**
Phytane	4.13	4.17	3.89	3.57	3.12	2.00	1.20	1.02
Olefins	**3.81**	**5.18**	**5.60**	**3.41**	**4.24**	**5.01**	**4.76**	**1.91**
Heptadecene	1.37	2.98	3.25	1.60	2.65	3.54	3.34	0.98
Octadecene	2.44	2.20	2.35	1.81	1.59	1.47	1.42	0.93

Table 4.6 GC-MS analysis of the liquid product mixtures in the catalytic upgrading of brown grease lipid feed (50 wt% in C12) over 20% Ni-5% Cu/Al_2O_3 at 325 °C and WHSV = 1.0 h^{-1}, in 100% H_2.

Compound	1 h	2 h	3 h	4 h	5 h	6 h	7 h	8 h
Normal Alkanes	**100.00**	**100.00**	**100.00**	**100.00**	**100.00**	**100.00**	**100.00**	**100.00**
Decane (C10)	4.03	3.68	3.37	3.34	3.59	3.52	3.63	3.29
Undecane (C11)	3.86	3.29	2.90	2.76	2.78	2.69	2.50	2.47
Tridecane (C13)	3.22	3.01	3.19	3.06	3.06	3.17	2.63	2.77
Tetradecane (C14)	2.26	2.06	2.06	1.95	1.90	1.89	1.95	1.93
Pentadecane (C15)	20.13	19.79	20.29	20.43	20.55	20.46	19.67	20.19
Hexadecane (C16)	7.67	7.32	6.82	6.82	6.83	6.77	6.84	7.20
Heptadecane (C17)	36.80	39.00	39.33	38.62	38.34	39.16	38.74	39.18
Octadecane (C18)	8.74	9.04	8.45	7.71	7.42	7.58	7.84	7.96
Nonadecane (C19)	1.13	1.21	1.27	1.26	1.24	1.25	1.29	1.25
Icosane (C20)	0.39	0.55	0.37	0.41	0.39	0.43	0.47	0.61
Heneicosane (C21)	0.44	0.50	0.56	0.52	0.59	0.60	0.69	0.64
Docosane (C22)	0.30	0.30	0.29	0.25	0.31	0.34	0.33	0.38
Tricosane (C23)	0.27	0.31	0.36	0.41	0.41	0.53	0.35	0.52
Tetracosane (C24)	0.19	0.20	0.33	0.32	0.31	0.38	0.36	0.28
Pentacosane (C25)	0.14	0.18	0.24	0.29	0.31	0.25	0.42	0.31
Hexacosane (C26)	0.11	0.13	0.21	0.22	0.26	0.23	0.26	0.27
Heptacosane (C27)	0.15	0.14	0.23	0.23	0.30	0.31	0.35	0.35
Octacosane (C28)	0.09	0.10	0.19	0.18	0.19	0.19	0.24	0.23
Nonacosane (C29)	0.07	0.10	0.18	0.20	0.23	0.24	0.26	0.27
Triacontane (C30)	0.03	0.07	0.10	0.12	0.14	0.14	0.18	0.17
Hentriacontane (C31)	0.08	0.15	0.31	0.29	0.34	0.36	0.45	0.48
Dotriacontane (C32)	0.03	0.06	0.06	0.11	0.11	0.13	0.19	0.12
Tritriacontane (C33)	0.08	0.28	0.47	0.54	0.60	0.63	0.83	0.85
Pentatriacontane (C35)	0.07	0.27	0.38	0.42	0.36	0.40	0.57	0.64
Unidentified HC	*9.74*	*8.27*	*8.05*	*9.51*	*9.43*	*8.35*	*8.97*	*7.62*

Table 4.7 GC-MS analysis of the liquid product mixtures in the catalytic upgrading of brown grease lipid feed (50 wt% in C12) over 20% Ni-5% Cu/Al_2O_3 at 375 °C and WHSV = 1.0 h^{-1}, in 20% H_2/Ar.

Compound	1 h	2 h	3 h	4 h	5 h	6 h	7 h	8 h
Normal Alkanes	**97.43**	**97.68**	**98.11**	**98.24**	**98.56**	**98.74**	**98.86**	**98.78**
Decane (C10)	6.91	5.18	4.09	3.74	2.98	2.03	2.78	1.81
Undecane (C11)	11.15	8.52	6.45	5.41	3.93	2.81	2.88	2.19
Tridecane (C13)	2.94	3.00	1.57	2.77	2.70	2.44	2.75	2.27
Tetradecane (C14)	3.34	3.63	3.21	3.29	3.09	3.08	2.72	2.72
Pentadecane (C15)	14.34	15.13	16.22	17.57	16.37	16.72	16.06	18.35
Hexadecane (C16)	8.68	9.03	8.81	0.62	8.68	9.15	7.65	0.94
Heptadecane (C17)	31.75	33.03	37.74	41.49	38.16	39.42	38.63	45.40
Octadecane (C18)	7.73	8.72	9.02	10.32	9.92	10.34	10.57	13.18
Nonadecane (C19)	1.31	1.59	1.72	1.94	1.83	1.82	1.75	1.85
Icosane (C20)	0.77	0.88	0.72	0.83	0.75	0.81	0.77	0.68
Heneicosane (C21)	0.55	0.67	0.71	0.87	0.80	0.68	0.82	0.76
Docosane (C22)	1.77	1.45	0.60	0.78	0.66	0.87	0.68	0.55
Tricosane (C23)	0.79	0.81	0.93	1.02	0.94	0.95	1.31	0.85
Tetracosane (C24)	0.89	0.88	1.00	1.10	1.04	1.12	1.55	0.93
Pentacosane (C25)	0.99	0.99	1.13	1.33	1.23	1.26	1.82	1.28
Hexacosane (C26)	1.04	1.07	1.12	1.51	1.63	1.50	1.99	1.35
Heptacosane (C27)	0.79	0.89	0.92	1.05	1.13	1.26	1.64	1.05
Octacosane (C28)	0.51	0.60	0.64	0.79	0.82	0.75	0.86	0.64
Nonacosane (C29)	0.48	0.59	0.64	0.83	0.91	0.77	0.82	0.75
Triacontane (C30)	0.30	0.40	0.36	0.38	0.40	0.32	0.30	0.59
Hentriacontane (C31)	0.40	0.62	0.51	0.60	0.59	0.64	0.51	0.64
Total Oxygenates	**2.60**	**2.33**	**1.87**	**1.76**	**1.43**	**1.28**	**1.13**	**1.21**
Cetyl Stearate	1.05	0.97	0.81	0.76	0.65	0.57	0.51	0.57
Stearyl Stearate	1.55	1.36	1.06	1.00	0.78	0.71	0.62	0.64

Table 4.8 GC-MS analysis of the liquid product mixtures in the catalytic upgrading of brown grease lipid feed (50 wt% in C12) over 20% Ni-5% Cu/Al_2O_3 at 375 °C and WHSV = 0.8 h^{-1}, in 100% H_2 for the first 100 h.

Compound	1 h	24 h	48 h	72 h	96 h
Normal Alkanes	**99.30**	**97.07**	**91.41**	**81.98**	**75.56**
Decane (C10)	4.56	2.15	3.13	2.89	3.01
Undecane (C11)	6.65	1.89	1.58	1.01	1.56
Tridecane (C13)	2.60	1.96	1.94	1.55	1.49
Tetradecane (C14)	2.73	1.59	1.54	1.20	1.11
Pentadecane (C15)	17.51	18.42	15.37	17.56	12.80
Hexadecane (C16)	9.23	5.54	4.03	4.26	-
Heptadecane (C17)	43.13	44.60	49.62	42.24	43.41
Octadecane (C18)	10.15	11.35	6.97	7.18	7.92
Nonadecane (C19)	0.74	1.16	0.81	0.89	0.90
Icosane (C20)	0.25	1.55	1.62	-	-
Heneicosane (C21)	0.26	0.47	0.25	0.29	0.30
Docosane (C22)	0.13	1.64	1.23	-	-
Tricosane (C23)	0.23	0.59	0.53	0.49	0.50
Tetracosane (C24)	0.18	0.69	0.44	0.44	0.44
Pentacosane (C25)	0.22	0.64	0.57	0.44	0.49
Hexacosane (C26)	0.26	0.79	0.78	0.66	0.66
Heptacosane (C27)	0.10	0.48	0.36	0.32	0.34
Octacosane (C28)	0.08	0.29	-	-	-
Nonacosane (C29)	0.07	0.31	-	-	-
Triacontane (C30)	0.06	0.09	-	-	-
Hentriacontane (C31)	0.08	0.28	0.25	0.20	0.20
Tritriacontane (C33)	0.09	0.39	0.23	0.22	0.26
Pentatriacontane (C35)	-	0.20	0.16	0.14	0.17
Branched Alkanes	**-**	**-**	**0.90**	**0.85**	**0.94**
Cholestane	-	-	0.31	0.30	0.33
Coprostane	-	-	0.33	0.29	0.33
Stigmastane	-	-	0.25	0.27	0.29
Olefins	**0.70**	**2.93**	**7.70**	**9.30**	**13.61**
2-Tetradecene (C14:1)	-	-	0.27	0.34	0.38
3-Hexadecene (C16:1)	-	-	-	0.85	3.95
8-Heptadecene (C17:1)	0.70	2.93	5.44	4.80	5.22
1-Octadecene (C18:1)	-	-	-	0.74	1.08
1-Tetracosene (C24:1)	-	-	0.13	0.39	0.47
1-Pentacosene (C25:1)	-	-	0.34	0.32	0.46
1-Hexacosene (C26:1)	-	-	0.37	0.47	0.53
1-Heptacosene (C27:1)	-	-	0.39	0.58	0.68
1-Octacosene (C28:1)	-	-	0.28	0.33	0.39
1-Nonacosene (C29:1)	-	-	0.48	0.47	0.46
Total Oxygenates	**-**	**-**	**-**	**7.86**	**9.89**
Fatty Acids	-	-	-	*6.93*	*8.15*
Glycerides	-	-	-	-	-
Alcohols	-	-	-	*0.93*	*1.74*

Table 4.9 GC-MS analysis of the liquid product mixtures in the catalytic upgrading of brown grease lipid feed (50 wt% in C12) over 20% Ni-5% Cu/Al_2O_3 at 375 °C and WHSV = 0.8 h^{-1}, in 100% H_2 for the second 100 h.

Compound	1 h	24 h	48 h	72 h	96 h
Normal Alkanes	**98.75**	**96.47**	**92.32**	**84.87**	**81.86**
Decane (C10)	0.73	0.87	-	-	-
Undecane (C11)	0.73	0.81	-	-	-
Tridecane (C13)	0.94	1.54	1.18	-	-
Tetradecane (C14)	0.92	1.02	0.60	-	-
Pentadecane (C15)	17.13	16.53	17.73	19.15	18.08
Hexadecane (C16)	5.47	6.87	5.75	5.19	1.43
Heptadecane (C17)	52.39	47.07	44.18	41.35	44.50
Octadecane (C18)	13.78	16.89	16.32	13.11	12.59
Nonadecane (C19)	0.91	0.73	0.59	0.60	0.52
Eicosane (C20)	0.36	0.33	0.93	-	-
Heneicosane (C21)	0.53	0.32	0.31	0.48	0.40
Docosane (C22)	0.31	0.36	1.24	0.83	-
Tricosane (C23)	0.60	0.44	0.54	0.66	0.68
Tetracosane (C24)	0.56	0.43	0.49	0.75	0.56
Pentacosane (C25)	0.62	0.51	0.55	0.61	0.53
Hexacosane (C26)	0.75	0.71	0.78	0.87	0.87
Heptacosane (C27)	0.46	0.33	0.36	0.36	0.35
Octacosane (C28)	0.23	0.19	0.20	0.25	0.24
Nonacosane (C29)	0.22	0.19	0.21	0.23	0.16
Triacontane (C30)	-	-	-	0.09	0.23
Hentriacontane (C31)	0.21	0.17	0.21	0.20	0.27
Tritriacontane (C33)	0.21	0.16	0.18	0.16	0.26
Pentatriacontane (C35)	0.69	-	-	-	0.20
Branched Alkanes	**-**	**-**	**-**	**-**	**0.27**
cholestane	-	-	-	-	0.16
stigmastane	-	-	-	-	0.11
Olefins	**1.25**	**3.53**	**7.68**	**11.24**	**11.65**
4-decene (C10:1)	-	-	1.07	1.19	0.44
5-Undecene (C11:1)	-	-	0.77	0.70	0.69
Tridecene (C13:1)	-	-	-	1.16	0.97
2-Tetradecene (C14:1)	-	-	-	0.87	0.93
8-Heptadecene (C17:1)	1.25	3.53	5.84	6.93	7.78
1-Tetracosene (C24:1)	-	-	-	-	0.16
1-Pentacosene (C25:1)	-	-	-	-	0.14
1-Hexacosene (C26:1)	-	-	-	0.16	0.24
1-Heptacosene (C27:1)	-	-	-	0.22	0.30
Total Oxygenates	**-**	**-**	**-**	**3.89**	**-**
Fatty acids	-	-	-	*3.89*	*5.48*
Glycerides	-	-	-	-	-
Alcohols	-	-	-	-	*0.75*

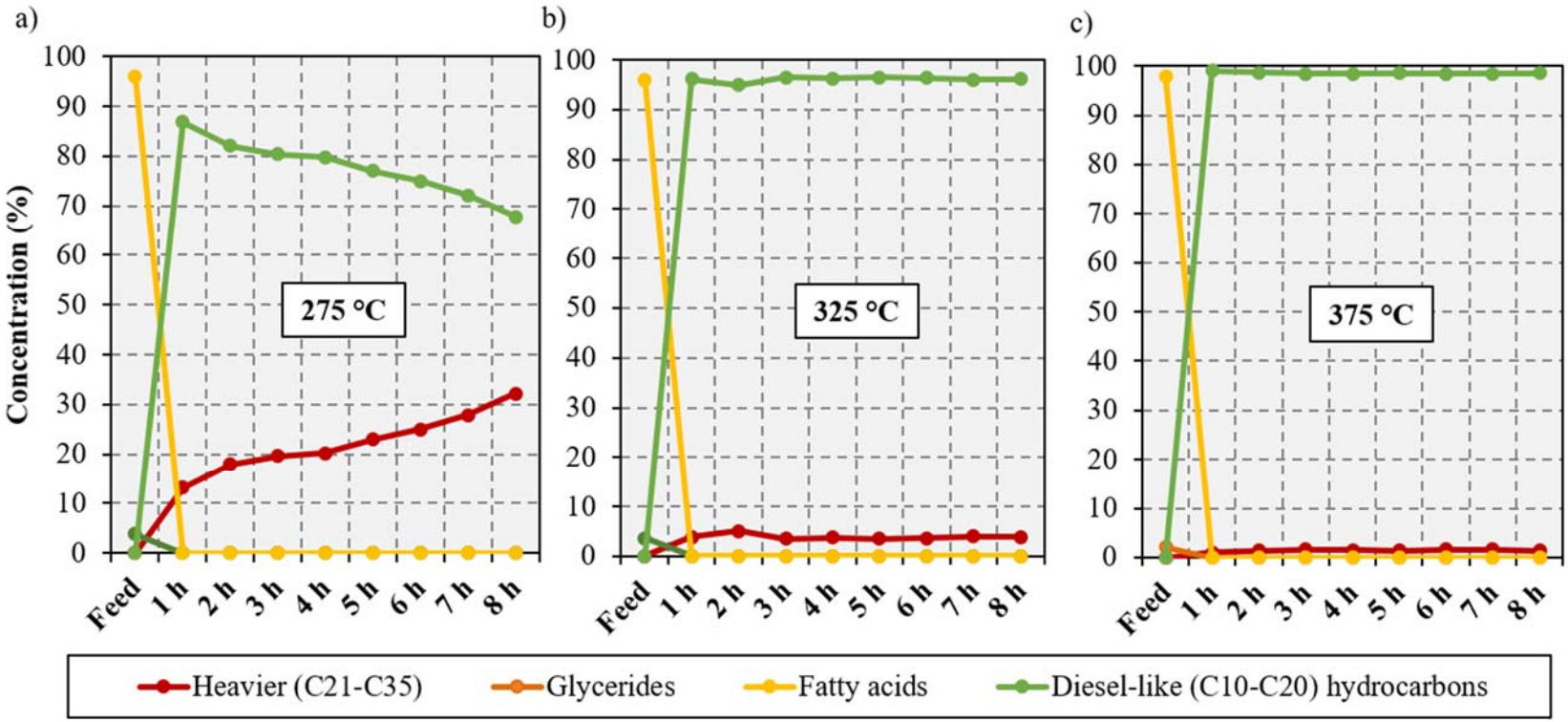

Figure 4.1 GC-MS analysis of the liquid product mixtures in the catalytic upgrading of fatty acid feed (25 wt% in C12) over 20% Ni-5% Cu/Al_2O_3 at a) 275 °C, b) 325 °C, c) 375 °C with a WHSV=1.0 h^{-1}, in 100% H_2.

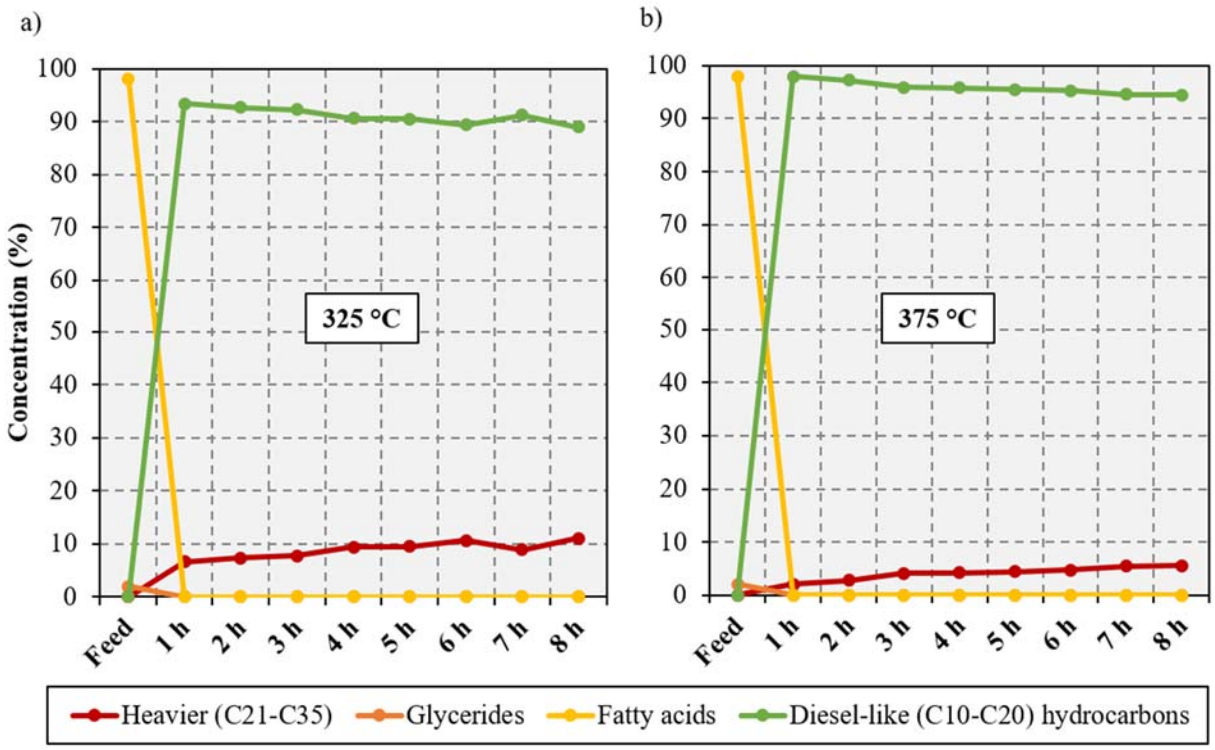

Figure 4.2 GC-MS analysis of the liquid product mixtures in the catalytic upgrading of brown grease lipid feed (25 wt% in C12) over 20% Ni-5% Cu/Al_2O_3 at a) 325 °C and b) 375 °C with a WHSV=1.0 h^{-1}, in 100% H_2.

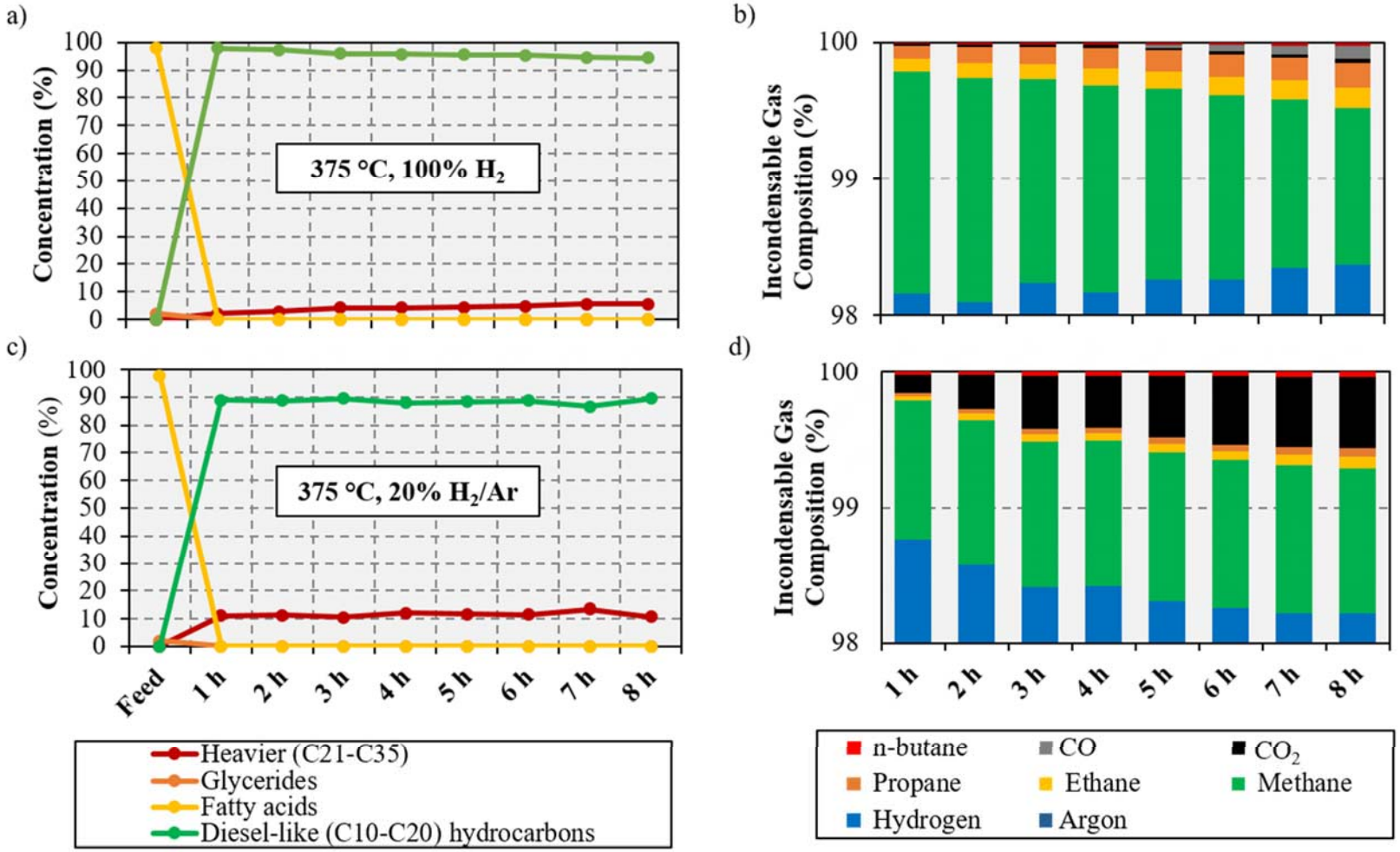

Figure 4.3. GC-MS of the liquid products (a and c) and refined gas analysis (b and d) of the gaseous products from the deoxygenation of brown grease lipids at different H_2 partial pressures.

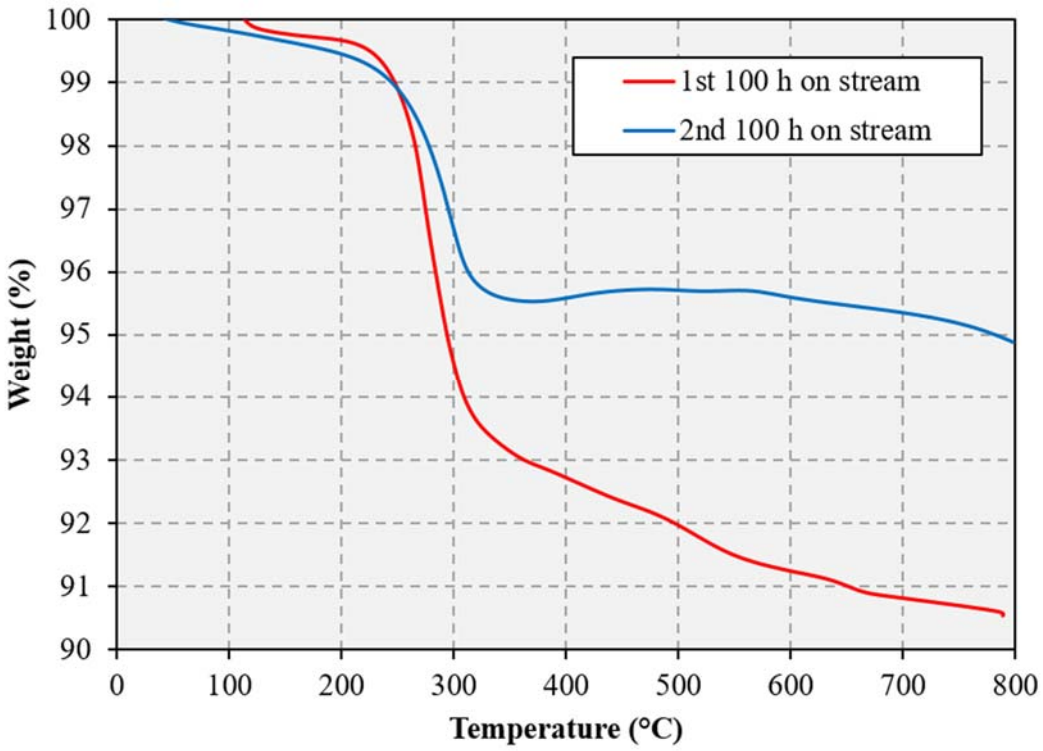

Figure 4.4. Thermogravimetric analysis of the dried spent catalyst from the deoxygenation of brown grease lipids at 375 °C and 580 psi of 100% H_2 after first 100 h and the second100 h on stream of the regenerated catalyst.

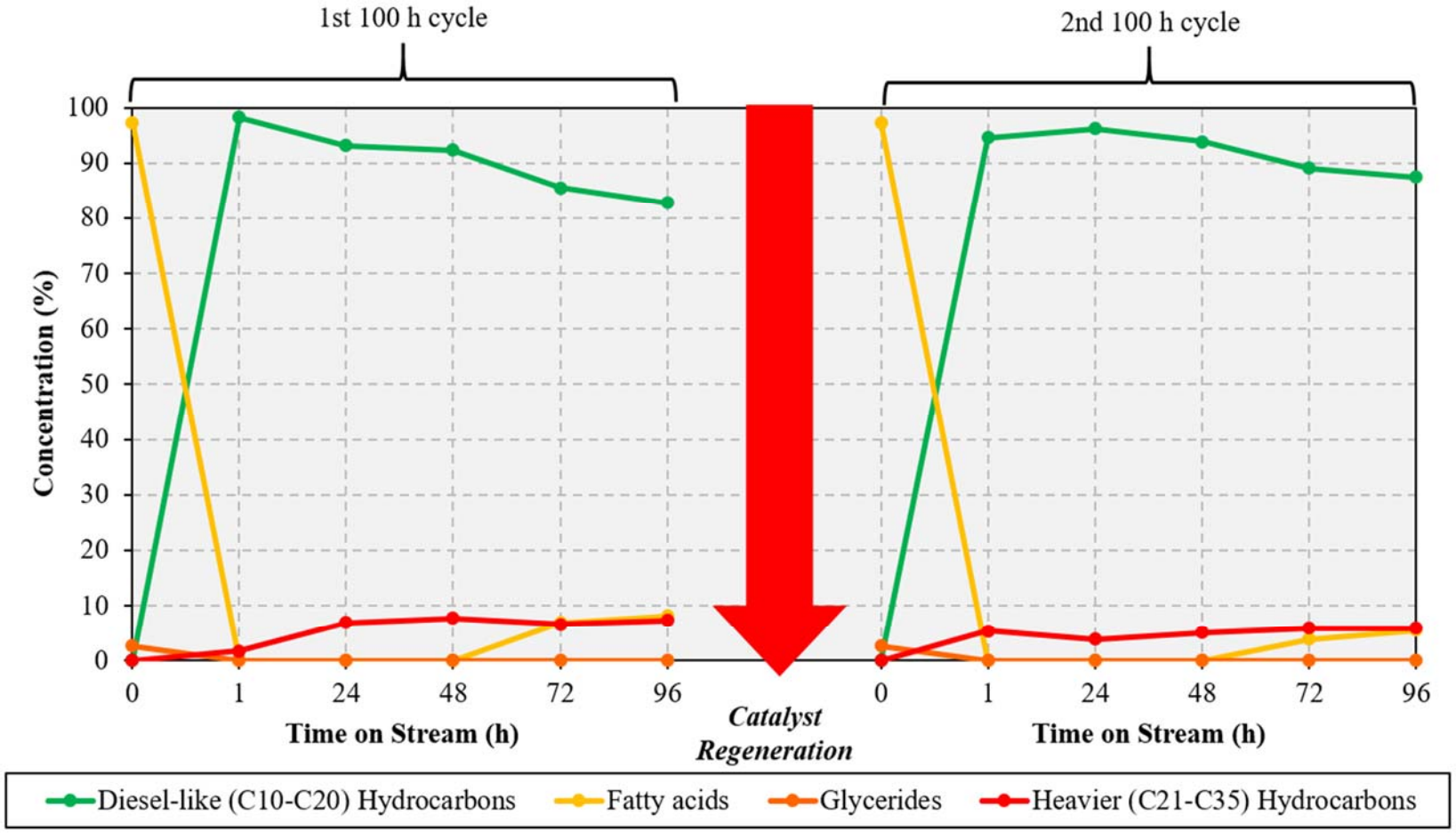

Figure 4.5. GC-MS analysis of select liquid samples for the deoxygenation of brown grease lipids after 100 h on stream, *in situ* catalyst regeneration, and a 2nd 100 h on stream at 375 °C and 580 psi of 100% H_2.

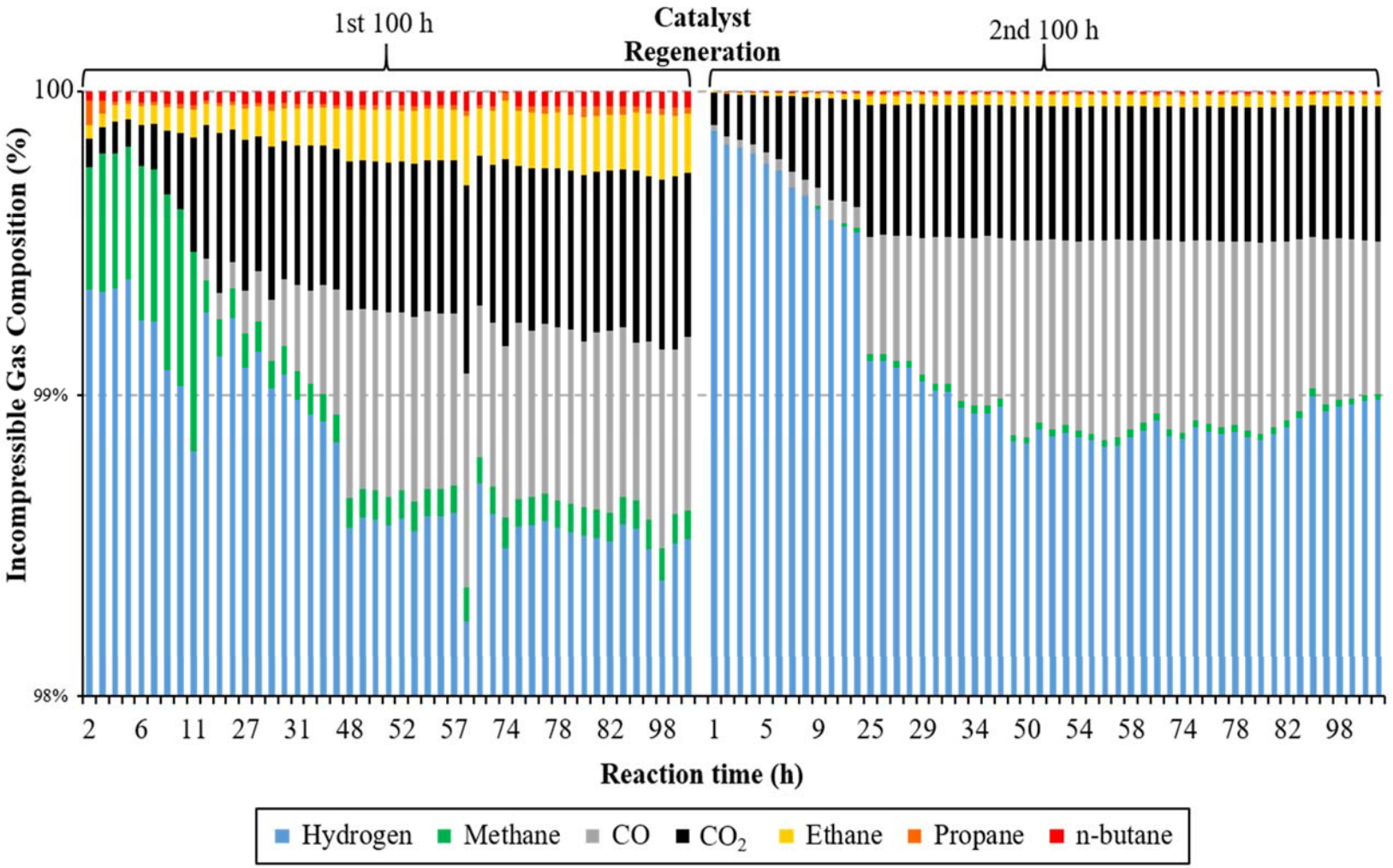

Figure 4.6. Refined gas analysis select gas samples from the deoxygenation of brown grease lipids after 100 h on stream, *in situ* catalyst regeneration, and a 2nd 100 h on stream at 375 °C and 580 psi of 100% H_2.

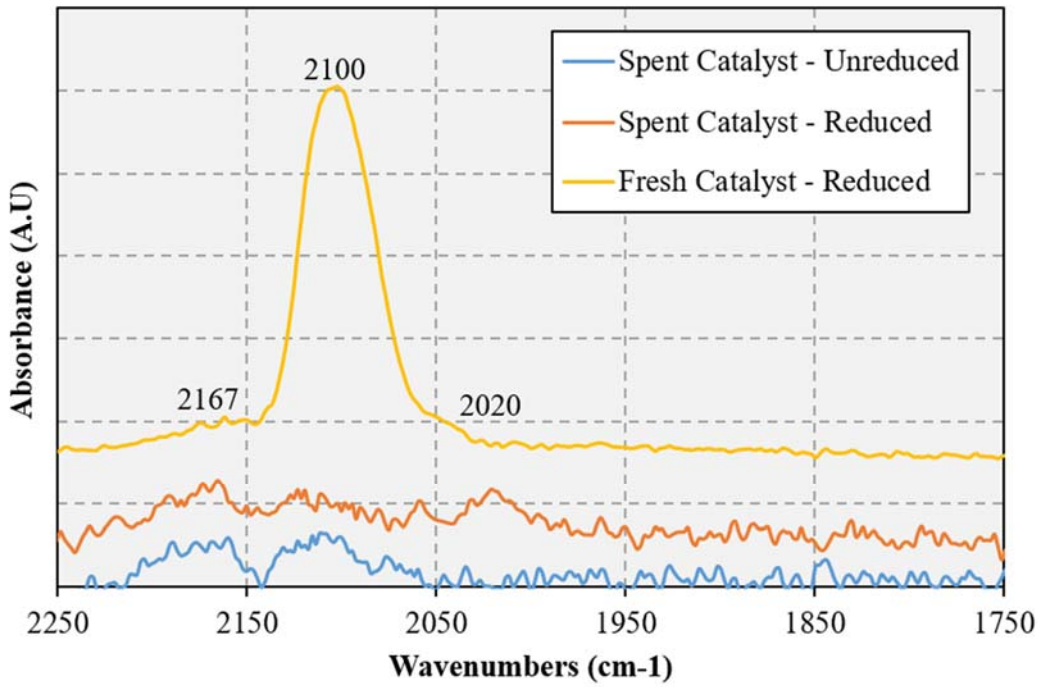

Figure 4.7. DRIFTS spectra of the fresh catalyst after reduction, spent catalyst, and the spent catalyst after reduction.

Chapter 5. Catalytic deoxygenation of tristearin using Pt as a promoter for supported Ni catalysts.

5.1. Introduction

The depletion of fossil fuels and environmental concerns surrounding their use demands the development of improved renewable energy systems. Biofuels, fuels derived from biomass, are renewable and have the potential to become carbon neutral without competing with the food supply if they are obtained from waste or non-edible feed stocks [3, 59, 60, 70]. Biodiesel (fatty acid methyl esters) is currently produced industrially through transesterification or esterification of the triglycerides and fatty acids in a variety of oils and fats. Although biodiesel is renewable, it has several drawbacks such as poor cold flow properties and storage stability. These are directly attributed to the oxygen content [8, 9]. Alternatively, processes are being developed to convert the same feed stocks used for biodiesel to fuel-like hydrocarbons by catalytically removing the oxygen present. These hydrocarbons provide a renewable biofuel source that is chemically identical to products obtained from fossil fuels. Investigations into such processes have revealed two dominant reaction pathways; 1) hydrodeoxygenation (HDO), oxygen is eliminated as water, and 2) decarbonylation/decarboxlation ($deCO_x$), in which the elimination of oxygen occurs as CO or CO_2. The HDO reaction pathway is typically selective in yielding the desired hydrocarbon products as well as saturating the C=C double bonds that are abundant in many feed sources. However, this requires high H_2 pressures and problematic sulfided catalysts. In contrast, the $deCO_x$ pathway yields hydrocarbons that contain one carbon less

than the original feed without the use of sulfided catalysts and requires little to no H_2 for oxygen removal [11].

In an effort to identify promising deoxygenation catalysts, Snåre et al. screened a number active metals on various supports for the deoxygenation of stearic acid, a model fatty acid compound, and found that deoxygenation activity follows the order Pd > Pt > Ni > Rh > IR > Ru > Os [84]. Unsurprisingly, the majority of deoxygenation studies since Snåre's work have focused on the use of the two most active metals, Pd [77, 78, 114, 116, 123, 127, 237-239] and Pt [79, 81, 103, 110, 126, 138, 141, 171]. Recently, Crocker and co-workers showed that Ni supported on carbon provides comparable results to Pd and Pt catalysts in the deoxygenation of triglycerides [15, 119]. The required Ni metal loading was significantly greater than the loading for precious metal catalysts; however, such catalysts are still desirable because of the considerably lower cost of Ni. Although promising, Ni catalysts typically yield more cracking products than their Pd and Pt analogs and Ni-based catalysts are prone to deactivation from coking. Although some cracking may be desirable to improve cold flow properties and produce hydrocarbon fuels that fall within the boiling point range of aviation fuels (150-300 °C) [11, 15], excessive cracking can lead to lower yields of fuel-like products and catalyst deactivation [75]. In light of this, the development and improvement of Ni-based catalysts is of significant interest.

In an effort to improve Ni deoxygenation catalysts, many authors have examined the use of a variety of supports, metal loadings, various reactor types and conditions. The conversion of lipids to fuel like-hydrocarbons using Ni catalysts was the subject of a recent

review by Kordulis [8]. Notably, metal oxide supported catalysts have shown acceptable conversion and selectivity compared to high surface area carbon supports [75, 95, 101, 112, 118, 121, 183]. Although carbon supported catalysts have generally shown better yields in the deCO_x pathway [82], the catalyst deactivation pathway for deoxygenation catalysts is mainly attributed to coke formation [157]. Consequentially, the regeneration of carbon supported catalysts can be challenging and requires the use of solvents which may or may not be effective in removing carbonaceous deposits. With metal oxide supports, the catalysts can be regenerated by combusting the coke deposits on the catalyst surface [118].

Efforts to identify a suitable Ni-based catalyst for the deoxygenation of lipids have not only incorporated the use of various supports but also modification of the active Ni phase [44, 74, 75, 153, 236, 240, 241]. Crocker and co-workers found the addition of small amounts of Cu to a 20 wt% Ni/Al_2O_3 catalyst facilitated NiO reduction at lower temperatures [75]. The bulk of the surface Ni could be reduced at 350 °C and below, compared to ~500 °C for the monometallic catalyst. This is beneficial for deoxygenation because the catalyst can be reactivated during the course of reaction. Moreover, supplying a continuous flow of H_2 in either a semi-batch or fixed bed reactor not only reactivates the catalyst, but it also removes CO_x generated during the process that might otherwise act as catalyst poisons [116]. Crocker and co-workers demonstrated this with the supported Ni-Cu catalyst which yielded near quantitative conversion of model lipid compounds, such as tristearin and stearic acid [75]. Remarkably, in hydrogen rich atmospheres and reaction temperatures as low as 260 °C, conditions typically favoring the HDO pathway [101, 124],

deoxygenation was observed to proceed via $deCO_x$ [74]. The promotion effect observed with the bimetallic catalyst was, in large part, attributed the ability of Cu to facilitate the reduction of Ni at lower temperatures.

The goal of the present study was to examine catalyst promotion using Pt. Pt is of particular interest in this regard because it can chemisorb H_2, leading to spill-over of atomic H on the support or surrounding metal sites through surface migration [242]. Since Pt reduces at a lower temperature than Ni, theoretically a similar catalytic promotion effect (as for Cu) can be obtained with small amounts of Pt. Interestingly, Pt has also been shown to lower the binding energy of CO to Ni that is either alloyed with the Pt or in close proximity [243], which could increase the $deCO_x$ activity of the Ni by decreasing the tendency of CO to adsorb on Ni. Therefore, this study will assess the possibility of using small amounts of Pt to act as a promotor for Ni catalysts in the deoxygenation of lipids.

5.2. Experimental

5.2.1. Catalyst preparation and characterization

Catalysts were prepared by excess wetness impregnation using $Ni(NO_3)_2 \cdot 6H_2O$ (Alfa Aesar) and $Pt(NH_3)_4(NO_3)_2$ (Sigma Aldrich) as the metal precursors. Beads of γ-Al_2O_3 (Sasol; surface area of 216 m^2/g) were used as the support and were crushed to a particle size of <150μm before the impregnation. Each catalyst contained 20 wt% Ni, while the Pt loading was varied at 0.1, 0.25, and 0.5 wt%. A monometallic 0.5 wt% Pt catalyst

was also prepared using the same method. The impregnated materials were dried overnight at 60 °C under vacuum prior to calcination for 3 h at 500 °C in static air.

The surface area, pore volume and average pore radius of the catalysts were determined by N_2 physisorption using previously described instruments and methods [15]. The average NiO particle size was calculated by applying the Scherrer equation to the NiO peaks observed in powder X-ray diffractograms. The equipment and procedures for acquiring the X-ray diffractograms are described elsewhere [112]. Thermogravimetric analysis (TGA) of the spent catalysts was performed under flowing air (50 mL/min) on a TA instruments Discovery Series thermogravimetric analyzer. The temperature was ramped from room temperature to 800 °C at a rate of 10 °C/min. Temperature-programmed reduction (TPR) and pulsed H_2 chemisorption were performed using calcined catalyst samples (150 mg). The catalyst was placed in a quartz, U-tube reactor inside a Micromeritics Autochem II chemisorption analyzer, equipped with a thermal conductivity detector (TCD). The temperature was monitored using a thermal couple situated in the catalyst bed. TPR measurements were performed using methods previously described [112]. For pulsed H_2 chemisorption calcined catalysts were reduced *in situ* under 10%H_2/Ar flow at 350 °C for 1 h. The reactor was purged with Ar (50 cm^3/min) at 450 °C for 30 min then cooled to 50 °C under flowing Ar. After the TCD signal stabilized, 0.025 cm^3 (STP) 10% H_2/Ar was pulsed into the Ar carrier gas flowing (50 cm^3/min) to the reactor. Pulsing of 10% H_2/Ar continued at 3 min intervals until the area of the H_2 peaks remained constant.

5.2.2. Deoxygenation experiments

The calcined catalyst (<150 μm particle size) was dried at 60 °C under vacuum overnight before use. The dried catalyst (0.5 g) was then placed into a 100 mL stainless steel, mechanically stirred, autoclave that was purged with Ar. The reactor was then pressurized to 70 psi with 10%H_2/Ar and a gas flow (60 mL/min). The flow and pressure were maintained during the catalyst reduction at 350 °C for 3 h. Temperature was measured by a K-type thermocouple placed inside a thermowell. The reactor was then cooled to room temperature and purged with Ar. After cooling, the liquid solvent (22 g) was added through an opening in the top of the reactor. The reactor was then opened to the atmosphere to add the solid feed (1.8 g). Tristearin (95%, from City Chemical) and dodecane (99+%, from Alfa Aesar) were used as the model triglyceride feed and the solvent, respectively. The reactor was resealed and purged 3 times with Ar prior to being pressurized with H_2 to 580 psi. Once at the desired pressure, the reactor was heated to 260 °C under a constant flow of H_2 (60 mL/min), while the contents were mechanically stirred (1000 rpm). Stirring and H_2 gas flow were held constant through the entirety of the experiment (3 h). Volatile liquid products were collected downstream of the reactor in a condenser. At the end of the experiment the reactor was cooled to room temperature using forced air and an ice bath. It was then depressurized and the liquid and solid products were removed and separated using gravity filtration. The solids were rinsed with chloroform to recover additional liquid

product from the spent catalyst. Excess chloroform was removed from the combined filtrate and washings by rotatory evaporation prior to analysis.

5.2.3. Liquid product analysis

The liquid products were analyzed using a combined Simulated Distillation-GC and GC-MS method specifically devised to identify and quantify the products obtained in the upgrading of fats and oils to hydrocarbons. Detailed information about the development and application of this method is available elsewhere [233]. The analyses were performed using an Agilent 7890B GC system equipped with an Agilent 5977A extractor MSD and flame ionization detector (FID). The multimode inlet, which contained a helix liner, was run in a split mode (15:1; split flow, 48 mL/min) with an initial temperature of 100 °C. Helium was used as the carrier gas and a 1 µL injection was employed. Upon injection, the inlet temperature was immediately increased to 380 °C at a rate of 8 °C/min, and the temperature was maintained for the course of the analysis. The oven temperature was increased upon injection from 40 °C to 325 °C at a rate of 4 °C/min, followed by a ramp of 10 °C/min to 400 °C, which was maintained for 12.5 min. The total analysis run time was 91.25 min. An Agilent J&W VF-5ht column (30 m × 250 µm × 0.1 µm) rated to 450 °C was used. Column eluents were directed to a Siltek MXT connector that split the flow into two streams, one leading to the MSD (J&W Ultimetal Plus Tubing, 11 m X 0.25 mm i.d.) and one leading to the FID (J&W Ultimetal Plus Tubing, 5 m X 0.25 mm i.d.). The MS zone temperatures (MS source at 230 °C and quadrupole at 150 °C) were held constant

for the duration of the analysis. A 1.75 min solvent delay was implemented and the MSD scanned from 10 to 700 Da. The FID was set to 390 °C with the following gas flow rates: H_2 at 40 mL/min; air = 400 mL/min; He makeup = 25 mL/min. Quantification was performed using cyclohexanone as an internal standard. Agilent MassHunter Acquisition and SimDis Expert 9 (purchased from Separation Systems Inc.) software were respectively used to perform chromatographic programming and to process GC-FID data acquired. Solvents (i.e., chloroform and dodecane) were quenched and/or subtracted prior to processing the data.

5.3. Results and Discussion

5.3.1. Catalyst Characterization

The X-ray diffractograms in Figure 4.1 show that all catalysts presented diffraction peaks at 37.2°, 43.4°, 63.1°, 75.5° and 79.4°, which points to the presence of NiO [187]. Unsurprisingly, Pt peaks are not observed due to the very low Pt metal loadings. The NiO particle sizes were obtained by applying the Scherrer equation to the 37.2° NiO peak, the calculated particle sizes as well as other textural properties being listed in Table 4.1. The particle size of the bimetallic catalysts remained similar to the monometallic catalyst indicating the additional calcination required for addition of the Pt did not result in sintering of the NiO to larger particles. The surface areas of 20%Ni/Al_2O_3 and the Ni-Pt bimetallic catalysts are relatively similar, which is expected. The 0.5%Pt/Al_2O_3 catalyst has a much higher surface area (196 m^2/g) than the others due to the absence of NiO.

The TPR profiles of the catalysts, shown in Figure 4.2, indicate the addition of Pt lowers the reduction temperature of NiO in the catalysts. The 20%Ni/Al_2O_3 catalyst has a broad reduction event with a maximum at 550 °C which is the result of the reduction of the NiO to catalytically active Ni^0 on the γ-Al_2O_3 support [190]. The broad reduction event has two shoulders, the first with a local maximum at 350 °C being attributed to the reduction of larger Ni clusters that have a weak interaction with support [190]. The shoulder at 650 °C is attributed to $NiAl_2O_4$ [75] and this event is observed in all catalysts studied between the temperature ranges 650-700 °C. The Pt catalysts exhibit several reduction events, the first occurring at 325-350 °C, which is most likely the reduction of larger Ni ensembles, for the monometallic Ni catalyst. The bimetallic catalysts have peak maxima at similar temperatures to the monometallic Ni catalyst, i.e., a broad peak between 550-650 °C attributed to surface Ni particle reduction and a shoulder at 700-750 °C attributed to $NiAl_2O_4$. The notable difference between the 20%Ni/Al_2O_3 catalyst and of the bimetallic catalysts is the major reduction maximum occurring between 439-450 °C in all the Ni-Pt bimetallic catalysts. The TPR profile of the 0.5%Pt/Al_2O_3 catalyst contains similar reduction maximum indicating the peaks at 450 °C are the reduction of surface Pt. In comparison, the reduction maximum for the bimetallic catalysts at 439-450 °C is significantly larger than the maximum observed for the Pt-only catalyst. This indicates the majority of the hydrogen uptake at this maximum must be due to the reduction of surface Ni on the bimetallic catalysts. Pt is known to facilitate hydrogen spillover [236], resulting in the observed shift in the reduction temperature for the majority of the surface Ni

particles. This is confirmed by a significant decrease in the reduction maximum at 550 °C that is attributed to monometallic Ni particles. However, this phenomenon does not appear to affect the reduction of the $NiAl_2O_4$ present.

H_2 chemisorption was performed on the catalysts used in this study to identify the number of active sites available after the catalysts were reduced at 350 °C, the reduction temperature used in the catalyst evaluation experiments. The amount of H_2 adsorbed and calculated theoretical H_2 adsorption are displayed in Table 4.2. Assuming dissociative adsorption of H_2, the amount of metal active sites can be estimated. The H_2 adsorption increases dramatically from 0.095 mL/g for 20%Ni/Al_2O_3 to 0.461 mL/g for 20%Ni-0.1% Pt/Al_2O_3. Assuming the Ni metal sites remain unaffected by the addition of Pt, the theoretical H_2 adsorption expected from 0.1% Pt addition (with an unlikely 100% metal dispersion) is calculated to be 0.152 mL/g. Given that the observed increase is three times the theoretical value, more reduced Ni sites are likely present. The amount of H_2 adsorption increased with the increased Pt metal loading; however, the additional Pt metal loading does not result in the dramatic adsorption differences observed with the monometallic catalyst and 20%Ni-0.1% Pt/Al_2O_3. In fact, under the assumption of 50% Pt metal dispersion, the H_2 adsorption trend corresponds to roughly the amount expected by only the additional Pt. For example, 20% Ni-0.25% Pt/Al_2O_3 and 20% Ni-0.5% Pt/Al_2O_3 adsorb 0.560 and 0.639 mL/g H_2, respectively. Theoretically, the adsorption would be 0.504 mL/g for 20% Ni-0.25% Pt/Al_2O_3 and 0.632 mL/g for 20% Ni-0.5% Pt/Al_2O_3 if additional Ni

was not affected by this increase in Pt loading. Therefore, albeit the addition of 0.1% Pt increases the number of adsorption sites from $2.55x10^{18}$/g and $1.24x10^{19}$ /g, additional Pt loading from 0.1% to 0.5% does not yield significant increases in the amount of reduced Ni.

5.3.2. Tristearin deoxygenation in semi-batch mode

The results of tristearin deoxygenation experiments are summarized in Table 4.3. Remarkably, whereas the monometallic catalyst afforded only 2% conversion at 260 °C, the 20% Ni-0.5% Pt/Al_2O_3 catalyst exhibited 100% conversion, the gas chromatograms and boiling point distribution plots (BPDPs) being shown in Figure 4.3. Catalysts utilizing Pt as the only active metal for deoxygenation have been reported [15, 79, 103, 126, 244] and it should be noted that Snåre et al. found Pt catalysts were only bettered in catalytic activity for deoxygenation of model lipid feeds by Pd [84]. Therefore, the highest Pt loading (0.5 wt%) for the bimetallic catalyst was prepared as a monometallic catalyst and subjected to the same reaction conditions. The 0.5% Pt/Al_2O_3 catalyst did indeed have a higher conversion (5%) than the 20% Ni/Al_2O_3 catalyst (2%); however, the bimetallic formulations achieved considerably greater tristearin conversion. The 20% Ni-0.1% Pt/Al_2O_3 catalyst had the lowest Pt loading and gave a conversion of 21% with a selectivity to diesel range hydrocarbons (C10-C17) of 93%. The increase in conversion of 16% achieved by the bimetallic formulation over the best performing monometallic catalyst indicates the improved performance stems from a synergistic effect between Ni and Pt and

not as a result of individual contributions. With increased Pt metal loading, 20% Ni-0.5% Pt/Al_2O_3 was found to be the optimal metal formulation for near quantitative conversion, producing 96% products that boil in the diesel range (identified as C10-C17) with a 65% selectivity to C17. MS analysis confirmed the products were indeed hydrocarbons, verifying that near complete deoxygenation was achieved, yielding only fuel-like hydrocarbons. The dramatic increase in tristearin conversion as Pt loading increases from 0.1-0.5% is curious given that pulsed H_2 chemisorption revealed the additional Pt loading did not significantly increase the amount of reduced Ni. Therefore, the increased conversion likely stems from another promotion effect that is not identified in this study. However, it is possible that Pt is lowering the binding energy of the products (i.e., CO) to the Ni active sites, resulting in increased product desorption rates and faster reactivation of the Ni active sites. The increased Pt loading would enhance this effect resulting in the observed promotion in conversion.

The deoxygenation reactions were performed in 100% H_2 atmosphere which has been shown to offer improved catalytic performance, even if the H_2 is not directly consumed [9, 56, 118, 119]. This is favorable because lower H_2 consumption is the advantage the $deCO_x$ pathway holds over the HDO pathway by significantly lowering the operating costs. However, the deoxygenation of lipids typically proceeds via HDO over $deCO_x$ at lower reaction temperatures in environments where both pathways are viable [16, 17, 55], which is possible for the experimental conditions employed in this study. Therefore, it is remarkable that all catalysts yielded 2% or less of C18, the primary HDO

product, indicating the deoxygenation pathway to be $deCO_x$ under these conditions. The majority of experiments also yielded small amounts (<1%) of stearyl stearate. This intermediate is formed in the deoxygenation of triglycerides by the transesterification of fatty acid and alcohol intermediates [121]. For one experiment involving 20%Ni-0.25%/Al_2O_3, the MS data (not shown) identified small amounts of stearic acid in the product mixture; however, neither fatty acids nor alcohols were identified in repeat experiments. The presence of the fatty acid can explain the stearyl stearate observed, as well as suggest that the deoxygenation pathway goes through a fatty acid intermediate. Notably, the small amounts of intermediates observed suggest the deoxygenation occurs rapidly after intermediate formation suggesting the latter to be the rate limiting step.

5.3.4. Spent catalyst characterization

Some authors have suggested the addition of Pt to Ni catalysts increases the catalyst stability under operating conditions by decreasing coke formation [243]. Coking has been shown to be the primary deactivation pathway of Ni catalysts. Therefore, representative spent catalysts were subjected to thermogravimetric analysis in air, the resulting profiles being shown in Figure 4.4. The TGA profiles show a major weight loss event below 400 °C , for all catalysts, which is attributed to the desorption and/or combustion of residual reactants, intermediates and/or products. Notably, the mass loss is minimal in most circumstances above 400 °C indicating that minimal amounts of graphitic or organized coke are present. Indeed, there is a trend in total weight loss with the Pt metal

loading for the catalysts. The total weight loss is 14.9%, 14.6%, 13.5%, and 12.2%, for 20%Ni/Al_2O_3, 20%Ni-0.1% Pt/Al_2O_3, 20%Ni-0.25% Pt/Al_2O_3, and 20%Ni-0.5% Pt/Al_2O_3, respectively. This follows the trend in catalytic activity observed, the 20%Ni/Al_2O_3 catalyst providing 2% conversion and 20%Ni-0.5% Pt/Al_2O_3 giving 100% conversion. The ability of Pt to facilitate surface migration of atomic H after adsorption [243] may result in the removal of adsorbed unsaturated species via hydrogenation (and hence the removal of material blocking pores [156]), resulting in the increased activity observed with increased Pt loading. However, given that the weight loss between the worst and best performing catalyst is only 2.49%, reduced coking does not appear to be a major promoting effect from Pt addition, although it does appear to be a minor contributing factor.

5.4. Conclusions

Catalyst evaluation in a semi-batch reactor results shows that Pt is an effective promoter for supported Ni catalysts in the deCO_x of tristearin at 260 °C. The tristearin conversion increased from 2% over 20% Ni/Al_2O_3 to 100% over 20% Ni-0.5% Pt/Al_2O_3 in 3 h of reaction time. In addition, 20% Ni-0.5% Pt/Al_2O_3 yielded a selectivity to diesel-like hydrocarbons (C10-C17) of 96% and 65% selectivity to C17, the primary deCO_x product. Notably, these improvements in deCO_x performance result from a synergistic effect of the two metals, indicated by the fact that monometallic 20% Ni/Al_2O_3 and 0.5% Pt/Al_2O_3 catalysts gave significantly lower conversion. Characterization of the catalysts reveal the superior activity of Ni-Pt relative to Ni-only catalysts is not a result of Ni particle

size effects or surface area differences, but rather stems from the improved reducibility of NiO when Pt is present. H_2 pulsed chemisorption identified roughly $2.55x10^{18}$/g and $1.72x10^{19}$/g adsorption sites on the 20% Ni/Al_2O_3 and 20% Ni-0.5% Pt/Al_2O_3 catalysts, respectively. This suggests the addition of a small amount of Pt to the supported Ni catalyst dramatically increases the amount of reduced metal, albeit all of which may not necessarily be catalytically active (i.e. reduced Ni in terrace sites). Thermogravimetric analysis of the spent catalysts from the deCO_x experiments suggest the beneficial effect of Pt on catalyst performance can also be explained by decreased coke formation. The primary coke formed corresponded to strongly adsorbed reactants, intermediates, or deoxygenation products and not graphic coke. The ability of Pt to chemisorb H_2 and facilitate H migration across the surface of the catalyst presumably helps to remove these adsorbents, resulting in the decreasing amount of coke observed on catalysts of increasing Pt loading.

Table 5.1. Textural properties and metal dispersion of the catalysts studied.

Active Phase	N_2 Physisorption			Avg. NiO particle size (nm)*
	BET surface area (m^2/g)	Pore vol. (cm^3/g)	Avg. pore diameter (nm)	
20% Ni	135	0.29	7.0	6.8
20% Ni-0.1% Pt	129	0.27	7.0	7.4
20% Ni-0.25% Pt	138	0.29	7.0	6.1
20% Ni-0.5% Pt	134	0.29	6.9	8.7
0.5%Pt	196	0.13	4.56	-

*Obtained from applying the Scherrer equation to the powdered X-ray diffractograms of the calcined catalysts.

Table 5.2. Pulsed H_2 chemisorption results of the catalysts screened for the deoxygenation of tristearin.

Active Phase	H_2 Ads. (mL/g)	Pt Ads. of H_2 for 50% Dispersion[a]	Pt H_2 Ads. of H_2 for 100% Dispersion[a]	H_2 Ads. of Ni-Pt for 100% Pt Dispersion[b]
20% Ni	0.095	-	-	-
20% Ni-0.1% Pt	0.461	0.028	0.057	0.152
20% Ni-0.25% Pt	0.560	0.071	0.144	0.239
20% Ni-0.5% Pt	0.639	0.144	0.287	0.382
0.5%Pt	0.371	0.144	0.287	0.287

[a]Values shown are calculated from the theoretical Pt metal dispersion and do not include Ni metal dispersion.

[b]Values shown are theoretical H_2 adsorptions if Ni metal sites were not affected by the addition of Pt.

Table 5.3. Semi-batch mode deoxygenation of tristearin over alumina-supported Ni-based catalysts (580 psi of H_2, 260 °C, 3 h reaction time).*

Active Phase	Conversion (%)[a]	Selectively to [Yield of] C10-C17 (%)[b, e]	Selectively to [Yield of] C17 (%)[c, e]	Selectively to [Yield of] C18 (%)[d, e]
20% Ni	2	83 [2]	83 [2]	3 [<1]
20% Ni-0.1% Pt	21	93 [20]	69 [15]	3 [1]
20% Ni-0.25% Pt	66	99 [65]	72 [48]	0 [0]
20% Ni-0.5% Pt	100	96 [96]	65 [65]	2 [0]
0.5% Pt	5	70 [4]	65 [3]	3 [0]

*All experiments for which results are shown were performed a minimum of two times and the values presented are averaged from the multiple experiments. The average standard deviations being 0.9, 0.9, and 2.4% for conversion, selectivity to C10-C17, and selectivity to C17, respectively.

[a] Conversion = wt% of product with b.p. < 375°C.

[b] Selectivity to C10-C17 = 100 × [(wt% of product with b.p. < 314°C – wt% of product with b.p. < 177°C)/(wt% of product with b.p. < 375°C)].

[c] Selectivity to C17 = 100 × [(wt% of product with b.p. < 314°C – wt% of product with b.p. < 295°C)/(wt% of product with b.p. < 375°C)].

[d] The corresponding yield (conversion × selectivity) values are shown between brackets.

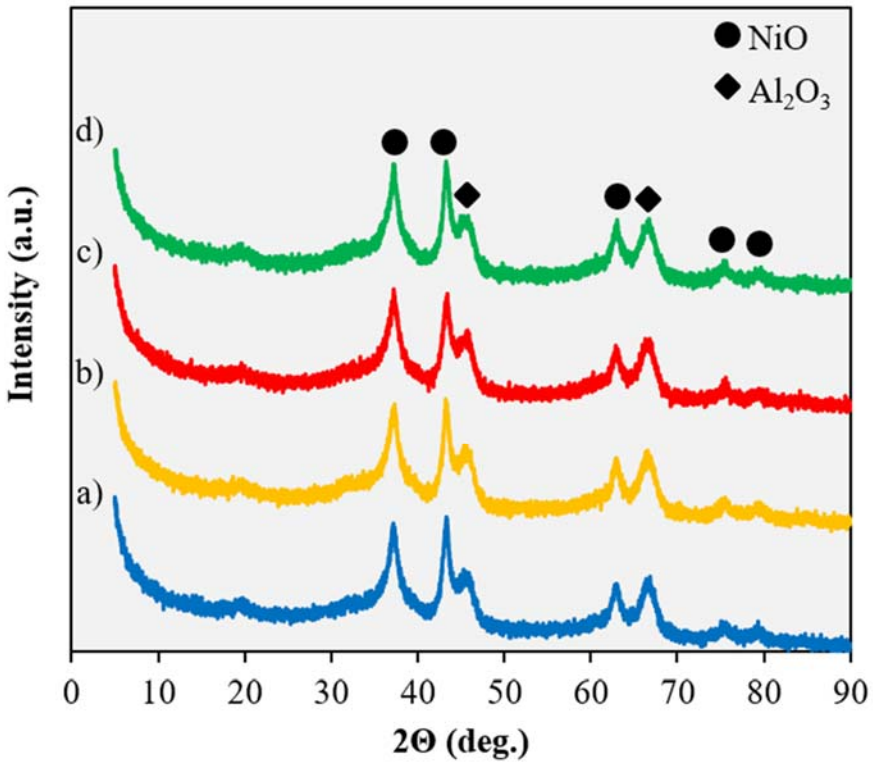

Figure 5.1. X-ray diffraction patterns for 20%Ni/Al_2O_3 (a), 20%Ni-0.1%Pt/Al_2O_3 (b), 20%Ni-0.25%Pt/Al_2O_3 (c), and 20%Ni-0.5%Pt/Al_2O_3 (d).

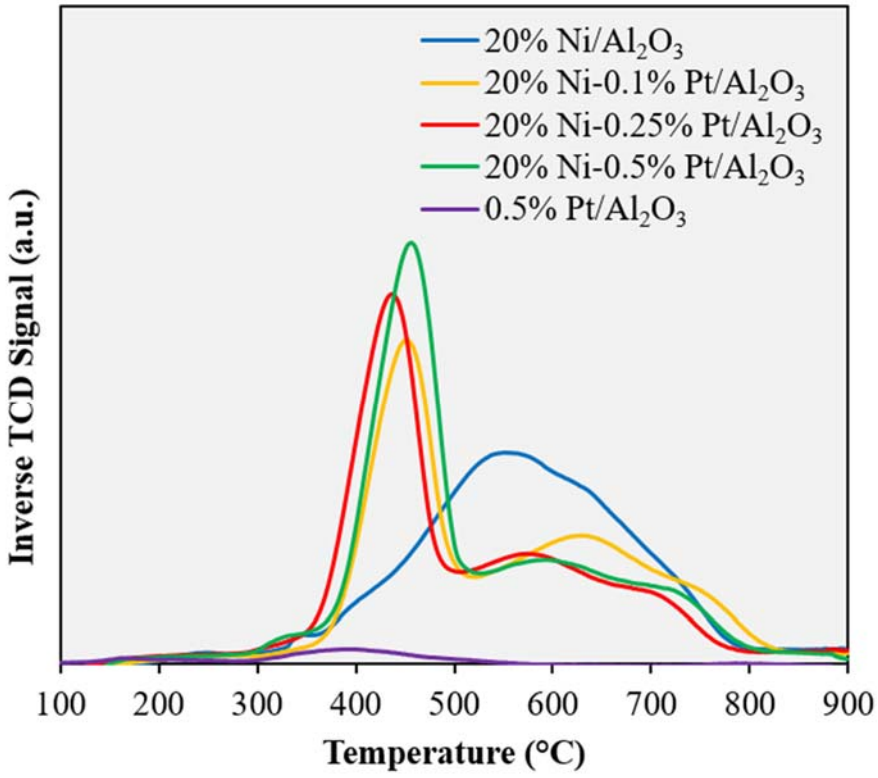

Figure 5.2. Temperature programmed reduction profile of the catalysts screened for the deoxygenation of tristearin

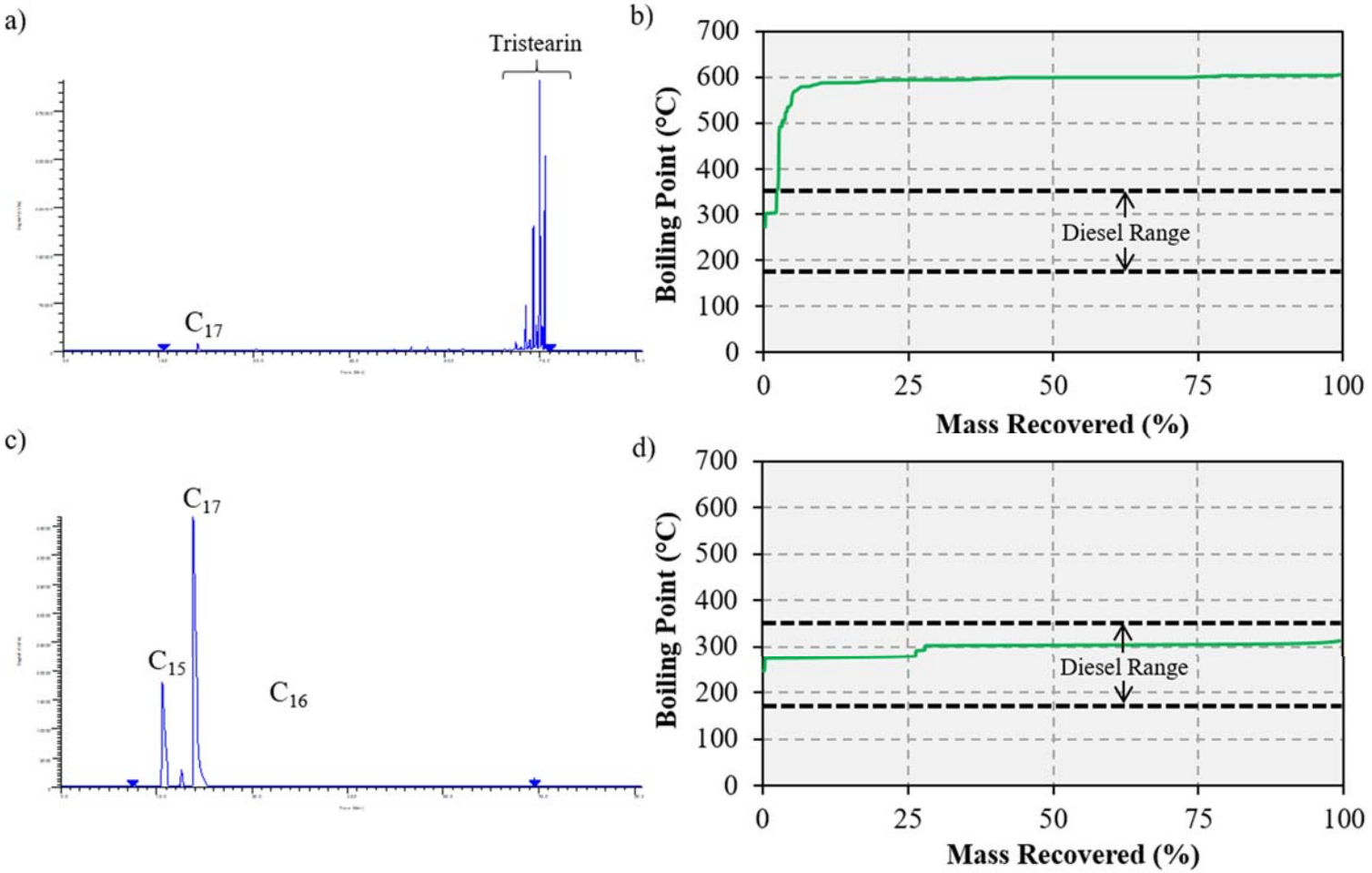

Figure 5.3. Gas chromatograms and BPDPs of the liquid products collected from the deoxygenation of tristearin with 20%Ni/Al_2O_3 (a and b) and 20%Ni-0.5%Pt/Al_2O_3 (c and d) at 260 °C.

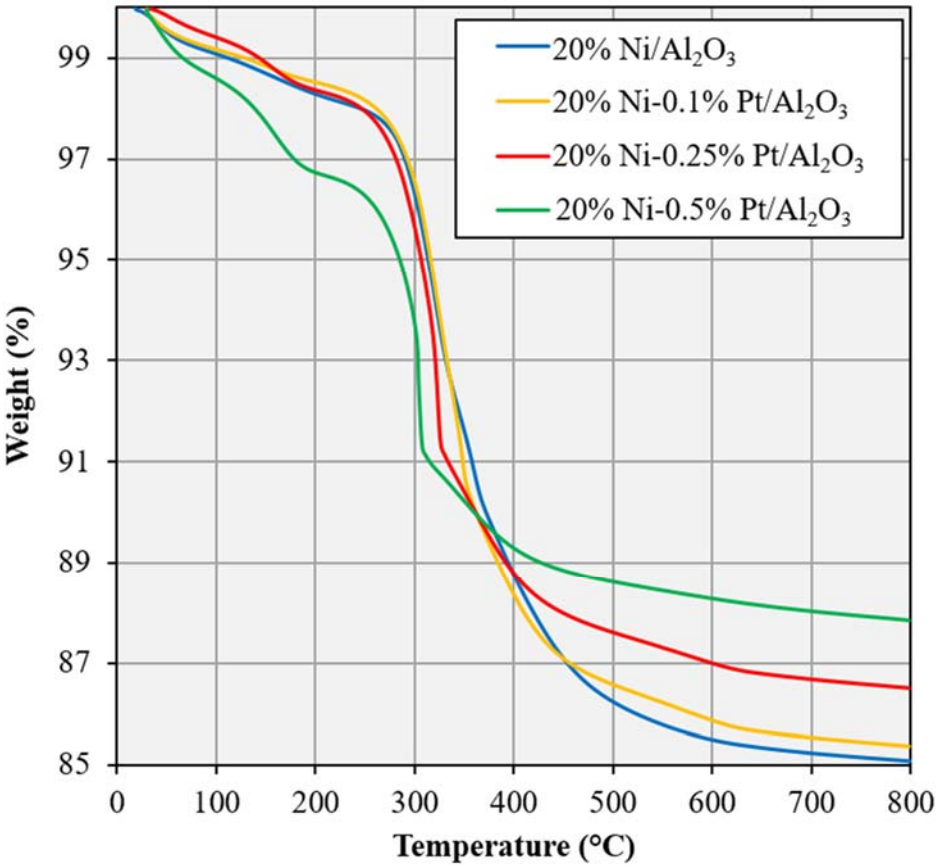

Figure 5.4. Thermogravimetric analysis of the spent catalysts from the deoxygenation of tristearin.

Chapter 6. Conclusions and future outlooks

6.1. Conclusions

The initial catalyst screening of Cu and Sn as promoter metals for 20% Ni/Al_2O_3 indicate that Cu is a very effective promoter of Ni for the $deCO_x$ of tristearin at 260 °C, tristearin conversion increasing from 27% over 20% Ni/Al_2O_3 to 97% over 20% Ni-5% Cu/Al_2O_3. Cu also promoted the deoxygenation of stearic acid in semi-batch mode, indicating 20% Ni-5% Cu/Al_2O_3 to be a promising catalyst for the catalytic deoxygenation of both esters and carboxylic acids. Improvements in $deCO_x$ performance arising from Cu addition to Ni catalysts does not appear related to particle size effects. The Cu promotion arises from a combination of factors including the destabilization of NiO and the consequent increase in the proportion of surface Ni^0, which is believed the catalytically active phase for lipid deoxygenation. Thermogravimetric analysis of spent catalysts from the semi-batch experiments suggests that an additional effect of Cu is the suppression of surface coking and hence catalyst deactivation. Enhanced resistance to coke-induced deactivation may reflect the ability of Cu to curb the cracking activity of Ni-only catalysts. Indeed, this effect is observed with the implementation of an industrially relevant fixed bed reactor and realistic feeds.

In a continuous fixed bed reactor, Ni/Al_2O_3 and $Ni\text{-}Cu/Al_2O_3$ were found to be effective catalysts for the conversion of yellow grease (25 wt% in dodecane) to linear alkanes at 350 °C. However, the Ni-Cu catalyst showed improved selectivity to long chain (C15-C17) hydrocarbons relative to the monometallic formulation. Chain shortening of the

produced hydrocarbons was found to occur mainly via the removal of terminal carbons, although a small amount of internal cracking. The Cu promoted catalysts exhibited significantly less end-chain cracking which additionally improves H_2 utilization. Ni-Cu catalyst was also effective in curbing cracking of a more unsaturated feed, hemp seed oil. Cu promotion was most pronounced in the upgrading of 75 wt% yellow grease, the Ni-Cu catalyst yielding ≥92% diesel-like hydrocarbons (regardless of the time on stream) whereas no liquid products were obtained over Ni/Al_2O_3.

Given that the concentrated feeds studied were primarily triglycerides, the 20% Ni-5% Cu/Al_2O_3 catalyst was further investigated using primarily fatty acid feeds. The Ni-Cu catalyst was found to be effective in this regard in that near quantitative conversion of the 25 wt% fatty acid (in dodecane) feed was achieved regardless of the reaction temperature employed in this study. C16 and C18 (primary HDO products) selectivity averaged ~15% of the total liquid products at 375 °C, the temperature that offered the highest diesel yield, whereas C15 and C17 (primary $deCO_x$ products) averaged 60%. Notably, the increase in lipid concentration from 25 wt% used in the fatty acid experiments to 50 wt% used in the brown grease experiments does not prevent the catalyst from achieving quantitative conversion of the brown grease lipids after 8 hours on stream. Under reduced H_2 partial pressure the 20% Ni-5% Cu/Al_2O_3 catalyst yielded a larger amount of heavy chain hydrocarbons; however, the H_2 consumed in methanation of the CO or CO_2 was significantly decreased.

Investigating the 20% Ni-5% Cu/Al_2O_3 catalyst for the deoxygenation of brown grease lipids in longer experimental conditions revealed the that >90% of the liquid products were diesel-like hydrocarbons after the first 48 h on stream. The diesel yield decreased each hour afterwards; however, the catalyst still yielded >80% fuel-like hydrocarbons after 100 h. The catalyst was regenerated *in situ* after the first 100 h on stream to assess the recyclability. The regenerated catalyst offered improved catalytic performance in that >90% of the liquid products obtained after 72 h were diesel-like hydrocarbons, decreasing to 88% by 100 h. Notably, methanation was negligible during the second 100 h on stream suggesting irreversible poisoning of CO adsorption sites or irreversible coke formation that decrease in the CO binding energy to the Ni sites occurs during the first 100 h.

Investigating other potential catalyst promoter metals showed that minimal amounts of Pt is an effective promoter for supported Ni catalysts in the deCO_x of tristearin at 260 °C. The catalyst evaluation in a semi-batch reactor showed tristearin conversion increased from 2% over 20% Ni/Al_2O_3 to 100% over 20% Ni-0.5% Pt/Al_2O_3 in 3 h of reaction time. In addition, 20% Ni-0.5% Pt/Al_2O_3 yielded a selectivity to diesel-like hydrocarbons (C10-C17) of 96%. Notably, improvements in deCO_x performance result from a synergistic effect of the two metals, indicated by poor catalytic activity of the monometallic 20% Ni/Al_2O_3 and 0.5% Pt/Al_2O_3 catalysts. Temperature programmed reduction experiments showed the addition of 0.1% Pt was effect if facilitating the reduction of Ni to lower temperatures. This is a similar promotional effect responsible for

the improved performance of the Ni-Cu catalyst; however, minimal increases in Ni reduction occurs when the Pt loading is increased from 0.1% to 0.5%. The difference in tristearin conversion from 20% Ni/Al_2O_3 to 20% Ni-0.5% Pt/Al_2O_3 was 21% and 100%, respectively, suggesting an alternative promotion effect must be occurring with increases in Pt loading. Thermogravimetric analysis of the spent catalysts from the deCO_x experiments show that an increase in Pt loading leads to a decrease in coke formation; however, the difference in coke formation from the most active and least active catalyst is minimal. It is possible that Pt is lowering the binding energy of the products (i.e., CO) to the Ni active sites, resulting in increased product desorption rates and faster reactivation of the Ni active sites. The increased Pt loading would enhance this effect resulting in the observed promotion in conversion; however, this was not tested in this study.

6.2. Future Outlooks

Although the results of the Ni-Cu and Ni-Pt catalysts were promising there are still a number of possibilities for further catalyst and process development. One possibility is the addition of alternative promoter metals such as Fe. Studies have shown Ni-Fe catalysts to exhibit increased catalytic activity in the HDO of m-cresol, a model bio-oil compound [245]. Recently, a 20% Ni-5% Fe/Al_2O_3 catalyst was screened alongside 20% Ni-5% Cu/ Al_2O_3 for the deoxygenation of tristearin at 260 °C for 3 h, resulting in a conversion of 100% and 59 %, respectively. The reasoning for the improved performance of the Fe catalyst and the optimal Fe metal loading have not yet been identified; however, the initial

results are encouraging. Additionally, reducible supports such as ZrO_2 have been shown to exhibit better catalytic performance due to the ability of the support to participate in the deoxygenation mechanism [121]. Therefore, a $CePrO_2$ support was briefly investigated and a monometallic 20 wt.% $Ni/Ce_{0.8}Pr_{0.2}O_2$ catalyst exhibited a 59% conversion of tristearin when subject to the same 260 °C, 3 h reaction times listed previously. This is a significant improvement over the monometallic Al_2O_3 supports and even rivals the promoted catalysts. This suggests further investigation into promoted formulations of this catalyst would be informative. Additionally, alternative supports may be necessary as the effect of water content in the feeds employed may prove problematic. The feeds employed in this study were dewatered; however, to dewater feeds on a large scale would be energy intensive and expensive. The dewatering step could be avoided by using a hydrothermally stable support, making the process could be more industrially feasible. The alumina support incorporated in this study is known to form boehmite (AlOOH) under hydrothermal conditions that results in a reduced catalyst surface area and sintering of the supported metal particles, hence severe catalyst deactivation, further increasing interest into the reducible support ZrO_2 and $CePrO_2$. Additional improvements would also consider simultaneous H_2 generation during the deoxygenation of lipids. This has been attempted by feeding methanol [246] or glycerol [247] in addition to the lipid feed stocks and selectivity reforming them to provide the needed H_2. This would significantly lower production costs as well and some attempts at simultaneous reforming of either glycerol or methanol have already been attempted by some authors with mixed success. Although there are several factors that can still be addressed in order to produce more efficient catalysts as well as

bifunctional reforming and deoxygenating catalysts, the results from this study are indeed encouraging.

REFERENCES

1. US Energy Information Administration, (2017). Internation Energy Outlook.
2. IEA Bioenergy Task 40 Sustainable Internation Bioenergy Trade, (2012). The potential role of biofuels in commercial air transport–biojetfuel.
3. Benazzi, E., Cameron, C., (2006). Boutique diesel in the on-road market, Hydrocarbon Process., 85 (3): DD17-DD18.
4. Chevron, (2006). Alternative jet fuels.
5. Pattanaik, B.P., Misra, R.D., (2017). Effect of reaction pathway and operating parameters on the deoxygenation of vegetable oils to produce diesel range hydrocarbon fuels: A review, Renew. Sustain. Energy Rev., 73: 545-557.
6. Naik, S.N., Goud, V.V., Rout, P.K., Dalai, A.K., (2010). Production of first and second generation biofuels: A comprehensive review, Renew. Sustain. Energy Rev., 14 (2): 578-597.
7. Knothe, G., (2010). Biodiesel and renewable diesel: A comparison, Prog. Energy Combust. Sci., 36 (3): 364-373.
8. Kordulis, C., Bourikas, K., Gousi, M., Kordouli, E., Lycourghiotis, A., (2016). Development of nickel based catalysts for the transformation of natural triglycerides and related compounds into green diesel: a critical review, Appl. Catal. B, 181: 156-196.
9. Kubičková, I., Snåre, M., Eränen, K., Mäki-Arvela, P., Murzin, D.Y., (2005). Hydrocarbons for diesel fuel via decarboxylation of vegetable oils, Catal. Today, 106 (1-4): 197-200.
10. Tran, N.H., Bartlett, J.R., Kannangara, G.S.K., Milev, A.S., Volk, H., Wilson, M.A., (2010). Catalytic upgrading of biorefinery oil from micro-algae, Fuel, 89 (2): 265-274.
11. Santillan-Jimenez, E., Crocker, M., (2012). Catalytic deoxygenation of fatty acids and their derivatives to hydrocarbon fuels via decarboxylation/decarbonylation, J. Chem. Technol. Biotechnol., 87 (8): 1041-1050.
12. Ameen, M., Azizan, M.T., Yusup, S., RamLi, A., Yasir, M., (2017). Catalytic hydrodeoxygenation of triglycerides: An approach to clean diesel fuel production, Renew. Sustain. Energy Rev., 80: 1072-1088.
13. Sotelo-Boyás, R., Trejo-Zárraga, F., de Jesús Hernández-Loyo, F., (2012), Hydroconversion of triglycerides into green liquid fuels, Hydrogenation, InTech, pp. 187-216.
14. Snåre, M., Mäki-Arvela, P., Simakova, I., Myllyoja, J., Murzin, D.Y., (2009). Overview of catalytic methods for production of next generation biodiesel from natural oils and fats, Russ. J. Phys. Chem. B, 3 (7): 1035-1043.
15. Morgan, T., Grubb, D., Santillan-Jimenez, E., Crocker, M., (2010). Conversion of triglycerides to hydrocarbons over supported metal catalysts, Top. Catal., 53 (11-12): 820-829.
16. Huber, G.W., O'Connor, P., Corma, A., (2007). Processing biomass in conventional oil refineries: Production of high quality diesel by hydrotreating vegetable oils in heavy vacuum oil mixtures, Appl. Catal. A, 329: 120-129.
17. Berenblyum, A.S., Danyushevsky, V.Y., Katsman, E.A., Podoplelova, T.A., Flid, V.R., (2010). Production of engine fuels from inedible vegetable oils and fats, Pet. Chem., 50 (4): 305-311.
18. Bertram, S.H., (1936). Action of selenium on stearic acid, ChemWeek, 33: 457-459.

19. Foglia, T., Barr, P., (1976). Decarbonylation dehydration of fatty acids to alkenes in the presence of transition metal complexes, J. Am. Oil Chem. Soc., 53 (12): 737-741.
20. Stern, R., Hillion, G., (1985), Process for manufacturing a linear olefin from a saturated fatty acid or fatty acid ester, US Patent 4,554,397, filed 24 August, 1984 and issued 19 November, 1985.
21. Maier, W.F., Roth, W., Thies, I., Schleyer, P.V.R., (1982). Hydrogenolysis, IV. Gas phase decarboxylation of carboxylic acids, Eur. J. Inorg. Chem., 115 (2): 808-812.
22. Knothe, G., Steidley, K.R., Moser, B.R., Doll, K.M., (2017). Decarboxylation of fatty acids with triruthenium dodecacarbonyl: Influence of the compound structure and analysis of the product mixtures, ACS Omega, 2 (10): 6473-6480.
23. Moser, B.R., Knothe, G., Walter, E.L., Murray, R.E., Dunn, R.O., Doll, K.M., (2016). Analysis and properties of the decarboxylation products of oleic acid by catalytic triruthenium dodecacarbonyl, Energy Fuels, 30 (9): 7443-7451.
24. Li, W., Gao, Y., Yao, S., Ma, D., Yan, N., (2015). Effective deoxygenation of fatty acids over $Ni(OAc)_2$ in the absence of H_2 and solvent, Green Chem., 17 (8): 4198-4205.
25. John, A., Dereli, B.s., Ortuño, M.A., Johnson, H.E., Hillmyer, M.A., Cramer, C.J., Tolman, W.B., (2017). Selective decarbonylation of fatty acid esters to linear α-olefins, Organometallics, 36 (15): 2956-2964.
26. John, A., Hillmyer, M.A., Tolman, W.B., (2017). Anhydride-additive-free nickel-catalyzed deoxygenation of carboxylic acids to olefins, Organometallics, 36 (3): 506-509.
27. Bie, Y., Lehtonen, J., Kanervo, J., (2016). Hydrodeoxygenation (HDO) of methyl palmitate over bifunctional Rh/ZrO_2 catalyst: Insights into reaction mechanism via kinetic modeling, Appl. Catal. A, 526: 183-190.
28. Murray, R.E., Walter, E.L., Doll, K.M., (2014). Tandem isomerization-decarboxylation for converting alkenoic fatty acids into alkenes, ACS Catal., 4 (10): 3517-3520.
29. Di, L., Yao, S., Song, S., Wu, G., Dai, W., Guan, N., Li, L., (2017). Robust ruthenium catalysts for the selective conversion of stearic acid to diesel-range alkanes, Appl. Catal. B, 201: 137-149.
30. Rodina, V., Ermakov, D.Y., Saraev, A., Reshetnikov, S., Yakovlev, V., (2017). Influence of reaction conditions and kinetic analysis of the selective hydrogenation of oleic acid toward fatty alcohols on $Ru\text{-}Sn\text{-}B/Al_2O_3$ in the flow reactor, Appl. Catal. B, 209: 611-620.
31. He, L., Wu, C., Cheng, H., Yu, Y., Zhao, F., (2012). Highly selective and efficient catalytic conversion of ethyl stearate into liquid hydrocarbons over a Ru/TiO_2 catalyst under mild conditions, Catal. Sci. Technol., 2 (7): 1328-1331.
32. Zhao, X., Wei, L., Cheng, S., Kadis, E., Cao, Y., Boakye, E., Gu, Z., Julson, J., (2016). Hydroprocessing of carinata oil for hydrocarbon biofuel over $Mo\text{-}Zn/Al_2O_3$, Appl. Catal. B, 196: 41-49.
33. Asikin-Mijan, N., Lee, H., Juan, J., Noorsaadah, A., Ong, H.C., Razali, S., Taufiq-Yap, Y., (2017). Promoting deoxygenation of triglycerides via Co-Ca loaded $SiO_2\text{-}Al_2O_3$ catalyst, Appl. Catal. A, 552: 38-48.
34. Cao, Y., Shi, Y., Bi, Y., Wu, K., Hu, S., Wu, Y., Huang, S., (2018). Hydrodeoxygenation and hydroisomerization of palmitic acid over bi-functional Co/H-ZSM-22 catalysts, Fuel Process. Technol., 172: 29-35.

35. Bian, J., Wang, Y., Zhang, Q., Fang, X., Feng, L., Li, C., (2017). Fatty acid decarboxylation reaction kinetics and pathway of co-conversion with amino acid on supported iron oxide catalysts, RSC Adv., 7 (75): 47279-47287.
36. Kandel, K., Anderegg, J.W., Nelson, N.C., Chaudhary, U., Slowing, I.I., (2014). Supported iron nanoparticles for the hydrodeoxygenation of microalgal oil to green diesel, J. Catal., 314: 142-148.
37. Al Alwan, B., Salley, S.O., Ng, K.Y.S., (2015). Biofuels production from hydrothermal decarboxylation of oleic acid and soybean oil over Ni-based transition metal carbides supported on Al-SBA-15, Appl. Catal. A, 498: 32-40.
38. Han, J., Duan, J., Chen, P., Lou, H., Zheng, X., Hong, H., (2011). Nanostructured molybdenum carbides supported on carbon nanotubes as efficient catalysts for one-step hydrodeoxygenation and isomerization of vegetable oils, Green Chem., 13 (9): 2561.
39. Rocha, A.S., Souza, L.A., Oliveira Jr., R.R., Rocha, A.B., da Silva, V.T., (2017). Hydrodeoxygenation of acrylic acid using Mo_2C/Al_2O_3, Appl. Catal. A, 531: 69-78.
40. Stellwagen, D.R., Bitter, J.H., (2015). Structure–performance relations of molybdenum- and tungsten carbide catalysts for deoxygenation, Green Chem., 17 (1): 582-593.
41. Wang, W., Zhang, K., Liu, H., Qiao, Z., Yang, Y., Ren, K., (2013). Hydrodeoxygenation of p-cresol on unsupported Ni–P catalysts prepared by thermal decomposition method, Catal. Commun., 41: 41-46.
42. Prins, R., Bussell, M.E., (2012). Metal Phosphides: Preparation, Characterization and Catalytic Reactivity, Catal. Lett., 142 (12): 1413-1436.
43. Peroni, M., Lee, I., Huang, X., Baráth, E., Gutiérrez, O.Y., Lercher, J.A., (2017). Deoxygenation of palmitic acid on Unsupported transition-metal phosphides, ACS Catal., 7 (9): 6331-6341.
44. Pan, Z., Wang, R., Nie, Z., Chen, J., (2016). Effect of a second metal (Co, Fe, Mo and W) on performance of Ni_2P/SiO_2 for hydrodeoxygenation of methyl laurate, J. Energy Chem., 25 (3): 418-426.
45. Liu, C., Hao, Y., Jing, Z., Xi, K., Qiao, C., (2016). Hydrodeoxygenation of fatty acid methyl esters and isomerization of products over NiP/SAPO-11 catalysts, J. Fuel Chem. Technol., 44 (10): 1211-1216.
46. Alvarez-Galvan, M.C., Blanco-Brieva, G., Capel-Sanchez, M., Morales-delaRosa, S., Campos-Martin, J.M., Fierro, J.L., (2018). Metal phosphide catalysts for the hydrotreatment of non-edible vegetable oils, Catal. Today, 302: 242-249.
47. Liu, Y., Yao, L., Xin, H., Wang, G., Li, D., Hu, C., (2015). The production of diesel-like hydrocarbons from palmitic acid over HZSM-22 supported nickel phosphide catalysts, Appl. Catal. B, 174-175: 504-514.
48. Ferrari, M., Maggi, R., Delmon, B., Grange, P., (2001). Influences of the hydrogen sulfide partial pressure and of a nitrogen compound on the hydrodeoxygenation activity of a CoMo/Carbon Catalyst, J. Catal., 198 (1): 47-55.
49. Yang, Y., Wang, Q., Zhang, X., Wang, L., Li, G., (2013). Hydrotreating of C18 fatty acids to hydrocarbons on sulphided $NiW/SiO_2–Al_2O_3$, Fuel Process. Technol., 116: 165-174.
50. Verma, D., Rana, B.S., Kumar, R., Sibi, M., Sinha, A.K., (2015). Diesel and aviation kerosene with desired aromatics from hydroprocessing of jatropha oil over hydrogenation catalysts supported on hierarchical mesoporous SAPO-11, Appl. Catal. A, 490: 108-116.

51. Priecel, P., Kubička, D., Čapek, L., Bastl, Z., Ryšánek, P., (2011). The role of Ni species in the deoxygenation of rapeseed oil over NiMo-alumina catalysts, Appl. Catal. A, 397 (1-2): 127-137.
52. Srifa, A., Viriya-empikul, N., Assabumrungrat, S., Faungnawakij, K., (2015). Catalytic behaviors of Ni/γ-Al_2O_3 and Co/γ-Al_2O_3 during the hydrodeoxygenation of palm oil, Catal. Sci. Technol., 5 (7): 3693-3705.
53. Srifa, A., Faungnawakij, K., Itthibenchapong, V., Assabumrungrat, S., (2015). Roles of monometallic catalysts in hydrodeoxygenation of palm oil to green diesel, Chem. Eng. J., 278: 249-258.
54. Onyestyák, G., Harnos, S., Szegedi, Á., Kalló, D., (2012). Sunflower oil to green diesel over Raney-type Ni-catalyst, Fuel, 102: 282-288.
55. Kikhtyanin, O.V., Rubanov, A.E., Ayupov, A.B., Echevsky, G.V., (2010). Hydroconversion of sunflower oil on Pd/SAPO-31 catalyst, Fuel, 89 (10): 3085-3092.
56. Sugami, Y., Minami, E., Saka, S., (2016). Renewable diesel production from rapeseed oil with hydrothermal hydrogenation and subsequent decarboxylation, Fuel, 166: 376-381.
57. Sugami, Y., Minami, E., Saka, S., (2017). Hydrocarbon production from coconut oil by hydrolysis coupled with hydrogenation and subsequent decarboxylation, Fuel, 197: 272-276.
58. Herskowitz, M., Landau, M.V., Reizner, Y., Berger, D., (2013). A commercially-viable, one-step process for production of green diesel from soybean oil on Pt/SAPO-11, Fuel, 111: 157-164.
59. Fargione, J., Hill, J., Tilman, D., Polasky, S., Hawthorne, P., (2008). Land clearing and the biofuel carbon debt, Science, 319 (5867): 1235-1238.
60. Tilman, D., Hill, J., Lehman, C., (2006). Carbon-negative biofuels from low-input high-diversity grassland biomass, Science, 314 (5805): 1598-1600.
61. Vásquez, M.C., Silva, E.E., Castillo, E.F., (2017). Hydrotreatment of vegetable oils: A review of the technologies and its developments for jet biofuel production, Biomass Bioenergy, 105: 197-206.
62. Amin, S., (2009). Review on biofuel oil and gas production processes from microalgae, Energy Convers. Manage., 50 (7): 1834-1840.
63. Zhao, C., Brück, T., Lercher, J.A., (2013). Catalytic deoxygenation of microalgae oil to green hydrocarbons, Green Chem., 15 (7): 1720-1739.
64. Posten, C., Schaub, G., (2009). Microalgae and terrestrial biomass as source for fuels—a process view, J. Biotechnol., 142 (1): 64-69.
65. Mata, T.M., Martins, A.A., Caetano, N.S., (2010). Microalgae for biodiesel production and other applications: a review, Renew. Sustain. Energy Rev., 14 (1): 217-232.
66. Brennan, L., Owende, P., (2010). Biofuels from microalgae—a review of technologies for production, processing, and extractions of biofuels and co-products, Renew. Sustain. Energy Rev., 14 (2): 557-577.
67. Bwapwa, J.K., Anandraj, A., Trois, C., (2017). Possibilities for conversion of microalgae oil into aviation fuel: A review, Renew. Sustain. Energy Rev., 80: 1345-1354.
68. Shi, F., Wang, P., Duan, Y., Link, D., Morreale, B., (2012). Recent developments in the production of liquid fuels via catalytic conversion of microalgae: experiments and simulations, RSC Adv., 2 (26): 9727-9747.

69. Chen, Y., Wu, Y., Hua, D., Li, C., Harold, M.P., Wang, J., Yang, M., (2015). Thermochemical conversion of low-lipid microalgae for the production of liquid fuels: challenges and opportunities, RSC Adv., 5 (24): 18673-18701.
70. Berenblyum, A.S., Podoplelova, T.A., Shamsiev, R.S., Katsman, E.A., Danyushevsky, V.Y., Flid, V.R., (2012). Catalytic chemistry of preparation of hydrocarbon fuels from vegetable oils and fats, Catal. Ind., 4 (3): 209-214.
71. Mäki-Arvela, P.i., Rozmysłowicz, B., Lestari, S., Simakova, O., Eränen, K., Salmi, T., Murzin, D.Y., (2011). Catalytic deoxygenation of tall oil fatty acid over palladium supported on mesoporous carbon, Energy Fuels, 25 (7): 2815-2825.
72. Jenišťová, K., Hachemi, I., Mäki-Arvela, P., Kumar, N., Peurla, M., Čapek, L., Wärnå, J., Murzin, D.Y., (2017). Hydrodeoxygenation of stearic acid and tall oil fatty acids over Ni-alumina catalysts: influence of reaction parameters and kinetic modelling, Chem. Eng. J., 316: 401-409.
73. Chhetri, A.B., Watts, K.C., Islam, M.R., (2008). Waste cooking oil as an alternate feedstock for biodiesel production, Energies, 1 (1): 3-18.
74. Santillan-Jimenez, E., Loe, R., Garrett, M., Morgan, T., Crocker, M., (2018). Effect of Cu promotion on cracking and methanation during the Ni-catalyzed deoxygenation of waste lipids and hemp seed oil to fuel-like hydrocarbons, Catal. Today, 302: 261-271.
75. Loe, R., Santillan-Jimenez, E., Morgan, T., Sewell, L., Ji, Y., Jones, S., Isaacs, M.A., Lee, A.F., Crocker, M., (2016). Effect of Cu and Sn promotion on the catalytic deoxygenation of model and algal lipids to fuel-like hydrocarbons over supported Ni catalysts, Appl. Catal. B, 191: 147-156.
76. Ford, J.P., Thapaliya, N., Kelly, M.J., Roberts, W.L., Lamb, H.H., (2013). Semi-batch deoxygenation of canola- and lard-derived fatty cids to diesel-range hydrocarbons, Energy Fuels, 27 (12): 7489-7496.
77. Sari, E., DiMaggio, C., Kim, M., Salley, S.O., Ng, K.Y.S., (2013). Catalytic conversion of brown grease to green diesel via decarboxylation over activated carbon supported palladium catalyst, Ind. Eng. Chem. Res., 52 (33): 11527-11536.
78. Simakova, I., Simakova, O., Mäki-Arvela, P., Murzin, D.Y., (2010). Decarboxylation of fatty acids over Pd supported on mesoporous carbon, Catal. Today, 150 (1-2): 28-31.
79. Fu, J., Lu, X., Savage, P.E., (2011). Hydrothermal decarboxylation and hydrogenation of fatty acids over Pt/C, ChemSusChem, 4 (4): 481-486.
80. Lestari, S., Mäki-Arvela, P., Simakova, I., Beltramini, J., Lu, G.Q.M., Murzin, D.Y., (2009). Catalytic Deoxygenation of Stearic Acid and Palmitic Acid in Semibatch Mode, Catal. Lett., 130 (1-2): 48-51.
81. Yang, L., Carreon, M.A., (2017). Deoxygenation of palmitic and lauric acids over Pt/ZIF-67 membrane/zeolite 5A bead catalysts, ACS Appl. Mater. Int., 9 (37): 31993-32000.
82. Ford, J.P., Immer, J.G., Lamb, H.H., (2012). Palladium catalysts for fatty acid deoxygenation: influence of the support and fatty acid chain length on decarboxylation kinetics, Top. Catal., 55 (3-4): 175-184.
83. Mohite, S., Armbruster, U., Richter, M., Martin, A., (2014). Impact of chain length of saturated fatty acids during their heterogeneously catalyzed deoxygenation, J. Sustain. Bioenergy Syst., 4 (3): 183-193.

84. Snåre, M., Kubičková, I., Mäki-Arvela, P., Eränen, K., Murzin, D.Y., (2006). Heterogeneous catalytic deoxygenation of stearic acid for production of biodiesel, Ind. Eng. Chem. Res., 45 (16): 5708-5715.
85. Wu, J., Shi, J., Fu, J., Leidl, J.A., Hou, Z., Lu, X., (2016). Catalytic decarboxylation of fatty acids to aviation fuels over nickel supported on activated carbon, Scientific Reports, 6: 27820.
86. Berenblyum, A.S., Shamsiev, R.S., Podoplelova, T.A., Danyushevsky, V.Y., (2012). The influence of metal and carrier natures on the effectiveness of catalysts of the deoxygenation of fatty acids into hydrocarbons, Russ. J. Phys. Chem. A, 86 (8): 1199-1203.
87. Madsen, A.T., Ahmed, E.H., Christensen, C.H., Fehrmann, R., Riisager, A., (2011). Hydrodeoxygenation of waste fat for diesel production: Study on model feed with Pt/alumina catalyst, Fuel, 90 (11): 3433-3438.
88. Lugo-José, Y.K., Monnier, J.R., Williams, C.T., (2014). Gas-phase, catalytic hydrodeoxygenation of propanoic acid, over supported group VIII noble metals: Metal and support effects, Appl. Catal. A, 469: 410-418.
89. Gong, S., Chen, N., Nakayama, S., Qian, E.W., (2013). Isomerization of n-alkanes derived from jatropha oil over bifunctional catalysts, J. Mol. Catal. A: Chem., 370: 14-21.
90. Chen, N., Gong, S., Shirai, H., Watanabe, T., Qian, E.W., (2013). Effects of Si/Al ratio and Pt loading on Pt/SAPO-11 catalysts in hydroconversion of Jatropha oil, Appl. Catal. A, 466: 105-115.
91. Sun, K., Wilson, A.R., Thompson, S.T., Lamb, H.H., (2015). Catalytic deoxygenation of octanoic acid over supported palladium: Effects of particle size and alloying with gold, ACS Catal., 5 (3): 1939-1948.
92. Kumar, P., Yenumala, S.R., Maity, S.K., Shee, D., (2014). Kinetics of hydrodeoxygenation of stearic acid using supported nickel catalysts: Effects of supports, Appl. Catal. A, 471: 28-38.
93. Zuo, H., Liu, Q., Wang, T., Shi, N., Liu, J., Ma, L., (2012). Catalytic hydrodeoxygenation of vegetable oil over Ni catalysts to produce second-generation biodiesel, J. Fuel Chem. Technol., 40 (9): 1067-1073.
94. Shi, N., Liu, Q.-y., Jiang, T., Wang, T.-j., Ma, L.-l., Zhang, Q., Zhang, X.-h., (2012). Hydrodeoxygenation of vegetable oils to liquid alkane fuels over Ni/HZSM-5 catalysts: Methyl hexadecanoate as the model compound, Catal. Commun., 20: 80-84.
95. Peng, B., Yuan, X., Zhao, C., Lercher, J.A., (2012). Stabilizing catalytic pathways via redundancy: selective reduction of microalgae oil to alkanes, J. Am. Chem. Soc., 134 (22): 9400-9405.
96. Yeh, T.M., Hockstad, R.L., Linic, S., Savage, P.E., (2015). Hydrothermal decarboxylation of unsaturated fatty acids over $PtSn_x$/C catalysts, Fuel, 156: 219-224.
97. Vardon, D.R., Sharma, B.K., Jaramillo, H., Kim, D., Choe, J.K., Ciesielski, P.N., Strathmann, T.J., (2014). Hydrothermal catalytic processing of saturated and unsaturated fatty acids to hydrocarbons with glycerol for in situ hydrogen production, Green Chem., 16 (3): 1507-1520.
98. Yakovlev, V.A., Khromova, S.A., Sherstyuk, O.V., Dundich, V.O., Ermakov, D.Y., Novopashina, V.M., Lebedev, M.Y., Bulavchenko, O., Parmon, V.N., (2009). Development of new catalytic systems for upgraded bio-fuels production from bio-crude-oil and biodiesel, Catal. Today, 144 (3-4): 362-366.

99. Gosselink, R.W., Xia, W., Muhler, M., de Jong, K.P., Bitter, J.H., (2013). Enhancing the activity of Pd on carbon nanofibers for deoxygenation of amphiphilic fatty acid molecules through support polarity, ACS Catal., 3 (10): 2397-2402.
100. Chen, H., Chen, K., Fu, J., Lu, X., Huang, H., Ouyang, P., (2017). Water-mediated promotion of the catalytic conversion of oleic acid to produce an alternative fuel using Pt/C without a H2 source, Catal. Commun., 98: 26-29.
101. Peng, B., Yao, Y., Zhao, C., Lercher, J.A., (2012). Towards quantitative conversion of microalgae oil to diesel-range alkanes with bifunctional catalysts, Angew. Chem., 124 (9): 2114-2117.
102. Duan, J., Han, J., Sun, H., Chen, P., Lou, H., Zheng, X., (2012). Diesel-like hydrocarbons obtained by direct hydrodeoxygenation of sunflower oil over Pd/Al-SBA-15 catalysts, Catal. Commun., 17: 76-80.
103. Ahmadi, M., Macias, E.E., Jasinski, J.B., Ratnasamy, P., Carreon, M.A., (2014). Decarboxylation and further transformation of oleic acid over bifunctional, Pt/SAPO-11 catalyst and Pt/chloride Al_2O_3 catalysts, J. Mol. Catal. A: Chem., 386: 14-19.
104. Smirnova, M.Y., Kikhtyanin, O.V., Smirnov, M.Y., Kalinkin, A.V., Titkov, A.I., Ayupov, A.B., Ermakov, D.Y., (2015). Effect of calcination temperature on the properties of Pt/SAPO-31 catalyst in one-stage transformation of sunflower oil to green diesel, Appl. Catal. A, 505: 524-531.
105. Wang, C., Liu, Q., Song, J., Li, W., Li, P., Xu, R., Ma, H., Tian, Z., (2014). High quality diesel-range alkanes production via a single-step hydrotreatment of vegetable oil over Ni/zeolite catalyst, Catal. Today, 234: 153-160.
106. Liu, Q., Zuo, H., Zhang, Q., Wang, T., Ma, L., (2014). Hydrodeoxygenation of palm oil to hydrocarbon fuels over Ni/SAPO-11 catalysts, Chin. J. Catal., 35 (5): 748-756.
107. Liu, Q., Zuo, H., Wang, T., Ma, L., Zhang, Q., (2013). One-step hydrodeoxygenation of palm oil to isomerized hydrocarbon fuels over Ni supported on nano-sized SAPO-11 catalysts, Appl. Catal. A, 468: 68-74.
108. Lee, S.-P., RamLi, A., (2013). Methyl oleate deoxygenation for production of diesel fuel aliphatic hydrocarbons over Pd/SBA-15 catalysts, Chem. Cent. J., 7 (1): 149.
109. Zuo, H., Liu, Q., Wang, T., Ma, L., Zhang, Q., Zhang, Q., (2012). Hydrodeoxygenation of methyl palmitate over supported Ni catalysts for diesel-like fuel production, Energy Fuels, 26 (6): 3747-3755.
110. Ahmadi, M., Nambo, A., Jasinski, J.B., Ratnasamy, P., Carreon, M.A., (2015). Decarboxylation of oleic acid over Pt catalysts supported on small-pore zeolites and hydrotalcite, Catal. Sci. Technol., 5 (1): 380-388.
111. Lestari, S., Mäki-Arvela, P., Eränen, K., Beltramini, J., Max Lu, G.Q., Murzin, D.Y., (2010). Diesel-like Hydrocarbons from Catalytic Deoxygenation of Stearic Acid over Supported Pd Nanoparticles on SBA-15 Catalysts, Catal. Lett., 134 (3-4): 250-257.
112. Morgan, T., Santillan-Jimenez, E., Harman-Ware, A.E., Ji, Y., Grubb, D., Crocker, M., (2012). Catalytic deoxygenation of triglycerides to hydrocarbons over supported nickel catalysts, Chem. Eng. J., 189-190: 346-355.
113. Mäki-Arvela, P., Snåre, M., Eränen, K., Myllyoja, J., Murzin, D.Y., (2008). Continuous decarboxylation of lauric acid over Pd/C catalyst, Fuel, 87 (17-18): 3543-3549.

114. Snåre, M., Kubičková, I., Mäki-Arvela, P., Chichova, D., Eränen, K., Murzin, D.Y., (2008). Catalytic deoxygenation of unsaturated renewable feedstocks for production of diesel fuel hydrocarbons, Fuel, 87 (6): 933-945.
115. Lestari, S., Maki-Arvela, P., Bernas, H., Simakova, O., Sjöholm, R., Beltramini, J., Lu, G.M., Myllyoja, J., Simakova, I., Murzin, D.Y., (2009). Catalytic deoxygenation of stearic acid in a continuous reactor over a mesoporous carbon-supported Pd catalyst, Energy Fuels, 23 (8): 3842-3845.
116. Immer, J.G., Kelly, M.J., Lamb, H.H., (2010). Catalytic reaction pathways in liquid-phase deoxygenation of C18 free fatty acids, Appl. Catal. A, 375 (1): 134-139.
117. Berenblyum, A.S., Podoplelova, T.A., Shamsiev, R.S., Katsman, E.A., Danyushevsky, V.Y., (2011). On the mechanism of catalytic conversion of fatty acids into hydrocarbons in the presence of palladium catalysts on alumina, Pet. Chem., 51 (5): 336-341.
118. Santillan-Jimenez, E., Morgan, T., Shoup, J., Harman-Ware, A.E., Crocker, M., (2014). Catalytic deoxygenation of triglycerides and fatty acids to hydrocarbons over Ni–Al layered double hydroxide, Catal. Today, 237: 136-144.
119. Santillan-Jimenez, E., Morgan, T., Lacny, J., Mohapatra, S., Crocker, M., (2013). Catalytic deoxygenation of triglycerides and fatty acids to hydrocarbons over carbon-supported nickel, Fuel, 103: 1010-1017.
120. Rozmysłowicz, B., Mäki-Arvela, P., Tokarev, A., Leino, A.-R., Eränen, K., Murzin, D.Y., (2012). Influence of hydrogen in catalytic deoxygenation of fatty acids and their derivatives over Pd/C, Ind. Eng. Chem. Res., 51 (26): 8922-8927.
121. Peng, B., Zhao, C., Kasakov, S., Foraita, S., Lercher, J.A., (2013). Manipulating catalytic pathways: deoxygenation of palmitic acid on multifunctional catalysts, Chem. Eur. J., 19 (15): 4732-4741.
122. Sun, K., Schulz, T.C., Thompson, S.T., Lamb, H.H., (2016). Catalytic deoxygenation of octanoic acid over silica- and carbon-supported palladium: Support effects and reaction pathways, Catal. Today, 269: 93-102.
123. Immer, J.G., Lamb, H.H., (2010). Fed-batch catalytic deoxygenation of free fatty acids, Energy Fuels, 24 (10): 5291-5299.
124. Li, X.-f., Luo, X.-g., (2015). Preparation of mesoporous activated carbon supported Ni catalyst for deoxygenation of stearic acid into hydrocarbons, Environ. Prog. Sustain. Energy, 34 (2): 607-612.
125. Boda, L., Onyestyák, G., Solt, H., Lónyi, F., Valyon, J., Thernesz, A., (2010). Catalytic hydroconversion of tricaprylin and caprylic acid as model reaction for biofuel production from triglycerides, Appl. Catal. A, 374 (1-2): 158-169.
126. Do, P.T., Chiappero, M., Lobban, L.L., Resasco, D.E., (2009). Catalytic deoxygenation of methyl-octanoate and methyl-stearate on Pt/Al_2O_3, Catal. Lett., 130 (1-2): 9-18.
127. Mäki-Arvela, P., Kubickova, I., Snåre, M., Eränen, K., Murzin, D.Y., (2007). Catalytic deoxygenation of fatty acids and their derivatives, Energy Fuels, 21 (1): 30-41.
128. Ding, R., Wu, Y., Chen, Y., Liang, J., Liu, J., Yang, M., (2015). Effective hydrodeoxygenation of palmitic acid to diesel-like hydrocarbons over MoO_2/CNTs catalyst, Chem. Eng. Sci., 135: 517-525.

129. Ito, T., Sakurai, Y., Kakuta, Y., Sugano, M., Hirano, K., (2012). Biodiesel production from waste animal fats using pyrolysis method, Fuel Process. Technol., 94 (1): 47-52.
130. Ochoa-Hernández, C., Yang, Y., Pizarro, P., Víctor, A., Coronado, J.M., Serrano, D.P., (2013). Hydrocarbons production through hydrotreating of methyl esters over Ni and Co supported on SBA-15 and Al-SBA-15, Catal. Today, 210: 81-88.
131. Bernas, H., Eränen, K., Simakova, I., Leino, A.-R., Kordás, K., Myllyoja, J., Mäki-Arvela, P., Salmi, T., Murzin, D.Y., (2010). Deoxygenation of dodecanoic acid under inert atmosphere, Fuel, 89 (8): 2033-2039.
132. Lestari, S., Simakova, I., Tokarev, A., Mäki-Arvela, P., Eränen, K., Murzin, D.Y., (2008). Synthesis of biodiesel via deoxygenation of stearic acid over supported Pd/C catalyst, Catal. Lett., 122 (3-4): 247-251.
133. Fu, J., Lu, X., Savage, P.E., (2010). Catalytic hydrothermal deoxygenation of palmitic acid, Energy Environ. Sci., 3 (3): 311.
134. Fu, J., Yang, C., Wu, J., Zhuang, J., Hou, Z., Lu, X., (2015). Direct production of aviation fuels from microalgae lipids in water, Fuel, 139: 678-683.
135. Miao, C., Marin-Flores, O., Davidson, S.D., Li, T., Dong, T., Gao, D., Wang, Y., Garcia-Pérez, M., Chen, S., (2016). Hydrothermal catalytic deoxygenation of palmitic acid over nickel catalyst, Fuel, 166: 302-308.
136. Kaewmeesri, R., Srifa, A., Itthibenchapong, V., Faungnawakij, K., (2015). Deoxygenation of waste chicken fats to green diesel over Ni/Al_2O_3: Effect of water and free fatty acid content, Energy Fuels, 29: 833-840.
137. Yang, L., Tate, K.L., Jasinski, J.B., Carreon, M.A., (2015). Decarboxylation of oleic acid to heptadecane over Pt supported on zeolite 5A beads, ACS Catal., 5 (11): 6497-6502.
138. Tian, Q., Qiao, K., Zhou, F., Chen, K., Wang, T., Fu, J., Lu, X., Ouyang, P., (2016). Direct production of aviation fuel range hydrocarbons and aromatics from oleic acid without an added hydrogen donor, Energy Fuels, 30 (9): 7291-7297.
139. Zhang, J., Zhao, C., (2016). Development of a bimetallic Pd-Ni/HZSM-5 catalyst for the tandem limonene dehydrogenation and fatty acid deoxygenation to alkanes and arenes for use as biojet fuel, ACS Catal., 6 (7): 4512-4525.
140. Rabaev, M., Landau, M.V., Vidruk-Nehemya, R., Koukouliev, V., Zarchin, R., Herskowitz, M., (2015). Conversion of vegetable oils on Pt/Al_2O_3/SAPO-11 to diesel and jet fuels containing aromatics, Fuel, 161: 287-294.
141. Chiappero, M., Do, P.T.M., Crossley, S., Lobban, L.L., Resasco, D.E., (2011). Direct conversion of triglycerides to olefins and paraffins over noble metal supported catalysts, Fuel, 90 (3): 1155-1165.
142. Domínguez-Barroso, M., Herrera, C., Larrubia, M., Alemany, L., (2016). Diesel oil-like hydrocarbon production from vegetable oil in a single process over $Pt–Ni/Al_2O_3$ and Pd/C combined catalysts, Fuel Process. Technol., 148: 110-116.
143. Vonghia, E., Boocock, D.G., Konar, S.K., Leung, A., (1995). Pathways for the deoxygenation of triglycerides to aliphatic hydrocarbons over activated alumina, Energy Fuels, 9 (6): 1090-1096.
144. Choudhary, T.V., Phillips, C.B., (2011). Renewable fuels via catalytic hydrodeoxygenation, Appl. Catal. A, 397 (1-2): 1-12.

145. Yokoyama, T., Yamagata, N., (2001). Hydrogenation of carboxylic acids to the corresponding aldehydes, Appl. Catal. A, 221 (1): 227-239.
146. Yokoyama, T., Setoyama, T., Fujita, N., Nakajima, M., Maki, T., Fujii, K., (1992). Novel direct hydrogenation process of aromatic carboxylic acids to the corresponding aldehydes with zirconia catalyst, Appl. Catal. A, 88 (2): 149-161.
147. Pestman, R., Koster, R., Boellaard, E., Van der Kraan, A., Ponec, V., (1998). Identification of the active sites in the selective hydrogenation of acetic acid to acetaldehyde on iron oxide catalysts, J. Catal., 174 (2): 142-152.
148. Hollak, S.A., Bitter, J.H., van Haveren, J., de Jong, K.P., van Es, D.S., (2012). Selective deoxygenation of stearic acid via an anhydride pathway, RSC Adv., 2 (25): 9387-9391.
149. Laurens, L., Nagle, N., Davis, R., Sweeney, N., Van Wychen, S., Lowell, A., Pienkos, P., (2015). Acid-catalyzed algal biomass pretreatment for integrated lipid and carbohydrate-based biofuels production, Green Chem., 17 (2): 1145-1158.
150. Ping, E.W., Pierson, J., Wallace, R., Miller, J.T., Fuller, T.F., Jones, C.W., (2011). On the nature of the deactivation of supported palladium nanoparticle catalysts in the decarboxylation of fatty acids, Appl. Catal. A, 396 (1-2): 85-90.
151. Wen, G., Xu, Y., Ma, H., Xu, Z., Tian, Z., (2008). Production of hydrogen by aqueous-phase reforming of glycerol, Int. J. Hydrogen Energy, 33 (22): 6657-6666.
152. Simakova, I., Simakova, O., Mäki-Arvela, P., Simakov, A., Estrada, M., Murzin, D.Y., (2009). Deoxygenation of palmitic and stearic acid over supported Pd catalysts: Effect of metal dispersion, Appl. Catal. A, 355 (1-2): 100-108.
153. Song, W., Zhao, C., Lercher, J.A., (2013). Importance of size and distribution of Ni nanoparticles for the hydrodeoxygenation of microalgae oil, Chem. Eur. J., 19 (30): 9833-9842.
154. Nguyen, H.S., Mäki-Arvela, P., Akhmetzyanova, U., Tišler, Z., Hachemi, I., Rudnäs, A., Smeds, A., Eränen, K., Aho, A., Kumar, N., (2017). Direct hydrodeoxygenation of algal lipids extracted from Chlorella alga, J. Chem. Technol. Biotechnol., 92 (4): 741-748.
155. Van Stiphout, P., Stobbe, D., Scheur, F.T.V., Geus, J., (1988). Activity and stability of nickel-copper/silica catalysts prepared by deposition-precipitation, Appl. Catal., 40: 219-246.
156. Chen, L., Li, H., Fu, J., Miao, C., Lv, P., Yuan, Z., (2016). Catalytic hydroprocessing of fatty acid methyl esters to renewable alkane fuels over Ni/HZSM-5 catalyst, Catal. Today, 259: 266-276.
157. Hollak, S.A.W., de Jong, K.P., van Es, D.S., (2014). Catalytic deoxygenation of fatty acids: elucidation of the inhibition process, ChemCatChem, 6 (9): 2648-2655.
158. Li, Y., Zhang, C., Liu, Y., Tang, S., Chen, G., Zhang, R., Tang, X., (2017). Coke formation on the surface of Ni/HZSM-5 and Ni-Cu/HZSM-5 catalysts during bio-oil hydrodeoxygenation, Fuel, 189: 23-31.
159. Yeh, T., Linic, S., Savage, P.E., (2014). Deactivation of Pt Catalysts during Hydrothermal Decarboxylation of Butyric Acid, ACS Sustain. Chem. Eng., 2 (10): 2399-2406.
160. Rozmysłowicz, B., Mäki-Arvela, P., Lestari, S., Simakova, O.A., Eränen, K., Simakova, I.L., Murzin, D.Y., Salmi, T.O., (2010). Catalytic deoxygenation of tall oil

fatty acids over a palladium-mesoporous carbon catalyst: A new source of biofuels, Top. Catal., 53 (15-18): 1274-1277.
161. Sari, E., Kim, M., Salley, S.O., Ng, K.Y.S., (2013). A highly active nanocomposite silica-carbon supported palladium catalyst for decarboxylation of free fatty acids for green diesel production: Correlation of activity and catalyst properties, Appl. Catal. A, 467: 261-269.
162. Zhao, X., Wei, L., Cheng, S., Julson, J., (2017). Review of heterogeneous catalysts for catalytically upgrading vegetable oils into hydrocarbon biofuels, Catalysts, 7 (3): 83-108.
163. Idesh, S., Kudo, S., Norinaga, K., Hayashi, J.-i., (2013). Catalytic Hydrothermal Reforming of Jatropha Oil in Subcritical Water for the Production of Green Fuels: Characteristics of Reactions over Pt and Ni Catalysts, Energy Fuels, 27 (8): 4796-4803.
164. Zhang, Z., Yang, Q., Chen, H., Chen, K., Lu, X., Ouyang, P., Fu, J., Chen, J.G., (2018). In situ hydrogenation and decarboxylation of oleic acid into heptadecane over a Cu–Ni alloy catalyst using methanol as a hydrogen carrier, Green Chem., 20 (1): 197-205.
165. Fargoine, J., Hill, J., Tilman, D., Polasky, S., Hawthorne, P., (2008). Land clearing and the biofuel carbon debt, Science, 319 (5867): 1235-1238.
166. Tilman, D., Socolow, R., Foley, J.A., Hill, J., Larson, E., Lynd, L., Pacala, S., Reilly, J., Searchinger, T., Somerville, C., Williams, R., (2009). Beneficial Biofuels-The Food, Energy, and Environment Trilemma, Science, 325 (5938): 270-271.
167. http://www.uop.com/processing-solutions/renewables/green-diesel/#biodiesel (accessed October 2015
168. Ogunkoya, D., Roberts, W.L., Fang, T., Thapaliya, N., (2015). Investigation of the effects of renewable diesel fuels on engine performance, combustion, and emissions, Fuel, 140: 541-554.
169. Donnis, B., Egeberg, R.G., Blom, P., Knudsen, K.G., (2009). Hydroprocessing of Bio-Oils and Oxygenates to Hydrocarbons. Understanding the Reaction Routes, Top. Catal., 52 (3): 229-240.
170. Snåre, M., Kubičková, I., Mäki-Arvela, P., Eränen, K., Wärnå, J., Murzin, D.Y., (2007). Production of diesel fuel from renewable feeds: Kinetics of ethyl stearate decarboxylation, Chem. Eng. J., 134 (1-3): 29-34.
171. Na, J.-G., Yi, B.E., Han, J.K., Oh, Y.-K., Park, J.-H., Jung, T.S., Han, S.S., Yoon, H.C., Kim, J.-N., Lee, H., Ko, C.H., (2012). Deoxygenation of microalgal oil into hydrocarbon with precious metal catalysts: Optimization of reaction conditions and supports, Energy, 47 (1): 25-30.
172. Lestari, S., Mäki-Arvela, P., Bernas, H., Simakova, O., Sjöholm, R., Beltramini, J., Lu, G.Q., Myllyoja, J., Simakova, I., Murzin, D.Y., (2009). Catalytic Deoxygenation of Stearic Acid in a Continuous Reactor over a Mesoporous Carbon-Supported Pd Catalyst, Energy Fuels, 23 (8): 3842-3845.
173. Botas, J.A., Serrano, D.P., García, A., de Vicente, J., Ramos, R., (2012). Catalytic conversion of rapeseed oil into raw chemicals and fuels over Ni- and Mo-modified nanocrystalline ZSM-5 zeolite, Catal. Today, 195 (1): 59-70.
174. Galea, N., Knapp, D., Ziegler, T., (2007). Density functional theory studies of methane dissociation on anode catalysts in solid-oxide fuel cells: Suggestions for coke reduction, J. Catal., 247 (1): 20-33.

175. Fierro, V., Akdim, O., Mirodatos, C., (2003). On-board hydrogen production in a hybrid electric vehicle by bio-ethanol oxidative steam reforming over Ni and noble metal based catalysts. , Green Chemistry, 5 (1): 20-24.
176. Boudjahem, A.G., Chettibi, M., Monteverdi, S., M. Bettabar, M., (2009). Acetylene hydrogenation over Ni-Cu nanoparticles supported on silica prepared by aqueous hydrazine reduction, Journal of Nanoscience and Nanotechnology, 9 (6): 3546-3554.
177. Guo, Q., Wu, M., Wang, K., Zhang, L., Xu, X., (2015). Catalytic Hydrodeoxygenation of Algae Bio-oil over Bimetallic Ni–Cu/ZrO2 Catalysts, Ind. Eng. Chem. Res., 54 (3): 890-899.
178. Van Stiphout, P.C.M., Stobbe, D.E., V.D. Scheur, F.T., Geus, J.W., (1988). Activity and stability of nickel--copper/silica catalysts prepared by deposition-precipitation, Appl. Catal., 40: 219-246.
179. Nikolla, E., Schwank, J., Linic, S., (2009). Comparative study of the kinetics of methane steam reforming on supported Ni and Sn/Ni alloy catalysts: The impact of the formation of Ni alloy on chemistry, J. Catal., 263 (2): 220-227.
180. Nikolla, E., Holewinski, A., Schwank, J., Linic, S., (2006). Controlling Carbon Surface Chemistry by Alloying: Carbon Tolerant Reforming Catalyst, Journal of American Chemical Society, 128 (35): 11354-11355.
181. Gosselink, R.W., Hollak, S.A.W., Chang, S.-W., Haveren, J.v., Jong, K.P.d., Es, D.S.v., (2013). Reaction Pathways for the Deoxygenation of Vegetable Oils and Related Model Compounds, ChemSusChem, 6: 1576-1597.
182. Santillan-Jimenez, E., Morgan, T., Shoup, J., Harman-Ware, A., Crocker, M., (2014). Catalytic deoxygenation of triglycerides and fatty acids to hydrocarbons over Ni-Al layered double hydroxide, Catal. Today, 237: 136-144.
183. Santillan-Jimenez, E., Morgan, T., Loe, R., Crocker, M., (2015). Continuous catalytic deoxygenation of model and algal lipids to fuel-like hydrocarbons over Ni–Al layered double hydroxide, Catal. Today, 258: 284-293.
184. Bligh, E.G., Dyer, W.J., (1959). A rapid method of total lipid extraction and purification, Canadian Journal of Biochemistry and Physiology, 37 (8): 911-917.
185. Wilson, M.H., Groppo, J., Placido, A., Graham, S., Morton, S.A., III, Santillan-Jimenez, E., Shea, A., Crocker, M., Crofcheck, C., Andrews, R., (2014). CO2 recycling using microalgae for the production of fuels, Appl. Petrochem. Res., 4: 41-53.
186. Morgan, T., Santillan-Jimenez, E., Crocker, M., (2014). Simulated Distillation Approach to the Gas Chromatographic Analysis of Feedstock and Products in the Deoxygenation of Lipids to Hydrocarbon Biofuels, Energy Fuels, 28 (4): 2654-2662.
187. Vizcaíno, A., Carrero, A., Calles, J., (2007). Hydrogen production by ethanol steam reforming over Cu–Ni supported catalysts, Int. J. Hydrogen Energy, 32 (10): 1450-1461.
188. Carrero, A., Calles, J., Vizcaíno, A., (2007). Hydrogen production by ethanol steam reforming over Cu-Ni/SBA-15 supported catalysts prepared by direct synthesis and impregnation, Appl. Catal. A, 327 (1): 82-94.
189. Lee, J.-H., Lee, E.-G., Joo, O.-S., Jung, K.-D., (2004). Stabilization of Ni/Al_2O_3 catalyst by Cu addition for CO2 reforming of methane, Appl. Catal. A, 269 (1-2): 1-6.
190. Rynkowski, J.M., Paryjczak, T., Lenik, M., (1993). On the nature of oxidic nickel phases in $NiO/\gamma\text{-}Al_2O_3$ catalysts, Appl. Catal. A, 106 (1): 73-82.

191. Miranda, B.C., Chimentão, R.J., Szanyi, J., Braga, A.H., Santos, J.B.O., Gispert-Guirado, F., Llorca, J., Medina, F., (2015). Influence of copper on nickel-based catalysts in the conversion of glycerol, Appl. Catal. B, 166-167: 166-180.
192. Li, Y., Chen, J., Chang, L., Qin, Y., (1998). The doping effect of copper on the catalytic growth of carbon fibers from methane over a Ni/Al_2O_3 catalyst prepared from Feitknecht compound precursor, J. Catal., 178 (1): 76-83.
193. Zieliński, J., (1982). Morphology of nickel/alumina catalysts, J. Catal., 76 (1): 157-163.
194. Castaño, P., Pawelec, B., Fierro, J.L.G., Arandes, J.M., Bilbao, J., (2007). Enhancement of pyrolysis gasoline hydrogenation over Pd-promoted Ni/SiO_2-Al_2O_3 catalysts, Fuel, 86 (15): 2262-2274.
195. Zhu, X., Zhang, Y.-p., Liu, C.-j., (2007). CO adsorbed infrared spectroscopy study of Ni/Al_2O_3 catalyst for CO_2 reforming of methane, Catal. Lett., 118 (3-4): 306-312.
196. Mihaylov, M., Lagunov, O., Ivanova, E., Hadjiivanov, K., (2011). Determination of polycarbonyl species on nickel-containing catalysts by adsorption of CO isotopic mixtures, Top. Catal., 54 (5-7): 308-317.
197. Kitla, A., Safonova, O.V., Fottinger, K., (2013). Infrared Studies on Bimetallic Copper/Nickel Catalysts Supported on Zirconia and Ceria/Zirconia, Catal Letters, 143 (6): 517-530.
198. Laperdrix, E., Justin, I., Costentin, G., Saur, O., Lavalley, J.C., Aboulayt, A., Ray, J.L., Nédez, C., (1998). Comparative study of CS_2 hydrolysis catalyzed by alumina and titania, Appl. Catal. B, 17 (1–2): 167-173.
199. Snåre, M., Kubičková, I., Mäki-Arvela, P., Eränen, K., Murzin, D.Y., (2006). Heterogeneous catalytic deoxygenation of stearic acid for production of biodiesel, Ind. Eng. Chem. Res., 45 (16): 5708-5715.
200. Berenblyum, A.S., Danyushevsky, V.Y., Katsman, E.A., Shamsiev, R.S., Flid, V.R., (2013). Specifics of the stearic acid deoxygenation reaction on a copper catalyst, Pet. Chem., 53 (6): 362-366.
201. Mahata, N., Vishwanathan, V., (2000). Influence of Palladium Precursors on Structural Properties and Phenol Hydrogenation Characteristics of Supported Palladium Catalysts, J. Catal., 196 (2): 262-270.
202. Parera, J.M., Figoli, N.S., Jablonski, E.L., Sad, M.R., Beltramini, J.N., (1980). Optimum Chlorine on Naphtha Reforming Catalyst Regarding Deactivation by Coke Formation, Stud. Surf. Sci. Catal., 6: 571-576.
203. Santillan-Jimenez, E., Crocker, M., (2012). Catalytic deoxygenation of fatty acids and their derivatives to hydrocarbon fuels via decarboxylation/decarbonylation, Journal of Chemical Technology & Biotechnology, 87 (8): 1041-1050.
204. Harnos, S., Onyestyák, G., Kalló, D., (2012). Hydrocarbons from sunflower oil over partly reduced catalysts, Reaction Kinetics, Mechanisms and Catalysis, 106 (1): 99-111.
205. Peng, B., Zhao, C., Kasakov, S., Foraita, S., Lercher, J.A., (2013). Manipulating catalytic pathways: deoxygenation of palmitic acid on multifunctional catalysts, Chemistry, 19 (15): 4732-4741.
206. Song, P., Wen, D., Guo, Z.X., Korakianitis, T., (2008). Oxidation investigation of nickel nanoparticles, PCCP, 10 (33): 5057-5065.

207. Tilman, D., Socolow, R., Foley, J.A., Hill, J., Larson, E., Lynd, L., Pacala, S., Reilly, J., Searchinger, T., Somerville, C., Williams, R., (2009). Beneficial Biofuels—The Food, Energy, and Environment Trilemma, Science, 325 (5938): 270-271.
208. http://www.uop.com/processing-solutions/renewables/green-diesel/#biodiesel (accessed November, 2016)
209. Santillan-Jimenez, E., Crocker, M., (2012). Catalytic deoxygenation of fatty acids and their derivatives to hydrocarbon fuels via decarboxylation/decarbonylation, J. Chem. Technol. Biotechnol., 87: 1041-1050.
210. Gosselink, R.W., Hollak, S.A., Chang, S.W., van Haveren, J., de Jong, K.P., Bitter, J.H., van Es, D.S., (2013). Reaction pathways for the deoxygenation of vegetable oils and related model compounds, ChemSusChem, 6 (9): 1576-1594.
211. Griffiths, M.J., van Hille, R.P., Harrison, S.T., (2010). Selection of direct transesterification as the preferred method for assay of fatty acid content of microalgae, Lipids, 45 (11): 1053-1060.
212. Arnold, R.T., Danzig, M.J., (1957). Thermal Decarboxylation of Unsaturated Acids. II, J. Am. Chem. Soc., 79 (4): 892-893.
213. Sebedio, J.L., Langman, M.F., Eaton, C.A., Ackman, R.G., (1981). Alteration of long chain fatty acids of herring oil during hydrogenation on nickel catalyst, J. Am. Oil Chem. Soc., 58 (1): 41-48.
214. Kaewmeesri, R., Srifa, A., Itthibenchapong, V., Faungnawakij, K., (2015). Deoxygenation of Waste Chicken Fats to Green Diesel over Ni/Al_2O_3: Effect of Water and Free Fatty Acid Content, Energy Fuels, 29 (2): 833-840.
215. Andersson, M.P., Abild-Pedersen, F., Remediakis, I.N., Bligaard, T., Jones, G., Engbæk, J., Lytken, O., Horch, S., Nielsen, J.H., Sehested, J., Rostrup-Nielsen, J.R., Nørskov, J.K., Chorkendorff, I., (2008). Structure sensitivity of the methanation reaction: H2-induced CO dissociation on nickel surfaces, J. Catal., 255 (1): 6-19.
216. Aziz, M.A.A., Jalil, A.A., Triwahyono, S., Mukti, R.R., Taufiq-Yap, Y.H., Sazegar, M.R., (2014). Highly active Ni-promoted mesostructured silica nanoparticles for CO_2 methanation, Appl. Catal. B, 147: 359-368.
217. Tada, S., Shimizu, T., Kameyama, H., Haneda, T., Kikuchi, R., (2012). Ni/CeO_2 catalysts with high CO_2 methanation activity and high CH_4 selectivity at low temperatures, Int. J. Hydrogen Energy, 37 (7): 5527-5531.
218. Guo, C., Wu, Y., Qin, H., Zhang, J., (2014). CO methanation over ZrO_2/Al_2O_3 supported Ni catalysts: A comprehensive study, Fuel Process. Technol., 124: 61-69.
219. Gao, J., Jia, C., Li, J., Zhang, M., Gu, F., Xu, G., Zhong, Z., Su, F., (2013). Ni/Al_2O_3 catalysts for CO methanation: Effect of Al_2O_3 supports calcined at different temperatures, J. Energy Chem., 22 (6): 919-927.
220. Krompiec, S., Mrowiec-Białoń, J., Skutil, K., Dukowicz, A., Pająk, L., Jarzębski, A.B., (2003). Nickel–alumina composite aerogel catalysts with a high nickel load: a novel fast sol–gel synthesis procedure and screening of catalytic properties, J. Non-Cryst. Solids, 315 (3): 297-303.
221. Peng, B., Yao, Y., Zhao, C., Lercher, J.A., (2012). Towards quantitative conversion of microalgae oil to diesel-range alkanes with bifunctional catalysts, Angewandte Chemie - International Edition, 51 (9): 2072-2075.

222. Veriansyah, B., Han, J.Y., Kim, S.K., Hong, S.-A., Kim, Y.J., Lim, J.S., Shu, Y.-W., Oh, S.-G., Kim, J., (2012). Production of renewable diesel by hydroprocessing of soybean oil: Effect of catalysts, Fuel, 94: 578-585.
223. Kim, S.K., Brand, S., Lee, H.S., Kim, Y., Kim, J., (2013). Production of renewable diesel by hydrotreatment of soybean oil: Effect of reaction parameters, Chem. Eng. J., 228: 114-123.
224. Arbeláez, O., Reina, T.R., Ivanova, S., Bustamante, F., Villa, A.L., Centeno, M.A., Odriozola, J.A., (2015). Mono and bimetallic Cu-Ni structured catalysts for the water gas shift reaction, Appl. Catal. A, 497: 1-9.
225. Saw, E.T., Oemar, U., Tan, X.R., Du, Y., Borgna, A., Hidajat, K., Kawi, S., (2014). Bimetallic Ni–Cu catalyst supported on CeO2 for high-temperature water–gas shift reaction: Methane suppression via enhanced CO adsorption, J. Catal., 314: 32-46.
226. Toops, T.J., Crocker, M., (2008). New sulfur adsorbents derived from layered double hydroxides: II. DRIFTS study of COS and H2S adsorption, Appl. Catal. B, 82 (3–4): 199-207.
227. Flaherty, D.W., Yu, W.-Y., Pozun, Z.D., Henkelman, G., Mullins, C.B., (2011). Mechanism for the water–gas shift reaction on monofunctional platinum and cause of catalyst deactivation, J. Catal., 282 (2): 278-288.
228. Benson, T.J., Hernandez, R., French, W.T., Alley, E.G., Holmes, W.E., (2009). Elucidation of the catalytic cracking pathway for unsaturated mono-, di-, and triacylglycerides on solid acid catalysts, J. Mol. Catal. A: Chem., 303 (1): 117-123.
229. Pimentel, D., Marklein, A., Toth, M.A., Karpoff, M.N., Paul, G.S., McCormack, R., Kyriazis, J., Krueger, T., (2009). Food versus biofuels: environmental and economic costs, Human ecology, 37 (1): 1.
230. None, N., Biofuels and Bioproducts from Wet and Gaseous Waste Streams: Challenges and Opportunities, EERE Publication and Product Library, 2017.
231. Laurent, E., Delmon, B., (1994). Study of the hydrodeoxygenation of carbonyl, car□ ylic and guaiacyl groups over sulfided CoMo/γ-Al_2O_3 and NiMo/γ- Al_2O_3 catalysts: I. Catalytic reaction schemes, Appl. Catal. A, 109 (1): 77-96.
232. Stacy, C.J., Melick, C.A., Cairncross, R.A., (2014). Esterification of free fatty acids to fatty acid alkyl esters in a bubble column reactor for use as biodiesel, Fuel Process. Technol., 124: 70-77.
233. Morgan, T., Santillan-Jimenez, E., Huff, K., Javed, K.R., Crocker, M., (2017). Use of dual detection in the gas chromatographic analysis of oleaginous biomass feeds and biofuel products to enable accurate simulated distillation and lipid profiling, Energy Fuels, 31 (9): 9498-9506.
234. Canakci, M., (2007). The potential of restaurant waste lipids as biodiesel feedstocks, Bioresour. Technol., 98 (1): 183-190.
235. Kim, M., DiMaggio, C., Yan, S., Wang, H., Salley, S.O., Ng, K.S., (2011). Performance of heterogeneous ZrO2 supported metaloxide catalysts for brown grease esterification and sulfur removal, Bioresour. Technol., 102 (3): 2380-2386.
236. Chen, H., Zhang, X., Zhang, J., Wang, Q., (2018). Tuning Decarboxylation Selectivity for Deoxygenation of Vegetable Oil over Pt-Ni Bimetal Catalysts via Surface Engineering, Catal. Sci. Technol.:

237. Simakova, I., Rozmysłowicz, B., Simakova, O., Mäki-Arvela, P., Simakov, A., Murzin, D.Y., (2011). Catalytic Deoxygenation of C18 Fatty Acids Over Mesoporous Pd/C Catalyst for Synthesis of Biofuels, Top. Catal., 54 (8-9): 460-466.
238. Hengst, K., Arend, M., Pfützenreuter, R., Hoelderich, W.F., (2015). Deoxygenation and cracking of free fatty acids over acidic catalysts by single step conversion for the production of diesel fuel and fuel blends, Appl. Catal. B, 174-175: 383-394.
239. de Sousa, F.P., Cardoso, C.C., Pasa, V.M., (2016). Producing hydrocarbons for green diesel and jet fuel formulation from palm kernel fat over Pd/C, Fuel Process. Technol., 143: 35-42.
240. Guo, Q., Wu, M., Wang, K., Zhang, L., Xu, X., (2015). Catalytic Hydrodeoxygenation of Algae Bio-oil over Bimetallic Ni–Cu/ZrO2Catalysts, Ind. Eng. Chem. Res., 54 (3): 890-899.
241. Shi, Y., Xing, E., Cao, Y., Liu, M., Wu, K., Yang, M., Wu, Y., (2017). Tailoring product distribution during upgrading of palmitic acid over bi-functional metal/zeolite catalysts, Chem. Eng. Sci., 166: 262-273.
242. Lu, S., Lonergan, W.W., Bosco, J.P., Wang, S., Zhu, Y., Xie, Y., Chen, J.G., (2008). Low temperature hydrogenation of benzene and cyclohexene: A comparative study between γ-Al_2O_3 supported PtCo and PtNi bimetallic catalysts, J. Catal., 259 (2): 260-268.
243. Tanksale, A., Beltramini, J., Dumesic, J., Lu, G., (2008). Effect of Pt and Pd promoter on Ni supported catalysts—A TPR/TPO/TPD and microcalorimetry study, J. Catal., 258 (2): 366-377.
244. Fisk, C.A., Morgan, T., Ji, Y., Crocker, M., Crofcheck, C., Lewis, S.A., (2009). Bio-oil upgrading over platinum catalysts using in situ generated hydrogen, Appl. Catal. A, 358 (2): 150-156.
245. Liu, X., An, W., Turner, C.H., Resasco, D.E., (2018). Hydrodeoxygenation of m-cresol over bimetallic NiFe alloys: Kinetics and thermodynamics insight into reaction mechanism, J. Catal., 359: 272-286.
246. Yfanti, V.-L., Vasiliadou, E., Lemonidou, A., (2016). Glycerol hydro-deoxygenation aided by in situ H 2 generation via methanol aqueous phase reforming over a Cu–ZnO–Al 2 O 3 catalyst, Catal. Sci. Technol., 6 (14): 5415-5426.
247. Hollak, S.A., Ariëns, M.A., de Jong, K.P., van Es, D.S., (2014). Hydrothermal deoxygenation of triglycerides over Pd/C aided by in situ hydrogen production from glycerol reforming, ChemSusChem, 7 (4): 1057-1062.

VITA

EDUCATIONAL INSTITUTIONS

2007-2011 **Muskingum University**
Bachelor of Science in Chemistry; Minor in Biology

2003-2007 **Pickerington North High School**

PROFESSIONAL POSITIONS

2012-Present **Graduate Student**
Mentor: Dr. Mark Crocker, Professor of Chemistry, Associate Director of Biofuels & Environmental Catalysis at the University of Kentucky Center for Applied Energy Research

2017-2018, 2012-2014 **Organic Chemistry Laboratory Teaching Assistant**
University of Kentucky

2013-2014 **General Chemistry Laboratory Teaching Assistant**
University of Kentucky

2011-2012 **Quality Control Technician**
Organic Technologies, Coshocton, Ohio

2010-2011 **Research Assistant**
Muskingum University
Mentor: Dr. Eric Schurter, Associate Professor of Chemistry

2009-2010 **Research Assistant**
Muskingum University
Mentor: Dr. Raymond Rataiczak, Science Division Coordinator, Professor of Chemistry

FELLOWSHIPS AND AWARDS

10/2017 Kokes Travel Award

07/2016 Travel Award

05/2016 NSF East Asia and Pacific Summer Institutes Fellowship

2012-2016 Max Steckler Fellowship

2015 Travel Award

2014 NSF Travel Award

PUBLICATIONS

[1] **R. Loe**, E. Santillan-Jimenez, M. Crocker, (2020). Upgrading of lipids to fuel-like hydrocarbons and terminal olefins via decarbonylation/decarboxylation. *Chemical Catalysts for Biomass Valorization*, Wiley-VCH. In Review.

[2] **R. Loe**, E. Santillan-Jimenez, T. Morgan, K. Huff, M. Crocker, (2018). Pt promotion of supported Ni catalysts on the catalytic deoxygenation of model lipids. Manuscript in preparation.

[3] **R. Loe**, E. Santillan-Jimenez, Y. Lavoignat, M. Maier, M. Abdallah, T. Morgan, M. Crocker, (2018). Effect of temperature and gas atmosphere on catalytic deoxygenation of brown grease lipids over supported Ni-Cu Catalysts. Manuscript in preparation.

[4] E. Santillan-Jimenez, **R. Loe**, M. Garrett, T. Morgan, M. Crocker, (2018). Effect of Cu Promotion on cracking and methanation during the Ni-catalyzed deoxygenation of waste lipids and hemp oil to fuel-like hydrocarbons. Catalysis Today. 302: 261-271.

[5] **R. Loe**, E. Santillan-Jimenez, T. Morgan, L. Sewell, Y. Ji, S. Jones, M.A. Is~~s~~aacs, A.F. Lee, M. Crocker, (2016). Effect of Cu or Sn promotion on the catalytic deoxygenation of model and algal lipids to fuel-like hydrocarbons over supported Ni catalysts. Applied Catalysis B: Environmental. 191: 147-156.

[6] E. Santillan-Jimenez, T. Morgan, **R. Loe**, M. Crocker, (2015). Continuous catalytic deoxygenation of model and algal lipids to fuel-like hydrocarbons over Ni-Al layered double hydroxide. Catalysis Today 258: 284-293